



TECHNISCHE UNIVERSITÄT MÜNCHEN

TUM School of Life Sciences

**Development of novel adipocyte sizing strategies to decipher
the genetic, transcriptomic and metabolic mechanisms of
adipocyte hypertrophy.**

Julius Honecker

Vollständiger Abdruck der von der TUM School of Life Sciences der Technischen Universität München zur Erlangung des akademischen Grades eines Doktors der Naturwissenschaften (Dr. rer. nat.) genehmigten Dissertation.

Vorsitz:

Prof. Dr. Martin Klingenspor

Prüfer*innen der Dissertation:

1. Prof. Dr. Johann J. Hauner

2. Prof. Dr. Melina Christine Clausnitzer

3. Prof. Dr. Matthias Blüher

Die Dissertation wurde am 02.02.2022 bei der Technischen Universität München eingereicht und durch die TUM School of Life Sciences am 04.07.2022 angenommen.

Table of contents

Table of contents	I
Abbreviations	III
Abstract	V
Zusammenfassung	VII
1 Introduction	1
1.1 The role of adipose tissue in the pathophysiology of obesity.....	1
1.2 The adipose organ in brief	1
1.3 Mechanisms of white adipose tissue expansion.....	2
1.4 Techniques to measure adipocyte size	3
1.5 Adipocyte size is related to anthropometry and systemic metabolic disorders	4
1.6 Adipocyte hypertrophy introduces pathophysiological changes to white adipose tissue structure and composition.....	6
1.7 Enlarged adipocytes display altered adipokine secretion patterns and show metabolic alterations.....	6
1.8 Data-driven “omics” studies and adipocyte hypertrophy.....	8
1.9 Limitations of current adipocyte sizing methods	9
2 Aims	10
3 Material and methods	12
3.1 Human samples and study cohorts.....	12
3.2 DNA isolation and genotyping.....	14
3.3 Histology and imaging.....	14
3.4 Adipocyte size determination from histological sections.....	15
3.5 Cell Culture.....	16
3.6 Respirometry in mature adipocytes.....	18
3.7 Cell culture sample processing	18
3.8 RNA sequencing.....	19

Table of contents

3.9 Adipose tissue fatty acid composition	21
3.10 MR based characterization of WAT.....	21
3.11 Statistics	22
4 Publications	24
Chapter I Development of a novel adipocyte sizing strategy that facilitates the study of potential genetic drivers behind adipocyte morphology.....	24
Chapter II A distribution-centered approach to analyze human adipocyte size estimates and their relationship with obesity-associated traits and mitochondrial respiration.....	27
Chapter III Deciphering the transcriptomic and fatty acid-related alterations that accompany adipocyte hypertrophy.	29
5 Discussion	32
6 References	45
7 Appendix	56
7.1 Original publications	56
7.2 Letters of approval.....	131
7.3 Key resources table	134
7.4 Approval for a publication-based dissertation.....	138
7.5 Declaration of Authorship.....	139
8 Publications and congress contributions.....	140
9 Acknowledgement.....	143

Abbreviations

General abbreviations

ADP	Adenosine diphosphate
BAT	Brown adipose tissue
BMI	Body mass index
CNN	Convolutional neuronal network
CP	CellProfiler
DM	Differentiation medium
DNA	Deoxyribonucleic acid
ETS	Electron transfer system capacity
FA	Fatty acid
FAME	Fatty acid methyl ester
FFA	Free fatty acid
FFPE	Formalin-fixed paraffin-embedded
GC-MS	Gas chromatography-mass spectrometry
GTE _x	Genotype tissue expression project
GWAS	Genome-wide association study
H&E	Hematoxylin & eosin
hAMSC	Human adipose mesenchymal stem cells
HbA _{1c}	Glycated hemoglobin
HDL	High-density lipoprotein
HOMA-IR	Homeostasis model assessment for insulin resistance
IM	Isolation medium
InM	Induction medium
KRP	Krebs Ringer phosphate buffer
LDL	Low-density lipoprotein
MR	Magnetic resonance
OXPHOS	Oxidative phosphorylation
PM	Proliferation medium
PUFA	Polyunsaturated fatty acid
RNA	Ribonucleic acid
SAT	Subcutaneous adipose tissue
SNP	Single nucleotide polymorphism
SVF	Stromal vascular fraction
T2D	Type 2 diabetes
VAT	Visceral adipose tissue
WAT	White adipose tissue
WHO	World health organization
WHR	Waist to hip ratio

Abbreviations

Gene names

<i>FTO</i>	Fat mass and obesity-associated
<i>KLF14</i>	Krüppel like factor 14
<i>PRDM16</i>	PR domain containing 16
<i>TNF-α</i>	Tumor necrosis factor α
<i>UCP-1</i>	Uncoupling protein 1
<i>EGFL6</i>	EGF like domain multiple 6
<i>SLC27A2</i>	Solute carrier family 27 member 2
<i>FASN</i>	Fatty acid synthase

RNA-Seq related abbreviations

DE	Differential expression
GO	Gene ontology
GSEA	Gene set enrichment analysis
KEGG	Kyoto encyclopedia of genes and genomes
STAR	Spliced transcripts alignments to a reference
TMM	Trimmed means of m-values
TPM	Transcripts per kilobase million

Abstract

Adipose tissue is an organ with unmatched plasticity that dynamically responds to energy intake and expenditure. With substantial changes in dietary habits and physical activity, a constant positive energy balance can be seen as the main driver behind the disproportionate accumulation of white adipose tissue and the manifestation of obesity as a major global health burden. On a microscopic scale, an increase in fat cell volume (adipocyte hypertrophy) has been identified as metabolically adverse and was shown to associate with obesity-related comorbidities such as type 2 diabetes and cardiovascular disease. While adipocyte size has been frequently associated with obesity and changes of the metabolic state, the underlying genetic architecture and transcriptomic changes associated with adipose morphology remain largely unknown.

To link genetic variation and gene expression changes to adipocyte size, this Ph.D. thesis aimed to establish novel, scalable adipocyte sizing strategies that are tailored towards large cohort studies.

To address current limitations in adipocyte sizing, a machine learning-based method (Adipocyte U-net) was developed to reliably obtain adipocyte area estimates from whole adipose slide scans. Validation experiments against current state-of-the-art adipocyte sizing methods showed excellent agreement and therefore the obtained area estimates were used in a genome-wide association study to gain insight into the genetic architecture of adipocyte morphology. Despite large sample numbers ($n = 820$), no genetic loci reaching genome-wide significance were found.

To obtain a more granular cell size characterization of adipocyte populations, a distribution-centered analysis strategy suggesting additional sizing parameters beyond measures of central tendency was established. The additional sizing parameters complemented previous analytical approaches and revealed important insights into the shape and modality of histology-derived adipocyte size distributions. Based on the extracted sizing parameters, possible correlations between adipocyte size, anthropometry, clinical parameters and mitochondrial function were explored. As a novel finding linking adipocyte hypertrophy and adipose tissue metabolism, an inverse relationship between adipocyte size estimates and mitochondrial respiration was found.

Transcriptomic profiling of white adipose tissue, and size-separated mature adipocytes by RNA-sequencing indicated a shift from an energy-dissipating towards an energy-storing and pro-inflammatory transcriptomic profile associated with adipocyte hypertrophy. In good agreement with the altered expression of fatty acid metabolism-related genes, a close relationship between white adipose tissue fatty acid composition and adipocyte size was discovered. To harness the

Abstract

diagnostic potential of the described laboratory findings, magnetic resonance spectroscopy-based strategies for the non-invasive, simultaneous characterization of adipose tissue morphology and composition were developed.

Altogether, the current work provides a novel, fully automated method for the reliable quantification of adipocyte size that is tailored towards large population-based studies. As key findings, substantial alterations in gene expression, mitochondrial function and fatty acid composition associated with adipocyte hypertrophy were discovered which at least partially lay the transcriptional and metabolic foundation for the manifestation and progression of obesity and its related disorders.

Zusammenfassung

Fettgewebe ist ein Organ mit enormer Plastizität und reagiert dynamisch auf Veränderungen der Energiezufuhr und des Energieverbrauchs. Eine dauerhaft positive Energiebilanz aufgrund substanzieller Veränderungen im Essverhalten, kombiniert mit reduzierter körperlicher Betätigung, wird als der zentrale Mechanismus für eine überproportionale Zunahme der Fettmasse angesehen und trägt dazu bei, dass Adipositas zu einem der größten gesundheitlichen Probleme des 21. Jahrhunderts geworden ist. Die Größenzunahme von bereits existierenden Fettzellen (Hypertrophie) gilt als eine der zentralen pathologischen Veränderungen im Fettgewebe von Personen mit Adipositas. Das sekretorische und metabolische Profil von hypertrophen Adipozyten gilt als schädlich und trägt maßgeblich zur Manifestation Adipositas-assoziiierter Erkrankungen bei (z.B. Typ 2 Diabetes & Kardiovaskuläre Erkrankungen). Bisher ist jedoch nicht bekannt, ob eine genetische Prädisposition für hypertrophe Fettzellen existiert und wie sich das Transkriptom, die mitochondriale Funktion und Fettsäurezusammensetzung in Abhängigkeit von der Adipozytengröße verändert.

Um genetische Prädisposition und Veränderungen der Genexpression in Abhängigkeit der Fettzellgröße zu untersuchen, war es daher das Ziel der Doktorarbeit neue, auf große Kohorten zugeschnittene Methoden zur Fettzellgrößenbestimmung zu entwickeln.

Basierend auf maschinellem Lernen wurde eine Methode zur Zellgrößenbestimmung entwickelt, welche ganze Objektträgerbilder als Datenquelle nutzt und Limitationen von derzeitigen Größenbestimmungsmethoden adressiert. Im ersten Schritt wurden die Fettzellgrößen des sogenannten „Adipocyte U-net“ mit Fettzellgrößen von bisher genutzten „state of the art“ Methoden verglichen. Basierend auf der neuen Fettzellgrößenbestimmungsmethode wurde als nächster Schritt in einer genomweiten Assoziationsstudie untersucht, ob bestimmte Einzel-Nukleotid-Polymorphismen die mittlere Fettzellgröße beeinflussen. Trotz der hohen Anzahl an Probanden in der Studie ($n = 820$), konnten keine Loci mit genomweiter Signifikanz identifiziert werden.

Um eine detailliertere Charakterisierung der gesamten Adipozytenpopulation zu erreichen, wurde eine verteilungsbasierte Methode zur Fettzellgrößenanalyse entwickelt. Die Analysestrategie schlägt zusätzliche Parameter zur Charakterisierung vor, die über die bisher verwendeten Lageparameter hinausgehen, und vervollständigt somit bisher publizierte Analysemethoden. Mittels der neuen statistischen Parameter konnten wichtige Erkenntnisse zur Form und Modalität von Histologie-basierten Fettzellgrößenverteilungen gewonnen werden. Basierend auf den gewonnenen Fettzellgrößenparametern wurden Korrelationsanalysen durchgeführt, um den

Zusammenfassung

Zusammenhang zwischen Fettzellgröße, anthropometrischen, sowie klinischen Parametern und mitochondrialer Funktion zu untersuchen. Die Studie belegt ein reziprokes Verhältnis zwischen Fettzellgröße und mitochondrialer Atmung und deckt somit neue metabolische Störungen, die mit vergrößerten Adipozyten einhergehen, auf.

Die Transkriptomanalysen von Fettgewebe und gröÙenseparierten Adipozyten basierend auf RNA Sequenzierung ergaben, dass in Individuen mit hypertrophen Fettzellen eine Veränderung der globalen Genexpression vorliegt. Detaillierte Analysen zeigten, dass das Transkriptom sich von einem energieverbrauchenden zu einem energiespeichernden und entzündungsfördernden Profil verändert. Zusätzlich zur veränderten Expression von Genen des Fettsäuremetabolismus konnten Assoziationen zwischen Fettsäuremustern und Fettzellgrößen nachgewiesen werden. Um das diagnostische Potential der genannten Forschungsergebnisse zu ergründen, wurden nicht-invasive Magnetresonanz-spektroskopie-Methoden zur morphologischen und kompositionellen Charakterisierung des Fettgewebes erprobt.

Zusammenfassend etabliert die beschriebene Arbeit eine neue und vollautomatisierte Methode zur Fettzellgrößenbestimmung, die auf populationsbasierte Studien zugeschnitten ist. Als zentrales Ergebnis konnten transkriptomweite Veränderungen in der Genexpression in Abhängigkeit der Fettzellgröße identifiziert werden. Die globalen Veränderungen in der Genexpression in Abhängigkeit von der Zellgröße könnten als ein zentraler mechanistischer Grundstein für das Entstehen und Fortschreiten von Adipositas sowie ihren verwandten metabolischen Erkrankungen gesehen werden.

1 | Introduction

1.1 | The role of adipose tissue in the pathophysiology of obesity

Obesity has reached epidemic proportions and is a central risk factor and driving force for the development of chronic, non-communicable diseases such as type 2 diabetes (T2D), nonalcoholic fatty liver disease, and coronary artery disease. In 2016, according to the World Health Organization (WHO), more than 1.9 billion adults were overweight relating to 39 % of the total adult population (1). Since 1980 the number of individuals with obesity has doubled (2). Recent projections, furthermore, suggest that the prevalence of obesity in adults will continue to increase and it is estimated that by 2030 approximately half of the United States population will suffer from obesity (3). Obesity can, therefore, be recognized as one of the most important global health burdens of the 21st century.

The mechanisms behind the development of obesity are multi-factorial and stem from both environmental and genetic factors (4, 5). From all factors contributing to the progression of obesity, an increased energy intake combined with decreased energy expenditure due to a sedentary lifestyle resulting in a persisting positive energy balance can be seen as one of the central developmental origins (4). A long-term positive energy balance results in the expansion of white adipose tissue (WAT) due to increased lipid storage in fat cells in the form of triglycerides. Except for serving as a site to store excess calories, WAT was seen as metabolically inactive for a long time. With methodological advances including the isolation of mature adipocytes from collagenase digested tissue samples it became clear that WAT plays a major role in nutrient homeostasis and whole-body energy metabolism (6). Later, the discovery of adipose-secreted factors like leptin, adiponectin, and tumor necrosis factor alpha (TNF- α) led to the recognition of WAT as an endocrine and inflammatory organ involved in multiple, systemic metabolic disorders (7).

1.2 | The adipose organ in brief

In contrast to other organs, adipose tissue is compartmentalized, and depots are scattered across the human body fulfilling various important functions ranging from energy storage and energy dissipation to mechanical support and cushioning (8, 9). Generally, adipose tissue can be classified into either brown adipose tissue (BAT) or WAT (10). WAT, by volume, is mainly comprised of adipocytes with a unilocular lipid droplet, serving as a storage site for triglycerides (11). BAT, in contrast, contains multilocular adipocytes and is a thermogenic organ as it can dissipate energy in the form of heat mediated by uncoupling protein 1 (UCP1) (12). Anatomically,

different adipose tissue depots can be broadly classified into either subcutaneous or visceral adipose tissue (SAT/VAT). Thereby, SAT is being located beneath the skin, while VAT resides in the abdominal cavity (13). The distribution of body fat between the two compartments is influenced by multiple factors (sex, age, nutrition) and large-scale genome-wide association studies (GWAS) suggest sexual dimorphisms in the genetics of body fat distribution (14-16). Additionally, both storage sites differ in volume and regarding their associations with metabolic disorders (8). While SAT has the highest contribution to total body fat the accumulation of VAT shows a stronger association with metabolic disorders (15). The cellular composition of WAT is ambiguous. While mature adipocytes make up for more than 90 % of fat pad volume, it is important to emphasize that a wide variety of other cells resides in WAT, including endothelial cells, fibroblasts, preadipocytes, and immune cells (7, 17). All together these cells form the stromal-vascular fraction (SVF) and make up for approximately 60 - 80 % of the WAT cell count (7). SVF cells are a double-edged sword as on the one hand they are crucial to maintain metabolically healthy WAT function by amongst other functions constant adipocyte renewal (18). On the other hand, immune-related SVF cells can substantially contribute to the progression of metabolic disorders as they are pivotal to the formation of a pro-inflammatory environment within WAT (7, 17).

1.3 | Mechanisms of white adipose tissue expansion

Besides being recognized as an endocrine organ, WAT has unmatched morphological plasticity that cannot be seen in any other organ (19). Studies measuring adipocyte size confirm this observation as there is considerable variation in fat cell size both within and between individuals (20). Thereby, the total WAT mass is mainly determined by the size and number of fat cells residing in the different depots. With the onset of obesity, WAT mass increases up to multiple folds, either due to an increase in fat cell size (hypertrophy) or number (hyperplasia). While adipocyte number is a major determinant of total fat mass, studies highlight that fat cell number remains largely stable during adulthood and is preferentially set during childhood and adolescence (21). Only in the context of severe obesity, an increase in fat cell number can be observed as well (21). Despite a mostly stable population of adipocytes being present in adults, this does not mean that there is no turnover and renewal of the existing cell population. Measurements of ¹⁴C-incorporation into genomic DNA suggest that approximately 10 % of the total adipocyte population are renewed annually, which relates to the replacement of 50 % of the fat cell population after 8 years (22). In humans, the two different morphological profiles show opposing effects regarding the development and progression of cardiometabolic diseases (23, 24). While WAT hyperplasia is generally considered benign, hypertrophic WAT expansion has been associated with adverse

outcomes including impaired lipid metabolism, hypoxia, and a pro-inflammatory environment leading to insulin resistance, T2D, dyslipidemia, and hypertension (6).

1.4 | Techniques to measure adipocyte size

Adipocyte size has been one of the earliest measured parameters to characterize adipose tissue morphology and function (25). Currently, three methods have emerged as standards to assess adipocyte size: Histological sections, collagenase digestion, and osmium tetroxide fixation. Adipocyte size determination from AT sections is most often carried out after hematoxylin & eosin (H&E) staining using manual gating or semi-automated image thresholding methods (26, 27). Size determination with collagenase digestion relies on adipocyte size measurements in a suspension of isolated mature adipocytes either based on direct microscopy with an object micrometer or with computer-based sizing methods (28, 29). Osmium tetroxide fixes intracellular lipids and adipocyte size is measured with a multisizer allowing for the quantification of multiple thousands of cells (30, 31). Both osmium fixation and collagenase-based size determination measure the maximum cell diameter as the adipocyte is liberated from connective tissue taking on spherical shape in suspension. With histology, adipocyte area is assessed in a certain plane of the tissue. Depending on where the adipocyte is cut the measured area does not necessarily correspond to the largest cross-sectional area of the cell (32). Histology is however the only method where spatial information, as well as other tissue structures and general tissue architecture, are preserved. Furthermore, samples from histology can be easily stored at different stages of processing either as formalin-fixed paraffin-embedded (FFPE) tissue or as stained and coverslipped slides. Additionally, reanalysis is straightforward while the sample is inevitably lost with the other described sizing methods. Due to differences in methodology mean adipocyte size and its underlying size distribution and modality differ from method to method while the “ground truth” adipocyte size in an unperturbed state remains unknown (33). A large systematic review confirmed this observation with histology consistently producing smaller estimates compared to collagenase digestion, while osmium fixation yielded larger size estimates than collagenase digestion in SAT (34). Despite systematic differences, all methods are largely coherent regarding their associations with anthropometric measures and markers of cardiometabolic diseases (33).

1.5 | Adipocyte size is related to anthropometry and systemic metabolic disorders

Hypertrophy is a known stress factor for WAT and up to date, multiple studies report associations of SAT and VAT adipocyte size with anthropometry, cardiometabolic markers, or certain types of metabolic diseases (23, 34). Independent of the depot, positive associations between adipocyte size and body mass index (BMI) as well as body composition (body fat percentage, body fat mass) have been frequently reported (33, 35, 36). Differences in fat cell size between SAT and VAT are well established with VAT adipocytes, in general, being smaller compared to their SAT counterpart (34, 37, 38). In line with body fat distribution being a sexual dimorph trait, adipocytes size was identified to show marked differences between males and females (8, 39). In the context of morbid obesity, these differences vanish and adipocyte size from males and females converges (8). Systematic reviews as well as a large study that meta-analyzed adipocyte area across multiple cohorts suggest that females are less susceptible to visceral adipocyte hypertrophy than males (34, 39). There is clear evidence that adipose morphology is associated with insulin resistance and T2D (Figure 1) (40-42). Results are however divergent concerning the depot-specificity of the described associations. Both SAT and VAT adipocyte size have been associated with T2D, insulin resistance, and laboratory values related to these metabolic diseases (homeostasis model assessment for insulin resistance (HOMA-IR), glycated hemoglobin (HbA_{1c}), glucose, Insulin) (33, 41-46). Further, VAT adipocyte size has been shown to have a detrimental influence on dyslipidemia and is associated with plasma apolipoprotein B, total cholesterol, low-density lipoprotein (LDL) cholesterol, and triacylglycerols (33, 41, 47). In conclusion, data from smaller studies as well as systematic analyses highlight that VAT compared to SAT adipocyte hypertrophy has a greater contribution to the manifestation of metabolic disorders and shows stronger associations with their respective laboratory parameters (34, 48). Studies investigating WAT morphology before and after bariatric surgery suggest that adipocyte hypertrophy and its associated metabolic disturbances are at least partially reversible with a marked long-term reduction in fat cell size and substantial improvements in systemic insulin sensitivity up to two years after surgery (49-51).

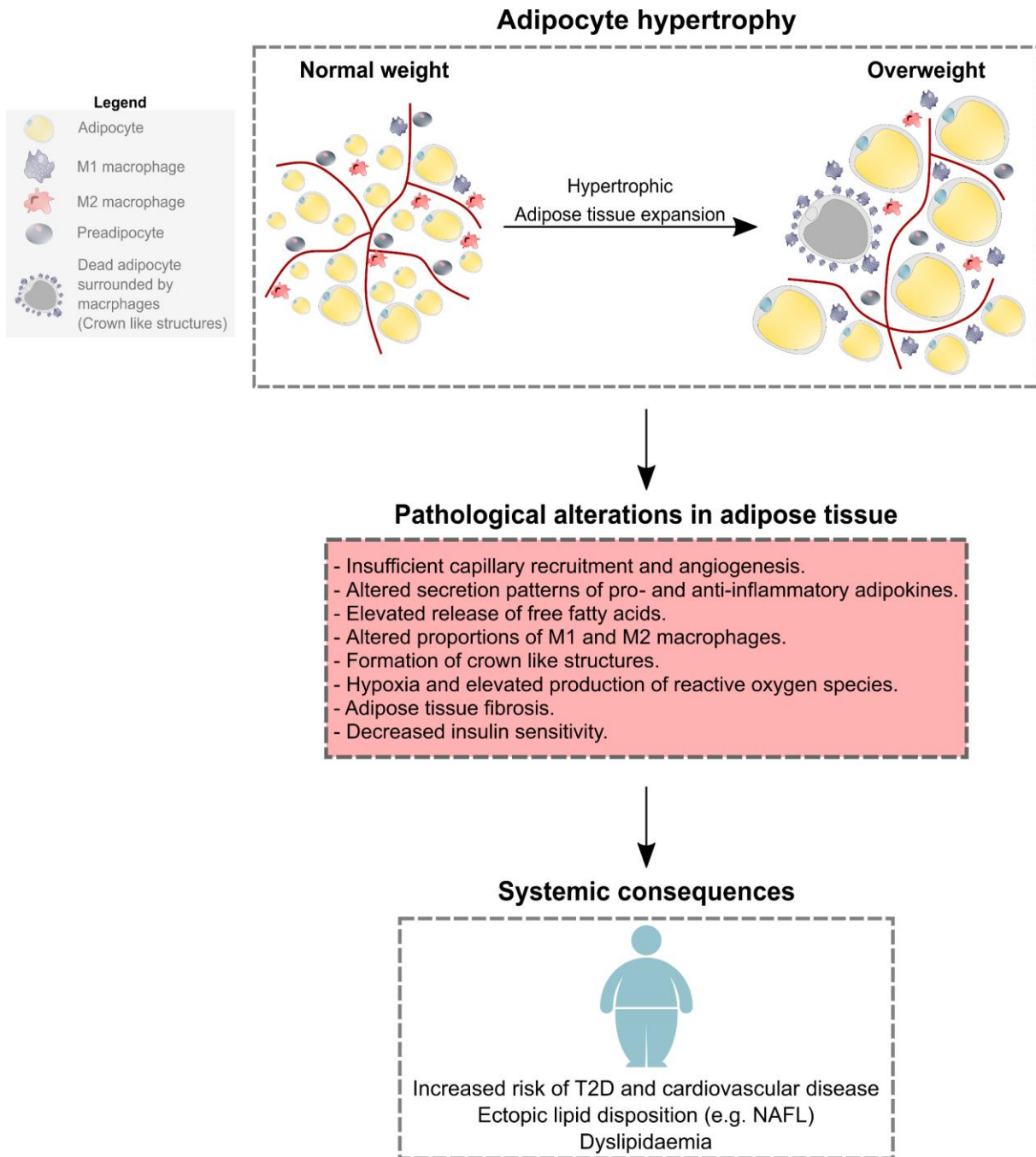


Figure 1: Adipocyte hypertrophy associated pathologic alterations in adipose tissue and their systemic consequences.

An expansion in the volume of existing adipocytes (hypertrophy) is accompanied by changes in structure, morphology and cellular composition of adipose tissue. The described pathological alterations manifest in systemic consequences such as T2D and cardiovascular diseases.

T2D, Type 2 Diabetes; NAFL, Non-alcoholic fatty liver

1.6 | Adipocyte hypertrophy introduces pathophysiological changes to white adipose tissue structure and composition

An increasing body of evidence suggests pathophysiological changes occurring along with adipocyte hypertrophy in WAT as a causal event for the manifestation of the disease phenotypes described above (19, 52). With increasing adipocyte size capillary density in WAT, blood flow and cardiac output do not increase even-handedly resulting in inadequate oxygenation (hypoxia) of the tissue (Figure 1) (53-55). To accommodate WAT growth extensive extracellular matrix remodeling is required leading to local fibrotic depositions (56-58). While immune cells are ordinary residents in WAT the hypertrophic expansion of adipose tissue has been associated with the infiltration of additional immune cells and introduces a shift in the polarization of residential immune cells (17). Amongst other immune cells, macrophages have been identified as a key player in promoting a pro-inflammatory environment during unhealthy WAT expansion (59). WAT macrophages can be broadly classified into two categories: M1 and M2 macrophages. The M2 population is mainly present in normal-weight individuals with metabolically healthy WAT and is thought to have an anti-inflammatory secretion profile. With increasing adipocyte size the macrophage polarization switches towards the M1 subtype with a pro-inflammatory secretion profile (42, 60, 61). Macrophages typically accumulate around death or senescent adipocytes, thereby forming “crown-like structures” (61). Along with this phenomenon, the expression of senescence marker genes and the shortening of telomeres were observed with increasing adipocyte size (62-64).

1.7 | Enlarged adipocytes display altered adipokine secretion patterns and show metabolic alterations.

Together with the discovery of leptin, numerous adipocyte-secreted factors such as TNF- α , Interleukin 6, and adiponectin have been identified, manifesting the adipocyte as an endocrine cell (65, 66). Besides changes in WAT microstructure and SVF composition, the secretory profile of the white adipocytes itself undergoes pathologic changes during its hypertrophic expansion (Figure 1). Studies on size-separated adipocytes suggest major differences between small and large fat cells from the same individual. Thereby, large fat cells display a more adverse secretion pattern that promotes inflammation and thus might facilitate the development of metabolic diseases (67, 68). Lipogenesis and lipolysis are key metabolic pathways of the adipocyte. Up to date, multiple studies have demonstrated increased lipolysis rates with adipocyte hypertrophy (69-71). De novo lipogenesis (DNL) in WAT on the other hand was found to be reduced in individuals with large fat cells (71, 72). Longitudinal analysis of lipid age in adults suggests that lipid turnover in SAT is age-dependent and decreased lipid removal rates are observed with higher age. Given

that lipid uptake remains constant, a long-term increase in fat mass and body weight is observed (73). The mitochondrion represents an essential organelle for adipocyte lipogenesis and lipolysis as it provides energy in the form of ATP and harbors multiple lipid metabolism-related processes. Further, clear evidence for an impairment of mitochondrial function in WAT with obesity exists (74-76). Whether mitochondrial dysfunction is related to adipocyte hypertrophy and fat cell size remains poorly investigated. So far, only two studies with size-separated adipocytes concluded that the respiratory capacity of small and large fat cells does not differ (77, 78).

Despite the adipocyte being mainly comprised of triglycerides (> 95 %) and numerous lipogenesis and lipolysis genes being related to adipocyte hypertrophy, studies relating WAT lipid composition to fat cell size remain scarce (79). *Roberts et al.* observed a negative relationship between adipocyte size and myristic acid (FA 14:0) as well as stearic acid (FA 18:0) (72). Another study investigating the relationship between fat cell size and fatty acid (FA) composition in overweight and obese individuals yields conflicting results observing a positive relationship between saturated fatty acids and adipocyte size (80). Further, obesity and insulin resistance have been associated with increased FA chain lengths and elevated levels of mono unsaturated fatty acid species in WAT (81).

1.8 | Data-driven “omics” studies and adipocyte hypertrophy

Despite adipocyte size being associated with obesity-related metabolic complications and markers thereof, the mechanisms, transcriptome-wide changes, and genetic predisposition for adipocyte hypertrophy remain largely unknown. Notwithstanding an important role of environmental factors, literature leaves no doubt that common obesity is under strong genetic control. Only a minor fraction of obesity cases, however, stems from monogenic alterations and the prevalence for the development of obesity can be attributed to a plethora of genetic risk loci that are also involved in a complex interplay with their environment (82). Up to date, GWAS studies have identified numerous genetic variants that are associated with measures of obesity, body fat distribution (waist-to-hip ratio), and metabolic disorders (14, 83-85). Even though many obesity-associated genetic variants have been identified, deciphering their mode of action and relevant target tissues remains a challenging task, especially if variants are located in noncoding genomic regions (5, 86-88). With a substantial body of evidence indicating that obesity is under (poly) genetic control, it seems likely that adipocyte morphology and expansion could be heritable traits as well. A single locus dissection study reports a relationship between rs1421085 (fat mass and obesity-associated, *FTO*) genotype and adipocyte size (86). Further, a female-specific effect of the Krüppel Like Factor 14 (*KLF14*) genotype on adipocyte size was identified (87). rs11614913, an expression quantitative trait locus for miRNA196a, was associated with adipocyte size as well (89). On a genome-wide scale, a study in over 900 individuals on adipocyte morphology identified 31 loci displaying suggestive associations ($p < 1e^{-05}$) with adipose morphology but none of the loci did reach genome-wide significance ($p < 5e^{-08}$) (90). Overall, evidence from a limited number of studies based on suggestive GWAS associations, heritability estimates, twin cohorts, and single-locus dissection indicates that adipocyte size is under (poly)-genetic control (86, 87, 90, 91).

Similar to genomic analyses, research investigating transcriptome-wide changes that might occur with adipocyte hypertrophy remain scarce. Microarray-based transcriptomic analysis using size-separated adipocytes was able to identify 14 mainly immune-related genes that were enriched in large compared to small adipocytes (68). Studies in twins discordant for obesity and adipocyte volume suggest an upregulation of inflammatory genes, while transcripts related to mitochondrial function were found to be reduced in the heavier twin (92). Recently, spatial transcriptome studies in SAT were able to shed light on the spatial organization of 18 different cell types within the tissue. Based on transcriptome data three different adipocyte types with distinct gene expression patterns were identified. Strikingly, out of the three adipocyte subtypes, only one class was shown to be insulin sensitive (93). While *Bäckdahl et al.* report that the transcriptome is fat cell-size dependent, adipocyte size per se did not explain the heterogeneity between the different adipocyte subtypes

(93). Although next-generation sequencing techniques became cheaper and more accessible evidence from hypothesis-free methods on the molecular pathways, genetic variants, and transcripts that are involved in the depot-specific regulation of adipocyte morphology and size remain largely unexplored.

1.9 | Limitations of current adipocyte sizing methods

While numerous smaller cohort studies on adipocyte size exist, it is striking that despite adipocyte size being one of the earliest measurable WAT traits large human cross-sectional or longitudinal studies are limited (50, 90, 94). One reason for this observation is that the biopsy procedure, especially for VAT, is highly invasive and tissue can only be obtained during medically indicated general surgery under anesthesia (95). The requirement of surgery to obtain WAT biopsies further proposes some limitations of its own: Cohorts are often biased towards individuals with medical conditions while samples from lean and healthy individuals remain scarce. Further, general anesthesia and surgical stress are known to induce substantial metabolic, inflammatory, and endocrine alterations that could influence the desired outcome measures (96). Very few studies rely on WAT samples obtained post-mortem with the advantage of being able to sample multiple WAT sites and larger amounts of tissue albeit care needs to be taken as sample ischemic times are known to influence specimen integrity (97, 98). After a biopsy is obtained, adipocyte sizing remains a labor-intensive task as mature adipocytes need to be isolated using collagenase digestion or extensive sample processing with fixation, tissue processing, embedding, and cutting is required before H&E staining. Following sample processing, only limited automation is present during the microscopic determination of adipocyte size from sections or with mature adipocytes (26, 27, 99). Commonly, adipocyte diameter after collagenase digestion is determined based on a few hundred cells using a built-in object micrometer or with a ruler tool. For histology, imaging mostly remains a manual process as digital pathology and whole slide scanning are not yet widely used in an exploratory research setting but rather in clinical laboratories (100). Existing proprietary microscope software and freeware to determine adipocyte size from histology are optimized towards smaller images using thresholding and watershed algorithms to separate foreground and background for the identification of adipocytes (26, 27, 99, 101). After object identification, manual inspection and flagging of improperly gated structures and artifacts is necessary to obtain reliable estimates. In conclusion, independent of the adipocyte-sizing strategy extensive processing and manual labor is required to obtain size estimates. In summary, the *in vivo* adipocyte size in an unperturbed state remains largely unknown and there is a need to develop fast, accurate, and fully automated adipocyte sizing approaches suitable for digital pathology.

2 | Aims

Adipocyte size is one of the most frequently measured parameters to describe adipose morphology. However, as only little automation is present with current sizing methods the applicability to harness the power of large biobanks that routinely archive and image WAT is limited. Accordingly, to date, the genetic predisposition for adipocyte hypertrophy and the transcriptomic alterations occurring with hypertrophic WAT expansion remain largely unknown. While recent studies suggest that adipocyte size can serve as a potential biomarker for metabolic diseases, a clinical application of the latter is still pending due to the invasiveness of the procedure.

Therefore, the goals of the thesis were to develop novel, automated, fast, precise, and less invasive methods for the determination of adipocyte size. The obtained size estimates from large cohort studies were then used to investigate the genetic predisposition, metabolic foundation, and the transcriptomic alterations of adipocyte hypertrophy (Figure 2).

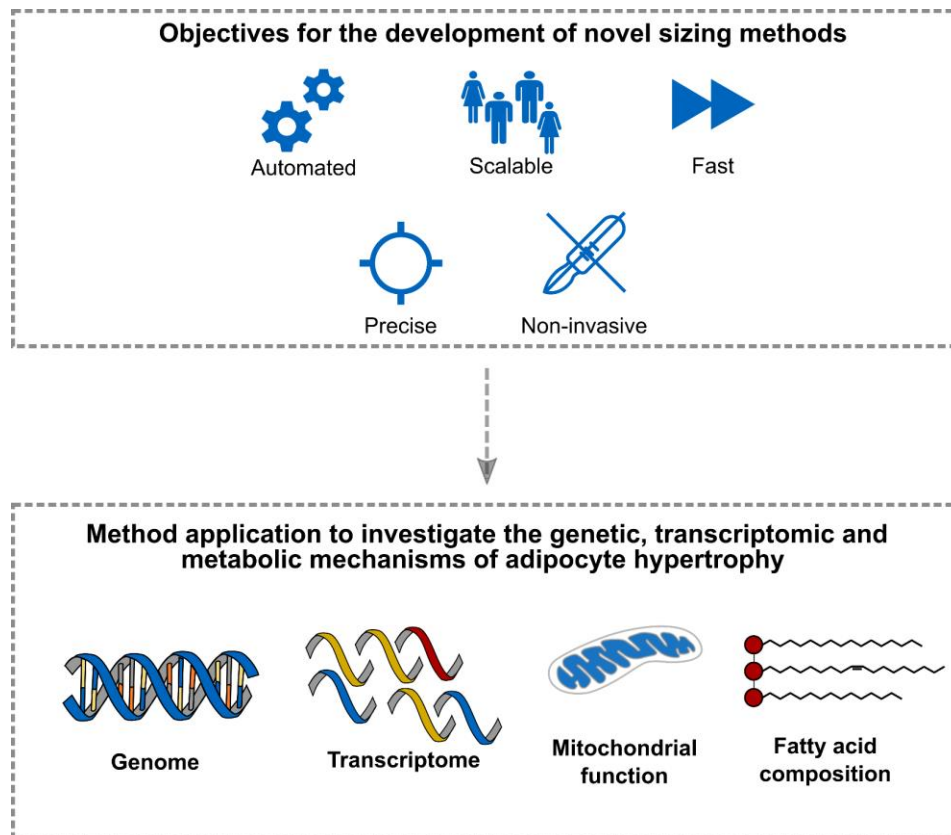


Figure 2: Aims and objectives

Due to the inherent limitations of currently existing adipocyte sizing methods, a central objective was to develop novel sizing strategies with higher degrees of automation and speed, thereby allowing for scalable, precise and accurate size prediction in a multitude of sections. Further, the potential of biopsy-free and thus non-invasive strategies for the measurement of adipocyte size was explored. After extensive method validation, the aim was to use the previously developed methods to reliably determine adipocyte size in large cohort studies to investigate the genetic, transcriptomic and metabolic mechanisms underlying adipocyte hypertrophy.

Chapter I *Development of a novel adipocyte sizing strategy that facilitates the study of potential genetic drivers behind adipocyte morphology.*

“Current histology-based adipocyte sizing methods rely on manual gating or are only semi-automated. Therefore, adipocyte sizing remains a rather time and labor-intensive procedure limiting its applicability to large cohort studies that are required to detect SNPs that are associated with WAT morphology in GWAS studies. To overcome the limitations described above a fully automated machine-learning-based adipocyte sizing method was developed and applied to whole-slide scans from four large cross-sectional cohorts. With the mean adipocyte area estimates obtained, a GWAS on adipose morphology was computed.”

Chapter II *A distribution-centered approach to analyze human adipocyte size estimates and their relationship with obesity-associated traits and mitochondrial respiration.*

“Measures of central tendency (mean & median) are commonly used to describe adipocyte populations. However, data on the similarity and differences of adipocyte size distributions in a method and sizing-parameter specific manner is limited and sometimes contradictory. A distribution-centered approach for the analysis of human adipocyte size was developed and outcome measures were associated with obesity-related traits and mitochondrial respiration.”

Chapter III *Deciphering the transcriptomic and fatty acid-related alterations that accompany adipocyte hypertrophy.*

“Hypertrophic WAT expansion has been associated with metabolic disorders and laboratory markers thereof. The global transcriptional alterations and changes in FA patterns that accompany pathological WAT expansion however remain unclear. Hence, RNA-Seq experiments were performed in bulk WAT biopsies, and size-separated mature adipocytes to unravel transcriptional patterns associated with adipocyte hypertrophy. Further, the relationship between adipocyte size and WAT FA composition was investigated. For a possible future translation of the findings into clinical practice the applicability of magnetic resonance spectroscopy (MRS) for the non-invasive characterization of WAT morphology and composition was explored.”

3 | Material and methods

3.1 | Human samples and study cohorts

Human WAT samples were obtained from either abdominal surgery or plastic surgery. Each participant gave written informed consent before inclusion and the study protocol was approved by the ethics committee of the Technical University of Munich (Study №: 5716/13; 1946/07, 409/16s). A summary of the different cohorts, the sampled biomaterials, related outcome measures, and references in various publications emerging from this thesis is given in Figure 3.

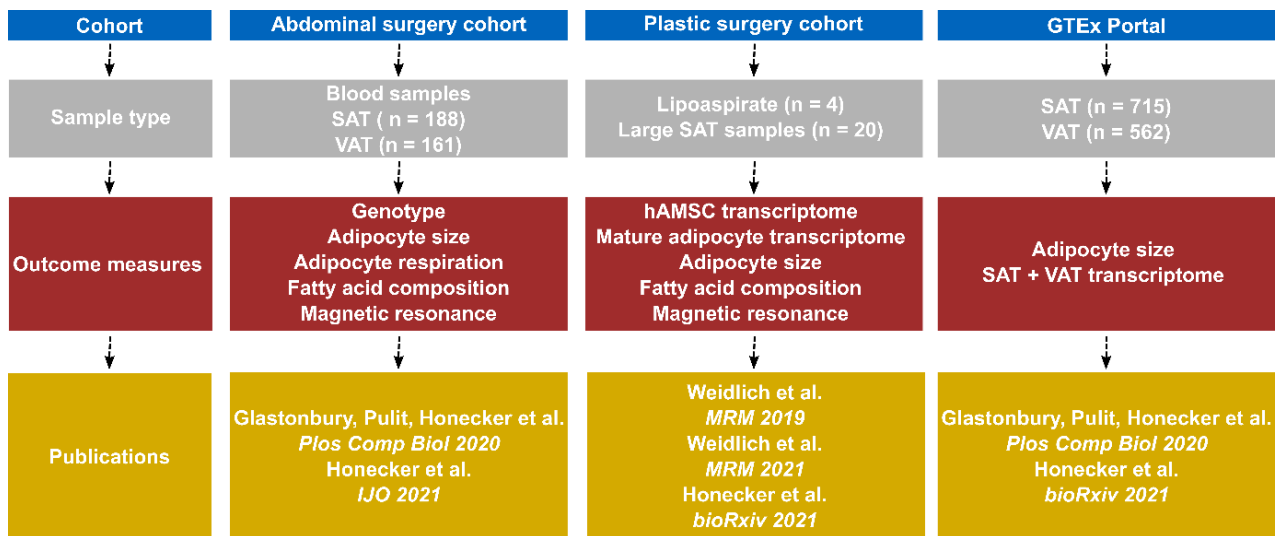


Figure 3: Cohorts, samples, outcome measures, and respective publications

The different cohorts that were recruited are shown in blue at the top of the figure. Sample types that were collected (Abdominal surgery & plastic surgery cohort) or used for downstream computational analysis (GTEEx) are depicted in grey. Outcome measures are shown in red and publications that the different cohorts appear in are pictured in yellow. SAT, subcutaneous adipose tissue; VAT, visceral adipose tissue; hAMSC, human adipose mesenchymal stem cell; GTEEx, Genotype-Tissue Expression Project

Abdominal surgery cohort (“Munich obesity biobank”)

SAT and VAT biopsies were obtained from adult individuals undergoing elective abdominal laparoscopic surgery (e.g. sleeve gastrectomy, fundoplication, appendectomy). SAT samples were collected at the site of the incision in the upper abdominal area. VAT samples were excised in the proximity of the angle of his. Venous blood was drawn intraoperatively using K3 EDTA collection tubes and immediately centrifuged at 4500 g for 10 min at room temperature. After centrifugation plasma and buffy coat were aliquoted and immediately snap-frozen on dry ice. Directly after the WAT biopsies were obtained two approximately 5 mm³ pieces were gross sectioned from the whole tissue and fixed in 4% formaldehyde for later use in histology. 10 – 20 mg of WAT were immediately snap-frozen on dry ice in tubes containing 700 mg of 1.4 mm diameter ceramic beads for later FA composition analysis. The remaining tissue was equally divided and either fixed in formalin for MR-based characterization or immersed in DMEM-F12 + 1% penicillin-streptomycin for the isolation of mature adipocytes, respectively. Clinical data of the participants was collected including the presence or absence of T2D as diagnosed by the treating physician, demographics (age, sex), anthropometry (weight before surgery, height, BMI) as well as laboratory values (HbA_{1c}, fasting plasma glucose, triglycerides, cholesterol, LDL-cholesterol, and high-density lipoprotein (HDL)-cholesterol). Briefly, samples originating from the abdominal surgery cohort were used for adipocyte sizing, respirometry measurements, FA composition analysis, and MR.

Plastic surgery cohort

Human liposuction material was used for the isolation of human adipose mesenchymal stem cells (hAMSCs) and mature adipocytes. Large WAT samples from abdominoplasty were gross sectioned into approximately 300 - 500 cm³ pieces. Smaller tissue biopsies were dissected from directly underneath the skin and from the bottom of the sample being formerly attached to the abdominal wall to account for possible heterogeneities in WAT microstructure. Smaller tissue biopsies were preserved for histology and FA composition analysis as described above. Two of the remaining large tissue pieces were placed in one liter straight-sided wide-mouth jars and immersed in 4 % formaldehyde with the skin side facing upwards for MR measurements.

Genotype-Tissue Expression (GTEx) project

Parts of the data and material used originates from the “Genotype-Tissue Expression (GTEx)” project. Briefly, GTEx is a public resource to study gene expression in various tissues and has been described elsewhere in detail (102, 103). Most GTEx samples are harvested post-mortem with SAT originating from beneath the legs skin sample located on the left or right leg 2 cm below patella on the medial side. VAT is obtained from the greater omentum. Detailed sampling instructions are given in the GTEx Tissue Harvesting Work Instruction and a visual representation of tissue sampling sites is given on the GTEx portal¹. Publicly available subject phenotypes (10 year age brackets, sex) were downloaded from GTEx analysis V8 (dbGap accession phs000424.v8.p2).

3.2 | DNA isolation and genotyping

DNA was isolated from 100 µl buffy coat using silica-based spin column DNA purification according to the manufacturer’s instructions (DNeasy Blood & Tissue, Qiagen). DNA concentration and quality were assessed photometrically by measuring wavelengths of 230 nm, 260 nm, and 280 nm. 260/280 ratios in a range between 1.7 and 1.8 as well as 260/230 ratios > 1.5 were considered as sufficient for further processing of the samples. As DNA concentration is often overestimated in spectrophotometer measurements, quantification with higher accuracy was additionally carried out using the DNA intercalating dye PicoGreen against a standard of known DNA concentrations (Quant-iT PicoGreen dsDNA Assay Kit, Thermo Fisher Scientific). DNA concentration was normalized to 50 ng/µl and 10 µl of DNA was shipped to the Oxford Genotyping Center for genotyping on the Infinium HTS assay on Global Screening Array bead chips (Illumina).

3.3 | Histology and imaging

All WAT samples used for histology were fixed in 4 % formaldehyde for at least 24 hours. Dehydration and clearing were carried out automatically (TP1020, Leica). After tissue processing samples were embedded in paraffin and at least three 5 µm thick sections with a minimum distance of 100 µm were cut on a rotary microtome (RM2255, Leica). After sectioning slides were stained with hematoxylin & eosin (H&E) in a fully automated multistainer (ST5020, Leica) and coverslipped immediately after the run was finished. Representative digital images of WAT from the abdominal surgery cohort were acquired in a lossless format using a fluorescence microscope with a texas red filter cube at 200x magnification (DMI 4000B, Leica). Whole slide scans were generated using an Aperio AT2 scanner (Leica) in collaboration with the Core Facility Comparative Experimental Pathology (Klinikum Rechts der Isar, Technical University of Munich). Stitched

¹ <https://gtexportal.org/home/samplingSitePage>

images from WAT sections originating from the plastic surgery cohort were taken in high-definition range at $\times 200$ magnification using a Keyence VHX-6000 microscope with a motorized stage.

3.4 | Adipocyte size determination from histological sections

Machine learning-based estimation of adipocyte size

To allow for the fast and accurate determination of adipocyte area from whole slide scans a machine learning-based adipocyte sizing method, the so-called “Adipocyte U-Net” was developed in a collaborative effort led by the University of Oxford’s Big Data Institute. Briefly, the Adipocyte U-net uses a convolutional neural network (CNN) to classify 1024×1024 pixel tiles derived from whole slide scans as either empty, adipocyte-only, or non-adipocyte-containing (104). For this purpose, transfer learning was applied to a CNN that was previously developed for complex object category classification and detection tasks (Inceptionv3) (105). The network was trained using a supervised learning approach on 2,729 image tiles. Tiles were equally distributed across SAT and VAT as well as across all tile categories with 80 % of the dataset being used for training and the remaining 20 % being used for validation. Tiles classified as adipocyte containing were then further processed to obtain fat cell counts and areas. For this purpose, a second CNN (U-net) designed for efficient image segmentation tasks in smaller biomedical datasets (e.g. microscopy images) was used (106). To train the model for adipocyte segmentation adipocytes on 175 tiles were manually annotated. As an output probability maps where each pixel was either classified as an adipocyte or background were generated. After transforming the probability maps into greyscale images, adipocyte area and count were measured. Objects with area estimates between $200 \mu\text{m}^2$ and $16,000 \mu\text{m}^2$ were used to generate descriptive statistics (mean \pm SD) based on a consistent number of 500 randomly sampled objects.

CellProfiler based adipocyte area measurements as a validation strategy for Adipocyte U-net derived area estimates

CellProfiler (CP) is a free open-source software that is based on image processing and measurement modules that can be arranged sequentially to generate custom-tailored analysis pipelines. Due to its flexibility, accessibility, and user-friendly interface that does not require extensive knowledge in computer vision or programming CP has become one of the most popular software for the quantitative analysis of microscopy images (26). For the reasons mentioned, CP was chosen to validate the Adipocyte U-net-derived area estimates based on an adipocyte sizing pipeline that was published by *Berry et al.* (107). Each image overlay generated by CP was analyzed manually, and improperly gated structures or artifacts were excluded after processing. A lower area limit of $314 \mu\text{m}^2$ ($\triangleq 20 \mu\text{m}$ diameter) was set to exclude small artifacts and debris. A

constant number of 200 randomly sampled objects was used to generate descriptive statistics (mean \pm SD).

Proprietary software-based adipocyte sizing

Adipocyte area of WAT sections originating from the plastic surgery cohort was determined using proprietary microscope software (VHX 6000, Keyence). A lower ($200 \mu\text{m}^2$) and upper size limit ($16,000 \mu\text{m}^2$) similar to the Adipocyte U-net's cut-off was used (39). Each image was manually inspected after automated identification and remaining artifacts were removed.

3.5 | Cell Culture

Both, the isolation of hAMSCs and mature adipocytes relies on the use of collagenases to dissociate WAT and liberate cells from the extracellular matrix. Filtration steps are afterwards used to remove the digested extracellular matrix and centrifugation results in the pelleting of the SVF. The SVF contains amongst other cell types hAMSCs. Mature adipocytes accumulate in the supernatant due to a low density ($\sim 0.9 \text{ g/ml}$) stemming from their large lipid droplet. The isolation of mature adipocytes based on this method has first been published by *Rodbell et al.* in the early sixties and since then has been refined to maximize yield and integrity of different cell types residing within WAT (108). The SVF can be plated and the growth of hAMSCs is promoted by specific culture media (109, 110). Despite multiple efforts being made the long-term cultivation of mature adipocytes remains a challenging task due to their fragility and non-adherent nature (111).

hAMSC isolation

hAMSCs were isolated from liposuction material as published (112). Briefly, 37.5 ml Krebs-ringer phosphate buffer (KRP) containing 4 % bovine serum albumin (BSA) and 200 u/ml collagenase were added to 12.5 ml of liposuction material and incubated for one hour at $37 \text{ }^\circ\text{C}$ under strong agitation in a water bath. After digestion, the supernatant containing mostly lipids from ruptured mature adipocytes was discarded, while the remaining volume was filtered through a nylon mesh with 2 mm pore size. The SVF was pelleted by centrifugation at 200 g for 10 minutes. The supernatant was removed and the pellet was resuspended in an ammonium chloride-containing buffer for the lysis of erythrocytes. The suspension then was filtered through $250 \mu\text{m}$ and $150 \mu\text{m}$ nylon meshes followed by centrifugation at 200 g for 10 minutes. The supernatant was discarded and the pellet was resuspended in isolation medium (IM). Subsequently, cells were seeded into T75 cell culture flasks. On the next day, cells were washed three times with phosphate-buffered saline (PBS) and the medium was changed to proliferation medium (PM). Following, the medium was changed every three days, and cells were grown until confluency and cryopreserved afterwards.

Differentiation of hAMSCs

Adipogenic differentiation of hAMSCs was induced by applying a method that was already described in detail (110, 112). Briefly, cells were supplemented with PM and grown until confluence in 6-well plates. At confluence, the medium was changed to induction medium (InM) containing rosiglitazone, the glucocorticoid dexamethasone, and the phosphodiesterase inhibitor IBMX (D0) to stimulate adipogenic differentiation. After three days (D3), the medium was changed to differentiation medium (DM) and cells were cultured until day 14 (D14) to allow for lipid accumulation. At D0 and D14 cells from two wells were harvested in 350 μ l of RLT buffer with 1 % β -mercaptoethanol for later RNA isolation. Oil Red O was used to stain lipids and to assess the differentiation capacity of hAMSCs.

Mature adipocyte isolation and size-separation

Isolation of mature adipocytes was carried out similar to the hAMSc isolation described above with the following differences: The collagenase concentration was reduced to 100 u/ml and incubation was shortened to 45 minutes with only mild agitation to prevent rupturing of mature adipocytes. The supernatant was filtered twice through meshes with pore sizes of 2,000 μ m and 200 μ m. Following, isolated mature adipocytes were washed with KRP 0.1 % BSA three times. Mature adipocytes were fractionated in a separating funnel based on the observation that large adipocytes contain higher amounts of lipids compared to their smaller counterparts and are thus more buoyant (67, 77). For size separation, 25 ml of mature adipocytes were gently mixed with 50 ml KRP 0.1 % BSA. After 45 s 25 ml of volume was withdrawn from the funnel representing the small adipocyte fraction. The missing volume in the funnel was replaced with KRP 0.1 % BSA and this procedure was repeated 4 times. Similarly, an intermediate fraction was obtained with a flotation time of 20 s. After this procedure, only large cells remain in the funnel which can be directly withdrawn. 600 μ l of each fraction were immediately snap-frozen in 600 μ l RLT buffer containing 1 % β -mercaptoethanol and 250 mg, 0.5 mm zirconia beads for later RNA isolation. To measure mature adipocyte diameter a glass-slide was wetted with 200 μ l of PBS and approximately 20 μ l of adipocytes were carefully pipetted onto the slide using a cut-off pipette tip to avoid shearing. Stitched, bright field images in high definition range were taken and adipocyte diameter was automatically determined using the microscope's software (VHX-6000, Keyence). Identified objects were inspected manually and artifacts were excluded from the analysis.

3.6 | Respirometry in mature adipocytes

High-resolution respirometry is considered a state-of-the-art approach to analyze respiration in intact cells or isolated mitochondria to gain detailed insights on mitochondrial (dys-)function (113). Thereby, an oxygen sensor is used to monitor oxygen concentration in an enclosed chamber while substrates, uncouplers, and inhibitors are injected allowing for a detailed investigation of the function of individual mitochondrial respiratory chain complexes and respiratory states (113, 114). Data on SAT and VAT mature adipocyte mitochondrial function was derived from an earlier project of our group and related to adipocyte area in further studies during this Ph.D. thesis (74). Therefore, a detailed description of the respirometry protocol is given in a publication by *Wessels, Honecker, et al.* (74). Briefly, 200 μ l of mature adipocytes were pipetted into the respirometry chamber of an Oxygraph-2k (Oroboros Instruments) and digitonin, pyruvate, malate, adenosine diphosphate (ADP), succinate, oligomycin, carbonyl cyanide-p-trifluoromethoxyphenylhydrazone, rotenone, and antimycin A were injected to assess among others, the following respiratory states: Free oxidative phosphorylation (OXPHOS) capacity, describing the respiratory capacity potentially available for ADP phosphorylation. OXPHOS capacity depicting the respiratory capacity of mitochondria in the ADP activated state. Electron transfer system capacity (ETS) being representative of the maximum respiratory chain capacity due to chemical uncoupling introducing proton reflux into the mitochondrial matrix. Leak respiration in the presence of oligomycin describing the dissipative component of respiration that it is not available for adenosine triphosphate synthesis. Oxygen consumption in pmol/s was normalized per ng of DNA. Mature adipocytes were chosen as a model system to measure respiration since cell-mitochondria interactions remain preserved and, compared to WAT pieces, a contribution of the SVF to respiration can be ruled out (7, 114).

3.7 | Cell culture sample processing

RNA isolation

RNA from mature adipocytes and hAMSCs was isolated using the mirVana, miRNA Isolation Kit, with phenol. Samples from hAMSCs intended for RNA isolation were allowed to thaw on ice and 350 μ l of mirVana lysis buffer was added to each tube. All following hAMSC RNA isolation steps were carried out as described in the manufacturer's protocol. Before isolation, samples from mature adipocytes were allowed to thaw on ice, the RLT containing, 1 % β -mercaptoethanol was carefully removed and replaced with mirVana lysis buffer. Mature adipocytes were lysed for 3 x 30 s in a homogenizer filled with dry ice set to 6.0 m/s and centrifuged at 12,000 xg for 10 minutes at 4 °C. Using an insulin syringe the adipocyte lysate located underneath the fatty layer was

3 | Material and methods

transferred to a new tube. All remaining steps were carried out as described by the manufacturer. RNA concentration was photometrically determined and the 260/280 ratio was used for quality control. Further, bioanalyzer RNA Nano chips (Agilent) were run to obtain RNA integrity number (RIN) and percentage of fragments of >200 nucleotides (DV_{200}) to assess RNA quality and integrity. An average RIN value of 9.0 ± 0.8 was observed across all samples.

Oil Red O staining

Oil Red O is a fat-soluble dye that stains neutral lipids such as triglycerides and, therefore, accumulates in lipid droplets of hAMSCs when differentiation has been induced. Staining intensity is used as an estimate for the differentiation capacity of the cultured cells as lipid droplets are stained in a distinct deep red color. At D0 and D14 of differentiation, the medium was removed and cells were washed with PBS. hAMSCs were covered with 4 % formaldehyde for one hour to fix the cells. Subsequently, cells were stained with a 0.3 % Oil Red O solution dissolved in a mixture of 60 % isopropanol and 40 % water (v/v). After one hour of incubation at room temperature the dye was removed and cells were washed with PBS twice and covered with an appropriate volume of PBS for storage. Representative images at 200x magnification were taken across the well (VHX-6000, Keyence).

3.8 | RNA sequencing

hAMSCs and mature adipocytes

Library preparation, sequencing, and reference genome alignment were carried out by the genomics services department of the Broad Institute of MIT and Harvard choosing a strand-specific, whole transcriptome sequencing approach. 250 ng of total RNA was used as an input for poly-A selection and strand-specific cDNA library preparation. After final quality control fragments with a mean length of 550 basepairs were sequenced on an Illumina platform generating a minimum sequencing depth of 50 million aligned reads. Reads were aligned to human genome assembly GRCh37 (hg19) using Spliced Transcripts Alignment to a Reference (STAR) (115). Raw read counts were determined using the feature counts function from the Rsubread package (116).

GTEX RNA sequencing data

GTEX RNA-seq data in the form of raw gene read counts and gene transcripts per kilobase million (TPM) were downloaded from the GTEX portal stemming from GTEX analysis V8 (dbGap accession phs000424.v8.p2) (103, 117).

Differential expression analysis

All RNA-seq data was analyzed using edgeR's quasi-likelihood pipeline (118, 119). As an initial step in the analysis, genes with very low counts across all libraries were removed. Second, normalization was carried out to adjust for different sequencing depths between samples. Additionally, technical influence on RNA-seq data can stem from the phenomenon when a small number of genes is highly expressed in a limited number of samples. These highly expressed genes can now make up for a substantial amount of the total library size, while the remaining genes with lower expression might be underrepresented (119). To account for this issue, normalization was carried out by edgeR's inbuilt trimmed mean of M values (TMM) function prior to downstream analysis (118, 119). Multi-dimensional scaling (MDS) and dendrograms based on euclidean distances were used to test if samples cluster in dependence of an experimental group. EdgeR's quasi-likelihood pipeline was used to test for significant differential expression (DE) (118).

Gene set enrichment analysis

While DE analysis tests for significant expression differences of a given gene in the context of an experimental condition compared to the baseline control, biological systems involve thousands of transcribed genes that are co-regulated, acting in networks, thereby orchestrating complex biological pathways and regulatory processes. Further, multiple genes involved in a certain biological process with only subtle expression differences might manifest in a phenotype but individually might not pass a certain significance threshold. The basis of Gene set enrichment analysis (GSEA) are lists of genes (gene sets) that for example act in synergy within a biological pathway or metabolic process. GSEA is then used to compute whether these predefined genes cluster together at either the top or bottom of the list of DE genes which indicates an enrichment or depletion in one of the experimental groups. Albeit custom gene sets can be generated, large curated repositories with predefined sets exist and the gene ontology (GO) and Kyoto Encyclopedia of Genes and Genomes (KEGG) database were used in this study for GSEA analysis. ClusterProfiler was utilized to compute the GSEA analysis and data was visualized in the form of pathway graphs with pathview (120).

BATLAS analysis to estimate the brown adipocyte content in bulk WAT biopsies

Briefly, BATLAS is a web tool based on deconvolution algorithms that estimates brown adipocyte content in heterogeneous cell populations as present in bulk WAT biopsies (121). A better understanding and relative quantification of cells with the potential to perform thermogenesis in various human adipose tissue depots is further of great relevance for a better understanding of whole-body energy homeostasis and metabolism. While most studies rely on single marker genes

(e.g. *UCP-1*, *PRDM16*) to estimate the thermogenic capacity of tissues or cell cultures, BATLAS takes into account the expression of 98 and 21 genes that have been identified as either BAT or WAT specific. A total of 119 marker genes were therefore identified in a data-driven approach by analyzing mouse and human transcriptomes of pure brown, brite and white adipocyte populations (121). For the estimation of GTEX SAT and VAT brown adipocyte content TPM expression value data was filtered for the relevant BATLAS marker genes. Before uploading the data on the BATLAS webtool homepage expression values of marker genes that were not expressed in the GTEX cohort were set to zero ². Brown adipocyte content estimates per individual and respective WAT depot were obtained from the web tool's results sheet and mean-centered for all later statistical analysis.

3.9 | Adipose tissue fatty acid composition

Gas chromatography–mass spectrometry (GC-MS) of fatty acid methyl esters (FAME) is one of the most common analyses in lipid research to assess the total FA composition of various specimens ranging from blood to tissue and cell cultures. A protocol initially published and described in detail by *Ecker et al.* was used to determine the total FA composition of WAT biopsies (122). Frozen samples were allowed to thaw on ice and dependent on sample weight a mixture of equal parts MeOH and water (v/v) was added to set the concentration to 0.05 mg/μl. Tissue was lysed using a homogenizer set to 30 s and 6 m/s. Transesterification was carried out by incubating the samples together with MeOH, acetyl chloride, and two internal FA standards (FA 13:0 iso, FA 21:0 iso) for one hour at 95 °C in a shaking water bath. Hexane was used to extract FAMEs and GC-MS, as well as post-run analysis, was carried out as described earlier (122). A total of 28 different fatty acid species with chain lengths between eight and 28 carbon atoms and different degrees of unsaturation were resolved by the method. Individual FA species were presented as molar percentages of the total FA profile.

3.10 | MR based characterization of WAT

Lipid emulsions

Lipid emulsions are an important model system to validate novel MR protocols, since water-fat content, FA composition, and droplet size can be precisely set up in a laboratory environment (123-125). To generate a reference that MR measurements could be validated against later in the process, the FA composition of store-bought linseed oil and sunflower seed oil was determined using FAME GC-MS. For this purpose, the oils were diluted at 1:500 (v/v) and 1:1000 (v/v) in 3:1 (v/v) isooctane isopropyl alcohol. Transesterification and GC-MS were carried out similarly to WAT

² <https://shiny.hest.ethz.ch/BATLAS/>

samples as described above. Together with the chair of food and bioprocess engineering (School of Life Sciences, Technical University of Munich) water-fat phantoms were manufactured with a fat content of 80 % and a water content of 20 % closely resembling human *in vivo* WAT composition (126, 127). Emulsions were manufactured with the two individual oils and by mixing them in a 1:2 (v/v) and 2:1 (v/v) ratio. 2 % tween 80 (v/v) was added to the aqueous phase as an emulsifier. 0.5 % sodium benzoate (m/v) was added as a preservative. Emulsification was carried out using a colloid mill (IKA Labor-Pilot 2000/4) set to 3000, 5000, 8000, and 12,000 rpm. Colloid mills operate on the rotor-stator principle where a rotor turns at an adjustable speed. Shear forces that are dependent on the speed and gap between rotor and stator result in the disintegration of droplets and emulsions with different particle sizes can be produced by varying the speed of the rotor. The lipid droplet sizes of the different manufactured emulsions were determined using a laser diffraction particle size analyzer (Mastersizer 2000 with Hydro 2000S dispersing unit).

Magnetic resonance measurements

Magnetic resonance imaging is an established method for the quantitative and spatial analysis of WAT abundance and distribution across the human body (128). In a collaborative effort together with the body magnetic resonance research group (Department of Diagnostic and Interventional Radiology, Klinikum Rechts der Isar, Technical University of Munich) the potential of novel MR-based strategies for the analysis of WAT morphology and composition were explored. For this purpose, magnetic resonance spectroscopy and imaging were applied to lipid emulsions and human WAT biopsies to assess adipocyte size and FA composition on a clinical 3 Tesla magnetic resonance scanner. Results from the MR measurements were referenced against gold standard methods for the measurement of adipocyte size (histology), particle size (laser diffraction), and fatty acid composition (FAME GC-MS). The different MR sequences and strategies that were tested and deemed as suitable to generate an MR signal from which adipocyte size and fatty acid composition can be estimated are described elsewhere in detail and were developed, tested, and applied by the body magnetic resonance research group (123, 129, 130).

3.11 | Statistics

All statistical analyses were conducted in R (131). If not specified otherwise results are given as mean \pm SD. Histograms, Q-Q plots, and Shapiro Wilk tests were used to test for/against normality of the measurement values. According to the sample distribution, variance, and experimental setting (paired vs. unpaired) parametric tests (paired samples t-test, independent samples t-test) or non-parametric tests (Mann-Whitney test, Wilcoxon signed-rank test) were used to test for/against differences between groups. Pearson or Spearman correlation was used to investigate

3 | Material and methods

the association between continuous variables. Multiple linear regression was used to model a linear relationship between an explanatory and a response variable, while at the same time being able to account for possible confounding effects of BMI. When numerous comparisons or correlations were run in parallel, Bonferroni adjustment was used to account for multiple testing. Across all analyses, p-values < 0.05 were considered significant.

4 | Publications

Chapter I Development of a novel adipocyte sizing strategy that facilitates the study of potential genetic drivers behind adipocyte morphology.

Title: Machine Learning based histology phenotyping to investigate the epidemiologic and genetic basis of adipocyte morphology and cardiometabolic traits.

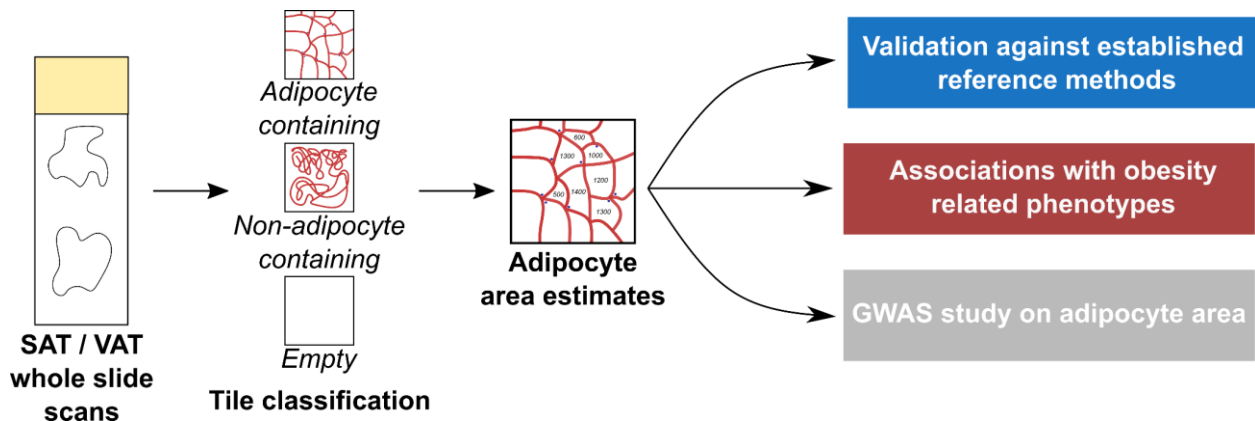
Authors: Glastonbury, C. A.*, Pulit, S. L.*, **Honecker, J.***, Censin, J. C., Laber, S., Yaghooskar, H., Rahmioglu, N., Pastel, E., Kos, K., Pitt, A., Hudson, M., Nellåker, C., Beer, N. L., Hauner, H., Becker, C. M., Zondervan, K. T., Frayling, T. M., Claussnitzer, M. & Lindgren, C. M
(* indicates equal contributions reflected in shared first authorship positions on this work)

Journal: PLOS COMPUTATIONAL BIOLOGY

Publication date: August 14, 2020

DOI: <https://doi.org/10.1371/journal.pcbi.1008044>

Personal Contributions: JH contributed substantially to the design of the study. He established methods, obtained samples, and performed all laboratory work/experiments related to the MOBB cohort. He was markedly involved in validating the novel machine learning adipocyte sizing method by providing adipocyte area estimates from two independent and established sizing strategies. He was involved to a great extent in the analysis of data and preparation of figures concerning model validation. He contributed significantly to the analysis investigating associations of adipocyte size with phenotypic variables, cardiometabolic traits and single nucleotide polymorphisms. JH contributed markedly to writing, editing and revising of the manuscript.

Graphical abstract:**Summary**

Adipocyte size has been frequently associated with cardiometabolic markers and metabolic disease. However, the genetic and mechanistic underpinnings of adipocyte hypertrophy remain elusive. This can be partially attributed to the fact that adipocyte sizing with current methods remains a laborious task due to limited automation and is therefore not well suited for large cross-sectional cohort studies that are necessary to unravel the genetic background and mechanisms leading to the manifestation of a phenotype. Therefore, a machine-learning based method, the “Adipocyte U-net” was developed to measure adipocyte area from H&E stained whole slide scans. Briefly, tiles from whole slide scans were automatically classified into either adipocyte-containing, non-adipocyte-containing, or empty. Afterwards, segmentation masks were generated from adipocyte-containing tiles and cell area was determined. Due to the automated tile classification, there is no further need for the manual inspection of identified objects and time-consuming exclusion of improperly gated structures. Performance benchmarking revealed that the Adipocyte U-net is computationally faster than previous conventional sizing approaches. Area estimates from the adipocyte U-net were compared against state-of-the-art approaches for the segmentation of adipocyte histology images (Adiposoft & CellProfiler) and against the size of mature floating adipocytes in two independent cohorts (MOBB & fatDIVA). Results from the U-net were highly concordant with the validation strategies. As validation and benchmarking proofed that the adipocyte U-net was a reliable method for the fast and accurate determination of adipocyte area, associations with obesity-related phenotypes were investigated next. Across all cohorts, a positive relationship between adipocyte area and BMI was found and subcutaneous adipocytes were on average larger compared to their visceral counterparts. With the obtained adipocyte area estimates a GWAS study with a subsequent meta-analysis across all cohorts ($n_{\text{SAT}} = 820$, $n_{\text{VAT}} = 564$) was performed. No SNP reaching genome-wide significance, most likely due to a for GWAS

studies relatively small sample set and heterogeneous sampling sites across the different cohorts, was observed. SNPs (*FTO*/rs1421085, *KLF14*/rs4731702) from single-locus dissection studies that were previously reported to be associated with adipocyte size could not be confirmed when area estimates from all cohorts were meta-analyzed. In conclusion, the study emphasizes the necessity of large cross-sectional cohorts with homogenous sampling to identify robust genetic associations. With the adipocyte U-net a fast and readily available tool for the reliable measurement of adipocyte size from whole slide sections, especially in large biobanks, is provided. The analysis of tissue endophenotypes in a GWAS network compared to clinical outcome measures represents a promising approach to detect novel genetic variants, as endophenotypes are most likely linked more directly to the underlying biological mechanisms.

Chapter II A distribution-centered approach to analyze human adipocyte size estimates and their relationship with obesity-associated traits and mitochondrial respiration.

Title: A distribution-centered approach for analyzing human adipocyte size estimates and their association with obesity related traits and mitochondrial function

Authors: **Honecker, J.**, Weidlich, D., Heisz, S., Lindgren, C. M., Karampinos, D. C., Claussnitzer, M. & Hauner, H.

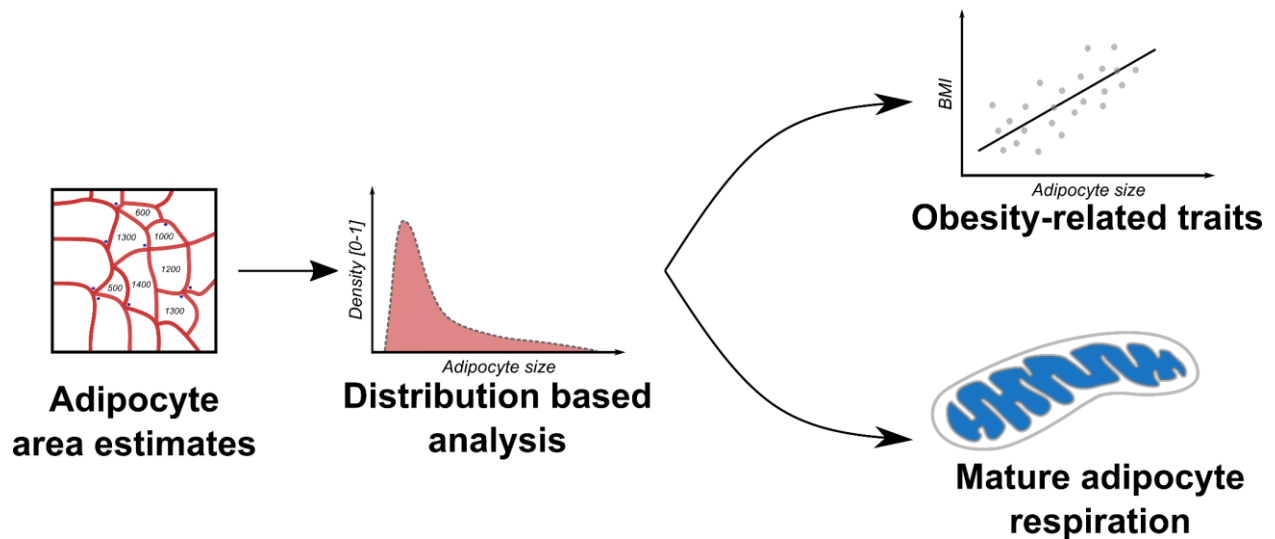
Journal: International Journal of Obesity

Publication date: June 25, 2021

DOI: <https://doi.org/10.1038/s41366-021-00883-6>

Personal Contributions: JH designed the study, performed experiments, analyzed the data, prepared figures, and wrote and revised the manuscript

Graphical abstract:



Summary

Measures of central tendency (mean & median) are frequently used to describe adipocyte area, diameter or volume derived from different sizing methods such as histology or collagenase digestion. Systematic approaches assessing the shape, symmetry, and modality of the underlying adipocyte size population are, however, scarce. Further, it is common practice to transform the initial measurement variable into another sizing parameter assuming spherical shape. How adipocyte distributions change regarding this mathematical transformation has not yet been reported. The described publication, therefore, aimed to complement previous approaches by an in-depth description of histology and collagenase-derived adipocyte size distributions. Next, the relationship of different adipocyte sizing variables with obesity-related traits was investigated. As mitochondria have a pivotal role in WAT metabolism and are impaired with obesity their relationship with adipocyte hypertrophy was assessed by high-resolution respirometry. The data indicated that adipocyte area estimates derived from histology are not distributed normally but are rather characterized by positive skewness. Mathematical transformation of adipocyte area into diameter or volume assuming spherical shape introduced substantial changes to the shape of the distribution. In contrast, distributions from collagenase-digested adipocytes closely followed the pattern of a normal distribution. Histology-derived adipocyte area, diameter, volume, and surface area were all equally correlated with obesity-associated traits. While BMI was the only parameter correlated with adipocyte size in SAT, robust associations with glucose, HbA_{1c}, HDL-cholesterol, and T2D were found in VAT. Further, VAT adipocyte size was identified as a sexual dimorph trait with males having significantly larger adipocytes compared to females. In conclusion, the study confirmed the strong link between VAT expansion and cardiometabolic disorders. Next, histology-derived adipocyte size was associated with different respiratory states derived from high-resolution respirometry in mature adipocytes to investigate the relationship between adipocyte hypertrophy and mitochondrial (dys)-function. Primarily in SAT, significant negative associations between adipocyte size, free OXPHOS capacity, and ETS capacity were observed. Results from the correlation analyses were confirmed in a multiple linear regression model, taking into account possible confounding by BMI. In summary, the study provides an original approach for the distribution-based examination of adipocyte size and draws important methodological considerations towards a distribution-centered analysis approach. As a novel finding, this work establishes for the first time a link between adipocyte size and mitochondrial function, thus providing new insights on the metabolic changes occurring with adipocyte hypertrophy.

Chapter III Deciphering the transcriptomic and fatty acid-related alterations that accompany adipocyte hypertrophy.

Title: Transcriptome and fatty-acid signatures of adipocyte hypertrophy and its non-invasive MR-based characterization in human adipose tissue

Authors: **Honecker, J.***, Ruschke, S.*, Selliger, C., Laber, S., Strobel, S., Pröll, P., Nellåker, C., Lindgren, C.M., Ecker, J., Karampinos, D.C., Claussnitzer, M., & Hauner H.
(* indicates equal contributions reflected in shared first authorship positions on this work)

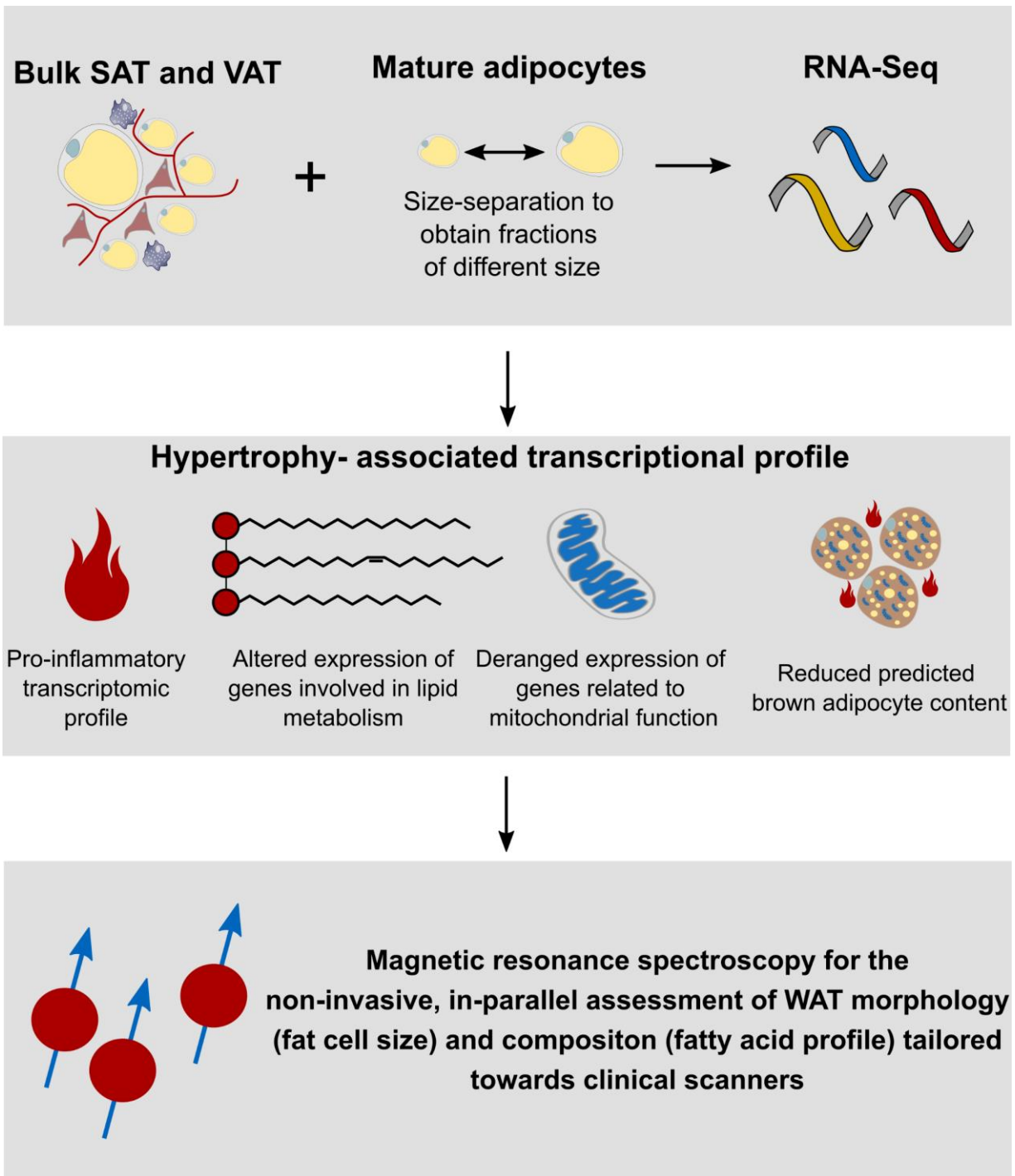
Journal: Preprint: *bioRxiv*, Under review: *EBioMedicine*

Publication date: November 20, 2021

DOI: <https://doi.org/10.1101/2021.11.20.468818> (bioRxiv preprint)

Personal Contributions: Except for the section on magnetic resonance spectroscopy, JH contributed substantially to the publication by designing the study, performing all experiments, analyzing all data, preparing all figures, as well as writing and revising the manuscript

Graphical abstract:



Summary

WAT is characterized by an unmatched plasticity and its expansion in volume through hypertrophic adipocyte expansion has been associated with adverse cardiometabolic outcomes. The causal transcriptional and metabolic alterations within WAT and especially adipocytes leading to this systemic phenotype, however, remain poorly investigated. Based on publicly available GTEx-derived SAT and VAT RNA-Seq data, the relationship between adipocyte size and global gene expression was investigated. The data indicate substantial transcriptomic alterations of genes involved in OXPHOS, biosynthesis, and elongation of FAs, FA degradation, and inflammation in individuals with large adipocytes. As a key finding, a reduction in the expression of thermogenesis-related genes and estimated brown adipocyte content with increasing adipocyte size was found. An increased brown adipocyte content in WAT could display an important protective mechanism against excessive lipid accumulation and adipocyte hypertrophy. Since WAT is a heterogeneous organ composed of many cell types mature adipocyte isolations were prepared to gain further insights on the cell types that could be detrimental to the observed transcriptomic alterations in bulk tissue. Mature adipocytes were separated into different size fractions based on their buoyancy and transcriptional differences between the fractions were assessed. Different transcriptomic patterns were observed between small and large adipocytes with an identical genetic background, suggesting enlarged adipocytes themselves as a causal cell type for transcriptomic changes in bulk WAT. As unilocular adipocytes account for over 90 percent of the total fat pad volume and our transcriptome analysis suggested that genes involved in fatty acid metabolism are regulated in a size-specific manner, it was next investigated whether the WAT FA pattern is affected by adipocyte hypertrophy. FA composition of WAT was found to be size and depot-specific, with a positive relationship between adipocyte size and certain polyunsaturated fatty acid (PUFA) species in SAT, while a negative relationship between adipocyte size and saturated fatty acids was seen in VAT. Taking into account the transcriptional and FA related patterns that most likely contribute to WAT dysfunction and metabolic disease, the reliable and fast quantification of FA composition and adipocyte size in a clinical setting would be highly desirable. With the use of water-fat phantoms and large WAT biopsies, MRS strategies tailored towards clinical scanners for the future non-invasive quantification of WAT adipocyte size and FA composition were developed. Excellent agreement between MRS and reference methods confirmed that MRS is suitable for the characterization of WAT morphology and composition. In summary, the present study unravels novel transcriptional and metabolic aberrations related to adipocyte hypertrophy and proposes MRS methods to detect the latter towards a better and earlier detection and diagnosis of metabolic disease.

5 | Discussion

Obesity is a major global health concern and is characterized by an unhealthy expansion of SAT and VAT. Especially an increase in volume of existing adipocytes (hypertrophy) has been identified as pivotal in the manifestation of systemic metabolic disorders such as T2D and cardiovascular disease. While associations of adipocyte size with systemic phenotypes and markers of the latter have frequently been made, the genetic, transcriptomic, and metabolic underpinnings of adipocyte hypertrophy remain poorly investigated. A sound understanding of the biological mechanisms and genetic determinants of WAT expansion is, however, imperative for the development of preventive strategies, an earlier diagnosis, and improved treatment of obesity and its related comorbidities.

Machine learning-based adipose tissue phenotyping

Whole slide scans of adipose tissue are a rich source of data that allow for the spatial, numerical, and morphological quantification of various cell types and structures within WAT (100, 132). Additionally, histology offers the major advantage that samples can be easily conserved and reanalyzed, either in digital or physical form, and are not lost during quantification. As histological samples can be easily obtained and archived this allows for the great opportunity to retrospectively harness the power of large, already existing biorepositories for basic and translational research. A bottleneck in the quantitative analysis of WAT sections, however, is that nearly all currently existing approaches rely on manual annotations or are only semi-automated (26, 27, 99, 107). Often, the knowledge of an expert in the field or pathologist is further required to carefully assess and review identified structures. In conclusion, long running times combined with manual examination and correction are major limitations for the application of current adipocyte sizing strategies to large cohort studies. To improve upon current sizing methods and to address the pitfalls described above, a deep learning-based method for the estimation of adipocyte area from H&E stained sections was developed (adipocyte U-net). Adipocyte area estimates from the adipocyte U-net were in excellent agreement with reference methods considered as gold standards for adipocyte sizing, while run times were drastically shorter. Therefore, the adipocyte U-net was deemed suitable for the fast, reliable, and accurate determination of adipocyte area in large cohort studies from thousands of sections. Despite high accuracy and speed, it should be acknowledged that extensive computational knowledge and specialized hardware requirements (graphics processing units) are necessary to obtain U-net-derived adipocyte area estimates. Previous segmentation algorithms on the other hand often do provide a graphical user interface and have fewer hardware requirements which might make them more feasible for a broad

application in the field of adipose biology. The adipocyte U-net in its current form uses a per-tile classification where intact objects are lost if the major area on the slide has been recognized as either damaged or empty. A large number of measured adipocytes comparable to counts from osmium tetroxide fixation would, however, be desirable to reliably assess the shape and modality of adipocyte size distributions. Therefore, the method is currently further developed to transition from a per-tile to an individual object classification approach. Besides adipocytes, other cell types (immune cells), structures (connective tissue & vasculature) and cellular compartments are involved in pathological alterations of WAT with obesity and have been frequently identified as important drivers for the systemic manifestation of metabolic disorders (52, 56-58, 61, 133, 134). Hence, a training data set with manual annotations is currently generated to expand the adipocyte U-net's capabilities towards identifying besides adipocytes other structures such as vessels, connective tissue and nuclei within WAT.

The genetic basis of adipocyte morphology

With adipocyte area estimates obtained from over 2000 SAT and VAT samples stemming from four different study cohorts, the genetic background of adipocyte hypertrophy was investigated by computing a GWAS study on adipocyte area. Despite a large sample size, no associations exceeding genome-wide significance were found. Similar to obesity itself and in agreement with monozygotic twin studies on adipocyte size and number, heritability estimates suggested that adipocyte area is a heritable trait. Since previous investigations on individual genetic risk loci report an association between genetic variants (rs1421085 (*FTO*), rs4731702 (*KLF14*)) and adipocyte size, validation experiments were carried out with sample numbers exceeding the cohort sizes of the initial publications by multiple folds (86, 87). Previously published genetic associations were not confirmed in a meta-analysis across all adipocyte U-net cohorts. Both studies listed above despite having smaller sample sizes, however, do provide orthogonal, mechanistic evidence on how genetic variants of *FTO* and *KLF14* are involved in the regulation of adipocyte size (86, 87). In a recent analysis with larger n-numbers, sex-specific significant associations between rs1421085 genotype and adipocyte area were observed for the abdominal surgery cohort. Results concerning the sex-specific effect of the rs1421085 genotype on adipocyte size are corroborated by a novel study indicating sexual dimorph steroid profiles regarding rs1421085 genotype (135). Conflicting results and a lack of significance in both the GWAS and single-locus analysis could be explained by heterogeneities and differing sampling sites between the cohorts that were enrolled for the adipocyte U-net publication. For instance, GTEx is a post-mortem cohort with WAT samples obtained from a broad study population with different causes of death and previous courses of disease. The ENDOX cohort is an endometriosis cohort, while samples from

the abdominal surgery cohort are mainly derived from severely obese individuals undergoing bariatric surgery. Similarly, SAT and VAT samples were harvested from different anatomical locations, further contributing to heterogeneity between the different cohorts and possibly blunting genetic associations. Together, the described findings confirm that it is of great importance that SAT/VAT stem from exactly matched anatomical sites if meta-analyses are performed and that sex-specific effects should always be taken into account. Especially the origin of GTEX SAT in proximity to the knee could provide a plausible explanation for missing significant associations within the GWAS study. While SAT from the abdominal area is considered to be crucial for energy storage, SAT from the knee could also have important biomechanical properties that are not related to metabolism. Up to date, there is no metabolic characterization comparing the two SAT depots with each other and it remains speculative to make assumptions about the similarities and differences between knee and abdominal SAT. A study characterizing the transcriptome of 15 different adipose depots identified that the gene expression pattern in SAT depots is rather diverse with the most distinct gene expression patterns for buccal, heel, and carotid sheath AT. Gene expression of samples from the upper leg, upper arm, and abdomen were comparable (98). RNA-Seq data is publicly available for GTEX SAT and VAT samples which allowed a comparison between the two depots regarding the expression of adipose marker genes. First, depot-specific developmental gene expression signatures of GTEX samples were in good agreement with previously published lineage tracing and transcriptomic studies (*HOX family, IRX3, IRX5, TBX15, SHOX2, NR2F1, EN1, WT1*) (98, 136-140). Second, the expression of adipogenic and lineage-specific marker genes from knee-derived SAT was compared with VAT (Figure 4). GTEX SAT from the knee showed expression patterns of depot-specific marker genes similar to motifs reported in the literature. Common adipogenic marker genes were expressed at comparable levels to VAT as well (Figure 4). It is, therefore, concluded that GTEX fat harvested from the knee is (a) representative for the subcutaneous depot and (b) expresses common adipogenic marker genes representative for energy-storing WAT sites that are involved in obesity and metabolic diseases. Nevertheless, direct comparisons between paired SAT from the knee and the abdomen from the same individual would be desirable to completely unravel similarities and differences between the two sites.

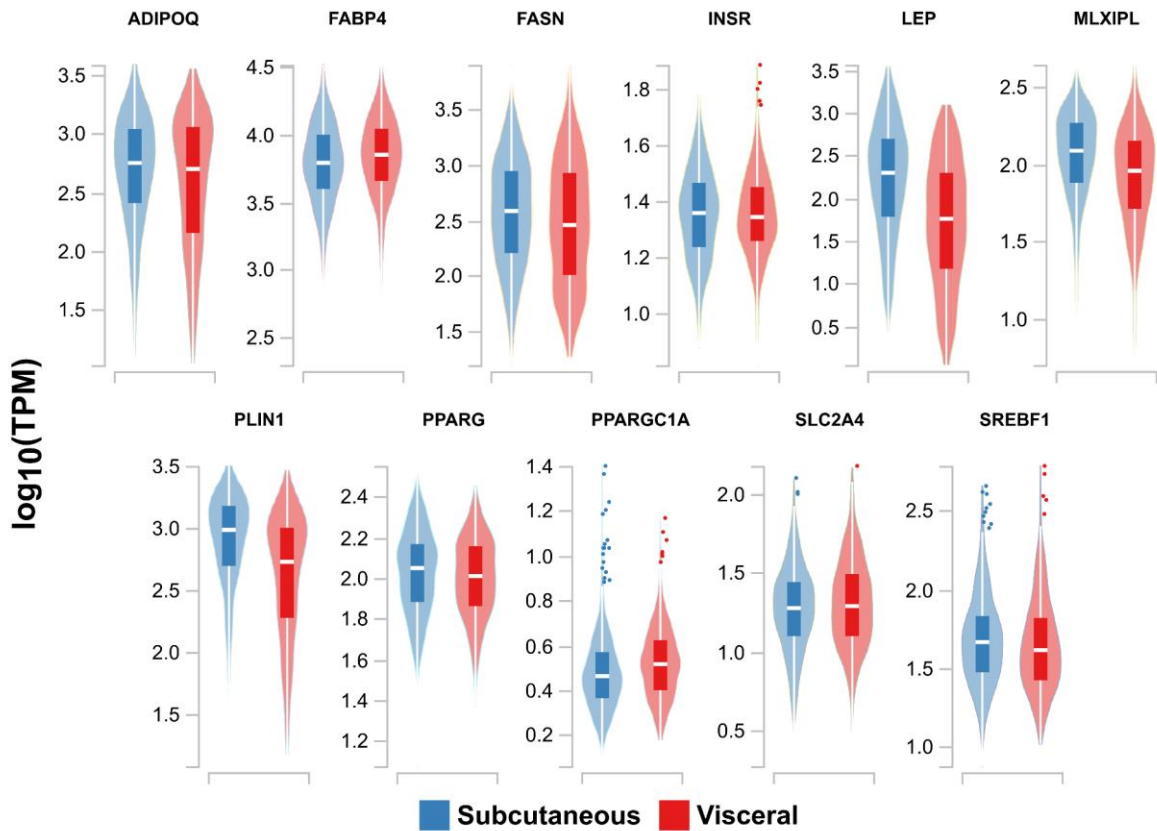
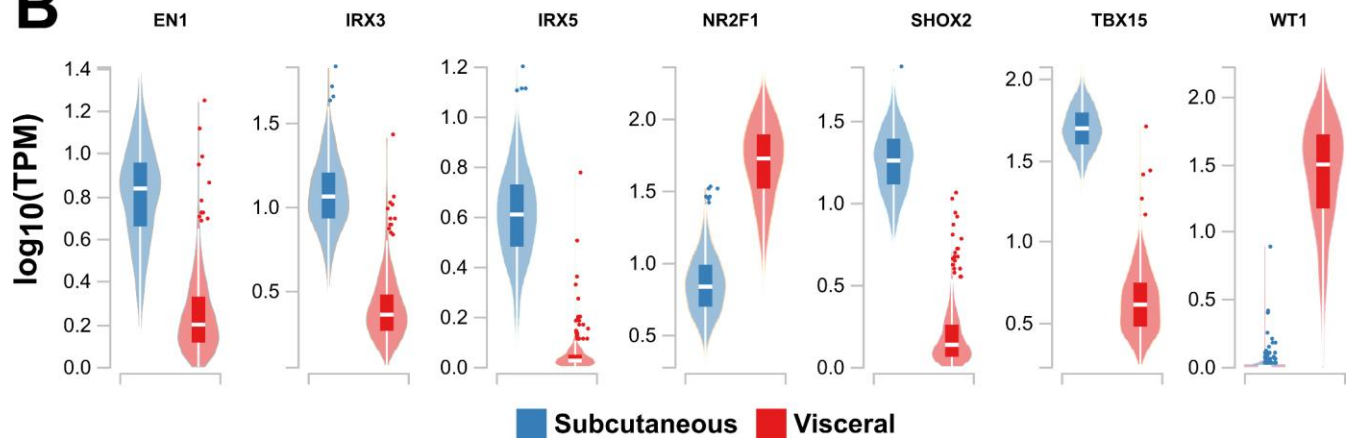
A**B**

Figure 4: Adipogenic and depot-enriched marker gene comparison between SAT and VAT

The expression of adipogenic (A) and depot-specific (B) marker genes was compared between SAT and VAT to test whether SAT from the knee shows an expression of common adipocyte and subcutaneous lineage-specific markers.

In conclusion, tying GWAS studies to robust WAT endophenotypes represents a promising approach for the more rapid discovery of genetic variants and their underlying biological mechanisms of action. Much larger sample sizes with highly standardized sampling procedures are, however, necessary to obtain robust genetic associations from GWAS studies. Therefore, in

close collaboration with the IFB adiposity diseases (University of Leipzig) SAT and VAT samples from approximately 1200 individuals are currently processed, stained, and imaged to address the issues raised above. Both, the IFB adiposity diseases cohort and the abdominal surgery cohort were initiated together under the umbrella of the German Obesity Biobank network with standard operating procedures for sample harvesting, preservation, and processing in place. This offers the unique opportunity to obtain adipocyte area estimates from SAT and VAT with homogenous and highly standardized sampling procedures in a well-powered study cohort with an estimate of 1500 individuals to be enrolled.

Distribution-centered analysis of human adipocyte size estimates

Using a systematic approach, a series of statistical parameters and graphical visualizations were computed from individual adipocyte-area estimates to obtain an in-depth and method-specific characterization of adipocyte size distributions. Histology-derived adipocyte size distributions showed substantial deviations from normality and were also influenced in their shape by mathematical transformation of the initial size measurement into another sizing variable. Therefore, measures of central tendency are not well suited to describe the most frequent cell population in skewed distributions, and results from studies where a mathematical transformation of the initial sizing variable was carried out need to be interpreted with care. Consequently, the study emphasizes the importance of ascertaining method, sizing parameter, and distribution shape when conducting adipocyte size analyses. A distribution-centered approach for the analysis of adipocyte size is also of high physiological relevance, as small and large adipocyte populations separated based on buoyancy show different gene expression and adipokine secretion patterns (67, 68). Besides distribution shape, adipocyte distribution modality is controversially discussed in the literature, with both unimodal and bimodal distributions being reported (33, 68, 141, 142). The data did not confirm the presence of a second local maximum in histology-derived adipocyte size distributions and adds further body of evidence to adipocyte size distributions being unimodal. Despite using a larger number of adipocytes ($n = 500$) for the distribution-based analysis compared to previous studies, higher counts would be desirable to reliably detect additional maxima with low frequencies. With the per-object classification strategy from whole slide scans described above it is to be expected that greater numbers of adipocyte area estimates will be obtained laying a sound foundation for further investigations on the question of adipocyte distribution modality. Despite substantial differences in distribution shape, the extracted adipocyte sizing parameters were all equally correlated with anthropometry and laboratory chemistry. The observed results are in good agreement with investigations by *Laforest et al.* suggesting that different adipocyte size estimates from various measurement techniques all show comparable

correlations with adiposity and cardiometabolic risk factors (33). In conclusion, small cohort sizes and limited adipocyte counts should propose greater limitations to significance and comparability between studies rather than different measurement techniques or outcome measures. Nonetheless, it is important to emphasize that adipocyte size itself cannot be generalized between studies and always needs to be seen in context and carefully interpreted regarding physiological relevance.

Individuals with enlarged adipocytes show decreased respiratory capacity

As a novel finding, the present work indicates that mature adipocyte respiratory chain capacity is decreased in individuals with enlarged adipocytes predominantly in SAT-derived samples. If mitochondria due to defects in the respiratory chain fail to provide sufficient ATP for cellular and lipid metabolic processes this could lead to enhanced levels of free fatty acids and reactive oxygen species. Altered mitochondrial function in turn could substantially contribute to differences in the adipocyte's energy homeostasis and secretory function. While the study does provide functional evidence for a reduction in respiratory chain capacity with adipocyte hypertrophy it should be acknowledged that further investigations are necessary to identify individual respiratory chain complexes or distinct biological pathways leading to the observed effects. Additionally, it would be of high physiological relevance to conduct follow-up experiments to gain more insights into a possible relationship between adipocyte size, free fatty acid release, ROS production, and pro-inflammatory signaling. The study for the first time reports a negative relationship between fat cell size and mature adipocyte respiratory chain function. Similar to the results described, multiple publications report a pivotal role of mitochondrial deficiencies in obesity (77, 143, 144). Perturbed respiratory chain capacity in individuals with large adipocytes, therefore, represents a highly plausible mechanism that could substantially contribute to WAT dysfunction, a harmful metabolic profile, and the systemic manifestation of metabolic disorders. While an inverse relationship between respiratory chain capacity and adipocyte size was predominantly observed in SAT, it is striking that no other anthropometric or laboratory variables besides BMI were associated with adipocyte size in this depot. Albeit weaker associations with respiratory chain function were seen in VAT, multiple significant relationships between adipocyte size and laboratory parameters representative for obesity-related disorders were present. The associations reported for VAT are in good agreement with the well-known and frequently reported close interrelationship between visceral obesity and metabolic disorders (8, 42). Both, the functional associations observed in SAT and the relationship between adipocyte size and laboratory markers of cardiovascular disease in VAT emphasize that metabolic alterations within a tissue do not necessarily manifest in a phenotype that is easily detectable and vice-versa. A detailed and comprehensive transcriptional

and functional characterization of WAT in relation to adipocyte size is, therefore, of utmost importance to obtain detailed insights how metabolic differences within a certain adipose depot are intertwined with obesity-associated disorders and markers thereof.

The white adipose tissue transcriptome and adipocyte size

WAT is an organ with unmet plasticity and expansion capacity when energy intake exceeds energy expenditure. How the WAT transcriptome differs between depots and changes with adipocyte hypertrophy remains poorly investigated. The GTEx project offers an unmatched dataset to address these research questions, as it is a public resource that allows studying tissue-specific gene expression at over 50 sites including SAT and VAT. Since H&E stained histology images are provided by the consortium as well, adipocyte area estimates and transcriptomics were tied together. As an initial analysis, RNA-Seq data from GTEx was used to compare global differences in gene expression between SAT and VAT. Later, differential expression analysis concerning adipocyte size was carried out both using a binned model grouping adipocyte area into four different size categories and with adipocyte area as a continuous variable. The RNA-Seq analysis comparing SAT and VAT showed that multiple developmental genes and transcription factors (HOX family, IRX family, BARX1) were differentially expressed between the two sites. With a large number of paired SAT and VAT samples ($n = 99$), the present study expands the existing body of evidence from smaller transcriptomics and lineage tracing studies suggesting that SAT and VAT white adipocytes arise from different progenitors (98, 136-140).

Besides developmental genes, arachidonate 15-Lipoxygenase (*ALOX15*) was found amongst the top differentially expressed genes, being significantly enriched in VAT. *ALOX15* can produce both pro and anti-inflammatory mediators depending on its FA substrates. While anti-inflammatory mediators mainly arise from ω -3 FAs, pro-inflammatory mediators are synthesized from ω -6 FA species such as arachidonic acid (145, 146). Due to a substantial enrichment of ω -6 FAs in westernized diets, production of pro-inflammatory mediators by *ALOX15* would be favored, displaying a possible novel link between diet, metabolism, and the harmful pro-inflammatory environment in VAT with progressing obesity (147, 148). Based on the findings from the described exploratory analysis it would be of great relevance to conduct a follow-up study that assesses the expression of *ALOX15* and measures its substrates/products with lipidomics techniques in relation to dietary intake or intervention.

On the single gene level, *EGFL6* and *SLC27A2* were amongst the top-ranked differentially expressed genes related to adipocyte size in SAT. *EGFL6* is a growth factor that has been previously associated with obesity and enhanced proliferation of adipose tissue-derived stromal vascular cells and was shown to be increased in individuals with large adipocytes (149). On the

contrary, *SLC27A2* was inversely related to adipocyte size and functions as an acyl-coA synthase and FA transporter showing substrate specificity towards long-chain FAs (150). *SLC27A2* levels are reduced after high-fat overfeeding and correlated negatively with obesity and diabetes-related traits (151-153). Interestingly, the expression of *SLC27A1*, a FA transporter highly expressed in WAT and BAT, was not influenced by cell size. As *SLC27A2* usually shows higher expression in liver or kidney compared to WAT, functional studies with orthogonal assays should be conducted to elucidate the role and importance of *SLC27A2* in WAT FA metabolism (150). Similarly, strong negative associations between transcripts involved in DNL (*FASN*) and elongation of its products (*ELOVL6*) were seen in VAT. Decreased expression of DNL related genes has been previously reported with obesity and T2D (154). The reduced expression of DNL related enzymes in VAT could display a physiological response to elevated dietary intake of fatty acids that is usually observed with obesity and western diets. Accordingly, DNL is suppressed by high-fat diets and stimulated through an increased intake of carbohydrates (155). In agreement with the observed gene expression patterns, DNL has been identified as an important metabolic pathway to maintain an anti-inflammatory and insulin-sensitive environment within WAT (156).

KEGG gene set enrichment analysis to identify classes of genes that are over- or under-represented in individuals with enlarged fat cells suggested that genes involved in OXPHOS, thermogenesis, lipolysis, and FA degradation were underrepresented. Orthogonal, functional evidence for this finding is provided by studies within this Ph.D. thesis clearly showing a negative relationship between respiratory capacity and fat cell size. Thermogenesis and lipolysis could display essential mechanisms to maintain healthy adipocyte size and a strategy to dispose excess dietary lipids in the form of heat. Based on this intriguing finding further investigations estimating the brown adipocyte content in heterogeneous WAT biopsies were carried out using a deconvolution tool (BATLAS) that was previously published (121). In both depots, a negative relationship between adipocyte size and estimated BAT content with stronger effects in VAT was observed. While pathways related to mitochondrial function and FA metabolism were found to be impaired with larger adipocyte size, an enrichment of genes related to immune and inflammatory processes was present. For the first time, the study reports that in individuals with large fat cells an energy-storing rather than energy-expending transcriptomic profile is present. Additionally, upregulation of genes involved in pro-inflammatory processes was observed. The present work, therefore, provides important novel insights on the transcriptional foundation leading to WAT dysfunction and excess lipid accumulation with obesity. A decreased brown adipocyte content in WAT of individuals with large adipocytes could facilitate white adipocyte hypertrophy and excess lipid accumulation.

As bulk tissue was used for the study a substantial contribution of other cell types from the SVF cannot be ruled out, and future single cell gene expression profiling will be important to link gene signatures across adipocyte cell state transitions to adipocyte size. Further, the SAT and VAT samples originate from different individuals with diverse genetic backgrounds that most likely influences WAT gene expression. To rule out these possible confounders, mature adipocytes from four individuals were separated by size and RNA from the different fractions was sequenced. The analysis revealed similar pathways and genes to be affected in size-separated adipocytes as in bulk tissue and indicated that large adipocytes display a metabolically more harmful transcriptional profile compared to their small counterparts. It is therefore concluded, that differences in gene expression in bulk tissue and the harmful transcriptional profile with larger adipocyte size can at least partially be attributed to hypertrophic adipocytes themselves. Findings from mature adipocytes were in good agreement with recent spatial transcriptomics experiments indicating that adipocytes grouped into different size quartiles, display distinct gene expression patterns (93). However, *Bäckdahl et al.* additionally conclude that adipocytes of similar size also have distinct transcriptional profiles clustering them into three different subtypes. According to these authors, fat cell size per se does not explain transcriptional differences between adipocyte subclasses that show remarkable differences in insulin sensitivity. Location, surrounding SVF cells, and lineage are major drivers of gene expression in adipocytes as well and add another layer of complexity to the data (93). As the categorization of human adipose tissue into either SAT or VAT is gross and intradepot variation exists, it cannot be ruled out that the observed effects are specific to the anatomical locations that were investigated (157). This is especially relevant in the context of GTEx SAT biopsies, which were harvested proximate to the knee. Detailed investigations that characterize gene expression at multiple WAT depots across the body and at different intra-depot sites would be of great interest and could shed further light on the generalizability of findings from distinct anatomical locations (98).

The fatty acid composition of WAT is depot dependent and adipocyte size specific

Since genes related to FA metabolism ranked with high significance in the DE analysis it was hypothesized that FA composition of WAT could be depot- and adipocyte size-specific. Hitherto, only limited data is available on FA patterns and fat cell size. Using FAME GC-MS the relative abundance of 28 different fatty acids between and 8 and 28 carbon atoms was measured and related to adipocyte size and WAT depots. In VAT relative to SAT, a lower proportion of ω -3 and ω -6 PUFAs was observed, while elevated levels of medium and long-chain saturated FAs were present. Lower amounts of ω -3 and ω -6 PUFAs in VAT could be attributed to an elevated expression of genes that utilize PUFAs for the synthesis of pro and anti-inflammatory mediators

(lipoxygenases, cyclooxygenases, epoxygenases) as seen in RNA-Seq experiments. As VAT directly drains through the portal circulation to the liver, it is also plausible that higher amounts of PUFAs are dispensed from the tissue with increasing adipocyte size. The in general high metabolic activity of VAT combined with elevated fatty acid fluxes and excess lipid accumulation in the liver with obesity would support this hypothesis (158).

Elevated levels of medium and long-chain saturated fatty acids in VAT could be explained by a higher expression of genes involved in DNL at this site as seen in our own RNA-seq data and previous publications (159). Organismal studies with isotope-labeled substrates would, however, be of great relevance to obtain a clear, organ-specific overview of the flux and origin of different fatty acid species. In SAT, a strong positive relationship between the relative abundance of eicosapentaenoic and arachidonic acid (FA 20:5(n-3), FA 20:4(ω -6)) with adipocyte size was seen, while medium and long-chain saturated fatty acids showed a strong negative correlation with adipocyte size in VAT. The observed results are somewhat counterintuitive, as in general a higher dietary intake of saturated fat is considered to be metabolically unhealthy. Similar results were, however, observed by *Roberts et al.* who report a negative association of myristic acid (FA 14:0) and adipocyte size (72). The strong negative correlation of DNL genes and adipocyte size in VAT as seen in our own RNA-seq experiments provides a plausible explanation for the observed inverse relationship between saturated fatty acids and fat cell size. Similar to the results observed in VAT, the positive relationship between PUFAs and fat cell size in SAT could stem from multiple origins. It is plausible that an increased abundance of PUFAs facilitates the expandability of existing fat cells due to greater conformational flexibility and fluidity of the adipocyte membrane (160). Concordantly, severe differences in the WAT membrane lipid composition were found in monozygotic twins discordant for obesity (161). Besides structural properties and functioning as an energy-dense medium to store excess energy, lipids, especially PUFAs, have been shown to have substantial signaling activity. For example, PUFAs are known to have signaling activity towards peroxisome proliferator-activated receptors and sterol regulatory element binding proteins that are abundantly expressed in WAT (162). Since total FAs were quantified no assumptions can be made about the individual lipid classes, the individual FA species were most abundant in or if certain lipid classes show a stronger relationship with adipocyte size compared to others. Lipidome studies concerning adipocyte size would represent a promising tool to follow up on these pending research questions. Cell culture studies assessing the adipogenic differentiation capacity of hAMSCs in the presence or absence of PUFAs could help to investigate the relationship between signaling activity and lipid accumulation.

Magnetic resonance spectroscopy as a promising strategy for the future in-vivo characterization of WAT morphology and composition

To obtain quantitative information about WAT morphology and FA composition a biopsy is typically required. While SAT is relatively easy to obtain, acquisition of the metabolically more harmful VAT becomes increasingly more difficult and requires general surgery. The requirement of general surgery to obtain VAT biopsies makes longitudinal studies of the respective depot almost impossible as surgery needs to be medically indicated. Also, this prerequisite makes it challenging to obtain samples from healthy and lean individuals. Further, surgical stress and anesthesia are known to alter glucose metabolism, enhance lipolysis and increase the release of pro-inflammatory mediators (96). Moreover, the amount of tissue and anatomical location where WAT can be excised is often limited due to ethical, anatomical or surgical reasons. For a comprehensive characterization of WAT in health and disease it would be desirable to achieve a longitudinal characterization of WAT with spatial resolution at multiple different sites in the body in an unperturbed state. Up to date, no feasible methods for the quantitative assessment of WAT morphology and composition in an *in vivo* state are available. Thus, in close collaboration with the Body Magnetic Resonance Research Group (Klinikum Rechts der Isar) the potential of magnetic resonance spectroscopy to simultaneously and non-invasively probe adipocyte size and FA composition of WAT were explored. As a model system, water-fat emulsions were manufactured in a colloid mill allowing to precisely modify the size of the lipid droplets generated based on stirrer speed. Thereby, the manufactured droplets closely resemble the round, unilocular shape and size of lipid droplets that are observed in mature adipocytes. As high fat emulsions were produced the fat content of 80 % and water content of 20 % closely resembled *in vivo* WAT composition (126, 127). Since ω -3 to ω -6 ratios in diet and tissues are considered to have a substantial impact on metabolic health and disease, two vegetable oils with drastically different ω -3 and ω -6 content (linseed oil and sunflower oil) were chosen to manufacture the emulsions (146, 163). MRS was validated against gold-standard methods for droplet sizing (laser diffraction) and FA composition (FAME-GCMS) showing excellent agreement for both parameters. After the proof-of-concept study with lipid emulsions, a similar approach comparing MR against state-of-the-art validation methods was chosen in SAT and VAT biopsies. Findings from the model systems were corroborated by good agreement between MR and reference methods. It should be noted that clinical MRS was able to discriminate well between different degrees of saturation, chain length and double bond position, but does not yet reach a resolution that is comparable to mass spectrometry that allows identifying individual FA species. With two successful validation strategies MRS represents an innovative approach for the simultaneous assessment of fat cell size and FA composition. Compared to diffusion-based MR strategies, the in-parallel quantification

of adipocyte size and FA composition using MRS offers the advantage to extract more quantitative WAT parameters with overall shorter measurement times. Further, MRS is less sensitive to breathing, vibration and motion. In conclusion, the application of MRS to probe adipocyte size and FA composition *in vivo* is highly feasible and prospect of future investigations. Non-invasive MRS would offer the opportunity to longitudinally study adipose morphology and composition in health, disease and ageing or as part of (dietary) intervention studies. Further, *in vivo* MRS could help to unravel questions about inter- and intra-depot WAT heterogeneity as accessibility and scanning locations are in contrast with biopsy-based techniques not limited.

Conclusion

The present work aimed to address limitations in adipocyte sizing approaches to unravel the genetic, metabolic and transcriptomic underpinnings of adipocyte morphology.

Therefore, the potential of novel, machine learning based strategies for the fast and accurate determination of adipocyte size from whole slide scans was explored. Machine learning proved feasible to reliably measure adipocyte size from histology images and estimates were used for an in-depth analysis of fat cell size distributions and to shed light on the genetic and transcriptional background of adipocyte morphology.

Orthogonal experiments (RNA-Seq, respirometry, FAME GC-MS) in complementary model systems (mature adipocytes) were carried out to validate and expand the initial findings. While no loci with genome-wide significance were found, in the present study, the data generated identified novel transcriptional and functional alterations of genes involved in OXPHOS, FA metabolism, thermogenesis, and inflammatory processes with adipocyte hypertrophy. In agreement with results from RNA-Seq, correlations between adipocyte size, mature adipocyte respiration and WAT FA composition were observed. Together, the identified transcriptional signatures can be considered as fundamental for WAT dysfunction and the manifestation of metabolic disorders.

The observed inverse relationship between adipocyte size and WAT thermogenic adipocyte content displays a novel mechanism that could facilitate hypertrophic adipocyte expansion. Further, a plethora of novel transcripts that are related to adipocyte size were found. As a follow-up, functional studies should be carried out from this rich dataset to decipher the mechanism of action of individual transcripts and evaluate their potential for pharmacological targeting. Changes in WAT morphology, gene expression, and FA patterns are most likely pivotal events that occur before obesity-related disorders become systemic. MRS represents a promising tool for the early and preventive detection of the described WAT phenotypes in a clinical setting.

In conclusion, the present Ph.D. thesis leads from methodological advances in adipocyte sizing to insights on the transcriptional and metabolic background of adipocyte hypertrophy with the possibility of a translational application towards a non-invasive characterization of WAT.

6 | References

1. World Health Organization (WHO). Obesity and overweight. <https://www.who.int/news-room/fact-sheets/detail/obesity-and-overweight>. Accessed 25.05.2021, 2021.
2. Afshin A, Forouzanfar MH, Reitsma MB, Sur P, Estep K, Lee A, et al. Health Effects of Overweight and Obesity in 195 Countries over 25 Years. *The New England journal of medicine*. 2017;377(1):13-27.
3. Ward ZJ, Bleich SN, Cradock AL, Barrett JL, Giles CM, Flax C, et al. Projected U.S. State-Level Prevalence of Adult Obesity and Severe Obesity. *The New England journal of medicine*. 2019;381(25):2440-50.
4. Heymsfield SB, and Wadden TA. Mechanisms, Pathophysiology, and Management of Obesity. *The New England journal of medicine*. 2017;376(3):254-66.
5. Claussnitzer M, Cho JH, Collins R, Cox NJ, Dermitzakis ET, Hurles ME, et al. A brief history of human disease genetics. *Nature*. 2020;577(7789):179-89.
6. Morigny P, Boucher J, Arner P, and Langin D. Lipid and glucose metabolism in white adipocytes: pathways, dysfunction and therapeutics. *Nature Reviews Endocrinology*. 2021;17(5):276-95.
7. Rosen Evan D, and Spiegelman Bruce M. What We Talk About When We Talk About Fat. *Cell*. 2014;156(1):20-44.
8. Lee MJ, Wu Y, and Fried SK. Adipose tissue heterogeneity: implication of depot differences in adipose tissue for obesity complications. *Molecular aspects of medicine*. 2013;34(1):1-11.
9. Cinti S. The adipose organ. *Prostaglandins, Leukotrienes and Essential Fatty Acids*. 2005;73(1):9-15.
10. Peirce V, Carobbio S, and Vidal-Puig A. The different shades of fat. *Nature*. 2014;510(7503):76-83.
11. Cinti S. The adipose organ at a glance. *Disease models & mechanisms*. 2012;5(5):588-94.
12. Cannon B, and Nedergaard J. Brown adipose tissue: function and physiological significance. *Physiological reviews*. 2004;84(1):277-359.
13. Shen W, Wang Z, Punyanita M, Lei J, Sinav A, Kral JG, et al. Adipose tissue quantification by imaging methods: a proposed classification. *Obesity research*. 2003;11(1):5-16.
14. Pulit SL, Stoneman C, Morris AP, Wood AR, Glastonbury CA, Tyrrell J, et al. Meta-analysis of genome-wide association studies for body fat distribution in 694 649 individuals of European ancestry. *Human molecular genetics*. 2019;28(1):166-74.
15. Schoettl T, Fischer IP, and Ussar S. Heterogeneity of adipose tissue in development and metabolic function. *The Journal of Experimental Biology*. 2018;221(Suppl 1):jeb162958.
16. Veilleux A, and Tchernof A. In: Symonds ME ed. *Adipose Tissue Biology*. New York, NY: Springer New York; 2012:123-66.
17. Kanneganti TD, and Dixit VD. Immunological complications of obesity. *Nature immunology*. 2012;13(8):707-12.

18. Berry R, Jeffery E, and Rodeheffer MS. Weighing in on adipocyte precursors. *Cell Metab.* 2014;19(1):8-20.
19. Sun K, Kusminski CM, and Scherer PE. Adipose tissue remodeling and obesity. *The Journal of clinical investigation.* 2011;121(6):2094-101.
20. Stenkula KG, and Erlanson-Albertsson C. Adipose cell size: importance in health and disease. *American journal of physiology Regulatory, integrative and comparative physiology.* 2018;315(2):R284-r95.
21. Arner P, and Spalding KL. Fat cell turnover in humans. *Biochemical and biophysical research communications.* 2010;396(1):101-4.
22. Spalding KL, Arner E, Westermark PO, Bernard S, Buchholz BA, Bergmann O, et al. Dynamics of fat cell turnover in humans. *Nature.* 2008;453(7196):783-7.
23. Tandon P, Wafer R, and Minchin JEN. Adipose morphology and metabolic disease. *J Exp Biol.* 2018;221(Pt Suppl 1).
24. Rutkowski JM, Stern JH, and Scherer PE. The cell biology of fat expansion. *The Journal of cell biology.* 2015;208(5):501-12.
25. Smith U, Sjöström L, and Björnstorpe P. Comparison of two methods for determining human adipose cell size. *Journal of lipid research.* 1972;13(6):822-4.
26. Carpenter AE, Jones TR, Lamprecht MR, Clarke C, Kang IH, Friman O, et al. CellProfiler: image analysis software for identifying and quantifying cell phenotypes. *Genome biology.* 2006;7(10):R100.
27. Galarraga M, Campión J, Muñoz-Barrutia A, Boqué N, Moreno H, Martínez JA, et al. Adiposoft: automated software for the analysis of white adipose tissue cellularity in histological sections. *Journal of lipid research.* 2012;53(12):2791-6.
28. Björnheden T, Jakubowicz B, Levin M, Odén B, Edén S, Sjöström L, et al. Computerized determination of adipocyte size. *Obesity research.* 2004;12(1):95-105.
29. Ashwell M, Priest P, Bondoux M, Sowter C, and McPherson CK. Human fat cell sizing--a quick, simple method. *Journal of lipid research.* 1976;17(2):190-2.
30. Hirsch J, and Gallian E. Methods for the determination of adipose cell size in man and animals. *Journal of lipid research.* 1968;9(1):110-9.
31. McLaughlin T, Sherman A, Tsao P, Gonzalez O, Yee G, Lamendola C, et al. Enhanced proportion of small adipose cells in insulin-resistant vs insulin-sensitive obese individuals implicates impaired adipogenesis. *Diabetologia.* 2007;50(8):1707-15.
32. Lenz M, Roumans NJ, Vink RG, van Baak MA, Mariman EC, Arts IC, et al. Estimating real cell size distribution from cross-section microscopy imaging. *Bioinformatics (Oxford, England).* 2016;32(17):i396-i404.
33. Laforest S, Michaud A, Paris G, Pelletier M, Vidal H, Geloën A, et al. Comparative analysis of three human adipocyte size measurement methods and their relevance for cardiometabolic risk. *Obesity (Silver Spring, Md).* 2017;25(1):122-31.
34. Ye RZ, Richard G, Gévry N, Tchernof A, and Carpentier AC. Fat Cell Size: Measurement Methods, Pathophysiological Origins, and Relationships With Metabolic Dysregulations. *Endocrine Reviews.* 2021.
35. van Harmelen V, Skurk T, Röhrig K, Lee YM, Halbleib M, Aprath-Husmann I, et al. Effect of BMI and age on adipose tissue cellularity and differentiation capacity in women. *International journal of obesity and related metabolic disorders :*

- journal of the International Association for the Study of Obesity*. 2003;27(8):889-95.
36. Tchoukalova YD, Koutsari C, Karpyak MV, Votruba SB, Wendland E, and Jensen MD. Subcutaneous adipocyte size and body fat distribution. *The American Journal of Clinical Nutrition*. 2008;87(1):56-63.
 37. Van Harmelen V, Reynisdottir S, Eriksson P, Thörne A, Hoffstedt J, Lönnqvist F, et al. Leptin secretion from subcutaneous and visceral adipose tissue in women. *Diabetes*. 1998;47(6):913-7.
 38. Reynisdottir S, Dauzats M, Thörne A, and Langin D. Comparison of hormone-sensitive lipase activity in visceral and subcutaneous human adipose tissue. *The Journal of Clinical Endocrinology and Metabolism*. 1997;82(12):4162-6.
 39. Glastonbury CA, Pulit SL, Honecker J, Censin JC, Laber S, Yaghoobkar H, et al. Machine Learning based histology phenotyping to investigate the epidemiologic and genetic basis of adipocyte morphology and cardiometabolic traits. *PLoS computational biology*. 2020;16(8):e1008044.
 40. Lonn M, Mehlig K, Bengtsson C, and Lissner L. Adipocyte size predicts incidence of type 2 diabetes in women. *FASEB journal : official publication of the Federation of American Societies for Experimental Biology*. 2010;24(1):326-31.
 41. Hoffstedt J, Arner E, Wahrenberg H, Andersson DP, Qvisth V, Löfgren P, et al. Regional impact of adipose tissue morphology on the metabolic profile in morbid obesity. *Diabetologia*. 2010;53(12):2496-503.
 42. Verboven K, Wouters K, Gaens K, Hansen D, Bijnen M, Wetzels S, et al. Abdominal subcutaneous and visceral adipocyte size, lipolysis and inflammation relate to insulin resistance in male obese humans. *Scientific reports*. 2018;8(1):4677.
 43. Lundgren M, Svensson M, Lindmark S, Renström F, Ruge T, and Eriksson JW. Fat cell enlargement is an independent marker of insulin resistance and 'hyperleptinaemia'. *Diabetologia*. 2007;50(3):625-33.
 44. McLaughlin T, Lamendola C, Coghlan N, Liu TC, Lerner K, Sherman A, et al. Subcutaneous adipose cell size and distribution: relationship to insulin resistance and body fat. *Obesity (Silver Spring, Md)*. 2014;22(3):673-80.
 45. Cotillard A, Poitou C, Torcivia A, Bouillot JL, Dietrich A, Klötting N, et al. Adipocyte size threshold matters: link with risk of type 2 diabetes and improved insulin resistance after gastric bypass. *The Journal of Clinical Endocrinology and Metabolism*. 2014;99(8):E1466-70.
 46. McLaughlin T, Craig C, Liu LF, Perelman D, Allister C, Spielman D, et al. Adipose Cell Size and Regional Fat Deposition as Predictors of Metabolic Response to Overfeeding in Insulin-Resistant and Insulin-Sensitive Humans. *Diabetes*. 2016;65(5):1245-54.
 47. Veilleux A, Caron-Jobin M, Noël S, Laberge PY, and Tchernof A. Visceral adipocyte hypertrophy is associated with dyslipidemia independent of body composition and fat distribution in women. *Diabetes*. 2011;60(5):1504-11.
 48. Honecker J, Weidlich D, Heisz S, Lindgren CM, Karampinos DC, Claussnitzer M, et al. A distribution-centered approach for analyzing human adipocyte size estimates and their association with obesity-related traits and mitochondrial function. *International Journal of Obesity*. 2021.

49. Andersson DP, Eriksson Hogling D, Thorell A, Toft E, Qvisth V, Naslund E, et al. Changes in subcutaneous fat cell volume and insulin sensitivity after weight loss. *Diabetes care*. 2014;37(7):1831-6.
50. Katsogiannos P, Kamble PG, Boersma GJ, Karlsson FA, Lundkvist P, Sundbom M, et al. Early Changes in Adipose Tissue Morphology, Gene Expression, and Metabolism After RYGB in Patients With Obesity and T2D. *The Journal of Clinical Endocrinology and Metabolism*. 2019;104(7):2601-13.
51. Tamez M, Ramos-Barragan V, Mendoza-Lorenzo P, Arrieta-Joffe P, López-Martínez S, Rojano-Rodríguez ME, et al. Adipocyte Size and Leptin Receptor Expression in Human Subcutaneous Adipose Tissue After Roux-en-Y Gastric Bypass. *Obesity surgery*. 2017;27(12):3330-2.
52. Crewe C, An YA, and Scherer PE. The ominous triad of adipose tissue dysfunction: inflammation, fibrosis, and impaired angiogenesis. *The Journal of clinical investigation*. 2017;127(1):74-82.
53. Pasarica M, Sereda OR, Redman LM, Albarado DC, Hymel DT, Roan LE, et al. Reduced adipose tissue oxygenation in human obesity: evidence for rarefaction, macrophage chemotaxis, and inflammation without an angiogenic response. *Diabetes*. 2009;58(3):718-25.
54. Virtanen KA, Lönnroth P, Parkkola R, Peltoniemi P, Asola M, Viljanen T, et al. Glucose Uptake and Perfusion in Subcutaneous and Visceral Adipose Tissue during Insulin Stimulation in Nonobese and Obese Humans. *The Journal of Clinical Endocrinology & Metabolism*. 2002;87(8):3902-10.
55. Kabon B, Nagele A, Reddy D, Eagon C, Fleshman JW, Sessler DI, et al. Obesity decreases perioperative tissue oxygenation. *Anesthesiology*. 2004;100(2):274-80.
56. Marcelin G, Silveira ALM, Martins LB, Ferreira AV, and Clément K. Deciphering the cellular interplays underlying obesity-induced adipose tissue fibrosis. *The Journal of clinical investigation*. 2019;129(10):4032-40.
57. Henegar C, Tordjman J, Achard V, Lacasa D, Cremer I, Guerre-Millo M, et al. Adipose tissue transcriptomic signature highlights the pathological relevance of extracellular matrix in human obesity. *Genome biology*. 2008;9(1):R14.
58. Divoux A, Tordjman J, Lacasa D, Veyrie N, Hugol D, Aissat A, et al. Fibrosis in human adipose tissue: composition, distribution, and link with lipid metabolism and fat mass loss. *Diabetes*. 2010;59(11):2817-25.
59. Mraz M, and Haluzik M. The role of adipose tissue immune cells in obesity and low-grade inflammation. *The Journal of endocrinology*. 2014;222(3):R113-27.
60. Lumeng CN, Bodzin JL, and Saltiel AR. Obesity induces a phenotypic switch in adipose tissue macrophage polarization. *The Journal of clinical investigation*. 2007;117(1):175-84.
61. Cinti S, Mitchell G, Barbatelli G, Murano I, Ceresi E, Faloia E, et al. Adipocyte death defines macrophage localization and function in adipose tissue of obese mice and humans. *Journal of lipid research*. 2005;46(11):2347-55.
62. Gustafson B, Nerstedt A, and Smith U. Reduced subcutaneous adipogenesis in human hypertrophic obesity is linked to senescent precursor cells. *Nature communications*. 2019;10(1):2757.
63. el Bouazzaoui F, Henneman P, Thijssen P, Visser A, Koning F, Lips MA, et al. Adipocyte telomere length associates negatively with adipocyte size, whereas adipose tissue telomere length associates negatively with the extent of fibrosis in severely obese women. *International journal of obesity (2005)*. 2014;38(5):746-9.

64. Monickaraj F, Gokulakrishnan K, Prabu P, Sathishkumar C, Anjana RM, Rajkumar JS, et al. Convergence of adipocyte hypertrophy, telomere shortening and hypoadiponectinemia in obese subjects and in patients with type 2 diabetes. *Clinical biochemistry*. 2012;45(16-17):1432-8.
65. Zhang Y, Proenca R, Maffei M, Barone M, Leopold L, and Friedman JM. Positional cloning of the mouse obese gene and its human homologue. *Nature*. 1994;372(6505):425-32.
66. Halberg N, Wernstedt-Asterholm I, and Scherer PE. The adipocyte as an endocrine cell. *Endocrinology and metabolism clinics of North America*. 2008;37(3):753-68, x-xi.
67. Skurk T, Alberti-Huber C, Herder C, and Hauner H. Relationship between adipocyte size and adipokine expression and secretion. *The Journal of Clinical Endocrinology and Metabolism*. 2007;92(3):1023-33.
68. Jernas M, Palming J, Sjöholm K, Jennische E, Svensson PA, Gabrielsson BG, et al. Separation of human adipocytes by size: hypertrophic fat cells display distinct gene expression. *FASEB journal : official publication of the Federation of American Societies for Experimental Biology*. 2006;20(9):1540-2.
69. Laurencikiene J, Skurk T, Kulyté A, Hedén P, Aström G, Sjölin E, et al. Regulation of lipolysis in small and large fat cells of the same subject. *The Journal of Clinical Endocrinology and Metabolism*. 2011;96(12):E2045-9.
70. Acosta JR, Douagi I, Andersson DP, Bäckdahl J, Rydén M, Arner P, et al. Increased fat cell size: a major phenotype of subcutaneous white adipose tissue in non-obese individuals with type 2 diabetes. *Diabetologia*. 2016;59(3):560-70.
71. Rydén M, and Arner P. Cardiovascular risk score is linked to subcutaneous adipocyte size and lipid metabolism. *Journal of internal medicine*. 2017;282(3):220-8.
72. Roberts R, Hodson L, Dennis AL, Neville MJ, Humphreys SM, Harnden KE, et al. Markers of de novo lipogenesis in adipose tissue: associations with small adipocytes and insulin sensitivity in humans. *Diabetologia*. 2009;52(5):882.
73. Arner P, Bernard S, Appelsved L, Fu KY, Andersson DP, Salehpour M, et al. Adipose lipid turnover and long-term changes in body weight. *Nature medicine*. 2019;25(9):1385-9.
74. Wessels B, Honecker J, Schöttl T, Stecher L, Klingenspor M, Hauner H, et al. Adipose Mitochondrial Respiratory Capacity in Obesity is Impaired Independently of Glycemic Status of Tissue Donors. *Obesity*. 2019;27(5):756-66.
75. Kraunsoe R, Boushel R, Hansen CN, Schjerling P, Qvortrup K, Stockel M, et al. Mitochondrial respiration in subcutaneous and visceral adipose tissue from patients with morbid obesity. *The Journal of physiology*. 2010;588(Pt 12):2023-32.
76. Heinonen S, Buzkova J, Muniandy M, Kaksonen R, Ollikainen M, Ismail K, et al. Impaired Mitochondrial Biogenesis in Adipose Tissue in Acquired Obesity. *Diabetes*. 2015;64(9):3135-45.
77. Fischer B, Schöttl T, Schempp C, Fromme T, Hauner H, Klingenspor M, et al. Inverse relationship between body mass index and mitochondrial oxidative phosphorylation capacity in human subcutaneous adipocytes. *American journal of physiology Endocrinology and metabolism*. 2015;309(4):E380-7.

78. Yin X, Lanza IR, Swain JM, Sarr MG, Nair KS, and Jensen MD. Adipocyte Mitochondrial Function Is Reduced in Human Obesity Independent of Fat Cell Size. *The Journal of Clinical Endocrinology and Metabolism*. 2014;99(2):E209-16.
79. Hodson L, Skeaff CM, and Fielding BA. Fatty acid composition of adipose tissue and blood in humans and its use as a biomarker of dietary intake. *Progress in lipid research*. 2008;47(5):348-80.
80. Garaulet M, Hernandez-Morante JJ, Lujan J, Tebar FJ, and Zamora S. Relationship between fat cell size and number and fatty acid composition in adipose tissue from different fat depots in overweight/obese humans. *International journal of obesity (2005)*. 2006;30(6):899-905.
81. Yew Tan C, Virtue S, Murfitt S, Roberts LD, Phua YH, Dale M, et al. Adipose tissue fatty acid chain length and mono-unsaturation increases with obesity and insulin resistance. *Scientific reports*. 2015;5(1):18366.
82. Rohde K, Keller M, la Cour Poulsen L, Blüher M, Kovacs P, and Böttcher Y. Genetics and epigenetics in obesity. *Metabolism: clinical and experimental*. 2019;92:37-50.
83. Shungin D, Winkler TW, Croteau-Chonka DC, Ferreira T, Locke AE, Mägi R, et al. New genetic loci link adipose and insulin biology to body fat distribution. *Nature*. 2015;518(7538):187-96.
84. Emdin CA, Khera AV, Natarajan P, Klarin D, Zekavat SM, Hsiao AJ, et al. Genetic Association of Waist-to-Hip Ratio With Cardiometabolic Traits, Type 2 Diabetes, and Coronary Heart Disease. *Jama*. 2017;317(6):626-34.
85. Kulyté A, Lundbäck V, Lindgren CM, Luan J, Lotta LA, Langenberg C, et al. Genome-wide association study of adipocyte lipolysis in the GENetics of adipocyte lipolysis (GENiAL) cohort. *Molecular metabolism*. 2020;34:85-96.
86. Claussnitzer M, Dankel SN, Kim KH, Quon G, Meuleman W, Haugen C, et al. FTO Obesity Variant Circuitry and Adipocyte Browning in Humans. *The New England journal of medicine*. 2015;373(10):895-907.
87. Small KS, Todorovic M, Civelek M, El-Sayed Moustafa JS, Wang X, Simon MM, et al. Regulatory variants at KLF14 influence type 2 diabetes risk via a female-specific effect on adipocyte size and body composition. *Nature genetics*. 2018;50(4):572-80.
88. Sobreira DR, Joslin AC, Zhang Q, Williamson I, Hansen GT, Farris KM, et al. Extensive pleiotropism and allelic heterogeneity mediate metabolic effects of IRX3 and IRX5. *Science (New York, NY)*. 2021;372(6546):1085-91.
89. Hilton C, Neville MJ, Wittemans LBL, Todorovic M, Pinnick KE, Pulit SL, et al. MicroRNA-196a links human body fat distribution to adipose tissue extracellular matrix composition. *EBioMedicine*. 2019;44:467-75.
90. Lundbäck V, Kulyté A, Arner P, Strawbridge RJ, and Dahlman I. Genome-Wide Association Study of Diabetogenic Adipose Morphology in the GENetics of Adipocyte Lipolysis (GENiAL) Cohort. *Cells*. 2020;9(5).
91. Heinonen S, Saarinen L, Naukkarinen J, Rodriguez A, Fruhbeck G, Hakkarainen A, et al. Adipocyte morphology and implications for metabolic derangements in acquired obesity. *International journal of obesity (2005)*. 2014;38(11):1423-31.
92. Heinonen S, Muniandy M, Buzkova J, Mardinoglu A, Rodriguez A, Fruhbeck G, et al. Mitochondria-related transcriptional signature is downregulated in adipocytes in obesity: a study of young healthy MZ twins. *Diabetologia*. 2017;60(1):169-81.

93. Bäckdahl J, Franzén L, Massier L, Li Q, Jalkanen J, Gao H, et al. Spatial mapping reveals human adipocyte subpopulations with distinct sensitivities to insulin. *Cell Metab.* 2021.
94. Arner E, Westermark PO, Spalding KL, Britton T, Ryden M, Frisen J, et al. Adipocyte turnover: relevance to human adipose tissue morphology. *Diabetes.* 2010;59(1):105-9.
95. Alderete TL, Sattler FR, Sheng X, Tucci J, Mittelman SD, Grant EG, et al. A novel biopsy method to increase yield of subcutaneous abdominal adipose tissue. *International Journal of Obesity.* 2015;39(1):183-6.
96. Duggan EW, Carlson K, and Umpierrez GE. Perioperative Hyperglycemia Management: An Update. *Anesthesiology.* 2017;126(3):547-60.
97. Ferreira PG, Muñoz-Aguirre M, Reverter F, Sá Godinho CP, Sousa A, Amadoz A, et al. The effects of death and post-mortem cold ischemia on human tissue transcriptomes. *Nature communications.* 2018;9(1):490.
98. Schleinitz D, Krause K, Wohland T, Gebhardt C, Linder N, Stumvoll M, et al. Identification of distinct transcriptome signatures of human adipose tissue from fifteen depots. *European Journal of Human Genetics.* 2020;28(12):1714-25.
99. Zhi X, Wang J, Lu P, Jia J, Shen HB, and Ning G. AdipoCount: A New Software for Automatic Adipocyte Counting. *Front Physiol.* 2018;9:85.
100. Maguire AS, Woodie LN, Judd RL, Martin DR, Greene MW, and Graff EC. Whole-slide image analysis outperforms micrograph acquisition for adipocyte size quantification. *Adipocyte.* 2020;9(1):567-75.
101. Chen HC, and Farese RV, Jr. Determination of adipocyte size by computer image analysis. *Journal of lipid research.* 2002;43(6):986-9.
102. Lonsdale J, Thomas J, Salvatore M, Phillips R, Lo E, Shad S, et al. The Genotype-Tissue Expression (GTEx) project. *Nature genetics.* 2013;45:580.
103. The GTEx Consortium atlas of genetic regulatory effects across human tissues. *Science (New York, NY).* 2020;369(6509):1318-30.
104. Szegedy C, Vanhoucke V, Ioffe S, Shlens J, and Wojna Z. 2016 *IEEE Conference on Computer Vision and Pattern Recognition (CVPR).* 2016:2818-26.
105. Russakovsky O, Deng J, Su H, Krause J, Satheesh S, Ma S, et al. ImageNet Large Scale Visual Recognition Challenge. *International Journal of Computer Vision.* 2015;115(3):211-52.
106. Ronneberger O, Fischer P, and Brox T. 2015:arXiv:1505.04597.
107. Berry R, Church CD, Gericke MT, Jeffery E, Colman L, and Rodeheffer MS. Imaging of adipose tissue. *Methods in enzymology.* 2014;537:47-73.
108. Rodbell M. Metabolism of isolated fat cells. I. Effects of hormones on glucose metabolism and lipolysis. *The Journal of biological chemistry.* 1964;239:375-80.
109. van Harmelen V, Skurk T, and Hauner H. Primary culture and differentiation of human adipocyte precursor cells. *Methods in molecular medicine.* 2005;107:125-35.
110. Skurk T, Ecklebe S, and Hauner H. A novel technique to propagate primary human preadipocytes without loss of differentiation capacity. *Obesity (Silver Spring, Md).* 2007;15(12):2925-31.
111. Harms MJ, Li Q, Lee S, Zhang C, Kull B, Hallen S, et al. Mature Human White Adipocytes Cultured under Membranes Maintain Identity, Function, and Can Transdifferentiate into Brown-like Adipocytes. *Cell Rep.* 2019;27(1):213-25.e5.

112. Sinnott-Armstrong N, Sousa IS, Laber S, Rendina-Ruedy E, Nitter Dankel SE, Ferreira T, et al. A regulatory variant at 3q21.1 confers an increased pleiotropic risk for hyperglycemia and altered bone mineral density. *Cell Metab.* 2021;33(3):615-28.e13.
113. Gnaiger E. Mitochondrial pathways and respiratory control. An introduction to OXPHOS analysis. 4th ed. Mitochondr Physiol Network 19.12. *OROBOROS MiPNet Publications.* 2014:Innsbruck, 80 pp.
114. Brand M D, and Nicholls D G. Assessing mitochondrial dysfunction in cells. *Biochemical Journal.* 2011;435(Pt 2):297-312.
115. Dobin A, Davis CA, Schlesinger F, Drenkow J, Zaleski C, Jha S, et al. STAR: ultrafast universal RNA-seq aligner. *Bioinformatics (Oxford, England).* 2013;29(1):15-21.
116. Liao Y, Smyth GK, and Shi W. The R package Rsubread is easier, faster, cheaper and better for alignment and quantification of RNA sequencing reads. *Nucleic acids research.* 2019;47(8):e47.
117. Lonsdale J, Thomas J, Salvatore M, Phillips R, Lo E, Shad S, et al. The Genotype-Tissue Expression (GTEx) project. *Nature genetics.* 2013;45(6):580-5.
118. Chen Y, Lun AT, and Smyth GK. From reads to genes to pathways: differential expression analysis of RNA-Seq experiments using Rsubread and the edgeR quasi-likelihood pipeline. *F1000Research.* 2016;5:1438.
119. Robinson MD, McCarthy DJ, and Smyth GK. edgeR: a Bioconductor package for differential expression analysis of digital gene expression data. *Bioinformatics (Oxford, England).* 2010;26(1):139-40.
120. Luo W, and Brouwer C. Pathview: an R/Bioconductor package for pathway-based data integration and visualization. *Bioinformatics (Oxford, England).* 2013;29(14):1830-1.
121. Perdikari A, Leparc GG, Balaz M, Pires ND, Lidell ME, Sun W, et al. BATLAS: Deconvoluting Brown Adipose Tissue. *Cell Reports.* 2018;25(3):784-97.e4.
122. Ecker J, Scherer M, Schmitz G, and Liebisch G. A rapid GC-MS method for quantification of positional and geometric isomers of fatty acid methyl esters. *Journal of chromatography B, Analytical technologies in the biomedical and life sciences.* 2012;897:98-104.
123. Weidlich D, Honecker J, Gmach O, Wu M, Burgkart R, Ruschke S, et al. Measuring large lipid droplet sizes by probing restricted lipid diffusion effects with diffusion-weighted MRS at 3T. *Magnetic resonance in medicine.* 2019;81(6):3427-39.
124. Gmach O, Bertsch A, Bilke-Krause C, and Kulozik U. Impact of oil type and pH value on oil-in-water emulsions stabilized by egg yolk granules. *Colloids and Surfaces A: Physicochemical and Engineering Aspects.* 2019;581:123788.
125. Guilmineau F, and Kulozik U. Influence of a thermal treatment on the functionality of hen's egg yolk in mayonnaise. *Journal of Food Engineering.* 2007;78:648-54.
126. Thomas LW. The chemical composition of adipose tissue of man and mice. *Q J Exp Physiol Cogn Med Sci.* 1962;47:179-88.
127. International Commission on Radiological Protection. *ICRP Publication 23, Reference Man: Anatomical, Physiological, and Metabolic Characteristics.* New York: Pergamon Press; 1975.

128. Franz D, Syväri J, Weidlich D, Baum T, Rummeny EJ, and Karampinos DC. Magnetic Resonance Imaging of Adipose Tissue in Metabolic Dysfunction. *Rofo*. 2018;190(12):1121-30.
129. Weidlich D, Honecker J, Boehm C, Ruschke S, Junker D, Van AT, et al. Lipid droplet-size mapping in human adipose tissue using a clinical 3T system. *Magnetic resonance in medicine*. 2021;86(3):1256-70.
130. Lundbom J, Hakkarainen A, Fielding B, Söderlund S, Westerbacka J, Taskinen MR, et al. Characterizing human adipose tissue lipids by long echo time 1H-MRS in vivo at 1.5 Tesla: validation by gas chromatography. *NMR in biomedicine*. 2010;23(5):466-72.
131. R Core Team. Vienna, Austria: R Foundation for Statistical Computing; 2021.
132. Casero R, Westerberg H, Horner NR, Yon M, Aberdeen A, Grau V, et al. Phenotyping of Klf14 mouse white adipose tissue enabled by whole slide segmentation with deep neural networks. *bioRxiv*. 2021:2021.06.03.444997.
133. Canello R, Henegar C, Viguerie N, Taleb S, Poitou C, Rouault C, et al. Reduction of Macrophage Infiltration and Chemoattractant Gene Expression Changes in White Adipose Tissue of Morbidly Obese Subjects After Surgery-Induced Weight Loss. *Diabetes*. 2005;54(8):2277-86.
134. Smith U, Li Q, Rydén M, and Spalding KL. Cellular senescence and its role in white adipose tissue. *International Journal of Obesity*. 2021;45(5):934-43.
135. Laber S, Forcisi S, Bentley L, Petzold J, Moritz F, Smirnov KS, et al. Linking the FTO obesity rs1421085 variant circuitry to cellular, metabolic, and organismal phenotypes in vivo. *Sci Adv*. 2021;7(30).
136. Chau YY, Bandiera R, Serrels A, Martínez-Estrada OM, Qing W, Lee M, et al. Visceral and subcutaneous fat have different origins and evidence supports a mesothelial source. *Nature cell biology*. 2014;16(4):367-75.
137. Tang W, Zeve D, Suh JM, Bosnakovski D, Kyba M, Hammer RE, et al. White fat progenitor cells reside in the adipose vasculature. *Science (New York, NY)*. 2008;322(5901):583-6.
138. Tchkonina T, Lenburg M, Thomou T, Giorgadze N, Frampton G, Pirtskhalava T, et al. Identification of depot-specific human fat cell progenitors through distinct expression profiles and developmental gene patterns. *American journal of physiology Endocrinology and metabolism*. 2007;292(1):E298-307.
139. White UA, and Tchoukalova YD. Sex dimorphism and depot differences in adipose tissue function. *Biochimica et biophysica acta*. 2014;1842(3):377-92.
140. Karastergiou K, Fried SK, Xie H, Lee MJ, Divoux A, Rosencrantz MA, et al. Distinct developmental signatures of human abdominal and gluteal subcutaneous adipose tissue depots. *The Journal of Clinical Endocrinology and Metabolism*. 2013;98(1):362-71.
141. Meyer LK, Ciaraldi TP, Henry RR, Wittgrove AC, and Phillips SA. Adipose tissue depot and cell size dependency of adiponectin synthesis and secretion in human obesity. *Adipocyte*. 2013;2(4):217-26.
142. Fang L, Guo F, Zhou L, Stahl R, and Grams J. The cell size and distribution of adipocytes from subcutaneous and visceral fat is associated with type 2 diabetes mellitus in humans. *Adipocyte*. 2015;4(4):273-9.
143. Kusminski CM, and Scherer PE. Mitochondrial dysfunction in white adipose tissue. *Trends in Endocrinology & Metabolism*. 2012;23(9):435-43.

144. Christe M, Hirzel E, Lindinger A, Kern B, von Flüe M, Peterli R, et al. Obesity affects mitochondrial citrate synthase in human omental adipose tissue. *ISRN obesity*. 2013;2013:826027-.
145. Singh NK, and Rao GN. Emerging role of 12/15-Lipoxygenase (ALOX15) in human pathologies. *Progress in lipid research*. 2019;73:28-45.
146. Schmitz G, and Ecker J. The opposing effects of n-3 and n-6 fatty acids. *Progress in lipid research*. 2008;47(2):147-55.
147. Cole BK, Morris MA, Grzesik WJ, Leone KA, and Nadler JL. Adipose Tissue-Specific Deletion of 12/15-Lipoxygenase Protects Mice from the Consequences of a High-Fat Diet. *Mediators of Inflammation*. 2012;2012:851798.
148. Micha R, Khatibzadeh S, Shi P, Fahimi S, Lim S, Andrews KG, et al. Global, regional, and national consumption levels of dietary fats and oils in 1990 and 2010: a systematic analysis including 266 country-specific nutrition surveys. *BMJ : British Medical Journal*. 2014;348:g2272.
149. Oberauer R, Rist W, Lenter MC, Hamilton BS, and Neubauer H. EGFL6 is increasingly expressed in human obesity and promotes proliferation of adipose tissue-derived stromal vascular cells. *Molecular and cellular biochemistry*. 2010;343(1-2):257-69.
150. Anderson CM, and Stahl A. SLC27 fatty acid transport proteins. *Molecular aspects of medicine*. 2013;34(2-3):516-28.
151. Gillberg L, Perfilyev A, Brøns C, Thomasen M, Grunnet LG, Volkov P, et al. Adipose tissue transcriptomics and epigenomics in low birthweight men and controls: role of high-fat overfeeding. *Diabetologia*. 2016;59(4):799-812.
152. Alligier M, Meugnier E, Debard C, Lambert-Porcheron S, Chanseau E, Sothier M, et al. Subcutaneous adipose tissue remodeling during the initial phase of weight gain induced by overfeeding in humans. *The Journal of Clinical Endocrinology and Metabolism*. 2012;97(2):E183-92.
153. Lappas M. Effect of pre-existing maternal obesity, gestational diabetes and adipokines on the expression of genes involved in lipid metabolism in adipose tissue. *Metabolism: clinical and experimental*. 2014;63(2):250-62.
154. Eissing L, Scherer T, Tödter K, Knippschild U, Greve JW, Buurman WA, et al. De novo lipogenesis in human fat and liver is linked to ChREBP- β and metabolic health. *Nature communications*. 2013;4(1):1528.
155. Song Z, Xiaoli AM, and Yang F. Regulation and Metabolic Significance of De Novo Lipogenesis in Adipose Tissues. *Nutrients*. 2018;10(10).
156. Smith U, and Kahn BB. Adipose tissue regulates insulin sensitivity: role of adipogenesis, de novo lipogenesis and novel lipids. *Journal of internal medicine*. 2016;280(5):465-75.
157. Kwok KHM, Lam KSL, and Xu A. Heterogeneity of white adipose tissue: molecular basis and clinical implications. *Experimental & Molecular Medicine*. 2016;48(3):e215-e.
158. Azzu V, Vacca M, Virtue S, Allison M, and Vidal-Puig A. Adipose Tissue-Liver Cross Talk in the Control of Whole-Body Metabolism: Implications in Nonalcoholic Fatty Liver Disease. *Gastroenterology*. 2020;158(7):1899-912.
159. Berndt J, Kovacs P, Ruschke K, Klötting N, Fasshauer M, Schön MR, et al. Fatty acid synthase gene expression in human adipose tissue: association with obesity and type 2 diabetes. *Diabetologia*. 2007;50(7):1472-80.

160. van Meer G, Voelker DR, and Feigenson GW. Membrane lipids: where they are and how they behave. *Nature reviews Molecular cell biology*. 2008;9(2):112-24.
161. Pietiläinen KH, Róg T, Seppänen-Laakso T, Virtue S, Gopalacharyulu P, Tang J, et al. Association of Lipidome Remodeling in the Adipocyte Membrane with Acquired Obesity in Humans. *PLOS Biology*. 2011;9(6):e1000623.
162. Bordoni A, Di Nunzio M, Danesi F, and Biagi PL. Polyunsaturated fatty acids: From diet to binding to ppars and other nuclear receptors. *Genes Nutr*. 2006;1(2):95-106.
163. Schulze MB, Minihane AM, Saleh RNM, and Risérus U. Intake and metabolism of omega-3 and omega-6 polyunsaturated fatty acids: nutritional implications for cardiometabolic diseases. *Lancet Diabetes Endocrinol*. 2020;8(11):915-30.

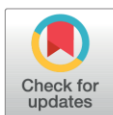
7 | Appendix

7.1 | Original publications

RESEARCH ARTICLE

Machine Learning based histology phenotyping to investigate the epidemiologic and genetic basis of adipocyte morphology and cardiometabolic traits

Craig A. Glastonbury^{1,2†*}, Sara L. Pulit^{1†}, Julius Honecker^{3†}, Jenny C. Censin^{1,4}, Samantha Laber^{1,5}, Hanieh Yaghoobkar^{6,7}, Nilufer Rahmioglu^{4,8}, Emilie Pastel⁶, Katerina Kos⁶, Andrew Pitt⁹, Michelle Hudson⁹, Christoffer Nellåker^{1,8}, Nicola L. Beer¹⁰, Hans Hauner^{3,11,12}, Christian M. Becker⁸, Krina T. Zondervan^{4,8}, Timothy M. Frayling^{6,9‡}, Melina Claussnitzer^{5,13,14‡}, Cecilia M. Lindgren^{1,4,5‡*}



OPEN ACCESS

Citation: Glastonbury CA, Pulit SL, Honecker J, Censin JC, Laber S, Yaghoobkar H, et al. (2020) Machine Learning based histology phenotyping to investigate the epidemiologic and genetic basis of adipocyte morphology and cardiometabolic traits. *PLoS Comput Biol* 16(8): e1008044. <https://doi.org/10.1371/journal.pcbi.1008044>

Editor: Lilia M. Iakoucheva, University of California San Diego, UNITED STATES

Received: November 10, 2019

Accepted: June 11, 2020

Published: August 14, 2020

Peer Review History: PLOS recognizes the benefits of transparency in the peer review process; therefore, we enable the publication of all of the content of peer review and author responses alongside final, published articles. The editorial history of this article is available here: <https://doi.org/10.1371/journal.pcbi.1008044>

Copyright: © 2020 Glastonbury et al. This is an open access article distributed under the terms of the [Creative Commons Attribution License](https://creativecommons.org/licenses/by/4.0/), which permits unrestricted use, distribution, and reproduction in any medium, provided the original author and source are credited.

Data Availability Statement: All Data, models and code are available through Github. <https://github.com/GlastonburyC/Adipocyte-U-net>.

1 Big Data Institute, University of Oxford, Oxford, United Kingdom, **2** BenevolentAI, London, United Kingdom, **3** Else Kröner-Fresenius-Center for Nutritional Medicine, School of Life Sciences, Technical University of Munich, Freising, Germany, **4** Wellcome Centre for Human Genetics (WCHG), Oxford, United Kingdom, **5** Broad Institute of MIT and Harvard, Cambridge Massachusetts, United States of America, **6** Genetics of Complex Traits, University of Exeter Medical School, Royal Devon & Exeter Hospital, Exeter, United Kingdom, **7** Research Centre for Optimal Health, School of Life Sciences, University of Westminster, London, United Kingdom, **8** Endometriosis CaRe Centre Oxford, Nuffield Department of Women's and Reproductive Health, University of Oxford, Oxford, United Kingdom, **9** NIHR Exeter Clinical Research Facility, University of Exeter Medical School, University of Exeter and Royal Devon and Exeter NHS Foundation Trust Exeter, United Kingdom, **10** Novo Nordisk Research Centre Oxford (NNRCO), Oxford, United Kingdom, **11** Institute of Nutritional Medicine, School of Medicine, Technical University of Munich, Munich, **12** German Center of Diabetes Research, Helmholtz Center Munich, Neuherberg, Germany, **13** University of Hohenheim, Stuttgart, Germany, **14** Beth Israel Deaconess Medical Center, Harvard Medical School, Boston, Massachusetts, United States of America

† CAG, SLP, and JH share first authorship on this work. TMF, MC, and CML are joint senior authors on this work.

* craig.glastonbury@benevolent.ai (CAG); celi@bdi.ox.ac.uk (CML)

Abstract

Genetic studies have recently highlighted the importance of fat distribution, as well as overall adiposity, in the pathogenesis of obesity-associated diseases. Using a large study ($n = 1,288$) from 4 independent cohorts, we aimed to investigate the relationship between mean adipocyte area and obesity-related traits, and identify genetic factors associated with adipocyte cell size. To perform the first large-scale study of automatic adipocyte phenotyping using both histological and genetic data, we developed a deep learning-based method, the Adipocyte U-Net, to rapidly derive mean adipocyte area estimates from histology images. We validate our method using three state-of-the-art approaches; CellProfiler, Adiposoft and floating adipocytes fractions, all run blindly on two external cohorts. We observe high concordance between our method and the state-of-the-art approaches (Adipocyte U-net vs. CellProfiler: $R^2_{\text{visceral}} = 0.94$, $P < 2.2 \times 10^{-16}$, $R^2_{\text{subcutaneous}} = 0.91$, $P < 2.2 \times 10^{-16}$), and faster run times (10,000 images: 6mins vs 3.5hrs). We applied the Adipocyte U-Net to 4 cohorts with histology, genetic, and phenotypic data (total $N = 820$). After meta-analysis, we found that mean adipocyte area positively correlated with body mass index (BMI) ($P_{\text{subq}} = 8.13 \times 10^{-69}$, $\beta_{\text{subq}} = 0.45$; $P_{\text{visc}} = 2.5 \times 10^{-55}$, $\beta_{\text{visc}} = 0.49$; average R^2 across cohorts =

Funding: C.A.G received a pump priming grant from Novo Nordisk to carry out this work. The funders had no role in study design, data collection and analysis, decision to publish, or preparation of the manuscript.

Competing interests: The authors have declared that no competing interests exist.

0.49) and that adipocytes in subcutaneous depots are larger than their visceral counterparts ($P_{\text{meta}} = 9.8 \times 10^{-7}$). Lastly, we performed the largest GWAS and subsequent meta-analysis of mean adipocyte area and intra-individual adipocyte variation ($N = 820$). Despite having twice the number of samples than any similar study, we found no genome-wide significant associations, suggesting that larger sample sizes and a homogenous collection of adipose tissue are likely needed to identify robust genetic associations.

Author summary

Fundamental aspects of biology such as how the size or number of adipocytes relates to obesity and cardiometabolic health are still unanswered. To answer such questions, fast, accurate and automated measurements need to be acquired, free from human biases. Glastonbury *et al.*, 2020 describe a novel machine learning method to perform rapid acquisition of adipocyte area estimates from histological imaging data. Using these imaging derived phenotypes, Glastonbury *et al.*, 2020 assess the relationship between adipocyte size and a range of cardio-metabolic comorbidities, demonstrating that adipocyte size can vary depending on where adipose is stored throughout the body. By tying genetics with imaging data, Glastonbury *et al.*, 2020 were able to demonstrate that previous findings associating adipocyte size with Type 2 Diabetes variants, are likely to be false positives. This study provides a means of being able to scale up GWAS type analyses to imaging derived phenotypes.

Introduction

Although obesity is a heritable and heterogeneous cardiometabolic risk factor, little is known about how genetic variation influences human adipocyte size across adipose depots or how such variability may confer risk to obesity and other cardiometabolic outcomes [1–4].

A defining feature of obesity is an excess of white adipose tissue (WAT). WAT mass expansion can occur in a range of adipose depots. The two most well defined depots are subcutaneous WAT and visceral WAT, where adipose accumulates in intra-abdominal depots present mainly in the mesentery and omentum and which drains through the portal circulation to the liver [5]. WAT expansion, both in normal development and in the development of obesity, is defined by two mechanisms: (i) *hyperplasia*, the increase in the number of adipocyte precursor cells, leading to an overall increase in the number of mature adipocytes; and (ii) *hypertrophy*, the increase in size of adipocytes due to lipid filling [6–8]. Reduced total adipocyte number has been associated with type 2 diabetes (T2D) [9], and increased adipocyte size has been associated with insulin resistance, dyslipidemia, hepatic steatosis, and the onset of T2D [10–11]. In addition, similar adipocyte sizes observed in BMI-concordant twins suggests a strong genetic background underlying adipocyte size [12]. To date, little is known about the genetic variation or molecular pathways that regulate adipocyte morphology (e.g., size, density, and morphology) [6,13], or how these link to biological mechanisms, whole-body obesity related traits such as BMI and waist-hip-ratio (WHR), and subsequent cardiometabolic disease [14].

We therefore sought to explore the relationship between mean adipocyte area and anthropometric traits like WHR and BMI, as well as investigate the genetic underpinnings of mean adipocyte area by combining histology data of fat tissue with accompanying genetic variation data from the same samples. Whilst adipocyte counting software exists [15], we chose to focus

on adipocyte area as a more tractable problem to solve. However, as a by-product of measuring adipocytes, we also get an approximate count (proportional to total fat mass).

To allow for rapid, automatic quantification and segmentation of mean adipocyte area in adipose histology slides from subcutaneous and visceral tissue collected from four independent research cohorts, we developed and applied a Convolutional Neural Network (CNN). For the first time to our knowledge, we couple the use of image-derived adipocyte area estimates to test for associations with BMI, WHR adjusted for BMI (WHRadjBMI), and a range of glycemic traits. Finally, we report the first genome-wide association study (GWAS) of adipocyte surface area to date, with the goal of identifying common genetic variants that associate with adipocyte morphology and to investigate previously published links to adipocyte morphology. Whilst several adipocyte measurement software exist [15–17], we demonstrate better accuracy and runtime.

Results

Applying a convolutional neural network to obtain region of interest proposals from thousands of histology slides and millions of cells

We ascertained histology and genotyping data from four independent cohorts (Table 1): (1) the Genotype-Tissue Expression (GTEx) Project, comprised of a multi-ancestry sample collected in the United States [18], with adipose tissue sampled from the lower leg (subcutaneous) and greater omentum (visceral); (2) the Endometriosis Oxford (ENDOX) project from the Endometriosis CaRe Centre, University of Oxford, with adipose tissue sampled from beneath peri-umbilical skin (subcutaneous) and from the bowel and omentum (visceral) of women undergoing laparoscopy for suspected endometriosis; (3) severely/morbidly obese patients undergoing elect abdominal laparoscopic surgery in the Munich Obesity BioBank (MOBB), with adipose tissue sampled from the upper abdominal area (subcutaneous) and the angle of His (visceral); and (4) a healthy cohort selected for not having type 2 diabetes (fatDIVA), with subcutaneous tissue sampled from the abdomen (see Methods for more detail).

To obtain adipocyte surface area measurements, we devised a deep learning pipeline that performs automatic classification of putative adipose cell containing Region of Interest (ROI) proposals in whole adipose tissue histology slides followed by segmentation of the images and then quantification, allowing us to filter tiles of slides that do not contain adipocytes (Fig 1).

Whole Slide Images are split into 1024 X 1024 pixel “tiles”. A Convolutional Neural Network (CNN), InceptionV3, pretrained on ImageNet and fine-tuned on adipose histology tiles, is used to assign probabilities to tiles containing adipocytes. Using high confidence adipocyte containing tiles (*Posterior Probability* > 0.9) alongside manually created binary segmentation masks, we implemented a U-net CNN to segment adipocytes. We then apply a probability threshold to each segmentation probability map [19] (see Data Availability and Code for

Table 1. Description of cohorts included in adipocyte morphology phenotyping and meta-analysis. | Histology sample sizes denote the number of tissue samples available in either the subcutaneous (subq) or visceral (visc) depots, after image quality control was complete (see Methods).

Cohort	N, histology (SC/VC) [†]		% female	Mean age	Mean BMI	% with T2D	N, both genetic and histology data	
	subq	visc					subq	visc
GTEx	715	562	34%	53.4	27.5	22%	504	410
ENDOX	308	42	100%	32.9	26.5	not available	105	23
MOBB	142	171	67%	46.5	44.4	30%	113	131
fatDIVA	123	0	58%	58.0	24.9	0%	98	0

<https://doi.org/10.1371/journal.pcbi.1008044.t001>

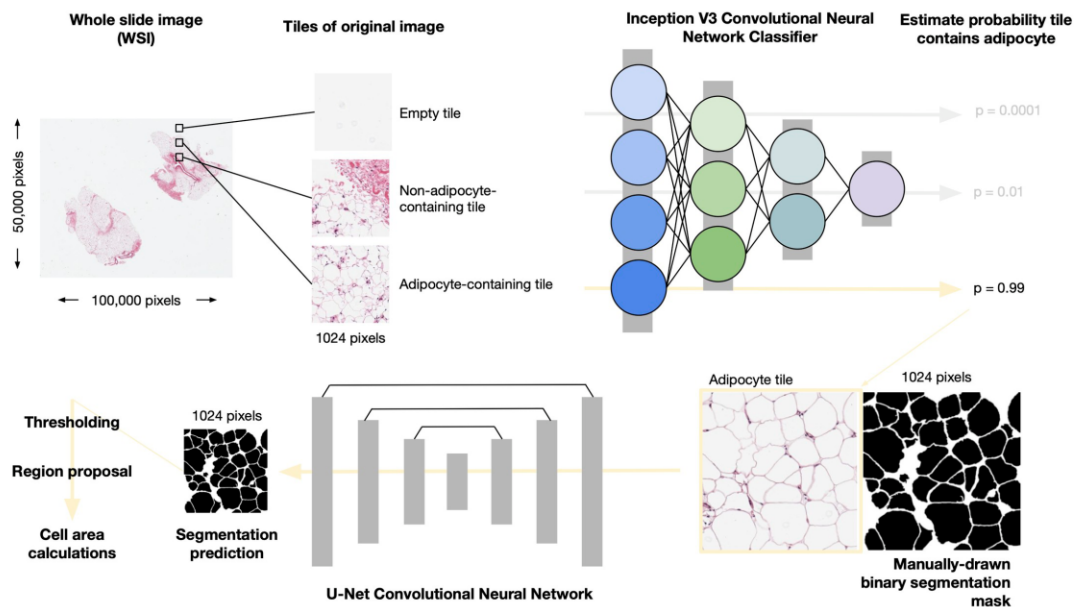


Fig 1. Overview of the pipeline to obtain adipocyte areas.

<https://doi.org/10.1371/journal.pcbi.1008044.g001>

details), regions are proposed using scikit-learn and areas calculated. Pixel areas are converted into μm^2 using the appropriate micron per pixel conversion factor per image.

First, we tiled each histology image slide using a sliding window of 1024×1024 pixels. We applied this tiling strategy across GTEx and ENDOX samples; the MOBB and fatDIVA cohorts already consisted of images containing adipocytes, and therefore required no tiling or filtering. Next, we manually selected tiles to form a training dataset of three distinct classes: (i) tiles containing adipocytes, (ii) tiles containing no adipocytes, and (iii) empty tiles. Example images of these three tile classes are shown in **Fig A in S1 Text**. To obtain only tiles containing adipocytes, we fine-tuned an InceptionV3 deep convolutional neural network (CNN) [20]; our CNN achieved 97% accuracy on our held out validation set (**Methods**). For each tile, we obtained the posterior probability that the tile belonged to one of the three defined tile classes (**Methods**) and defined the set of tiles containing adipocytes as those tiles exceeding a posterior probability threshold of $P > 0.90$ for being in that particular class. Choosing such a large posterior probability ensured we obtained images of just adipocytes and no other contaminant tissue (resulting in a low false positive rate and a high false negative rate). Examples of image tiles classified as adipocyte, non-adipocyte or empty at $P > 0.90$ are presented in **Fig B in S1 Text**.

Using deep adipocyte U-net to robustly segment cells and estimate cell area

To measure adipocyte surface area, we treated the task as a segmentation problem. We created a training dataset of 175 high resolution, hand drawn, manually segmented ($1024 \text{ pixels} \times 1024 \text{ pixels}$) binary segmentation masks across all four cohorts (**Methods**). Binary segmentation masks are images in which adipocyte/foreground are represented by white pixels taking on

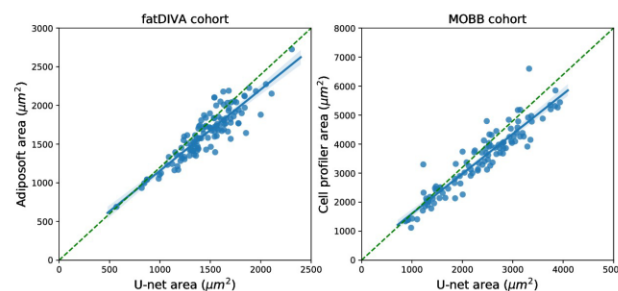


Fig 2. Comparison of Adipocyte U-net-estimated adipocyte area with Adiposoft and CellProfiler-estimated adipocyte area across fatDIVA and MOBB cohort. Estimates from our Adipocyte U-Net and from Adiposoft or CellProfiler are highly correlated, indicating concordance between our method and the two current gold standards for measuring cell morphology. The time necessary to compute these estimates with Adipocyte U-net was several orders of magnitude faster than the time required by Adiposoft/CellProfiler to generate the same measures.

<https://doi.org/10.1371/journal.pcbi.1008044.g002>

value 1 and the background pixels are black, represented as 0 (normalised from pixel space [0–255] to [0–1]) (Methods). While automated segmentation methods such as watershed and adaptive thresholding methods (as implemented in Adiposoft and CellProfiler [17,21]) can be effective for some image analysis, deep learning has shown state-of-the-art performance in semantic segmentation, object recognition and biomedical segmentation tasks [22–25]. Additionally, our approach benefits from GPU-acceleration, as it is currently not feasible to analyse tens of hundreds to millions of images with traditional methods relying on serial CPU compute, Graphical User Interfaces (GUI), or both. Therefore, we trained a U-net architecture, which we call the Adipocyte U-net (Methods), to produce binary segmentation masks of adipocytes that are then trivial to count and measure computationally. Our Adipocyte U-net achieved a held-out performance dice coefficient of 0.84 (Methods), indicating a high degree of overlap between our predicted segmentation and the ground truth known segmentation in the heldout test set (see Methods).

To benchmark and validate our Adipocyte U-net, we used two cohorts that had previously independently (blindly) estimated adipocyte surface area for all individuals using Adiposoft (fatDIVA) and CellProfiler (MOBB), alongside significant manual gating and expert correction of area predictions. These two methods are the current state of the art approaches for segmenting both adipocyte histology images (Adiposoft) and images of a wider array of cells more generally (CellProfiler) [16,26,27]. We show significant concordance between independent adipocyte area estimates between either FatDIVA ($r_{\text{subq}} = 0.91$, $P = 8.3 \times 10^{-45}$) or MOBB ($r_{\text{visc}} = 0.94$, $P < 2.2 \times 10^{-16}$, $r_{\text{subq}} = 0.91$, $P 2.2 \times 10^{-16}$) and our novel adipocyte estimation method, Adipocyte U-net (Fig 2). Adipocyte area estimates from the Adipocyte U-net were, on average smaller, compared to the area estimates obtained by other methods. This can be attributed to a difference in cutoff values of cell size being used to exclude small, improperly gated objects between methods.

As a second, non-histology based validation strategy, we compared fat cell size from collagenase digestion to adipose U-net area estimates in the MOBB cohort. Independent of the depot, and similar to the histological validation above, we observed agreement between both methods ($n_{\text{subq}} = 46$, $r_{\text{subq}} = 0.41$, $P_{\text{subq}} = 5.0 \times 10^{-3}$; $n_{\text{visc}} = 65$, $r_{\text{visc}} = 0.59$, $P_{\text{visc}} = 2 \times 10^{-7}$) (Fig O in S1 Text). As previously reported, we find that whilst adipocyte area estimates vary substantially dependent on the method used for quantification, the correlation of adipocyte size and obesity is robust to these differences [28].

Our Adipocyte U-net required less than 6 minutes to predict adipocyte surface area across the ~10,000 images included in fatDIVA and MOBB. In comparison, Adiposoft took ~3.5 hours. GTEEx and ENDOX, our largest cohorts, each consisting of approximately 250,000 images, took ~1 hour using the Adipocyte U-net, whilst we estimate Adiposoft would take 19 days for a single run. Additionally, our method captured adipocytes that are absent in Adiposoft produced segmentation masks (Fig C and Fig D in S1 Text). Examples of the test segmentation quality are presented in Fig E in S1 Text (all data and code available, see Data Availability & Code).

Adipocyte area differences from adipose depots throughout the human body

We next utilised our Adipocyte U-net to obtain area estimates from our four cohorts. These cohorts totaled 2,176 samples (multiple distinct adipose depots per subject) (Table 2) making it the largest study of adipocyte morphology of its kind.

For adipocyte area estimation, we obtained estimates for the mean as well as the standard deviation of adipocyte size for 500 unique cells/per sample/per depot (subcutaneous and visceral). We determined 500 unique cells to be a necessary minimum for stable, low variance estimates of adipocyte surface area by applying Monte Carlo sampling (Fig F in S1 Text). Given the different metabolic and physiological roles subcutaneous and visceral adipose tissue depots play [29], we compared their mean adipocyte cell surface area and performed a random-effects meta analysis to compare adipocytes across visceral and subcutaneous adipose depots. A depot-specific effect was observed ($P_{\text{meta}} = 9.8 \times 10^{-7}$, $\beta = -0.55$), with larger cells on average observed in subcutaneous adipose depots, as previously reported [30] (Fig G in S1 Text). ENDOX cohort samples showed no significant, but directionally consistent, differences across the two depots (t-statistic = -1.52, $P = 0.13$), likely due to limited power in this cohort ($N = 42$ visceral samples vs. $N = 562$ in GTEEx; Fig 3). Finally, we observed variation within each depot, further demonstrating how adipocyte size within a single depot can vary substantially (Fig 3 and Fig I in S1 Text).

As body fat distribution and its genetic basis is sexually dimorphic [1,3], we tested for sexual dimorphic effects in adipocyte morphology. A depot-specific meta-analysis showed that mean adipocyte area in visceral, but not subcutaneous adipose, is sexually dimorphic (Fig G in S1 Text). Our meta-analysis indicated that women had smaller adipocytes in visceral fat ($P_{\text{meta}} = 3.05 \times 10^{-7}$, $\beta = -0.34$, $I^2 = 0$). While females have larger adipocytes in subcutaneous adipose as compared to men, this result was not significant when meta-analysed across cohorts ($P_{\text{meta}} = 0.08$, $\beta = 0.186$, $I^2 = 53.2$), adjusting for BMI, age and ancestry (Fig G and Fig J in S1 Text). Due to the heterogeneity of subcutaneous adipose tissue being derived from various anatomical locations ($I^2 = 53.2$), it is possible there is a sexually dimorphic effect that is specific to precise anatomical subcutaneous adipose depots. For example, an effect ($\beta = 0.32$, $P = 3.0 \times 10^{-6}$)

Table 2. Summary of adipocyte measurements per cohort.

Cohort	Mean adipocyte area estimates (μm^2)	
	Subcutaneous	Visceral
GTEEx	2,813 \pm 717	2,352 \pm 866
ENDOX	1,842 \pm 484	1,711 \pm 518
MOBB	3,239 \pm 880	2,513 \pm 850
fatDIVA*	1,461 \pm 276	N/A

*The cohort fatDIVA were ascertained to fall within a healthy BMI range and to be free of type 2 diabetes. MOBB, with the largest cell size estimates, are primarily morbidly obese subjects.

<https://doi.org/10.1371/journal.pcbi.1008044.t002>

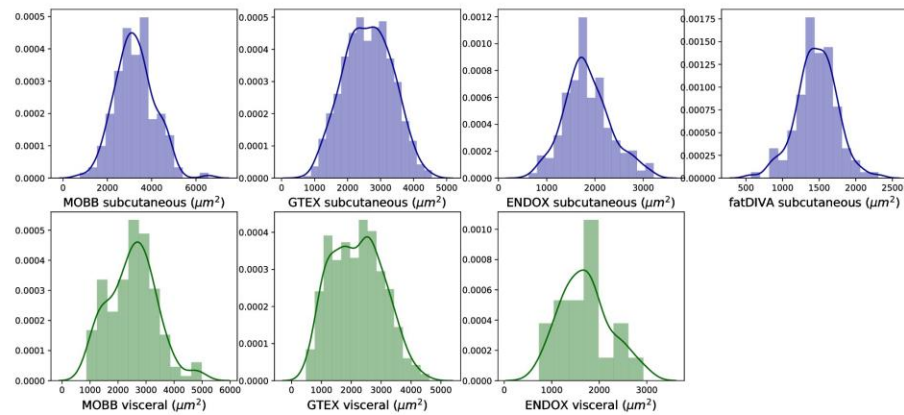


Fig 3. Mean adipocyte area across adipose depots (subcutaneous: blue, visceral: green) per sample. Visceral adipose tissue tends to have a bimodal distribution of mean adipocyte areas as compared to subcutaneous adipose tissue.

<https://doi.org/10.1371/journal.pcbi.1008044.g003>

was present in GTEx (derived from the lower leg), one of the four cohorts analysed (**Fig G in SI Text**).

Next, we assessed the relationship between adipocyte area in each depot and a range of disease relevant covariates. Previous studies have observed that obese individuals have larger adipocytes, but the vast majority of these analyses have been carried out using small sample sizes ($N < 100$) [30–31]. We recapitulate the relationship between adipocyte size and BMI in both subcutaneous and visceral depots across all four cohorts with an effective BMI range of 17–80, a range of collection methods and disease states. We observed an association between mean adipocyte area and BMI. We find that the mean adipocyte surface area in visceral fat correlates more strongly with BMI than adipocyte size in subcutaneous depots ($r_{\text{subq}} = 0.47$, $r_{\text{visc}} = 0.50$; **Fig 4**, $P_{\text{meta}} = 8.13 \times 10^{-69}$, $\beta = 0.45$), significant after adjustment for sex, age, T2D status, and

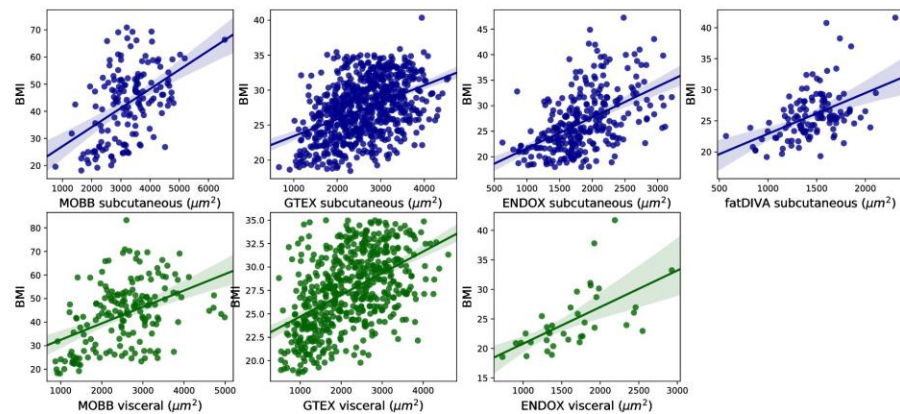


Fig 4. Association between mean adipocyte area and BMI across subcutaneous and visceral adipose tissue depots. We observe a strong correlation between BMI and mean adipocyte size across both subcutaneous and visceral depots in all cohorts.

<https://doi.org/10.1371/journal.pcbi.1008044.g004>

self-reported ethnicity (**Fig G in S1 Text**). We also find a significant positive association between adipocyte area and subject age in visceral, but not subcutaneous adipose tissue, when meta-analysed across all available cohorts ($P_{\text{subq meta}} = 0.09$, $\beta = 0.09$; $P_{\text{visc meta}} = 0.01$, $\beta = 0.12$) (**Fig G in S1 Text**).

As GTEx samples are collected post-mortem, and numerous publications have shown a range of significant associations between sample ischemic time and assays performed on GTEx subjects [32–33], we assessed the relationship between our adipocyte area estimates, and sample ischemic time across depots. We find a positive association between mean adipocyte area and sample ischemic time ($P_{\text{subq}} = 1.7 \times 10^{-4}$, $\beta_{\text{subq}} = 0.14 \pm 0.037$; $P_{\text{visc}} = 6.8 \times 10^{-4}$, $\beta = 0.14 \pm 0.042$) suggesting a relationship between longer ischemic time and larger cells, most likely due to cell degradation and/or bursting, leading to overestimation of cell surface area from broken or joining cell membranes or due to failed staining. Additionally, we found no association between cell estimates and self-reported ethnicity for both depots ($P = 0.59$). Finally, studies have found conflicting evidence regarding a relationship (or lack thereof) between adipocyte size and insulin resistance or T2D status [31,34,35]. We meta-analyzed GTEx and MOBB, as T2D status was available for both, and did not observe a significant relationship between adipocyte size and T2D for either depot ($P_{\text{visc meta}} = 0.11$, $\beta = 0.12$; $P_{\text{subq meta}} = 0.37$, $\beta = -0.19$) (**Fig G** and **Fig K in S1 Text**). As a range of glycemic state variables (HbA_{1C} and fasting blood glucose) were available for the MOBB cohort, we ran a multiple linear regression adjusting for BMI and age to investigate the relationship between adipocyte size and glucose homeostasis. Independent of the depot, no significant associations between glucose or HbA_{1C} and adipocyte size were found (Glucose: $n_{\text{subq}} = 110$, $p_{\text{subq}} = 0.71$, $n_{\text{visc}} = 124$, $p_{\text{visc}} = 0.061$; HbA_{1C}: $n_{\text{subq}} = 79$, $p_{\text{subq}} = 0.75$, $n_{\text{visc}} = 86$, $p_{\text{visc}} = 0.059$). While this suggests that BMI might act as the primary modifier of adipocyte size in these depots, further studies in larger cohorts including clinical biochemistry parameters of glucose homeostasis are necessary to clearly elucidate the role between diabetic state and adipocyte size.

For the MOBB cohort, we had additional extensive clinical measurements, including C-reactive protein, glucose, triglycerides and 12 additional clinical chemistry-derived phenotypes (**Fig H in S1 Text**). We observed several relationships between increased adipocyte size and WHR ($r_{\text{subq}} = 0.28$, $r_{\text{visc}} = 0.33$), C-reactive protein ($r_{\text{subq}} = 0.17$, $r_{\text{visc}} = 0.26$), prealbumin ($r_{\text{visc}} = 0.21$), gGT ($r_{\text{subq}} = 0.17$, $r_{\text{visc}} = 0.21$), thyroxine T3 ($r_{\text{visc}} = 0.3$) and triglycerides ($r_{\text{visc}} = 0.18$), demonstrating a wide range of depot-specific associations. Of these associations, only BMI ($P_{\text{subq}} = 3.6 \times 10^{-10}$; $P_{\text{visc}} = 5.6 \times 10^{-11}$) remained significant after adjustment for multiple testing in 19 phenotypes ($P = 2.6 \times 10^{-3}$). Together, these analyses suggest that obesity, as measured through BMI, is the dominant phenotype associated with adipocyte size, with mean adipocyte size in visceral fat accounting for, on average, 25% of the variance of BMI (**Fig 4**).

GWAS meta-analysis of depot-specific adipocyte surface area estimates

We sought to use our histology-derived phenotype data to identify common genetic variants (single nucleotide polymorphisms, SNPs) that associate with mean adipocyte size or variance of adipocyte size in subcutaneous and visceral tissue. After data quality control and imputation using the Haplotype Reference Consortium [36] for those cohorts with SNP array data (**Methods**), we used the histology phenotypes to perform genome-wide association testing in each depot and for each cohort. We then meta-analysed the results in an inverse variance fixed effects meta-analysis. In addition to performing the meta-analysis across the combined sample, we performed sex-specific analyses for each depot and each phenotype (mean adipocyte size and variance of adipocyte size).

Our meta-analysis in the combined sample in the subcutaneous depot examined 820 samples (424 women and 396 men) with available subcutaneous histology data, while our meta-

analysis in the visceral depot tested 564 samples (259 women and 305 men) with relevant available histology data. We performed all GWAS analyses using Plink 1.9 and adjusted analyses for sex, age, BMI, and the first 10 principal components (**Methods**). As the ENDOX cohort was genotyped on two separate platforms, we additionally adjusted these GWAS for genotyping platform. Due to ancestral heterogeneity in GTEx, we reduced our sample to just those individuals of European descent (**Methods**). We accounted for testing two separate depots by setting genome-wide significance at $P < 2.5 \times 10^{-8}$.

No SNP in our meta-analysis achieved genome-wide significance ($P < 2.5 \times 10^{-8}$), likely due to limited power given the small sample size. A small number of loci in our meta-analyses contained common SNPs at $P < 5 \times 10^{-7}$ with consistent direction of effect across all available cohorts (see summary-level results in **Data and Code Availability**), representing regions of interest for further genome-wide association testing.

Finally, we used our largest cohort (GTEx) to estimate the SNP-based heritability of the adipose histology phenotypes analysed here (**Fig L in S1 Text**). We used Genome-wide Complex Trait Analysis (GCTA) [37] to perform Restricted Maximum Likelihood (REML) analysis to estimate SNP-based heritability in each cell phenotype and across all sample groups (combined samples, women only, and men only). Cell phenotypes in both depots appear to be heritable traits, but error estimates were broad (h^2 of mean cell size in subcutaneous tissue = 35.3%, \pm 38.4%; h^2 of mean cell size in visceral tissue = 22.4%, \pm 48.5%; **Fig A in S1 Text**) reflecting that analysis of a larger set of samples is necessary for more accurate estimates of trait heritability.

Association signals at previously published adipocyte size loci

Two adipocyte size common variant associations exist in the literature: the *KLF14* locus (rs4731702, found in 18 men and 18 women) and the *FTO* locus (rs1421085, found in 16 risk and 26 non risk-allele carriers). While the *KLF14* locus was characterised using adipose tissue histology from non-obese female individuals, the *FTO* locus was characterized using isolated floating mature adipocytes in subcutaneous adipose tissue from lean ($20 < \text{BMI} < 24$), population-level male individuals [38–39]. In our meta-analysis, we find no evidence to support associations for either rs4731702 ($P_{\text{combined}} = 0.925$, $P_{\text{females}} = 0.662$, and $P_{\text{males}} = 0.158$ for mean adipocyte size in subcutaneous tissue) or rs1421085 ($P_{\text{combined}} = 0.735$, $P_{\text{females}} = 0.426$, $P_{\text{males}} = 0.609$ for mean adipocyte size in subcutaneous tissue; **Fig B in S1 Text & S2 Table**).

KLF14 is a female-specific type 2 diabetes-imprinted locus, it is only expressed from the maternally inherited allele. Additionally, rs4731702 has been linked to T2D risk in recent GWAS, with the locus only significant in female samples [38]. Because of this, we took further steps to mirror the original study design as best as possible in each of our cohorts. We excluded heterozygotes, only considering non-risk allele and risk-allele homozygotes, only considered genotype data from pre-menopausal women and subjects within a normal BMI range: $18 < \text{BMI} < 30$. After this stratification we observe a nominal association similar to the original study ($P = 0.012$ $n = 18$ risk allele carriers (CC) and $n = 14$ non-risk subjects (TT), having larger subcutaneous adipocytes (**Fig M in S1 Text**)). However, when we repeat this analysis in GTEx visceral fat samples and ENDOX subcutaneous fat samples, we see no evidence of association (GTEx, $P = 0.68$, n_{CC} individuals = 9, n_{TT} individuals = 9; ENDOX $P = 0.91$, $n_{\text{CC}} = 19$, $n_{\text{TT}} = 19$; **Fig N in S1 Text**). We were unable to perform these analyses in either fatDIVA or MOBB due to the absence of non-risk allele carriers remaining after sample filtering (fatDIVA) or due to the nature of the study design (MOBB, which contains a majority of morbidly obese subjects).

For *FTO* we were unable to similarly mirror the study design as we were able to do for the *KLF14* locus, given that the reported effect was specific to lean male individuals. Nevertheless,

we performed analysis to test for association between *FTO*-rs1421085 and adipocyte size in GTE_x (n risk allele carriers (CC) = 73, n non-risk allele carriers (TT) = 246). In subcutaneous fat, *FTO*-rs1421085 was not significantly associated to adipocyte surface area in joint ($P = 0.39$, n = 319), female ($P = 0.75$, n = 125) or male-specific analysis ($P = 0.08$, n = 194), controlling for the effects of age and BMI. In visceral fat, *FTO*-rs1421085 was also not significantly associated to adipocyte surface area in joint ($P = 0.59$, n = 248), female ($P = 0.98$, n = 98) or male-specific analysis ($P = 0.34$, n = 150), controlling for age and BMI. Lastly, *FTO*-rs1421085 was not significant in ENDOX (female-specific subcutaneous cohort) ($P = 0.78$, N = 40), MOBB (morbidly obese) ($P_{\text{subq}} = 0.67$, $n_{\text{subq}} = 68$; $P_{\text{visc}} = 0.86$, $n_{\text{visc}} = 74$) or fatDIVA (normal range BMI and T2D free) ($P = 0.34$, n = 52).

Association signals at previously published loci associated to obesity and fat distribution

We additionally sought to test whether known obesity and fat distribution loci were enriched for signal in our histology GWAS. We therefore looked up the index SNPs at loci associated to BMI and WHRadjBMI in our meta-analyses [3]. Of the 670 index SNPs associated to BMI and the 346 index SNPs associated to WHRadjBMI, approximately 3–7% of these SNPs achieved $p < 0.05$ in our histology GWAS. Similarly, of the index SNPs associated to either BMI or WHRadjBMI in sex-specific analyses, 2–5% achieved $p < 0.05$ in our sex-specific histology GWAS. These results indicate no significant enrichment for signal at BMI- or WHRadjBMI-associated SNPs in our histology GWAS, consistent with the limited power we see in our overall analysis.

We additionally looked up those SNPs in our histology GWAS achieving a 'suggestive' p-value ($p < 5 \times 10^{-7}$) in large-scale meta-analysis of BMI or WHRadjBMI. Only one SNP, rs72811236, achieves nominal significance ($p < 0.05$) in a GWAS of BMI restricted to women only. This SNP may represent a bona fide association to adipocyte size, but additional samples are necessary to establish whether or not a true association exists in this region.

Associations between obesity-trait genetic risk scores and adipocyte area

We tested for associations between genetic risk scores (GRSs) for BMI, WHR, and WHRadjBMI and mean adipocyte area in both subcutaneous and visceral fat depots (**Methods**). We observed a nominal ($P < 0.05$) association between the BMI GRS and subcutaneous mean adipocyte area. Each 1-unit higher BMI GRS (corresponding to a predicted 1-standard deviation higher BMI) was associated with $210 \mu\text{m}^2$ (95% CI 23–397 μm^2 , $P = 0.03$) larger mean adipocyte area, with comparable results for standardized adipocyte area (**S2 Table** and **S3 Table**). However, the association did not surpass our Bonferroni correction threshold of $P < 0.008$ (adjusting for three obesity trait GRSs and two fat depots). We observed no other associations between the obesity-trait GRSs and mean adipocyte area, but the confidence intervals were large, suggesting that larger sample sizes are needed to reliably assess these relationships.

Discussion

Imaging data provides a rich resource to perform rapid, accurate, and large-scale cellular phenotyping. Here, we developed the adipocyte U-net, an image segmentation machine learning model, to rapidly and accurately obtain measurements of adipocyte area from multiple human adipose depots across the human body. Whilst previous studies have used unsupervised learning methods to extract unknown cellular phenotypes and then performed GWAS on these latent representations [40], this study is the first to our knowledge that ties specific

(supervised) machine learned image phenotypes to genetic variants. We used these image-derived phenotypes to establish relationships between obesity, age, sex, T2D, and a range of clinical covariates. However, most associations we find are attenuated and no longer significant after conditioning on BMI, suggesting BMI is the primary driver of adipocyte size ($r = 0.43\text{--}0.59$ across cohorts and adipose depots). Using adipocyte surface area as a cellular phenotype, we performed the first GWAS of adipocyte surface area. Genome-wide association testing revealed no SNP exceeding genome-wide significance ($P < 2.5 \times 10^{-8}$ after multiple test correction). Heritability estimates also indicated that adipocyte area is likely heritable, but much larger sample sizes are required to obtain tight confidence bounds.

Our approach represents an additional opportunity for the application of machine learning in genomics. The Adipocyte U-net not only enables rapid phenotyping (our method is many orders of magnitude faster than current state-of-the-art approaches), but also demonstrates how genetic association studies could begin to examine endophenotypes, such as histology imaging, rather than clinically-measured phenotypes, such as BMI or waist-to-hip ratio. Being able to interrogate high-dimensional endophenotypes in a GWAS framework may yield a more rapid uncovering of genetic variants directly linked to the biological mechanisms that underpin clinically-measured outcomes. Many such methods to derive phenotypes from images are currently being developed [22,25,41,42].

A small number of studies have previously identified common genetic variants as associated to adipocyte morphology phenotypes. We report mixed replication results at both rs4731702 (at the *FTO* locus) and rs1421085 (at the *KLF14* locus). Our initial meta-analysis results indicate no evidence for association at either SNP (S1 Table & S2 Table). It is likely given the weakness of the initial results published and their lack of power ($n < 50$) that these loci do not reflect true adipocyte size associated loci. Additionally, whilst our study has variable sample ascertainment between cohorts (for example, ENDOX is an endometriosis cohort while GTEX are population-level ascertained postmortem samples), any single cohort described here is at least twice the size of the original publications. The potential signals at these loci will require further validation in much larger meta-analyses.

We have performed the largest study of automated histology measurements using a GWAS approach. Despite this being the largest study of its kind, our total sample size is $< 1,000$ samples and we find no genome-wide associated SNPs. Our findings suggest that larger samples will be necessary to uncover associated genetic variants and more accurately estimate heritability and polygenic risk of these phenotypes. Whilst we were underpowered to obtain meta-analysis heterogeneity statistics with tight confidence intervals, and by using random-effects to account for additional per-cohort variability, we do indeed see significant heterogeneity (I^2) for phenotype-adipocyte size analyses, likely reflecting the heterogeneous collection of subcutaneous and visceral adipose tissue depots across cohorts, including differences in anatomical locations from which tissues were collected. Larger, more homogeneous samples will be especially useful to investigate sex-specific effects [1,3]. Finally, our study focuses exclusively on samples of European-ancestry, a well-described bias in human genomics, [43–44] and studies in diverse ancestral populations will be necessary to fully understand the biology of adipocyte morphology and how this links to obesity, a condition that affects populations worldwide.

Adipose tissue represents quite a homogenous and therefore easy tissue for segmentation, with many other tissues, such as the placenta, being a much more complicated mix of cells and structures [25]. Adipocyte U-net could be rapidly adapted to other cell types using as few as 50 annotations and the principles of transfer learning [45]. We envisaged future work to take advantage of the recent successes of meta-learning, in which many similar tasks, such as classifying or segmenting cells across a range of image types, are solved at the same time and any future task can be adapted to work with very few gradient updates [46].

We have developed a method to enable rapid and accurate phenotyping from histology data, enabling integration of larger histology and GWAS datasets with highly-scalable computational phenotyping methods for future studies. Such an approach can accelerate the exploration of the genetic underpinnings of cell phenotypes or other endophenotypes measured via imaging data, thus paving the way for further insights into how genetic variation may contribute to adipocyte morphology and how these mechanisms may contribute to downstream cardiometabolic disease.

Methods

Data and code availability

Relevant code and data, including images and annotations can be found at the following GitHub repository: <https://github.com/GlastonburyC/Adipocyte-U-net>. Here, you can also find links to download the summary-results from our GWAS analyses.

GWAS summary statistics used for PRS:

<https://github.com/lindgengroup/fatdistnGWAS/tree/master/SuppTable1>

Cohort collection, curation, and quality control

GTEX. The Genotype Tissue and Expression (GTEX) Project was initiated to measure gene expression and identify expression quantitative trait loci (eQTLs) in 53 tissues. The project has been previously described [18]. Briefly, samples were collected in the United States. The vast majority of samples were collected postmortem. Tissues were collected and stored according to a released protocol.

We obtained 722 subcutaneous and 567 visceral/omentum adipose tissue GTEX histology slides. All histology images were stored as whole-slide, high-resolution binary 'svs' files. All histology slides were obtained at scale 0.4942 μ m per pixel and were therefore comparable across samples. To obtain images that were of reasonable resolution for downstream processing and analysis, we tiled across each of the histology slides, producing 1024 \times 1024 pixel tiles.

All samples had missingness < 5%. We excluded samples based on the suggested sample exclusions from GTEX. These samples include large chromosomal abnormalities (e.g., trisomies, large deletions) and mosaics. Principal component analysis (PCA) indicated the cohort to be a multi-ancestry cohort (including African-, East Asian-, and European-descent samples), to be expected given that samples were collected from many different locations in the United States. Within ancestral groups, no sample had an outlying inbreeding coefficient (defined as ≥ 6 standard deviations from the coefficient distribution).

To clean SNPs, we split the samples (roughly) into subsamples of reasonably homogenous ancestral groups (for QC purposes only). We dropped all SNPs out of Hardy Weinberg equilibrium (HWE) with $P < 1 \times 10^{-6}$.

Because samples were sequenced on two sequencing platforms (HiSeq 2000, HiSeq X) we performed an association test between the SNPs on each platform and removed any SNPs with substantially different frequencies ($P < 5 \times 10^{-8}$). We ran the same association test, but this time checking for frequency differences by library preparation group and removed any associated SNP ($P < 5 \times 10^{-8}$).

After checking transition/transversion ratio by (i) site missingness, (ii) quality-by-depth (QD), and (iii) depth of coverage, we removed all sites with missingness > 0.5%, sites with QD < 5, and sites with total depth < 9000 or > 33,000. The final dataset included 635 samples and >35M genetic variants with a minor allele count > 1.

We assessed the association of adipocyte area to a range of whole-body traits that were available in the GTEX dataset (BMI, Weight, Ischemic time & Type 2 Diabetes status).

Abdominal laparoscopy cohort—Munich Obesity BioBank / MOBB. We obtained subcutaneous and visceral adipose tissue histology slides from a total of 188 morbidly obese male (35%) and female (65%) patients undergoing a range of abdominal laparoscopic surgeries (sleeve gastrectomy, fundoplication or appendectomy). The visceral adipose tissue is derived from the proximity of the angle of His and subcutaneous adipose tissue obtained from beneath the skin at the site of surgical incision. Images were acquired at 20× magnification with a micron per pixel value of 0.193μm/pixel. Collagenase digestion and size determination of mature adipocytes was performed as described previously [47]. All samples had genotypes called using the Illumina Global Screening beadchip array.

Collaborators from MOBB—the abdominal laparoscopy cohort, sent DNA extracted from 192 samples to the Oxford Genotyping Center for genotyping on the Infinium HTS assay on Global Screening Array bead-chips. Genotype QC was done using GenomeStudio and genotypes were converted into PLINK format for downstream analysis. We checked sample missingness but found no sample with missingness > 5%.

To perform the remaining sample quality control (QC) steps, we reduced the genotyping data down to a set of high-quality SNPs. These SNPs were:

- a. Common (minor allele frequency > 10%)
- b. Had missingness < 0.1%
- c. Independent, pruned at a linkage disequilibrium (r^2) threshold of 0.2
- d. Autosomal only
- e. Outside the lactase locus (chr2), the major histocompatibility complex (MHC, chr6), and outside the inversions on chr8 and chr17.
- f. In Hardy-Weinberg equilibrium ($P > 1 \times 10^{-3}$)

Relevant information, including code and region annotations, can be found in the GitHub repository provided in the Data and Code Availability section at the beginning of the

Methods.

Using this high-quality set of ~65,000 SNPs, we checked samples for inbreeding and heterozygosity (—het in PLINK), but found no samples with excess homozygosity or heterozygosity (no sample >6 standard deviations from the mean). We also checked for relatedness (—genome in PLINK) and found one pair of samples to be identical; we kept the sample with the higher overall genotyping rate. Finally, we performed PCA using EIGENSTRAT and projected the samples onto data from HapMap3, which includes samples from 11 global populations. Six samples appeared to have some amount of non-European ancestral background, while the majority of samples appeared to be of European descent. We removed no samples at this step, selecting to adjust for principal components in genome-wide testing. However, adjustment for principal components failed to eliminate population stratification, and we therefore restricted to samples of European descent only, defined as samples falling within +/- 10 standard deviations of the first and second principal component values of the CEU (Northern and Western European-ancestry samples living in Utah) and TSI (Tuscans in Italy) samples included in the HapMap 3 dataset [48–49]. Finally, sex information was received after initial sample QC was complete. As a result, one sample with potentially mismatching sex information (comparing genotypes and phenotype information) was discovered after analyses were complete and therefore remained in the analysis.

Beginning with all SNPs available in the MOBB dataset (~800,000), we first removed all SNPs with missingness > 5% and out of HWE, $P < 1 \times 10^{-6}$. We also removed monomorphic

SNPs. Finally, we set heterozygous haploid sites to missing, in order to enable downstream imputation.

The final cleaned dataset included 190 samples and ~700,000 SNPs. We note that histology data was not available for all genotyped samples.

fatDIVA. “fatDIVA” (Function of Adipose Tissue for DIabetes VARIants) is a recruit-by-genotype study aiming to understand more about the mechanisms of differences in adipose tissue function. Research volunteers were identified by the NIHR Exeter Clinical Research Facility (Exeter CRF) and recruitment facilitated within the Exeter CRF. Before recruitment into fatDIVA, approximately 6,000 anonymised DNA samples from the Exeter 10,000 (EXTEND) study were genotyped on the Global Screening Array and imputed to the Haplotype Reference Consortium reference panel. A genetic risk score of 11 variants was then calculated for each individual and weighted by effects on fasting insulin. These 11 variants formed an early version of a “favourable adiposity” genetic score—where collectively the alleles associated with higher fat mass were associated with a favourable metabolic profile, and vice versa [50].

Individuals falling into the 5% lowest tail of the weighted genetic score were contacted and, if agreeing to take part in the study, matched to age (± 4 years), sex and BMI (± 1 unit) to an individual in the highest 20% of the weighted genetic score. Inclusion criteria were age 18–75 and exclusion criteria were: treated Diabetes (including insulin and GLP-1 analogues), history of bariatric surgery and recent significant weight loss/gain (± 3 kgs in the last 3 months); connective tissue disease, pregnancy and lactation, inflammatory or consuming conditions, and the following medications: prescribed glucose-lowering medication, lipid-lowering treatment (such as statins, fibrates or ezetimibe) or other medication that alters lipids (such as beta blockers and diuretics), oral/IV corticosteroid treatment or loop diuretics (furosemide, bumetanide), antiplatelet and anticoagulation medication, methotrexate. All participants were asked to refrain from strenuous exercise and from eating very fatty meals in the 48 hours prior to coming into the clinic, then fast overnight prior to attending a one-off morning visit at the Exeter CRF. A sample of abdominal fat was obtained by firstly injecting some local anaesthetic into an accessible area of the abdomen. Using a scalpel, a small incision (approx 2-3cm) was made to a depth of approx 15mm and a small (pea-sized) sample of fat removed. The wound was closed with simple sutures or steristrips. Part of the fat sample was stored in formalin for later H&E staining. For each individual, a H&E stained slide was examined under a microscope and ten photographs of different parts of the slide taken, with the operator choosing sections with a clear vision of adipocytes wherever possible. Adiposoft software was used to identify and quantify the area of adipocytes.

Samples had previously been imputed using the HRC panel and sent in best-guess genotype format.

Phenotypic and genetic sex information was consistent for all samples with available sex information. For all samples with sex information missing in the phenotype data, we used the genotypic sex to infer sex of the sample. A relatedness check found two pairs of related samples ($\pi\text{-hat} > 0.125$). Because all samples were imputed (missingness is 0) we arbitrarily removed one sample from each pair. One sample had an inbreeding coefficient > 6 s.d from the mean of the inbreeding coefficient distribution, and was therefore removed. PCA indicated all samples to be of European descent.

We removed all monomorphic SNPs from the dataset and removed any SNP out of HWE ($P < 1 \times 10^{-6}$). The final dataset comprised 254 samples and > 8.8 M SNPs.

ENDOX Endometriosis case/control study. Samples were genotyped at the Oxford genotyping center on two arrays: the Affymetrix Axiom (UK Biobank chip) ($n = 56$) and the Illumina Infinium Global Screening Array ($n = 127$).

Samples were cleaned in a manner identical to those samples in the abdominal laparoscopy (MOBB) and fatDIVA cohorts. No samples had missingness >5% and all samples were consistent in phenotypic and genotypic sex (all female). No sample was an outlier in the inbreeding check, and no pair of samples appeared to be related (pi-hat threshold of 0.125, equivalent to a cousin relationship). PCA using HapMap 3 data showed that all samples were of European descent.

SNPs were cleaned in a manner identical to those samples in the abdominal laparoscopy and fatDIVA cohorts. The final cleaned dataset included 127 samples and ~685,000 SNPs on the Illumina Array and 56 samples and 655,000 SNPs on the Affymetrix array.

For the genotyped cohorts without imputation data (ENDOX and MOBB) we performed imputation via the Michigan Imputation Server. We aligned SNPs to the positive strand, and then uploaded the data (in VCF format) to the server. We imputed the data with the Haplotype Reference Consortium (HRC) panel, to be consistent with the fatDIVA data which was already imputed with the HRC panel. We selected EAGLE as the phasing tool to phase the data. To impute chromosome X, we followed the server protocol for imputing this chromosome (including using SHAPEIT to perform the phasing step).

Region of Interest proposal: InceptionV3 CNN. We defined our Regions of Interest (ROIs) “adipocyte-only” training set tiles as having little to no vessels, smooth muscle or other tissue/contaminate present and that were composed of well shaped, viable, non-ruptured adipocytes that filled the majority of the tile (>80%). To automate this procedure, we trained an InceptionV3 deep convolutional neural network (CNN) architecture using transfer learning [20]. Whilst the original InceptionV3 network was trained on 1000 ImageNet classes [51], we only wanted to classify empty, adipocyte-only and non-adipocyte containing tiles. To do this, we removed the final dense layer and replaced it with an AveragePooling layer with (8,8) convolutions and a stride of 8. Our final layer consisted of a fully connected layer with outputs representing our three classes. We used a softmax activation to obtain posterior probabilities of any given tile belonging to one of our three classes. For a tile to be classified as containing adipocytes, we use only high confidence calls (Posterior Probability > 0.9). We used Stochastic Gradient Descent (SGD) with Nesterov momentum (0.9) and a learning rate of 1.0×10^{-4} . We trained the network on 2,729 tiles, approximately equally distributed across each class from both subcutaneous and visceral depots. We used a 80:20 train:validation split. The model reached a training accuracy of 95% and validation accuracy of 96.6%. Our trained classifier and weights are available to use in a Jupyter notebook (see: **Data and Code Availability**) [52].

U-net architecture. To obtain robust count and area estimates of adipocytes we used a deep convolutional neural network architecture based on a modified U-net, originally designed to perform biomedical image segmentation in a low sample size regime [23]. We used 175 manually created ground-truth segmentations of adipocyte tiles of resolution 1024×1024 . We demonstrate our network learns the correct segmentation mask and predicts adipocytes that are commonly missed by Adiposoft (**S3 Fig**). Each adipocyte tile and corresponding mask were concatenated to create a large ‘ensemble image’ which we then sampled 1024×1024 input images from. For validation, we used 10% of the data ensuring that the same image samples never overlapped for training and validation. Our loss function was a dice binary cross-entropy loss, and a dice coefficient metric was used to assess performance. The Dice coefficient measures the degree of overlap between two segmentations (A: ground truth, B: predicted) and takes on a value between 0 and 1, with 1 representing a perfect score:

$$Dice_{A,B} = \frac{2(A \cap B)}{(A + B)}$$

The final validation Dice coefficient was 0.844. As an output, we obtain a pixel-wise probability map per input image of the same dimensions with each pixel classified as an adipocyte or not. The trained U-net model architecture, corresponding weights, and jupyter notebooks are all publicly available (see: **Data and code availability**).

Adipocyte area estimation. To obtain robust adipocyte area estimates we utilised the output of our Adipocyte U-net. To further refine our predictions, we thresholded the probability maps and transformed them into grey-scale images. To obtain counts and area estimates for every cell in the image, we used the *'regprop'* function in the scikit-learn library. As a quality control step, we removed cell area estimates less than $200\mu\text{m}^2$ and greater than $16,000\mu\text{m}^2$, which typically represented cell debris and joined adipocytes where H&E staining had failed, respectively. As the quality of the histology slides varied significantly, our ROI method and use of a fixed number of cells per sample was essential to avoid any significant sample specific biases.

Network training hardware and software specification. U-net training took approximately 20 hours and the InceptionV3 fine tuning ran in under one hour. Inception tile classification for all samples took 13 hours (classification of more than 2 Million images) and Inference/Prediction on 1024×1024 images for the U-net took 22 hours (240,000 images). All models were implemented in Keras/Tensorflow. All networks were trained on a single server with a one Titan X pascal NVIDIA card, 12Gb of GPU memory and 64Gb of RAM.

Phenotype-Adipocyte size meta-analysis. All phenotype-adipocyte meta-analyses were conducted using the R package *'meta'* and *'metafor'* [53]. As our cohorts come from heterogeneous populations and both subcutaneous and visceral adipose depots are taken from various anatomical locations, we chose to use a random effects meta-analysis to capture the distributional differences in adipocyte size across cohorts. Whilst underpowered to estimate heterogeneity accurately, we calculated I^2 , a statistic that quantifies the proportion of the variance in the meta-analysis attributable to heterogeneity.

Genome-wide association testing and meta-analysis. In each cohort, we implemented a genome-wide association study (GWAS) of the available histology phenotypes. The GWAS in the GTEx data was performed directly on the genotypes generated from whole-genome sequencing [18]. For the other three cohorts, we performed GWAS on the best-guess genotypes resulting from imputation with the Haplotype Reference Consortium (HRC) [36]. Imputation dosages were converted to best-guess genotypes using Plink 2.0 [54]. Due to limited data availability for the X chromosome, we restricted our GWAS to the autosomal chromosomes.

We performed GWAS in each cohort using linear regression implemented in Plink 2.0 (—glm). We adjusted all GWAS for sex, age, BMI and the top ten principal components calculated from common genetic variation in the cohort using a high-quality set of markers (see **Cohort collection, curation and quality control**). For the imputed genotype cohorts, we restricted regression to those SNPs with an imputation quality (INFO) score > 0.3 . We applied no minor allele frequency threshold at this step and opted instead to filter on allele frequency once the meta-analysis was complete.

After performing GWAS within each cohort for each group of samples (all samples, women only, men only) and each phenotype (mean cell size, cell size variance) we generated quantile-quantile (QQ) plots stratified by both imputation quality score and minor allele count (**Data and Code Availability** for details) to check for excessive genomic inflation in particular bins of SNPs. We observed no evidence for stratification in any GWAS, and therefore proceeded with meta-analysis.

Once GWAS within each cohort were complete, we performed an inverse-variance fixed effects meta-analysis for each phenotype (in the combined and sex-stratified samples). We

implemented the meta-analysis in METAL [55]. Once the meta-analyses were complete, we again plotted stratified QQ plots (**Data and Code Availability** for details) to check for evidence of population stratification or other sources of confounding. We set genome-wide significance at $P < 2.5 \times 10^{-8}$, reflecting a Bonferroni correction for testing tissue from two adipose depots. As adipocyte mean size and adipocyte variance are highly correlated to one another ($r_{\text{subq}} = 0.914$ and $r_{\text{visc}} = 0.963$), we did not count the two phenotypes as independent tests.

Genetic risk scores for obesity-related traits and adipocyte area. We constructed GRSs for BMI, WHR, and WHRadjBMI using independent ($r^2 < 0.05$) primary (“index”, associated with each obesity trait $P < 5 \times 10^{-9}$) SNPs in the combined-sexes analyses in a recent GWAS [3] (see **data availability**). We excluded SNPs with duplicated positions, missingness > 0.05 , HWE $P < 1 \times 10^{-6}$, and minor allele frequency < 0.05 in the imputed data, after filtering on imputation info > 0.3 in the imputed cohorts and restricting the GTEx cohort to those of European ancestry and excluding one individual due to relatedness. For these analyses, the individual in MOBB with potential sex mismatch between genotypic and phenotypic sex was removed. Only SNPs available in all cohorts after quality control was included, resulting in a final set of 530, 259, and 274 SNPs for BMI, WHR and WHRadjBMI, respectively. The SNPs were aligned so that the effect allele corresponded to the obesity-trait increasing allele. GRSs were then computed for each participant by taking the sum of the participant’s obesity-increasing alleles weighted by the SNPs effect estimate, using plink v1.90b3 [56].

We then investigated associations with subcutaneous and visceral mean adipocyte area per 1-unit higher obesity GRS, corresponding to a predicted one standard deviation higher obesity trait, using linear regression in R version 3.4. [57]. All analyses were performed both with adipocyte area in μm^2 and in standard deviation units, computed through rank inverse normal transformation of the residuals and adjusting for any covariates at this stage. We adjusted for age, sex, and ten principal components, and with and without adjusting for BMI in the GTEx, MOBB, and fatDIVA cohorts. As we did not have access to data about age and BMI in the all-female ENDOX cohort, we only adjusted for ten principal components in that cohort and with and without adjusting for chip type. We then meta-analysed the cohorts, assuming a fixed-effects model. In the main meta-analysis model, ENDOX was included using the adjusted for chip type estimates. As a sensitivity analysis, we also reran the meta-analyses using the ENDOX estimates unadjusted for chip type and completely excluding the ENDOX cohort, yielding highly similar results.

Supporting information

S1 Text. Contains Fig A-O and Table A.
(DOCX)

S1 Table. Look-up of *KLF14* SNP reported to associate with adipocyte morphology phenotypes. We looked up rs4731702, previously reported to be associated with adipocyte morphology phenotypes, in our own genome-wide association results. We find no evidence for association at this SNP ($p > 0.05$ for all phenotypes and all sample groups).
(TXT)

S2 Table. Look-up of *FTO* SNP reported to associate with adipocyte morphology phenotypes. We looked up rs1421085, a SNP previously reported to be associated with adipocyte morphology phenotypes, in our own genome-wide association results. We find no evidence for association at this SNP ($p > 0.05$ for all phenotypes and all sample groups).
(XLSX)

S3 Table. Effect of obesity genetic risk scores on standardized and non-standardized adipocyte area in μm^2 in different fat depots. Estimates derived from a linear regression model with estimates of adipocyte area in μm^2 per 1-unit higher genetic risk score, corresponding to a predicted 1 standard deviation higher obesity trait and adjusting for 10 principal components in all cohorts. In GTEx, fatDIVA and MOBB, adjustments were also made for age and sex, and with and without adjusting for BMI. In the all-female ENDOX cohort, adjustments were made for 10 principal components and with and without adjusting for chip type as the other covariates were unavailable. In the main meta-analysis model (assuming a fixed-effect model), ENDOX was included adjusted for chip type. Two sensitivity meta-analyses were performed; including ENDOX unadjusted for chip type and excluding the ENDOX cohort. (XLSX)

Acknowledgments

We thank study participants who donated adipose tissue to this study.

Author Contributions

Conceptualization: Craig A. Glastonbury.

Data curation: Craig A. Glastonbury, Samantha Laber, Emilie Pastel.

Formal analysis: Craig A. Glastonbury, Sara L. Pulit, Julius Honecker.

Funding acquisition: Craig A. Glastonbury, Cecilia M. Lindgren.

Investigation: Craig A. Glastonbury.

Methodology: Craig A. Glastonbury.

Project administration: Craig A. Glastonbury, Nicola L. Beer.

Resources: Craig A. Glastonbury, Timothy M. Frayling.

Software: Craig A. Glastonbury.

Supervision: Christoffer Nellåker, Cecilia M. Lindgren.

Validation: Julius Honecker, Jenny C. Censin, Hanieh Yaghootkar, Nilufer Rahmioglu, Katerina Kos, Andrew Pitt, Michelle Hudson, Hans Hauner, Christian M. Becker, Krina T. Zondervan, Timothy M. Frayling, Melina Claussnitzer.

Visualization: Craig A. Glastonbury, Sara L. Pulit.

Writing – original draft: Craig A. Glastonbury.

Writing – review & editing: Craig A. Glastonbury, Sara L. Pulit, Julius Honecker, Cecilia M. Lindgren.

References

1. Shungin D. et al. New genetic loci link adipose and insulin biology to body fat distribution. *Nature* 518, 187–196 (2015). <https://doi.org/10.1038/nature14132> PMID: 25673412
2. Locke A. E. et al. Genetic studies of body mass index yield new insights for obesity biology. *Nature* 518, 197–206 (2015). <https://doi.org/10.1038/nature14177> PMID: 25673413
3. Pulit S. L. et al. Meta-analysis of genome-wide association studies for body fat distribution in 694,649 individuals of European ancestry. *Hum. Mol. Genet.* 1–9 (2018). <https://doi.org/10.1093/hmg/ddx374>

4. Yengo L. et al. Meta-analysis of genome-wide association studies for height and body mass index in ~700 000 individuals of European ancestry. *Human Molecular Genetics* 3641–3649 (2018). <https://doi.org/10.1093/hmg/ddy271> PMID: 30124842
5. Pulit S. L., Laber S., Glastonbury C. A. & Lindgren C. M. The genetic underpinnings of body fat distribution. *Expert Rev. Endocrinol. Metab.* 12, 417–427 (2017). <https://doi.org/10.1080/17446651.2017.1390427> PMID: 30063432
6. Berry R., Jeffery E. & Rodeheffer M. S. Weighing in on adipocyte precursors. *Cell Metab.* 19, 8–20 (2014). <https://doi.org/10.1016/j.cmet.2013.10.003> PMID: 24239569
7. Arner E. et al. Adipocyte turnover: relevance to human adipose tissue morphology. *Diabetes* 59, 105–109 (2010). <https://doi.org/10.2337/db09-0942> PMID: 19846802
8. Jo J. et al. Hypertrophy and/or Hyperplasia: Dynamics of Adipose Tissue Growth. *PLoS Comput. Biol.* 5, e1000324 (2009). <https://doi.org/10.1371/journal.pcbi.1000324> PMID: 19325873
9. Pasarica M. et al. Lower total adipocyte number but no evidence for small adipocyte depletion in patients with type 2 diabetes. *Diabetes Care* 32, 900–902 (2009). <https://doi.org/10.2337/dc08-2240> PMID: 19228873
10. Salans L. B., Knittle J. L. & Hirsch J. The role of adipose cell size and adipose tissue insulin sensitivity in the carbohydrate intolerance of human obesity. *Journal of Clinical Investigation* vol. 47 153–165 (1968). <https://doi.org/10.1172/JCI105705> PMID: 16695937
11. Lönn M., Mehlhig K., Bengtsson C. & Lissner L. Adipocyte size predicts incidence of type 2 diabetes in women. *FASEB J.* 24, 326–331 (2010). <https://doi.org/10.1096/fj.09-133058> PMID: 19741173
12. Heinonen S. et al. Adipocyte morphology and implications for metabolic derangements in acquired obesity. *Int. J. Obes.* 38, 1423–1431 (2014).
13. Glastonbury C. A., Couto Alves A., El-Sayed Moustafa J. S. & Small K. S. Cell-Type Heterogeneity in Adipose Tissue Is Associated with Complex Traits and Reveals Disease-Relevant Cell-Specific eQTLs. *Am. J. Hum. Genet.* 104, 1013–1024 (2019). <https://doi.org/10.1016/j.ajhg.2019.03.025> PMID: 31130283
14. Glastonbury C. A. et al. Adiposity-Dependent Regulatory Effects on Multi-tissue Transcriptomes. *Am. J. Hum. Genet.* 99, 567–579 (2016). <https://doi.org/10.1016/j.ajhg.2016.07.001> PMID: 27588447
15. Zhi X. et al. AdipoCount: A New Software for Automatic Adipocyte Counting. *Front. Physiol.* 9, 85 (2018). <https://doi.org/10.3389/fphys.2018.00085> PMID: 29515452
16. Galarraga M. et al. Adiposoft: automated software for the analysis of white adipose tissue cellularity in histological sections. *J. Lipid Res.* 53, 2791–2796 (2012). <https://doi.org/10.1194/jlr.D023788> PMID: 22993232
17. Dao D. et al. CellProfiler Analyst: interactive data exploration, analysis and classification of large biological image sets. *Bioinformatics* 32, 3210–3212 (2016). <https://doi.org/10.1093/bioinformatics/btw390> PMID: 27354701
18. Lonsdale J. et al. The Genotype-Tissue Expression (GTEx) project. *Nat. Genet.* 45, 580–585 (2013). <https://doi.org/10.1038/ng.2653> PMID: 23715323
19. Sankur B. Survey over image thresholding techniques and quantitative performance evaluation. *Journal of Electronic Imaging* vol. 13 146 (2004).
20. Szegedy, C., Vanhoucke, V., Ioffe, S., Shlens, J. & Wojna, Z. Rethinking the Inception Architecture for Computer Vision. in 2016 IEEE Conference on Computer Vision and Pattern Recognition (CVPR) (2016). <https://doi.org/10.1109/cvpr.2016.308>
21. McQuin C. et al. CellProfiler 3.0: Next-generation image processing for biology. *PLoS Biol.* 16, e2005970 (2018). <https://doi.org/10.1371/journal.pbio.2005970> PMID: 29969450
22. Cohen, J. P., Boucher, G., Glastonbury, C. A., Lo, H. Z. & Bengio, Y. Count-ception: Counting by Fully Convolutional Redundant Counting. *arXiv preprint arXiv:1703.08710* (2017).
23. Ronneberger O., Fischer P. & Brox T. U-Net: Convolutional Networks for Biomedical Image Segmentation. in *Lecture Notes in Computer Science* 234–241 (2015).
24. Deng, L., Yang, M., Qian, Y., Wang, C. & Wang, B. CNN based semantic segmentation for urban traffic scenes using fisheye camera. in *2017 IEEE Intelligent Vehicles Symposium (IV)* (2017). <https://doi.org/10.1109/ivs.2017.7995725>
25. Ferlaino, M. et al. Towards Deep Cellular Phenotyping in Placental Histology. *arXiv [cs.CV]* (2018).
26. Berry R. et al. Imaging of adipose tissue. *Methods Enzymol.* 537, 47–73 (2014). <https://doi.org/10.1016/B978-0-12-411619-1.00004-5> PMID: 24480341
27. Carpenter A. E. et al. CellProfiler: image analysis software for identifying and quantifying cell phenotypes. *Genome Biol.* 7, R100 (2006). <https://doi.org/10.1186/gb-2006-7-10-r100> PMID: 17076895

28. Laforest S. et al. Comparative analysis of three human adipocyte size measurement methods and their relevance for cardiometabolic risk. *Obesity* 25, 122–131 (2017). <https://doi.org/10.1002/oby.21697> PMID: 27883275
29. Lebovitz H. E. & Banerji M. A. Point: visceral adiposity is causally related to insulin resistance. *Diabetes Care* 28, 2322–2325 (2005). <https://doi.org/10.2337/diacare.28.9.2322> PMID: 16123512
30. Fang L., Guo F., Zhou L., Stahl R. & Grams J. The cell size and distribution of adipocytes from subcutaneous and visceral fat is associated with type 2 diabetes mellitus in humans. *Adipocyte* 4, 273–279 (2015). <https://doi.org/10.1080/21623945.2015.1034920> PMID: 26451283
31. McLaughlin T. et al. Adipose Cell Size and Regional Fat Deposition as Predictors of Metabolic Response to Overfeeding in Insulin-Resistant and Insulin-Sensitive Humans. *Diabetes* 65, 1245–1254 (2016). <https://doi.org/10.2337/db15-1213> PMID: 26884438
32. Melé M. et al. Human genomics. The human transcriptome across tissues and individuals. *Science* 348, 660–665 (2015). <https://doi.org/10.1126/science.aaa0355> PMID: 25954002
33. McCall M. N., Illei P. B. & Halushka M. K. Complex Sources of Variation in Tissue Expression Data: Analysis of the GTEx Lung Transcriptome. *Am. J. Hum. Genet.* 99, 624–635 (2016). <https://doi.org/10.1016/j.ajhg.2016.07.007> PMID: 27588449
34. Acosta J. R. et al. Increased fat cell size: a major phenotype of subcutaneous white adipose tissue in non-obese individuals with type 2 diabetes. *Diabetologia* 59, 560–570 (2016). <https://doi.org/10.1007/s00125-015-3810-6> PMID: 26607638
35. Verboven K. et al. Abdominal subcutaneous and visceral adipocyte size, lipolysis and inflammation relate to insulin resistance in male obese humans. *Sci. Rep.* 8, 4677 (2018). <https://doi.org/10.1038/s41598-018-22962-x> PMID: 29549282
36. McCarthy S. et al. A reference panel of 64,976 haplotypes for genotype imputation. *Nat. Genet.* 48, 1279–1283 (2016). <https://doi.org/10.1038/ng.3643> PMID: 27548312
37. Yang J., Lee S. H., Goddard M. E. & Visscher P. M. GCTA: A tool for genome-wide complex trait analysis. *Am. J. Hum. Genet.* 88, 76–82 (2011). <https://doi.org/10.1016/j.ajhg.2010.11.011> PMID: 21167468
38. Small K. S. et al. Regulatory variants at KLF14 influence type 2 diabetes risk via a female-specific effect on adipocyte size and body composition. *Nat. Genet.* 50, 572–580 (2018). <https://doi.org/10.1038/s41588-018-0088-x> PMID: 29632379
39. Claussnitzer M. et al. FTO Obesity Variant Circuitry and Adipocyte Browning in Humans. *N. Engl. J. Med.* 373, 895–907 (2015). <https://doi.org/10.1056/NEJMoa1502214> PMID: 26287746
40. Ash J. T., Darnell G., Munro D. & Engelhardt B. E. Joint analysis of gene expression levels and histological images identifies genes associated with tissue morphology. (2018) <https://doi.org/10.1101/458711>
41. Pawlowski N., Caicedo J. C., Singh S., Carpenter A. E. & Storkey A. Automating Morphological Profiling with Generic Deep Convolutional Networks. *bioRxiv* 085118 (2016) <https://doi.org/10.1101/085118>
42. Glastonbury, C. A., Ferlaino, M., Nellåker, C. & Lindgren, C. M. Adjusting for Confounding in Unsupervised Latent Representations of Images. *arXiv [cs.CV]* (2018).
43. Petrovski S. & Goldstein D. B. Unequal representation of genetic variation across ancestry groups creates healthcare inequality in the application of precision medicine. *Genome Biol.* 17, 157 (2016). <https://doi.org/10.1186/s13059-016-1016-y> PMID: 27418169
44. Mills M. C. & Rahal C. A scientometric review of genome-wide association studies. *Commun Biol* 2, 9 (2019). <https://doi.org/10.1038/s42003-018-0261-x> PMID: 30623105
45. Lu Y. *Transfer Learning for Image Classification*. (2017).
46. Thrun S. & Pratt L. *Learning to Learn*. (Springer Science & Business Media, 2012).
47. Skurk T., Alberti-Huber C., Herder C. & Hauner H. Relationship between adipocyte size and adipokine expression and secretion. *J. Clin. Endocrinol. Metab.* 92, 1023–1033 (2007). <https://doi.org/10.1210/jc.2006-1055> PMID: 17164304
48. The International HapMap Consortium. et al. The International HapMap Project. *Nature* 426, 789–796 (2003). <https://doi.org/10.1038/nature02168> PMID: 14685227
49. Altshuler D. M. et al. Integrating common and rare genetic variation in diverse human populations. *Nature* 467, 52–58 (2010). <https://doi.org/10.1038/nature09298> PMID: 20811451
50. Yaghoobkar H. et al. Genetic evidence for a normal-weight ‘metabolically obese’ phenotype linking insulin resistance, hypertension, coronary artery disease, and type 2 diabetes. *Diabetes* 63, 4369–4377 (2014). <https://doi.org/10.2337/db14-0318>
51. Russakovsky O. et al. ImageNet Large Scale Visual Recognition Challenge. *Int. J. Comput. Vis.* 115, 211–252 (2015).
52. Perez F. & Granger B. E. IPython: A System for Interactive Scientific Computing. *Comput. Sci. Eng.* 9, 21–29 (2007).

53. Schwarzer G., Carpenter J. R. & Rücker G. Meta-Analysis with R. *Use R!* (2015) <https://doi.org/10.1007/978-3-319-21416-0>
54. Chang C. C. et al. Second-generation PLINK: rising to the challenge of larger and richer datasets. *Giga-science* 4, 1–16 (2015). <https://doi.org/10.1186/2047-217X-4-1> PMID: 25838885
55. Willer C. J., Li Y. & Abecasis G. R. METAL: Fast and efficient meta-analysis of genomewide association scans. *Bioinformatics* 26, 2190–2191 (2010). <https://doi.org/10.1093/bioinformatics/btq340> PMID: 20616382
56. Purcell S. et al. PLINK: a tool set for whole-genome association and population-based linkage analyses. *Am. J. Hum. Genet.* 81, 559–575 (2007). <https://doi.org/10.1086/519795> PMID: 17701901
57. R Core Team. R: A language and environment for statistical computing. <https://www.r-project.org/>.

ARTICLE OPEN



Adipocyte and Cell Biology

A distribution-centered approach for analyzing human adipocyte size estimates and their association with obesity-related traits and mitochondrial function

Julius Honecker¹, Dominik Weidlich², Simone Heisz¹, Cecilia M. Lindgren^{3,4}, Dimitrios C. Karampinos^{1,2}, Melina Claussnitzer^{4,5,6} and Hans Hauner^{1,7}

© The Author(s) 2021

OBJECTIVE: Cell diameter, area, and volume are established quantitative measures of adipocyte size. However, these different adipocyte sizing parameters have not yet been directly compared regarding their distributions. Therefore, the study aimed to investigate how these adipocyte size measures differ in their distribution and assessed their correlation with anthropometry and laboratory chemistry. In addition, we were interested to investigate the relationship between fat cell size and adipocyte mitochondrial respiratory chain capacity.

METHODS: Subcutaneous and visceral histology-based adipocyte size estimates from 188 individuals were analyzed by applying a panel of parameters to describe the underlying cell population. Histology-based adipocyte diameter distributions were compared with adipocyte diameter distributions from collagenase digestion. Associations of mean adipocyte size with body mass index (BMI), glucose, HbA_{1c}, blood lipids as well as mature adipocyte mitochondrial respiration were investigated.

RESULTS: All adipocyte area estimates derived from adipose tissue histology were not normally distributed, but rather characterized by positive skewness. The shape of the size distribution depends on the adipocyte sizing parameter and on the method used to determine adipocyte size. Despite different distribution shapes histology-derived adipocyte area, diameter, volume, and surface area consistently showed positive correlations with BMI. Furthermore, associations between adipocyte sizing parameters and glucose, HbA_{1c}, or HDL specifically in the visceral adipose depot were revealed. Increasing subcutaneous adipocyte diameter was negatively correlated with adipocyte mitochondrial respiration.

CONCLUSIONS: Despite different underlying size distributions, the correlation with obesity-related traits was consistent across adipocyte sizing parameters. Decreased mitochondrial respiratory capacity with increasing subcutaneous adipocyte diameter could display a novel link between adipocyte hypertrophy and adipose tissue function.

International Journal of Obesity (2021) 45:2108–2117; <https://doi.org/10.1038/s41366-021-00883-6>

INTRODUCTION

Adipose tissue is a unique organ with great plasticity displaying unmatched expansion and shrinkage capacities during periods of caloric excess or deprivation which is directly reflected in up to multiple fold changes in fat cell volume [1–3]. The onset of obesity in adults is characterized by an increase in adipose tissue mass mostly due to the enlargement of existing fat cells (hypertrophy) [4, 5]. Hyperplasia, which describes an increase in fat cell number is considered to only play a minor role in the expansion of adipose tissue mass in adults [5].

To measure adipocyte size, three methods have emerged as standards: histological sections, collagenase digestion, and

osmium tetroxide fixation. Despite systematic size differences, all methods are largely coherent regarding their size estimate association with obesity-related traits [6]. However, adipocyte size distributions from different adipocyte sizing methods vary in characteristic features of the distribution (i.e., modality and symmetry) [6]. Furthermore, distributions from one sizing method may not always be comparable since different variables such as area or feret diameter can be used as output measurements [7, 8]. In addition, the transformation of the initial size measurement into another sizing variable assuming a spherical shape might reduce comparability due to the nonlinear transformation of the data (diameter = $\sqrt{4 \cdot \text{area} / \pi}$; volume = $1/6 \cdot \text{diameter}^3 \cdot \pi$) [8–10].

¹Technical University of Munich, Else Kröner-Fresenius-Center for Nutritional Medicine, Chair of Nutritional Medicine, School of Life Sciences, Gregor-Mendel-Straße 2, 85354 Freising-Weißenstephan, Germany. ²Department of Diagnostic and Interventional Radiology, School of Medicine, Technical University of Munich, Munich, Germany. ³Big Data Institute at the Li Ka Shing Centre for Health Information and Discovery, University of Oxford, Oxford, UK. ⁴Broad Institute of MIT and Harvard, Cambridge, MA, USA. ⁵Division of Gerontology, Department of Medicine, Beth Israel Deaconess Medical Center, Boston, MA, USA. ⁶Harvard Medical School, Harvard University, Boston, MA, USA. ⁷Institute for Nutritional Medicine, School of Medicine, Technical University of Munich, Georg-Brauchle-Ring 62, 80992 Munich, Germany. [✉]email: hans.hauner@tum.de

Received: 14 December 2020 Accepted: 10 June 2021

Published online: 25 June 2021

SPRINGER NATURE

Adipocyte diameter and volume are usually related to anthropometry, metabolic outcomes, or adipocyte function [5, 10, 11]. Due to the introduction of fast and automated adipocyte size determination software, adipocyte area is currently reported more frequently [12, 13]. Adipocyte volume as a measure of fat cell size has high physiological relevance and is directly related to lipid storage capacity and adipose tissue cellularity [5, 6, 14, 15]. Furthermore, associations of fat cell size with comorbidities of obesity (Type 2 diabetes (T2D), dyslipidemia, and cardiovascular disease) have been reported and insulin-resistant individuals were found to exhibit larger visceral adipocytes compared to insulin-sensitive controls [16–20]. In addition, studies on size-separated fat cells provide evidence for functional differences between small and large adipocytes from the same individual [10, 21, 22]. However, cross-sectional studies assessing the genetic and metabolic underpinnings of adipocyte hypertrophy remain scarce [12, 14, 23–25]. Despite their low content in comparison with other tissues, adipocyte mitochondria are essential organelles for adipocyte differentiation, lipogenesis, adipokine secretion, and browning [26–29]. Emerging evidence indicates a fundamental relationship between obesity and altered adipocyte mitochondrial metabolism [30–32]. Considering the central role of mitochondria in adipose tissue metabolism and their association with obesity-related traits it seems likely that adipose tissue mitochondrial function could be associated with fat cell size. However, the relationship between adipocyte size and mitochondrial function has not yet been investigated cross-sectionally in humans, but solely in size-separated adipocytes [33, 34].

Therefore, this study aimed to achieve a comprehensive overview of similarities and differences in fat cell size distribution shape dependent on the adipocyte sizing method and the extracted sizing parameter. Furthermore, we sought to relate measurements of adipocyte size to phenotypic and laboratory variables. We used mature adipocyte respirometry data to investigate if the mitochondrial function is associated with adipocyte size.

MATERIALS AND METHODS

Study participants and phenotypic data

Sc and vc adipose tissue samples were obtained from 188 adult individuals (129 female, 59 male) undergoing elective abdominal surgery. Each participant gave written informed consent before inclusion and the study protocol was approved by the ethics committee of the Technical University of Munich (Study No. 5716/13). Collected data included the presence or absence of T2D as diagnosed by the treating physician, demographics (age and sex), anthropometry (weight before surgery, height, and BMI) as well as laboratory values (glycated HbA_{1c}, fasting plasma glucose, triglycerides, cholesterol, LDL, and HDL).

Study participants were on average 48 ± 13 years old with a mean BMI of 43.6 ± 13.3 kg/m². According to BMI categories 23 individuals with normal weight (12.2%), 18 individuals with overweight (9.6%), 8 individuals with obesity class I (4.3%), 13 individuals with obesity class II (6.9%), and 122 individuals with obesity class III (64.9%) participated in the study.

T2D was diagnosed in 45 individuals (24.3%), while 140 participants were free of T2D (3 not known). The study populations' characteristics are summarized in Table 1 and Table S1.

Adipose tissue sampling and adipocyte isolation

Sc ($n = 161$) and vc ($n = 188$) adipose tissue biosamples were obtained from the upper abdominal area at the site of incision and in the proximity of the angle of his, respectively. Paired sc and vc adipose tissue were available from 146 individuals. After excision, samples were immediately fixed in 4% formaldehyde for later use in histology. Tissue samples for mature adipocyte isolation were transported to the laboratory in DMEM-F12 (Thermo Fisher Scientific, Waltham, Massachusetts) + 1% penicillin-streptomycin (Merck, Darmstadt, Germany) where collagenase-based mature adipocyte isolation was carried out as described previously [33].

Diameter determination of floating mature adipocytes

Approximately, 50 μ l of the adipocyte suspension was pipetted onto a glass slide and the diameter of 100 cells was manually determined under a

Table 1. Study participants' characteristics.

Variable	Mean \pm SD	Range (min–max)
<i>Anthropometry</i>		
Age [years]; $n = 188$	48 ± 13	18–78
BMI [kg/m ²]; $n = 184$	43.6 ± 13.3	18.2–83.3
<i>Glucose homeostasis</i>		
Glucose [mmol/l]; $n = 139$	6.0 ± 3.0	2.2–22.1
HbA _{1c} [%]; $n = 99$	6.0 ± 1.2	4.6–11.5
<i>Lipids</i>		
Total cholesterol [mmol/l] $n = 97$	5.1 ± 1.0	1.4–8.0
LDL [mmol/l]; $n = 92$	3.1 ± 0.8	1.3–5.3
HDL [mmol/l]; $n = 94$	1.3 ± 0.4	0.6–2.4
Triglycerides [mmol/l]; $n = 96$	1.9 ± 1.0	0.6–6.8

light microscope. Adipocyte diameter from collagenase digestion was available for 84 sc and 97 vc samples.

Histology-based adipocyte cross-sectional area determination

At least three 5 μ m thick hematoxylin and eosin-stained sections with a minimum distance of 100 μ m or from different blocks were used for microscopy and size determination. The adipocyte size estimates used for analysis were assessed retrospectively based on a recently published method, the Adipocyte U-Net [12]. Objects with an area smaller than 200 μ m² and larger than 16,000 μ m² were excluded as they typically represent artifacts from tissue processing and histology.

Adipocyte area parameters

Totally, 500 cell cross-sectional area estimates and 100 cell diameter estimates were used for data analysis on histology and collagenase-digested adipocytes, respectively. If not given by the initial measurement adipocyte area, diameter, volume or surface area were calculated based on the assumption of spherical shape. Descriptive statistics (density plots and quantile-quantile plots), as well as measures for central tendency (arithmetic mean and median), were calculated. In addition, the first and ninth decile were determined and the interdecile range (IDR) was calculated as a measure of the dispersion of adipocyte sizes. Skewness was used as a distribution asymmetry measure and kurtosis was used to assess distribution tailedness.

Respirometry

Data on mature adipocyte mitochondrial function was available for 24 sc and 35 vc samples originating from an earlier project of our group [30]. Briefly, 200 μ l of packed isolated adipocytes were pipetted into the experimental chamber of an Oxygraph-2k (Oroboros Instruments, Innsbruck, Austria) and substrate-uncoupler-inhibitor titration was carried out to assess the following respiratory states: (I) Free OXPHOS capacity which describes the respiratory capacity potentially available for ADP phosphorylation, (II) OXPHOS capacity describing the respiratory capacity of mitochondria in the ADP activated state, (III) electron transfer system capacity (ETS) describing the maximum respiratory chain capacity due to chemical uncoupling introducing proton reflux into the mitochondrial matrix, and (IV) leak respiration in the presence of oligomycin describing the dissipative component of respiration that does not contribute to ATP synthesis [35]. DNA from adipocytes was isolated for normalization purposes and results were given as picomoles of oxygen consumed per second and nanogram of DNA. Respiration was measured in mature adipocytes since cell-mitochondrion interactions are preserved [36]. In addition, isolated adipocytes offer the advantage that confounding effects from the stromal vascular fraction on respiration and normalization can be ruled out [37].

Statistics

Shapiro Wilk tests and quantile-quantile plots were used to test for/against normality. All data were presented as mean \pm SD. If not stated otherwise, Pearson correlation was used to test for associations between adipocyte size, anthropometry, laboratory values, and mitochondrial respiration. To further explore the relationship between adipocyte size and phenotype

data multiple linear regression was used to adjust for differences in BMI between individuals. P values below 0.05 were considered significant. All analyses were conducted in R [38].

RESULTS

Histology-based calculation of adipocyte diameter or volume from adipocyte area changes the adipocyte size distribution shape

The adipocyte area distributions across all individuals (Fig. 1A, B) did not fit a normal distribution and consistently showed positive skewness for both adipose depots (Table 2). This observation based on pooled data was in agreement with the subject and depot-specific distributions, consistently showing asymmetry as measured by positive skewness values (data not shown). P values < 0.05 from the Shapiro Wilk tests and large deviations in the correlation between a normal distribution and sample distribution displayed by quantile–quantile plots further supported the hypothesis of histology-derived adipocyte areas being non-normally distributed. Density plots, histograms, and quantile–quantile plots for each individual and depot are provided in Supplemental Figs. S1–S3. Due to the positive skew mean and median adipocyte area was not overlapping with the maximum of the distribution (mode) and therefore did not reflect the major fraction of the adipocyte population (Table 2). The calculation of adipocyte diameter from adipocyte area, which represents a non-linear square root transformation resulted in a broader distribution of the data (Fig. 1C, D). This observation was verified by decreased adipocyte diameter distribution skewness and kurtosis in comparison to the adipocyte area distributions ($skew_{sc\ area} = 1.1 \pm 0.4$, $skew_{sc\ diameter} = 0.3 \pm 0.2$; $skew_{vc\ area} = 1.3 \pm 0.4$, $skew_{vc\ diameter} = 0.4 \pm 0.2$; Table 2). Calculation of adipocyte volume from adipocyte area represents exponentiation of the data by the power of 3 and resulted in a sharper distribution shape with greater asymmetry compared to the adipocyte area distributions (Fig. 1E, F). In agreement, skewness and kurtosis of the adipocyte volume distribution increased in comparison to the adipocyte area distribution ($skew_{sc\ area} = 1.1 \pm 0.4$, $skew_{sc\ volume} = 1.9 \pm 0.6$; $skew_{vc\ area} = 1.3 \pm 0.4$, $skew_{vc\ volume} = 2.3 \pm 0.8$; Table 2). Since the surface area of a sphere equals four times the largest cross-sectional area ($A_{surface} = 4\pi r^2$, $A_{great\ circle} = \pi r^2$, therefore $A_{surface} = 4 \cdot A_{great\ circle}$), calculation of adipocyte surface area from adipocyte cross-sectional area does neither change distribution shape, nor statistical outcome measures.

Comparison between histological and collagenase-based adipocyte diameter distributions

Overall, mean adipocyte diameter derived from histology and collagenase digestion showed a good correlation with each other ($r_{Pearson} = 0.46$, $p = 3.2 \times 10^{-8}$; Fig. 2A). The mean adipocyte diameter from histology was, however, consistently smaller than the mean collagenase adipocyte diameter as shown by the Bland–Altman method comparison plotting (Table 2, Fig. 2B). This can be attributed to the fact that the adipocyte diameter from histology might not always be equivalent to the maximal diameter of the cell in vivo [8]. With collagenase digestion, mature adipocytes are liberated from their connective tissue and take on a spherical shape allowing to measure the maximal cell diameter under the microscope. Adipocyte diameter histograms indicate that the diameter distribution from collagenase digestion did fit the shape of a normal distribution (Fig. 2C, D) and was considerably less skewed in comparison to adipocyte diameter distributions from histology (Table 2).

Mean adipocyte size measurements from histology show similar correlations with anthropometric variables and laboratory values

As previously published, measures of mean adipocyte size showed strong correlations with BMI in both adipose tissue depots (Fig. 3,

Table S2). Significance levels and Pearson correlation coefficients were in a comparable range independent of the adipocyte sizing parameter that was used ($r_{Pearson} = 0.46\text{--}0.49$, $p = 9 \times 10^{-12}\text{--}1 \times 10^{-10}$). Other than BMI no significant associations with mean adipocyte size were found in sc fat. In addition to BMI, mean adipocyte size correlated with glucose (mean diameter: $n = 139$, $r_{Pearson} = 0.26$, $p = 0.002$), HbA_{1c} (mean diameter: $n = 99$, $r_{Pearson} = 0.31$, $p = 0.002$) and HDL (mean diameter: $n = 94$, $r_{Pearson} = -0.32$, $p = 0.002$) in the vc fat depot (Fig. 3, Table S2). Notably, despite different individual distribution shapes, mean adipocyte cross-sectional area, diameter, volume, and surface area were all similarly correlated with BMI and laboratory values (Fig. 3, Table S2). Since our data and results from previous studies show that BMI is strongly correlated with adipocyte size multiple linear regression was used to rule out any possible effect of differences in BMI on the association of laboratory values with mean adipocyte diameter (Table S3). Results from our multiple linear regression analysis were in agreement with results from the correlation analysis. Mean sc adipocyte diameter was only associated with BMI, while mean vc adipocyte diameter was significantly associated with age, fasting plasma glucose, HbA_{1c}, HDL and triglycerides ($p < 0.05$, Table S3). Besides the continuous variables that were considered in the correlation analysis sex and the absence or presence of T2D were added as categorical variables to our multiple linear regression model. The mean visceral adipocyte diameter of males was significantly larger compared to females in our multiple linear regression model ($p = 0.006$, Table S3). In agreement with the positive correlations of mean visceral adipocyte diameter with glucose and HbA_{1c}, respectively, adipocytes of individuals with T2D were larger compared to the control group in a multiple linear regression model ($p = 0.01$, Table S3). Together, the observed changes in adipocyte distribution shape did not influence the correlation of extracted mean values with obesity-related traits.

Associations of adipocyte size and mitochondrial function

Since all mean adipocyte size parameters showed comparable correlations with anthropometry and laboratory chemistry, the relationship between adipocyte size and mitochondrial respiratory capacity was only investigated using mean adipocyte diameter. Correlation analysis showed an inverse relationship between sc free OXPHOS capacity and mean adipocyte diameter (Fig. 4, $n = 24$, $r_{Pearson} = -0.41$, $p = 0.045$). In addition, significant correlations between mean adipocyte diameter and OXPHOS capacity ($n = 24$, $r_{Pearson} = -0.53$, $p = 0.008$) as well as ETS capacity ($n = 24$, $r_{Pearson} = -0.59$, $p = 0.003$) were observed (Fig. 4, Table S4). Both sc and vc mean adipocyte diameter showed negative correlations with leak respiration in the presence of oligomycin (Table S4). We observed a weaker though significant association of OXPHOS capacity with mean adipocyte diameter in the vc depot ($n = 35$, $r_{Pearson} = -0.36$, $p = 0.035$) (Table S4). When adjusting for the effect of BMI on the association between mitochondrial respiration and mean adipocyte diameter, we did not observe a significant effect (Table S5). Initially, 500 sampled cells per depot and individual were used to obtain individual histology-derived adipocyte size distributions. This, however, resulted in the exclusion of study participants where only a little adipose tissue was available for histology. In a second analysis, we, therefore, reduced the number of sampled cells per individual and depot to 200, thereby increasing paired adipocyte size and respirometry data ($n_{sc} = 32$, $n_{vc} = 41$). Mean adipocyte diameters from 500 and 200 sampled cells were highly correlated ($r_{Pearson} = 0.97$, $p < 2.2 \times 10^{-16}$, Fig. S4). Sc and vc mean adipocyte diameter from 200 cells was correlated with OXPHOS capacity, leak respiration, and ETS capacity while free OXPHOS capacity was solely associated with sc mean adipocyte diameter (Table S6, Fig. S5). Significant associations between OXPHOS capacity ($\beta = -0.16$, $p = 0.007$), leak respiration ($\beta = -0.29$, $p = 0.011$) and ETS capacity ($\beta = -0.221$, $p = 0.001$) with mean adipocyte diameter from 200 cells were present for the sc depot after adjusting for the effect of BMI in a

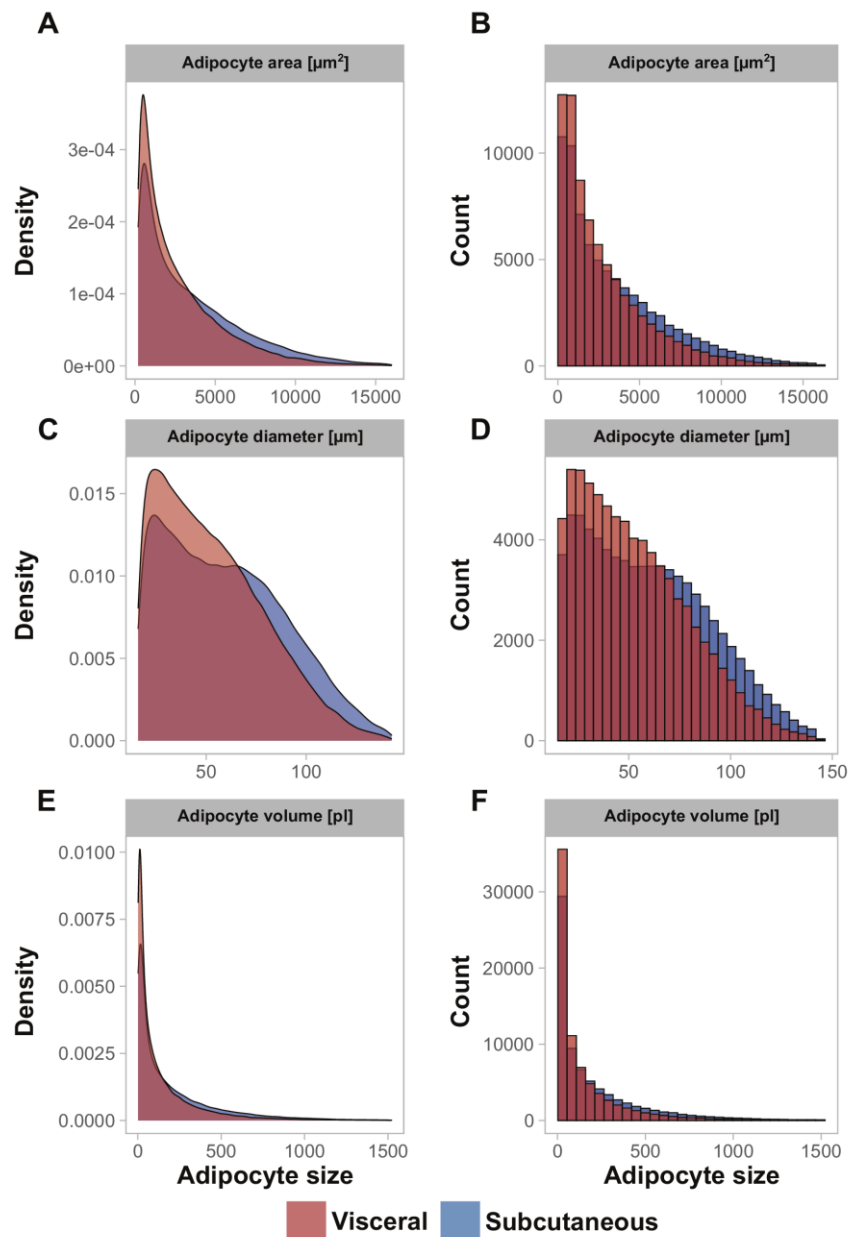


Fig. 1 Histology-derived adipocyte size distributions for adipocyte area, diameter, and volume. Density plots (left) and histograms (right) are shown for adipocyte area (A, B), adipocyte diameter (C, D), and adipocyte volume (E, F). Density plots and histograms were calculated for the whole cohort, separated on adipose tissue depot (sc $n = 161$, vc $n = 188$) and each individual is equally represented with 500 adipocyte size estimates. Independent of the size parameter assessed all distributions are showing positive skewness. It is, however, visible that the calculation of adipocyte diameter from the area which represents a square root transformation ($d = \sqrt{(4 \cdot A) / \pi}$), broadens the distribution shape and results in less positive skewness. Calculation of volume from adipocyte area ($V = 1/6 \cdot d^3 \cdot \pi$) results in a sharper distribution of values with increased positive skewness in comparison to the adipocyte area distribution.

Table 2. Adipocyte size summary.

Histology	Depot	Mean	Median	First Decile	Ninth decile	IDR	Skewness	Kurtosis
<i>Histology</i>								
Area [μm^2]	sc (n = 161)	3472.0	2678.8	443.2	7726.3	7283.1	1.1	4.0
		±	±	±	±	±	±	±
		886.8	795.4	76.7	2069.0	2030.1	0.4	1.7
	vc (n = 188)	2748.8	2099.8	407.7	6043.0	5635.3	1.3	5.1
		±	±	±	±	±	±	±
		863.6	718.7	68.1	2049.8	2013.6	0.4	2.5
Diameter [μm]	sc (n = 161)	59.6	57.7	23.7	98.2	74.6	0.3	2.3
		±	±	±	±	±	±	±
		7.8	8.8	2.0	13.8	12.8	0.2	0.4
	vc (n = 188)	53.1	50.9	22.7	86.3	63.6	0.4	2.6
		±	±	±	±	±	±	±
		8.4	8.9	1.9	15.8	14.8	0.2	0.6
Volume [pL]	sc (n = 161)	198.1	107.7	7.1	524.7	517.6	1.9	7.8
		±	±	±	±	±	±	±
		73.2	47.4	1.9	204.1	203.1	0.6	5.1
	vc (n = 188)	141.5	75.5	6.3	369.0	362.7	2.3	11.0
		±	±	±	±	±	±	±
		64.1	38.3	1.6	176.9	176.0	0.8	7.8
Surface area [μm^2]	sc (n = 161)	13887.9	10715.0	1772.6	30905	29132.5	1.1	4.0
		±	±	±	±	±	±	±
		3547.0	3181.5	8276.0	8267.0	8120.2	0.4	1.7
	vc (n = 188)	10,995	8399.2	1630.9	24172.1	22541.2	1.3	5.1
		±	±	±	±	±	±	±
		3454.4	2875.0	272.5	8199.2	8054.3	0.4	2.5
<i>Collagenase digestion</i>								
Area [μm^2]	sc (n = 84)	9523.7	9356	4259.9	14775.4	10515.5	0.6	5.4
		±	±	±	±	±	±	±
		2375.1	2659.6	2307.4	3042.1	2784.8	1.3	10.7
	vc (n = 97)	8292.5	7949	3661.0	12955.0	9294.0	0.9	6.3
		±	±	±	±	±	±	±
		2363.5	2507.2	1870.6	3384.7	2819.7	1.3	9.3
Diameter [μm]	sc (n = 84)	105.6	107.9	70.5	136.4	65.9	-0.2	3.9
		±	±	±	±	±	±	±
		14.7	16.3	21.3	14.5	20.0	0.9	5.3
	vc (n = 97)	98.3	99.2	66.0	127.2	61.2	0.1	4.1
		±	±	±	±	±	±	±
		15.3	16.8	17.4	17.7	16.9	0.8	4.0
Volume [pL]	sc (n = 84)	778.0	701.8	232.4	1372.6	1140.3	1.3	8.1
		±	±	±	±	±	±	±
		273.9	286.4	173.8	412.9	352.0	1.7	15.1
	vc (n = 97)	639	553.4	182.4	1138.1	955.6	1.8	10.2
		±	±	±	±	±	±	±
		258.7	248.6	137.9	427.2	367.0	1.6	13.6
Surface area [μm^2]	sc (n = 84)	38094.8	37427.7	17039.5	59101.6	42062.1	0.6	5.4
		±	±	±	±	±	±	±
		9500.3	10638.4	9229.8	12168.5	11139.3	1.3	10.7
	vc (n = 97)	33170.2	31796.8	14644.1	51820.1	37176.0	0.9	6.3
		±	±	±	±	±	±	±
		9453.9	10028.7	7482.5	13538.7	11278.7	1.3	9.3

multiple linear regression model (Table S7). No significant associations between mean adipocyte diameter and respiratory chain function except for ETS capacity ($\beta = -0.14$, $p = 0.045$) were found when applying the multiple linear regression model to the vc depot (Table S7). In conclusion, adipocyte respiratory capacity was predominantly associated with mean adipocyte diameter in the sc depot.

DISCUSSION

We applied a series of analytical approaches to histology and collagenase-derived adipocyte size estimates with the goal to

obtain an in-depth characterization of the underlying adipocyte size distributions and compare their relationship with phenotype or laboratory chemistry. Since mitochondrial dysfunction is related to obesity and/or T2D we investigated whether mitochondrial respiration is associated with adipocyte hypertrophy.

Our data indicate that histology-derived adipocyte cross-sectional area is characterized by positive skewness. Similar distribution shapes have been previously reported in rodents and humans [8, 39, 40]. We show that calculation of adipocyte diameter, volume or surface area from cross-sectional area introduces substantial changes to distribution shape. These changes are caused by mathematical data transformation and

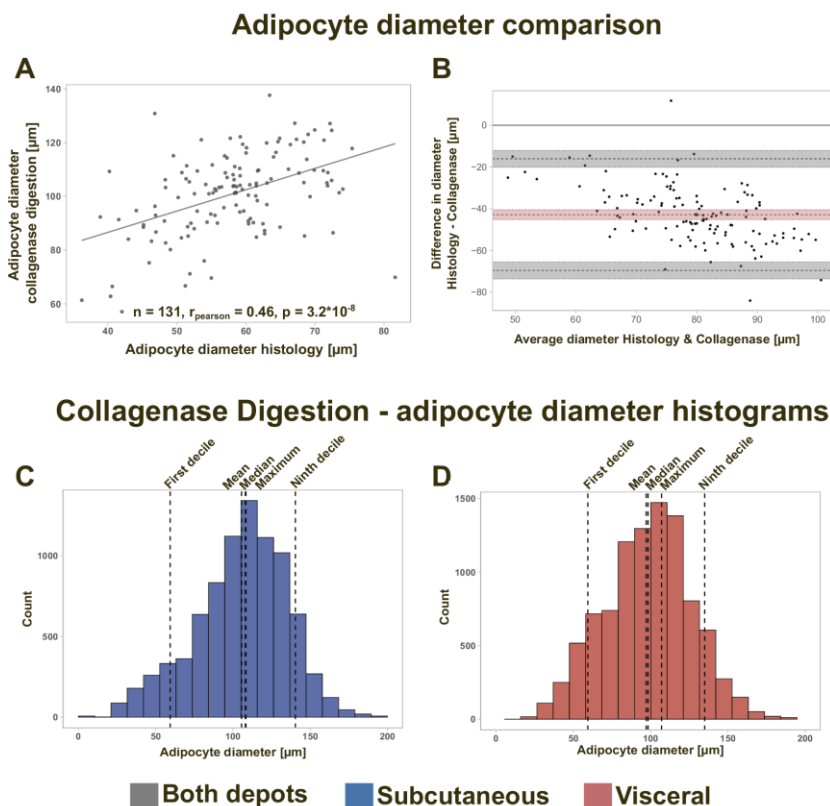


Fig. 2 Comparison of mean adipocyte diameter between histology and collagenase digestion and collagenase-based adipocyte diameter distributions. A scatterplot (A) as well as a Bland–Altman plot (B) are shown for comparing mean adipocyte diameter from histology and collagenase digestion. For method comparison (A, B) sc and vc samples were pooled ($n_{\text{tot}} = 131$, $n_{\text{sc}} = 56$, $n_{\text{vc}} = 75$). Histograms were plotted for sc (C, blue) and visceral adipose tissue (D, red) to visualize adipocyte diameter distributions from collagenase digestion. Each individual is equally represented with 100 adipocyte size estimates from a total of 84 individuals (sc) and 97 individuals (vc). Dotted vertical lines show where the first decile, ninth decile, mean, median, and modal adipocyte diameter are located in the histogram. Mean adipocyte diameter from histology and collagenase digestion are concordant as indicated by Pearson-correlation ($r_{\text{pearson}} = 0.46$, $p = 3.2 \times 10^{-8}$). However, as shown by the Bland–Altman plot (B) mean adipocyte diameter from histology was consistently smaller than mean adipocyte diameter from collagenase digestion. Independent of the depot, diameter histograms from collagenase digestion were following the pattern of a normal distribution (C, D).

are therefore not only limited to human adipose tissue sections but apply to all species with similar underlying size distributions. In agreement with previous studies, adipocyte diameter distributions from collagenase digestion show greater symmetry, follow the shape of a normal distribution and the mean collagenase diameter is consistently larger than the mean histology diameter [6, 7, 41]. With isolated adipocytes, both Gaussian distributions and bimodal distributions containing a second smaller cell population are reported [6, 21, 42, 43]. Our study cannot confirm the presence of the second peak in adipocyte size distributions from isolated adipocytes and therefore supports the notion that size distributions from isolated adipocytes are unimodal and normally distributed. Density histograms from our study suggest that adipocyte size distributions from histology are unimodal but differ from isolated adipocytes by showing considerable skew (Figs. S1–S3). Despite 500 counted cells being sufficient to extract mean adipocyte size estimates it should be acknowledged that higher cell counts would in our opinion be desirable to reliably

detect (if present) additional modes at lower frequencies [40, 44]. Using whole slide scans could display one method to achieve greater counts and therefore the question of modality should be addressed in future studies [12]. While the mean collagenase-derived adipocyte diameter represents the most frequent adipocyte population this is not the case for histology-derived distributions due to positive skew. Therefore, alternative measurements of adipocyte size such as IDR or modal adipocyte size are proposed to better describe non-normal distributions.

Besides different distribution shapes, we demonstrate that adipocyte area, diameter, volume, and surface area are equally correlated with common anthropometry and laboratory values. Across different sizing parameters, the correlation between adipocyte size and measures of glucose homeostasis and blood lipids was limited to the vc depot. Similar results were observed in previous studies and our results are in agreement with the well-known association between visceral obesity and metabolic disorders [11, 45]. Therefore, non-linear data transformation of

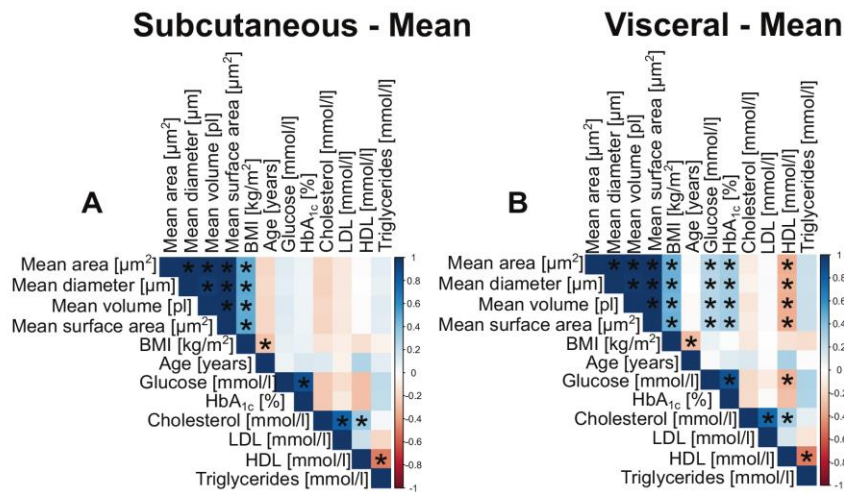


Fig. 3 Correlations between mean adipocyte size, anthropometric variables, and laboratory values. Data are shown as a Pearson correlation matrix. Positive correlations are depicted in shades of blue while negative correlations are shown in shades of red. Asterisks indicate significant associations. *P* values were Bonferroni corrected to account for multiple testing. In the sc depot (A), only BMI showed significant associations with measures of mean adipocyte size. In the vc depot (B) BMI, glucose and HbA_{1c} showed positive associations with measures of mean adipocyte size. HDL was negatively associated with vc mean adipocyte size.

the initial output variable (area) assuming spherical shape does not influence the associations between adipocyte size and obesity-related traits. Similar to inter-method comparisons we conclude that transformed adipocyte sizing parameters from the same method are equally related to measures of metabolic health and obesity [6]. Our data suggests that while the “ground truth” adipocyte size remains unknown and shows variation between studies reported associations with adipocyte size should in general be comparable. In our opinion, small cohort sizes and limited adipocyte counts propose greater limitations to significance and comparability rather than the utilization of different measurement methods or sizing parameters.

Mean adipocyte diameter, volume, and area are the most common adipocyte size measures [6, 11–13]. Since mature adipocytes are three-dimensional in shape and mainly comprised of a triglyceride-containing unilocular lipid droplet, volume is of high biological relevance for many research questions including fat mass and cellularity calculations [5, 46, 47]. Less biological relevance can be attributed to adipocyte area or diameter as they do not directly resemble the physiological properties of the adipocyte. Surface area is reported less frequently and is directly proportional to the largest cross-sectional area when the spherical shape is assumed. Since the surface area is proportional to membrane area it is relevant for receptor binding and signaling. Due to its linear relationship with adipocyte surface area, cross-sectional area could also be used as a meaningful readout of adipocyte size when signaling or biochemical processes are investigated. It is, however, important to emphasize that the cross-sectional area measured in histology is not necessarily equal to the largest cross-sectional area of the cell.

Considering the inherent advantages and limitations of each adipocyte sizing method as well as the different underlying distributions our study emphasizes that adipocyte size cannot be generalized, but always needs to be seen in context and interpreted regarding physiological relevance.

As a novel finding, our study correlates mean adipocyte diameter with mitochondrial function and our data indicate that individuals with larger sc adipocytes show decreased mature

adipocyte respiratory capacity. To the best of our knowledge, there are no previous studies investigating adipocyte size and mitochondrial respiration and data is solely available for size-separated adipocytes where no differences in mitochondrial function between large and small adipocytes from the same individual were observed [33, 34]. Therefore, it can be speculated that individuals with hypertrophic adipocytes exhibit an overall decreased mitochondrial respiratory capacity independent of intrinsic adipocyte size variation. Our findings regarding the association of mean adipocyte diameter and respiratory chain function are in line with data suggesting that adipocyte mitochondrial function is altered in individuals with obesity [30, 48].

If mitochondria of hypertrophic adipocytes cannot provide sufficient ATP for cellular processes and lipid metabolism due to e.g., defects in the respiratory chain it is likely that this could manifest for example in elevated free fatty acid levels and increased production of reactive oxygen species (ROS) both promoting a pro-inflammatory environment. Independent of adipocyte size we could not detect differences in respiratory states between depots except for leak respiration in the presence of oligomycin ($p = 0.003$, Figure S6). Proton leak is thought to be the predominant component of leak respiration and has been identified as an important mechanism to protect against ROS [49]. As ROS are able to induce proton leak thus suggesting a feedback loop, elevated leak respiration in vc adipocytes could also resemble a cytoprotective mechanism against increased oxidative stress. Decreased leak respiration with larger adipocyte size and thus less protection against ROS could provide an explanation for the pro-inflammatory profile of hypertrophic adipocytes. Both hypotheses would be in line with literature reporting that vc adipose tissue and hypertrophic adipocytes are more prone to provide a pro-inflammatory environment compared to their sc and hyperplastic counterparts [10, 11, 50]. Additional studies that directly measure mitochondrial superoxide production and inducible uncoupling are however necessary to clearly elucidate the amount of ROS production in dependency of fat cell size and depot.

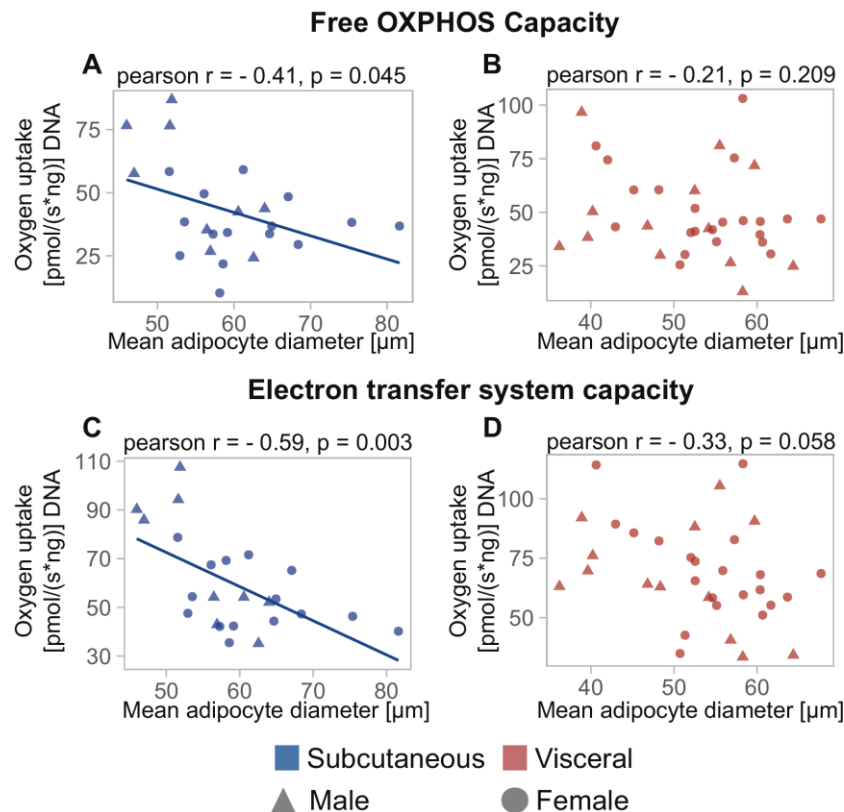


Fig. 4 Correlations between mean adipocyte diameter and mitochondrial respiratory capacity of mature adipocytes. Data are shown in form of scatterplots. **A, B** The correlation between free OXPHOS capacity and mean adipocyte diameter for sc and vc adipocytes respectively. **C, D** The correlations between mean adipocyte diameter and electron transfer system capacity. Significant correlations between free OXPHOS capacity ($r_{\text{Pearson}} = -0.41, p = 0.045$) and electron transfer system capacity ($r_{\text{Pearson}} = -0.59, p = 0.003$) were observed for sc adipose tissue (**A, C**).

As respiration was shown to be cell type-specific differences in respiration and its relationship with cell diameter could also originate from the fact that sc and vc adipocytes arise from different precursors [51, 52]. Transcriptome profiling studies from multiple different adipose tissue sites further support this observation as sc and vc adipose tissues are clearly separated by gene expression [53]. Since vc adipose tissue was sampled in the proximity of the angle of his we cannot rule out that our results are specific to this compartment. Intra-visceral depot comparisons however suggest that different vc adipose tissue depots show similarity regarding their gene expression [53]. Thus, comparability between our biopsy site with other vc sites should be given. Intra-depot comparisons from the same subject should however be the objective of future studies to identify similarities and differences in metabolic function and to further stratify the current adipose tissue classification.

In conclusion, the results of the present study highlight the importance of ascertaining method, sizing parameter, and distribution when analyzing adipocyte size. The data suggest that mean and median adipocyte area can deviate substantially from the most frequent cell population if the underlying distribution is non-normal. Additional parameters are, therefore, proposed to complement previous adipocyte sizing methods to enable a more

in-depth description of histology-derived adipocyte size towards a distribution-centered approach. Despite different distribution shapes histology-based adipocyte area, diameter, volume, and surface area are all equally related to clinical variables that have been frequently associated with adipocyte size. The association between sc mean adipocyte diameter and mitochondrial respiration represents a new finding of how adipose tissue metabolism is linked to adipocyte hypertrophy.

REFERENCES

1. Sun K, Kusminski CM, Scherer PE. Adipose tissue remodeling and obesity. *J Clin Investig.* 2011;121:2094–101.
2. Tchoukalova YD, Votruba SB, Tchkonja T, Giorgadze N, Kirkland JL, Jensen MD. Regional differences in cellular mechanisms of adipose tissue gain with over-feeding. *Proc Natl Acad Sci USA.* 2010;107:18226–31.
3. Hoffstedt J, Andersson DP, Eriksson Hogling D, Theorell J, Naslund E, Thorell A, et al. Long-term protective changes in adipose tissue after gastric bypass. *Diabetes Care.* 2017;40:77–84.
4. Bjorntorp P. Effects of age, sex, and clinical conditions on adipose tissue cellularity in man. *Metabolism.* 1974;23:1091–102.
5. Spalding KL, Amer E, Westermark PO, Bernard S, Buchholz BA, Bergmann O, et al. Dynamics of fat cell turnover in humans. *Nature.* 2008;453:783–7.

6. Laforest S, Michaud A, Paris G, Pelletier M, Vidal H, Geloan A, et al. Comparative analysis of three human adipocyte size measurement methods and their relevance for cardiometabolic risk. *Obesity* (Silver Spring, Md). 2017;25:122–31.
7. Galarraga M, Campión J, Muñoz-Barrutia A, Boqué N, Moreno H, Martínez JA, et al. Adiposoft: automated software for the analysis of white adipose tissue cellularity in histological sections. *J Lipid Res*. 2012;53:2791–6.
8. Lenz M, Roumans NJ, Vink RG, van Baak MA, Mariman EC, Arts IC, et al. Estimating real cell size distribution from cross-section microscopy imaging. *Bioinformatics* 2016;32:396–404.
9. Di Girolamo M, Mendlinger S, Fertig JW. A simple method to determine fat cell size and number in four mammalian species. *Am J Physiol*. 1971;221:850–8.
10. Skurk T, Alberti-Huber C, Herder C, Hauner H. Relationship between adipocyte size and adipokine expression and secretion. *The J Clin Endocrinol Metab*. 2007;92:1023–33.
11. Verboven K, Wouters K, Gaens K, Hansen D, Bijnen M, Wetzels S, et al. Abdominal subcutaneous and visceral adipocyte size, lipolysis and inflammation relate to insulin resistance in male obese humans. *Sci Rep*. 2018;8:4677.
12. Glastonbury CA, Pulit SL, Honecker J, Censin JC, Laber S, Yaghoobkar H, et al. Machine Learning based histology phenotyping to investigate the epidemiologic and genetic basis of adipocyte morphology and cardiometabolic traits. *PLoS Comput Biol*. 2020;16:e1008044.
13. Maguire AS, Woodie LN, Judd RL, Martin DR, Greene MW, Graff EC. Whole-slide image analysis outperforms micrograph acquisition for adipocyte size quantification. *Adipocyte*. 2020;9:567–75.
14. Lundbäck V, Kulyté A, Arner P, Strawbridge RJ, Dahlman I. Genome-wide association study of diabetogenic adipose morphology in the GENetics of adipocyte lipolysis (GENIAL) cohort. *Cells*. 2020;9:1085.
15. van Harmelen V, Skurk T, Röhrig K, Lee YM, Halbleib M, Aprath-Husmann I, et al. Effect of BMI and age on adipose tissue cellularity and differentiation capacity in women. *Int J Obes*. 2003;27:889–95.
16. Lonn M, Mehlig K, Bengtsson C, Tataranni PA, Pratley RE. Enlarged subcutaneous type 2 diabetes in women. *FASEB J*. 2010;24:326–31.
17. Veilleux A, Caron-Jobin M, Noel S, Laberge PY, Tchernof A. Visceral adipocyte hypertrophy is associated with dyslipidemia independent of body composition and fat distribution in women. *Diabetes*. 2011;60:1504–11.
18. Weyer C, Foley JE, Bogardus C, Tataranni PA, Pratley RE. Enlarged subcutaneous abdominal adipocyte size, but not obesity itself, predicts type II diabetes independent of insulin resistance. *Diabetologia*. 2000;43:1498–506.
19. Klötting N, Fasshauer M, Dietrich A, Kovacs P, Schon MR, Kern M, et al. Insulin-sensitive obesity. *Am J Physiol Endocrinol Metab*. 2010;299:E506–15.
20. Rydén M, Arner P. Cardiovascular risk score is linked to subcutaneous adipocyte size and lipid metabolism. *J Intern Med*. 2017;282:220–8.
21. Jernas M, Palming J, Sjöholm K, Jennische E, Svensson PA, Gabriellsson BG, et al. Separation of human adipocytes by size: hypertrophic fat cells display distinct gene expression. *FASEB J*. 2006;20:1540–2.
22. Laurencikienė J, Skurk T, Kulyté A, Hedén P, Aström G, Sjölin E, et al. Regulation of lipolysis in small and large fat cells of the same subject. *J Clin Endocrinol Metab*. 2011;96:E2045–9.
23. Claussnitzer M, Dankel SN, Kim KH, Quon G, Meuleman W, Haugen C, et al. FTO obesity variant circuitry and adipocyte browning in humans. *N Engl J Med*. 2015;373:895–907.
24. Small KS, Todorovic M, Civelek M, El-Sayed Moustafa JS, Wang X, Simon MM, et al. Regulatory variants at KLF14 influence type 2 diabetes risk via a female-specific effect on adipocyte size and body composition. *Nat. Genet*. 2018;50:572–80.
25. Hilton C, Neville MJ, Wittemans LBL, Todorovic M, Pinnick KE, Pulit SL, et al. MicroRNA-196a links human body fat distribution to adipose tissue extracellular matrix composition. *EBioMedicine*. 2019;44:467–75.
26. Kusminski CM, Scherer PE. Mitochondrial dysfunction in white adipose tissue. *Trends Endocrinol Metab*. 2012;23:435–43.
27. Kaaman M, Sparks LM, van Harmelen V, Smith SR, Sjölin E, Dahlman I, et al. Strong association between mitochondrial DNA copy number and lipogenesis in human white adipose tissue. *Diabetologia*. 2007;50:2526–33.
28. Keuper M, Jastroch M, Yi CX, Fischer-Posovszky P, Wabitsch M, Tschöp MH, et al. Spare mitochondrial respiratory capacity permits human adipocytes to maintain ATP homeostasis under hypoglycemic conditions. *FASEB J*. 2014;28:761–70.
29. Koh EH, Park JY, Park HS, Jeon MJ, Ryu JW, Kim M, et al. Essential role of mitochondrial function in adiponectin synthesis in adipocytes. *Diabetes*. 2007;56:2973–81.
30. Wessels B, Honecker J, Schöttl T, Stecher L, Klingenspor M, Hauner H, et al. Adipose mitochondrial respiratory capacity in obesity is impaired independently of glycemic status of tissue donors. *Obesity*. 2019;27:756–66.
31. Kraunsoe R, Boushel R, Hansen CN, Schjerling P, Qvortrup K, Stockel M, et al. Mitochondrial respiration in subcutaneous and visceral adipose tissue from patients with morbid obesity. *J Physiol*. 2010;588:2023–32.
32. Heinonen S, Buzkova J, Muniandy M, Kaksonen R, Ollikainen M, Ismail K, et al. Impaired mitochondrial biogenesis in adipose tissue in acquired obesity. *Diabetes*. 2015;64:3135–45.
33. Fischer B, Schottl T, Schempp C, Fromme T, Hauner H, Klingenspor M, et al. Inverse relationship between body mass index and mitochondrial oxidative phosphorylation capacity in human subcutaneous adipocytes. *Am J Physiol Endocrinol Metab*. 2015;309:E380–7.
34. Yin X, Lanza IR, Swain JM, Sarr MG, Nair KS, Jensen MD. Adipocyte mitochondrial function is reduced in human obesity independent of fat cell size. *J Clin Endocrinol Metab*. 2014;99:E209–16.
35. Gnaiger E. Mitochondrial pathways and respiratory control. An introduction to OXPHOS analysis. 4th ed. *Mitochondr Physiol Network* 19.12. Innsbruck: OROBOROS MIPNet Publications; 2014. p. 80.
36. Brand MD, Nicholls DG. Assessing mitochondrial dysfunction in cells. *Biochem J*. 2011;435:297–312.
37. Rosen ED, Spiegelman BM. What we talk about when we talk about fat. *Cell* 2014;156:20–44.
38. R Development Core Team. A language and environment for statistical computing. Vienna, Austria: R Foundation for Statistical Computing; 2019.
39. Ibáñez CA, Vázquez-Martínez M, León-Contreras JC, Reyes-Castro LA, Rodríguez-González GL, Bautista CJ, et al. Different statistical approaches to characterization of adipocyte size in offspring of obese rats: effects of maternal or offspring exercise intervention. *Front Physiol*. 2018;9:1571.
40. Parlee SD, Lentz SI, Mori H, MacDougald OA. Quantifying size and number of adipocytes in adipose tissue. *Methods Enzymol*. 2014;537:93–122.
41. Björnheden T, Jakubowicz B, Levin M, Odén B, Edén S, Sjöström L, et al. Computerized determination of adipocyte size. *Obes Res*. 2004;12:95–105.
42. Meyer LK, Ciaraldi TP, Henry RR, Wittgrove AC, Phillips SA. Adipose tissue depot and cell size dependency of adiponectin synthesis and secretion in human obesity. *Adipocyte*. 2013;2:217–26.
43. Fang L, Guo F, Zhou L, Stahl R, Grams J. The cell size and distribution of adipocytes from subcutaneous and visceral fat is associated with type 2 diabetes mellitus in humans. *Adipocyte*. 2015;4:273–9.
44. Tandon P, Wafer R, Minchin JEN. Adipose morphology and metabolic disease. *J Exp Biol*. 2018;221(Suppl_1).
45. Lee MJ, Wu Y, Fried SK. Adipose tissue heterogeneity: implication of depot differences in adipose tissue for obesity complications. *Mol Asp Med*. 2013;34:1–11.
46. Arner P, Bernard S, Appelsved L, Fu KY, Andersson DP, Salehpour M, et al. Adipose lipid turnover and long-term changes in body weight. *Nat Med*. 2019;25:1385–9.
47. Hodson L, Skeaff CM, Fielding BA. Fatty acid composition of adipose tissue and blood in humans and its use as a biomarker of dietary intake. *Prog Lipid Res*. 2008;47:348–80.
48. Christe M, Hirzel E, Lindinger A, Kern B, von Flüe M, Peterli R, et al. Obesity affects mitochondrial citrate synthase in human omental adipose tissue. *ISRN Obes*. 2013;2013:826027.
49. Jastroch M, Divakaruni AS, Mookerjee S, Treberg JR, Brand MD. Mitochondrial proton and electron leaks. *Essays Biochem*. 2010;47:53–67.
50. Acosta JR, Douagi I, Andersson DP, Bäckdahl J, Rydén M, Arner P, et al. Increased fat cell size: a major phenotype of subcutaneous white adipose tissue in non-obese individuals with type 2 diabetes. *Diabetologia*. 2016;59:560–70.
51. Chau YY, Bandiera R, Serrels A, Martínez-Estrada OM, Qing W, Lee M, et al. Visceral and subcutaneous fat have different origins and evidence supports a mesothelial source. *Nat Cell Biol*. 2014;16:367–75.
52. Brand MD. The efficiency and plasticity of mitochondrial energy transduction. *Biochem Soci Trans*. 2005;33:897–904.
53. Schleinitz D, Krause K, Wohland T, Gebhardt C, Linder N, Stumvoll M, et al. Identification of distinct transcriptome signatures of human adipose tissue from fifteen depots. *Eur J Hum Genet*. 2020;28:1714–25.

ACKNOWLEDGEMENTS

We are grateful to Prof. Dr. T. Huettli, Dr. O. Dietl, Dr. P. Stauch, and their team (Surgical Clinic of Munich-Bogenhausen) for obtaining adipose tissue samples. Portions of this article are available online as part of a dissertation (<https://d-nb.info/1149824301/34>). The data of this study are available from the corresponding author upon reasonable request.

AUTHOR CONTRIBUTIONS

J.H., M.C. and H.H. designed the study; J.H. and S.H. performed the histology, image acquisition, and isolation of mature adipocytes; J.H., D.W., S.H., C.M.L., M.C., D.K. and H. H. analyzed the data and interpreted the results; all authors were involved in drafting and revising the paper.

FUNDING

This study was supported in part by a grant from the Kompetenznetz Adipositas (Competence 421 Network for Obesity) funded by the Federal Ministry of Education and Research (FKZ 422 01G1128) and by the European Research Council (grant agreement No. 677661, ProFatMRI and grant agreement No. 875488, FatVirtual-Biopsy). Parts of the study were funded by the Else Kröner-Fresenius-Foundation, Bad Homburg. M.C. received funding from the Next Generation Fund at the Broad Institute of MIT and Harvard. C.M.L. is supported by the Li Ka Shing Foundation, WT-SSI/John Fell funds, and the National Institute for Health Research Oxford Biomedical Research Center. The funding bodies were not involved in study design, data collection, and analysis, decision to publish, or paper preparation. Open Access funding enabled and organized by Projekt DEAL.

COMPETING INTERESTS

The authors declare that they have no conflicts of interest. C.M.L. has collaborated with Novo Nordisk and Bayer in research, and in accordance with a university agreement, did not accept any personal payment.

ADDITIONAL INFORMATION

Supplementary information The online version contains supplementary material available at <https://doi.org/10.1038/s41366-021-00883-6>.

Correspondence and requests for materials should be addressed to H.H.

Reprints and permission information is available at <http://www.nature.com/reprints>

Publisher's note Springer Nature remains neutral with regard to jurisdictional claims in published maps and institutional affiliations.



Open Access This article is licensed under a Creative Commons Attribution 4.0 International License, which permits use, sharing, adaptation, distribution and reproduction in any medium or format, as long as you give appropriate credit to the original author(s) and the source, provide a link to the Creative Commons license, and indicate if changes were made. The images or other third party material in this article are included in the article's Creative Commons license, unless indicated otherwise in a credit line to the material. If material is not included in the article's Creative Commons license and your intended use is not permitted by statutory regulation or exceeds the permitted use, you will need to obtain permission directly from the copyright holder. To view a copy of this license, visit <http://creativecommons.org/licenses/by/4.0/>.

© The Author(s) 2021

bioRxiv preprint doi: <https://doi.org/10.1101/2021.11.20.468818>; this version posted November 20, 2021. The copyright holder for this preprint (which was not certified by peer review) is the author/funder, who has granted bioRxiv a license to display the preprint in perpetuity. It is made available under aCC-BY-NC-ND 4.0 International license.

TITLE

Transcriptome and fatty-acid signatures of adipocyte hypertrophy and its non-invasive MR-based characterization in human adipose tissue

AUTHORS

Julius Honecker^{1*}, Stefan Ruschke^{2*}, Claudine Seeliger¹, Samantha Laber³, Sophie Strobel³, Priska Pröll⁴, Christoffer Nellaker^{5,6}, Cecilia M. Lindgren^{3,5}, Ulrich Kulozik⁴, Josef Ecker⁷, Dimitrios C. Karampinos^{2,8}, Melina Claussnitzer^{3,9,10,‡}, Hans Hauner^{1,11,‡}

* JH and SR share first authorship on this work, ‡MC and HH are joint senior authors on this work

AFFILIATIONS

¹ Else Kröner-Fresenius-Center for Nutritional Medicine, Chair of Nutritional Medicine, TUM School of Life Sciences, Technical University of Munich, Gregor-Mendel-Straße 2, 85354 Freising-Weihenstephan, Germany

² Department of Diagnostic and Interventional Radiology, School of Medicine, Technical University of Munich, Munich, Germany

³ Broad Institute of MIT and Harvard, Cambridge, MA, USA

⁴ Food- and Bioprocess Engineering, TUM School of Life Sciences, Technical University of Munich, Weihenstephaner Berg 1, 85354 Freising, Germany.

⁵ Big Data Institute, Li Ka Shing Centre for Health Information and Discovery, University of Oxford, Oxford OX3 7FZ, UK.

⁶ Nuffield Department of Women's and Reproductive Health, University of Oxford, Women's Centre, John Radcliffe Hospital, Oxford, UK

⁷ ZIEL - Institute for Food & Health, Research Group Lipid Metabolism, Technical University of Munich, Freising, Germany.

⁸ Munich Institute of Biomedical Engineering, Technical University of Munich, Munich, Germany

⁹ Center for Genomic Medicine and Endocrine Division, Massachusetts General Hospital, Boston, MA, USA

¹⁰ Harvard Medical School, Harvard University, Boston, MA, USA

¹¹ Institute for Nutritional Medicine, School of Medicine, Technical University of Munich, Georg-Brauchle-Ring 62, 80992 Munich, Germany

bioRxiv preprint doi: <https://doi.org/10.1101/2021.11.20.468818>; this version posted November 20, 2021. The copyright holder for this preprint (which was not certified by peer review) is the author/funder, who has granted bioRxiv a license to display the preprint in perpetuity. It is made available under a [CC-BY-NC-ND 4.0 International license](#).

ABSTRACT

Adipose tissue is an organ with great plasticity and its hypertrophic expansion is associated with adipocyte dysfunction. How changes in adipocyte morphology are linked to gene expression and which cellular functions are affected remains elusive. We show that adipocyte hypertrophy is associated with transcriptomic changes using RNA-Seq data obtained from adipose tissue and size-separated adipocytes. Genes involved in oxidative phosphorylation, protein biosynthesis and fatty acid metabolism were down-regulated in large adipocytes while genes involved in inflammation were upregulated. For mitochondrial function, a reduction in the expression of thermogenesis related genes and estimated brown/beige adipocyte content was observed in individuals with large adipocytes. As a novel finding the total adipose tissue fatty acid composition was dependent on cell size and depot. MR spectroscopy methods for clinical scanning were developed to characterize adipocyte size and fatty acid composition in a fast and non-invasive manner. Together, the present data provides mechanistic insights on how adipocyte hypertrophy contributes to the manifestation of metabolic disease at the molecular and cellular level. MR spectroscopy was identified as a promising technique for an in-parallel assessment of adipose morphology and fatty acid composition allowing to translate our findings into an improved, non-invasive phenotyping of adipose tissue.

bioRxiv preprint doi: <https://doi.org/10.1101/2021.11.20.468818>; this version posted November 20, 2021. The copyright holder for this preprint (which was not certified by peer review) is the author/funder, who has granted bioRxiv a license to display the preprint in perpetuity. It is made available under aCC-BY-NC-ND 4.0 International license.

INTRODUCTION

A higher body fat percentage and thus an expanded white adipose tissue (WAT) mass is a central hallmark of obesity. An increase in the number of small adipocytes (hyperplasia) is considered as a metabolically less harmful mechanism of WAT growth, than an expansion in volume (hypertrophy) of already existing fat cells which is recognized as a pathological form of WAT remodeling that is associated with adverse cardiometabolic outcomes (1, 2). While hypertrophy in visceral adipose tissue (VAT) is associated with dyslipidemia and a pro-inflammatory state, both subcutaneous white adipose tissue (SAT) and VAT hypertrophy can contribute to systemic insulin resistance (3-8). With progressing obesity, recent studies report a decrease in lipid turnover which can be attributed to elevated rates of triglyceride storage and decreased lipolytic activity (9, 10). Additionally, differences in the secretion pattern of pro- and anti-inflammatory adipokines between small and large fat cells derived from the same individual were reported (11). The similarities and differences regarding measurement methods for adipocyte size and the pathophysiological implications of adipocyte hypertrophy have been extensively and systematically reviewed (12). Large-scale studies trying to unravel the causal transcriptional mechanisms behind adipocyte hypertrophy however, remain scarce (13).

One of the largest public biobanks that includes both tissue histology together with concordant RNA-Seq data is the Genotype-Tissue expression (GTEx) project (14, 15). Since our group previously estimated adipocyte size from over 500 SAT and VAT GTEx samples, we combined adipocyte size and RNA-Seq data from this cohort to investigate the transcriptomic changes that occur between different fat depots and depending on adipocyte hypertrophy (16).

Considering the relevance of fatty acid (FA) composition and fat cell size for WAT function and metabolic disease there is a need to develop novel, less invasive, yet highly accurate methods for the characterization of WAT. However, the feasibility of the simultaneous characterization of both FA composition and adipocyte size by magnetic resonance imaging (MRI) has not been shown yet and remains unclear. Furthermore, the motion sensitivity of magnetic resonance (MR)

bioRxiv preprint doi: <https://doi.org/10.1101/2021.11.20.468818>; this version posted November 20, 2021. The copyright holder for this preprint (which was not certified by peer review) is the author/funder, who has granted bioRxiv a license to display the preprint in perpetuity. It is made available under aCC-BY-NC-ND 4.0 International license.

diffusion-based adipocyte size estimations appears to be challenging in a clinical context given the required long diffusion times (17, 18). Thus, an MR relaxation-based characterization of adipocyte size – which is less sensitive to motion – combined with a chemical shift-based FA decomposition technique is desirable in the clinical context.

Therefore, the present study aimed to provide a comprehensive overview of gene expression changes associated with adipocyte hypertrophy on a variety of representative samples. Further, we investigated two of the potential underlying mechanisms, including mitochondrial activity and FA metabolism. For the latter, adipocyte size was related to FA composition and an advanced multi-parametric MRS-based method for the translational application towards an earlier and non-invasive diagnosis of WAT related metabolic diseases was developed.

MATERIAL

Study cohorts, sample origin and conducted experiments

All general study participants' characteristics, cohorts and related outcome measures are summarized in Table 1.

GTE_x

Parts of the data used in this study to investigate the relationship between adipocyte area and WAT transcriptome originate from the "Genotype-Tissue Expression (GTEx)" project (14, 15). GTEx SAT samples originate from beneath the leg's skin sample located below the patella on the medial site. VAT was obtained from the greater omentum. Sex and age in 10 year brackets derived from the GTEx publicly available subject phenotypes were used to characterize the donors.

Samples for FA composition and MRS measurements

Larger SAT pieces (~ 500 cm³) were obtained from abdominoplasty. Paired SAT and VAT samples were collected during general surgery or abdominal laparoscopic surgery. The described samples were used for MRS measurements, histology-based adipocyte sizing and to determine the FA composition by fatty-acid methyl ester (FAME) GC-MS. Collected phenotypic data included sex, age and BMI.

Samples for mature adipocyte isolation

Liposuction material was used to prepare and fractionate mature adipocytes for later isolation of RNA and transcriptomic characterization. Sex, age and BMI were given for the clinical characterization of the samples.

Cell culture

Adipocyte isolation and fractionation

Mature adipocytes were isolated from liposuction material based on collagenase-digestion as described previously (19). After isolation adipocytes were washed with Krebs-Ringer phosphate (KRP) buffer containing 0.1 % BSA for three times. Mature adipocytes were fractionated based on buoyancy in a separating funnel (11, 19). For size separation, 25 ml of mature adipocytes were

bioRxiv preprint doi: <https://doi.org/10.1101/2021.11.20.468818>; this version posted November 20, 2021. The copyright holder for this preprint (which was not certified by peer review) is the author/funder, who has granted bioRxiv a license to display the preprint in perpetuity. It is made available under aCC-BY-NC-ND 4.0 International license.

gently mixed with 50 ml KRP 0.1 % BSA. After 45 s 25 ml were withdrawn from the funnel representing the small adipocyte fraction. The missing volume in the funnel was replaced with KRP 0.1 % BSA and this procedure was repeated 4 times. Similarly, an intermediate fraction was obtained with a flotation time of 20 s. Afterwards, only large cells remained in the funnel which were directly withdrawn.

Adipocyte size determination

Computationally derived adipocyte size estimates from histology samples

GTEX adipocyte area estimates originated from an earlier analysis and published method, the Adipocyte U-Net (16). For additional RNA-Seq analysis of the GTEX samples and to factorize adipocyte area individuals were assigned to one of four bins with equally spaced area intervals (bin_{small} , bin_{medium} , bin_{large} , $bin_{X-large}$). Summary statistics on bin-specific phenotypes and adipocyte areas are given in Table 2.

Histology-based adipocyte sizing of samples used for FA composition measurements and MRS

At least three 5 μm sections with a minimum distance of 100 μm between sections were cut from FFPE WAT. Sections were H&E stained and stitched high definition range bright-field images at 200x magnification were taken (VHX 6000, Keyence). Adipocyte area was determined using the microscope's in-built image analysis software and diameter was calculated assuming spherical shape (VHX-6000, Version 3.2.0.121). A lower bound threshold of 200 μm^2 and an upper bound threshold of 16,000 μm^2 was set to remove artefacts (16). Identified objects were inspected manually and artifacts were excluded from the analysis. Summary statistics on adipocyte area and diameter of the samples that were either used to correlate adipocyte size with FA levels or results derived from MRS are given in Tables S5 & S6, respectively.

Mature adipocytes

To measure mature adipocyte diameter a glass-slide was wetted with 200 μl of PBS and approximately 20 μl of adipocytes were pipetted onto the slide. Stitched, bright-field images in high definition range were taken and adipocyte diameter was automatically determined using the

bioRxiv preprint doi: <https://doi.org/10.1101/2021.11.20.468818>; this version posted November 20, 2021. The copyright holder for this preprint (which was not certified by peer review) is the author/funder, who has granted bioRxiv a license to display the preprint in perpetuity. It is made available under aCC-BY-NC-ND 4.0 International license.

microscope's software (VHX-6000). Identified objects were inspected manually and artifacts were excluded from the analysis.

RNA isolation, sequencing and differential expression analysis

Mature adipocyte RNA isolation

600 μ l of adipocytes were pipetted into microtubes containing 600 μ l of RLT (Qiagen) 1 % β -mercaptoethanol (Merck), 200 mg of 0.5 mm ceramic beads (Carl-Roth), inverted and immediately snap-frozen. Samples were allowed to thaw on ice, the RLT 1 % β -Mercaptoethanol solution was removed and replaced with mirVana lysis buffer (Thermo Fisher Scientific). Samples were lysed for 3x 30 s in a homogenizer filled with dry ice set to 6.0 m/s (FastPrep, MP biomedical). Samples were centrifuged at 12,000 g for 10 min. at 4 °C. Using an insulin syringe (B. Braun) the adipocyte lysate located underneath the fat layer was transferred to a new tube. All remaining steps were carried out as described by the manufacturer.

RNA quality control of mature adipocytes

RNA concentration and 260/280 ratios from mature adipocytes were photometrically determined (Infinite 200 PRO, Tecan). The quality of isolated RNA was assessed based on RNA integrity number (RIN) obtained by using a Bioanalyzer RNA Nano chip (2100 Bioanalyzer, Agilent). Across all samples, high RNA integrity was observed with an average RIN of 9.0 ± 0.8 .

Mature adipocyte RNA sequencing

Library preparation, sequencing, and reference genome alignment of RNA isolated from mature adipocytes was carried out by the genomics services department of the Broad Institute. Reads were aligned to human genome assembly GRCh37 (hg19) using STAR (20). The number of raw read counts was determined using the feature counts function from the Rsubread package (21).

GTEX RNA-Seq data

Raw gene read counts and gene transcripts per kilobase million (TPM) were obtained through the GTEX portal from GTEX analysis V8 (dbGap accession phs000424.v8.p2) (14, 15).

bioRxiv preprint doi: <https://doi.org/10.1101/2021.11.20.468818>; this version posted November 20, 2021. The copyright holder for this preprint (which was not certified by peer review) is the author/funder, who has granted bioRxiv a license to display the preprint in perpetuity. It is made available under aCC-BY-NC-ND 4.0 International license.

Differential expression analysis

All RNA-Seq data was analyzed using edgeR (22-24). Multidimensional scaling (MDS) plots and dendrograms were generated to visualize clustering of samples dependent on experimental groups. EdgeR's quasi-likelihood pipeline was used to test for differential gene expression (24). Differential expression analysis was used to compare gene expression between GTEx-derived SAT and VAT samples. A differential expression model with adipocyte size as a categorical variable ($\text{bin}_{\text{small}}$ vs. $\text{bin}_{\text{X-large}}$) was applied to GTEx SAT and VAT samples. Additionally, a model relating gene expression to SAT or VAT adipocyte size expressed as a continuous variable was computed for the GTEx cohort. P-values from GTEx RNA-Seq analysis were FDR corrected and genes with an FDR < 0.05 and a \log_2 fold change > 1 were considered as significant.

In another differential expression analysis, the transcriptome of size-separated adipocytes (small fraction vs. large fraction) was compared. P-values from size-separated adipocytes were FDR corrected and genes with an FDR < 0.05 were considered as significant.

Gene set enrichment analysis

Gene set enrichment analysis based on the Kyoto Encyclopedia of Genes and Genomes (KEGG) was carried out using clusterProfiler (25). Data visualization in the form of pathway graphs was achieved using pathview (26).

BATLAS analysis

SAT and VAT TPM expression values obtained from the GTEx portal were filtered for the relevant BATLAS marker genes (27). TPM expression values of marker genes that were not expressed in the GTEx cohort were set to zero. Brown and beige adipocyte content estimates per individual and respective WAT depot were obtained from the BATLAS web tools results sheet (<https://shiny.hest.ethz.ch/BATLAS/>) and mean-centered for all later statistical analysis .

bioRxiv preprint doi: <https://doi.org/10.1101/2021.11.20.468818>; this version posted November 20, 2021. The copyright holder for this preprint (which was not certified by peer review) is the author/funder, who has granted bioRxiv a license to display the preprint in perpetuity. It is made available under aCC-BY-NC-ND 4.0 International license.

Adipose tissue fatty acid composition

Adipose tissue FA composition was determined based on FAME GC-MS in samples from abdominoplasty, general surgery or laparoscopy (28). 10 – 20 mg of wet adipose tissue were snap-frozen on dry ice immediately after excision in tubes containing 700 mg lysing matrix D (MP biomedical). Samples were weighed, allowed to thaw on wet ice, and concentration was set to 0.05 mg/μl using equal parts MeOH and water (LiChrosolv, Merck). Tissue was lysed using a homogenizer (FastPrep) set to 30 s and 6 m/s. Transesterification was carried out as described earlier and FAMES were extracted using hexane (LiChrosolv, Merck) (28, 29). GC-MS based total FA analysis was performed as previously published (28). Individual FA species were presented as molar percentages of the total FA profile.

Magnetic resonance spectroscopy

Lipid droplet phantom studies

As a validation strategy and to further elucidate the interplay of lipid droplet size and the degree of FA unsaturation in the formation of MR signals, lipid droplet phantoms were manufactured (30). Preceding emulsification, the FA composition and degree of unsaturation of different vegetable oils were validated using FAME GC-MS. Sunflower seed oil and linseed oil were diluted 1:500 and 1:1000 in 3:1 isooctane isopropyl alcohol (LiChrosolv, Merck). Transesterification and GC-MS were carried out similarly to WAT samples as described above. Lipid droplet phantoms were manufactured with the following ratios of sunflower and linseed oil: 1:0, 1:2, 2:1, 0:1. All lipid droplet phantoms were produced with a fat content of 80 % and a water content of 20 % closely resembling human WAT composition (31, 32). For emulsification and conservation purposes the aqueous phase contained 2 % (v/v) tween 80 (Merck) and 0.5 % (m/m) sodium benzoate (Merck). Emulsification was carried out using a colloid mill (Labor-Pilot 2000/4, IKA-Werke) set to 3000, 5000, 8000, and 12,000 rpm to obtain different lipid droplet sizes within the water matrix as described earlier (30, 33, 34). The generated lipid droplet size spectrum was determined using a

bioRxiv preprint doi: <https://doi.org/10.1101/2021.11.20.468818>; this version posted November 20, 2021. The copyright holder for this preprint (which was not certified by peer review) is the author/funder, who has granted bioRxiv a license to display the preprint in perpetuity. It is made available under aCC-BY-NC-ND 4.0 International license.

laser diffraction particle size analyzer (Mastersizer 2000 with Hydro 2000S dispersing unit, Malvern Instruments).

Adipose tissue sample preparation

All human WAT samples originating from abdominoplasty, general surgery or laparoscopy used for MRS were fixed in 4 % formaldehyde (Histofix, Carl-Roth) for 24 hours and immediately measured afterwards.

Magnetic resonance spectroscopy

Lipid droplet phantoms and WAT were measured using a single-voxel short-TR multi-TI multi-TE (SHORTIE) stimulated echo acquisition mode (STEAM) MRS acquisition scheme (Figure 7A) (35). Both lipid droplet phantoms and WAT samples were measured using equivalent sequence parameters: Inversion time (TI) of 8, 83, 233, 458, 833, 1133 ms, echo time(TE) of 10, 15, 20, 25, 70 ms, mixing time (TM) of 16 ms, minimum repetition time (TR) of 801 ms, τ of 774 ms, 4 phase cycles in 4 averages, 2048 sampling points, spectral bandwidth of 3000 Hz, default voxel-size of 12x12x12 mm³ and a total scan time of 02:32 min. Spectra were obtained for all combinations of TI and TE. All measurements were performed at room temperature (21±1°C) on a clinical whole-body 3T MRI scanner (Ingenia Elition X, Philips Healthcare, The Netherlands). For signal reception, either the clinical 8-channel small extremity coil or the clinical 8-channel wrist coil was used depending on sample size. The acquired MRS data was processed using SVD-based coil combination followed by simple averaging and zero-order phase correction (36). Signal fitting was carried out using a time domain-based joint-series model fitting routine implemented in MATLAB (R2019b) using NL2SOL (37). The SHORTIE signal as a function of time S(t) was modeled as:

$$S(t) = e^{j\phi} \sum_i \rho_i e^{(j2\pi\omega_i - d_i - g_i t)t} \left(1 - 2e^{-\frac{TI}{T_{1,i}}} + e^{-\frac{\tau+TI}{T_{1,i}}} \right) e^{-\frac{TM}{T_{1,i}} - \frac{TE}{T_{2,i}}}$$

where ϕ represents a common phase term, ρ_i is the proton density, ω_i is the precession frequency, d_i and g_i are the Lorentzian and Gaussian damping factors, and $T_{1,i}$ and $T_{2,i}$ are the relaxation times of the i th frequency component, respectively. TI is the inversion time; TM is the mixing time and

bioRxiv preprint doi: <https://doi.org/10.1101/2021.11.20.468818>; this version posted November 20, 2021. The copyright holder for this preprint (which was not certified by peer review) is the author/funder, who has granted bioRxiv a license to display the preprint in perpetuity. It is made available under aCC-BY-NC-ND 4.0 International license.

TE is the echo time. The proton MR-based FA profile characterization is based on the assumption that all MR-detectable FAs are present in the form of triglycerides and that all MR-detectable signals originate from water and triglycerides. Consequently, a 11-peak-signal-model was fitted with in total 21 degrees of freedom including constraints for a 10-peak-triglyceride-model and relaxation properties (Table S7) (38). In course of the parametrization of the triglyceride model, the FA profile characterization results from three triglyceride characteristics: the mean number of double bounds per triglyceride (ndb), the mean number of methylene interrupted double bounds per triglyceride (nmidb) and the mean fatty acid carbon chain length (CL).

Statistical analysis

Data analysis was carried out using R (39). If not specified otherwise all results were given as mean \pm SD. According to the sample distribution, variance, and experimental setting (paired vs. unpaired) parametric tests (paired samples t-test, independent samples t-test) or non-parametric tests (Mann-Whitney test, Wilcoxon signed-rank test) were used to test for/against differences between groups. Similarly, Pearson or Spearman correlation analysis was applied to investigate the association between continuous variables. One-sided tests were used within the BATLAS analysis to investigate whether a decrease in brown/beige adipocyte content was observed with larger fat cell size. Bonferroni correction was used to adjust for multiple testing in the FA composition analysis. Across all analyses p-values < 0.05 were considered significant. Linear regression analysis of the MRS data was carried out in python (V3.6.10) using the scipy package (V1.4.1).

Study approval

All tissue donors gave written informed consent. The study protocols were approved by the ethics committee of the Technical University of Munich (Study №: 5716/13, 1946/07, 409/16s)

RESULTS

SAT and VAT display different gene expression signatures

To assess the overall gene expression differences between SAT and VAT, GTEx derived bulk tissue RNA-Seq data was used. As visible by two distinct clusters in the MDS plot and two separate branches in the dendrogram, global SAT and VAT gene expression were clearly distinguishable from each other ($n_{\text{paired}} = 99$, Figure 1A, 1B). Differential gene expression analysis revealed a total of 689 genes characterized by positive fold changes (FC) and thus higher expression levels in SAT compared to VAT (FDR < 0.05, $\log_2(\text{FC}) > 1$; Figure 1C, Table S1_A), while 1437 genes were higher expressed in VAT compared to SAT (FDR < 0.05, $\log_2(\text{FC}) > 1$; Figure 1C, Table S1_A). A large fraction of the top differentially expressed targets were identified as genes of “developmental origin” (*HOX family*, *IRX3*, *IRX5*, *TBX15*, *SHOX2*, *NR2F1*; Figure 1C). Amongst genes that were not related to cell fate and development, *MMP3*, known to be involved in the breakdown of extracellular matrix, showed strong enrichment in SAT ($\log_2(\text{FC}) = -7.82$, FDR = 2.71×10^{-31} , Figure 1C). On the contrary, *ALOX15* expression was multiple fold higher in VAT compared to SAT and among the top 20 differentially expressed genes in the present analysis ($\log_2(\text{FC}) = -10.11$, FDR = 2.49×10^{-62} , Figure 1C, Table S1_A). *ALOX15*, is involved in the metabolism of poly-unsaturated FAs (PUFAS), producing both pro- and anti-inflammatory mediators, dependent on its FA substrates (40). KEGG gene set enrichment analysis revealed differences between the two different depots revolving around chemokine and cytokine related signaling (*hsa04060*:Cytokine-cytokine receptor interaction, FDR = 1.63×10^{-6} ; *hsa04062*:Chemokine signaling pathway, FDR = 3.44×10^{-4}), inflammatory processes (*hsa04668*:TNF signaling, FDR = 0.0084; *hsa04064*:NF-kappa b signaling, FDR = 7.51×10^{-4}) as well as energy metabolism (*hsa00190*:Oxidative phosphorylation, FDR = 0.010). An overview of the top 20 enriched KEGG pathways with an adjusted p-value < 0.05 is given in Figure 1D and all significantly enriched KEGG pathways are depicted in Table S1_B.

The SAT and VAT transcriptome is altered with adipocyte hypertrophy

To evaluate the link between adipocyte area and gene expression profiles, individuals from GTEx were stratified into four equally spaced adipocyte area bins (16). A 2.75 fold change in SAT mean adipocyte area was observed between individuals assigned to either bin_{small} (n = 20, mean adipocyte area = 1,383 ± 241 μm²) or bin_{X-large} (n = 28, mean adipocyte area = 3,797 ± 235 μm²) (Table 2). Substantial changes in SAT gene expression were observed when comparing small with X-large adipocytes, including increased expression of 621 genes in bin_{X-large} compared to bin_{small} (FDR < 0.05, log₂(FC) > 1; Figure 2A, Table S2_A). 369 genes were characterized by higher expression in the small compared to the X-large bin (FDR < 0.05, log₂(FC) > 1; Table S2_A). Amongst the top-ranked genes, *SLC27A2* exhibited significantly higher expression in the group with small adipocytes (FDR = 6.33e⁻⁰⁹, log₂(FC) = -3.90, Figure 2A, Table S2_A). Further *SLC27A2* ranked highest by FDR in a differential expression analysis where SAT adipocyte area was set as a continuous covariate (n = 153, FDR = 1.74e⁻¹⁴; Figure 2C, Table S2_B). *SLC27A1* (alias FATP1), the very long-chain FA transporter that is mainly expressed in WAT and that has been previously associated with obesity was not found to be differentially expressed concerning SAT adipocyte area (FDR_{binned} = 0.70, FDR_{continuous} = 0.33) (41, 42). Furthermore, *EGFL6* which has been previously related to obesity and the proliferation of human adipose mesenchymal stem cells was found to be higher expressed in individuals with larger SAT adipocyte areas (FDR = 2.83e⁻⁰⁵, log₂(FC) = 4.67, Figure 2A)(43). In the SAT differential gene expression model with adipocyte area as a continuous covariate *SLC27A2* (FDR = 1.74e⁻¹⁴), *AMN* (5.89e⁻¹⁴), *TC36* (FDR = 8.02e⁻¹⁴), *PTPN3* (FDR = 6.03e⁻¹³), and *TOX3* (2.46e⁻¹²) were found as the top 5 genes by FDR (Figure 2C, top row; Table S2_B). An overview of all genes with an FDR < 0.05 overlapping between the binned and continuous model is given in Table S2_C and Figure S1A. The present work is consistent and expands on recent studies to link gene expression with obesity, adipogenesis and fat cell size (12, 44). Amongst others, negative associations between SAT adipocyte area, *SLC2A4* (alias *GLUT4*, FDR = 1.72e⁻⁰⁴), *INSR* (FDR = 0.0013) and *CS* (FDR =

bioRxiv preprint doi: <https://doi.org/10.1101/2021.11.20.468818>; this version posted November 20, 2021. The copyright holder for this preprint (which was not certified by peer review) is the author/funder, who has granted bioRxiv a license to display the preprint in perpetuity. It is made available under aCC-BY-NC-ND 4.0 International license.

0.0016) were found, while *TNF* ($3.07e^{-04}$) and *EGFL6* (0.014) were positively related with adipocyte area (Figure 2C, bottom row; Table S2_B). KEGG gene set analysis in SAT revealed significant positive enrichment of genes involved in immune-related and inflammatory processes for individuals assigned to the bin_{XL} group (*hsa04640*:Hematopoietic cell lineage, FDR = $1.05e^{-07}$; *hsa04060*:Cytokine-cytokine receptor interaction, FDR = $5.47e^{-09}$; *hsa04064*:NF-kappa B signaling pathway, FDR = $6.48e^{-08}$; Figure 2B; Table S2_D). On the contrary, negative enrichment was seen for gene sets involved in key adipose tissue metabolic processes, such as *hsa04923*:Regulation of lipolysis in adipocytes (FDR = $1.13e^{-05}$; Figure 2B; Table S2_D) and *hsa00620*:Pyruvate metabolism (FDR = $6.48e^{-06}$; Figure 2B; Table S2_D). The analysis further revealed highly significant negative enrichment for *hsa03010*:Ribosome (FDR = $5.47e^{-09}$, Figure 2B; Table S2_D) and *hsa00190*:Oxidative phosphorylation (FDR = $5.47e^{-09}$, Figure 2B; Table S2_D). Pathway analysis confirmed this finding and revealed a consistent negative enrichment of subunits from the mitochondrial respiratory chain in SAT from individuals with enlarged adipocytes (Figure 2D).

VAT adipocyte area binning resulted in a 3.54 fold change in fat cell size between the smallest and largest bin (Table 2). Differences in VAT adipocyte area were reflected by size-bin specific transcriptomic signatures with 500 genes showing higher expression in $bin_{X-large}$ compared to bin_{small} and 327 genes showing higher expression in bin_{small} versus $bin_{X-Large}$ (FDR < 0.05, $\log_2(FC) > 1$ or $\log_2(FC) < -1$, respectively; Table S3_A). A differential gene expression model with adipocyte area as a continuous covariate was applied to account for unequal group sizes and sex distributions. The continuous model revealed a higher number of significant genes with an FDR < 0.05 (continuous: 4,194 genes; categorical: 1,896 genes; Figure S1B, Table S3_B) most likely due to higher sample sizes ($n_{cont} = 141$). Differentially expressed genes from the categorical model were overlapping with the genes from the continuous model with only 208 differentially expressed genes specific to the categorical model (Figure S1B, Table S3_C). An overview of ten exemplary genes that were found amongst the top 20 adipocyte size dependent genes in VAT by the

bioRxiv preprint doi: <https://doi.org/10.1101/2021.11.20.468818>; this version posted November 20, 2021. The copyright holder for this preprint (which was not certified by peer review) is the author/funder, who has granted bioRxiv a license to display the preprint in perpetuity. It is made available under aCC-BY-NC-ND 4.0 International license.

continuous model is given in Figure 3A. All differentially expressed genes from the continuous model are listed in Table S3_B. With both models a strong negative relationship between *ELOVL6* and adipocyte area was found ($FDR_{\text{continuous}} = 1.92e^{-12}$, $FDR_{\text{cat}} = 9.88e^{-05}$, $\log_2(\text{FC})_{\text{cat}} = -4.21$, Figure 3A). As depicted in Figure 3B, KEGG gene set enrichment analysis revealed significant negative enrichment for genes involved in metabolic pathways (*hsa00620*:Pyruvate metabolism, $FDR = 3.66e^{-05}$; *hsa00020*:Citric acid cycle (TCA), $FDR = 1.17e^{-05}$; *hsa01212*:Fatty acid metabolism, $FDR = 9.70e^{-07}$; Table S3_D), signaling (*hsa03320*:PPAR signaling pathways, $FDR = 8.80e^{-06}$; *hsa04910*:Insulin signaling, $FDR = 4.21e^{-05}$; Table S3_D) and energy homeostasis (*hsa00190*:Oxidative phosphorylation, $FDR = 2.29e^{-05}$; *hsa04714*:Thermogenesis, $FDR = 6.60e^{-09}$; Table S3_D). In line with findings from KEGG enrichment analysis suggesting that the FA metabolism of individuals with large adipocytes is perturbed and an inverse relationship between adipocyte area and *ELOVL6*, a negative relationship between adipocyte area and *FASN* expression ($FDR_{\text{cat}} = 0.004$, $\log_2(\text{FC})_{\text{cat}} = -3.23$; $FDR_{\text{cont}} = 2.02e^{-06}$) was observed in both models (Figure 3C). In agreement with the KEGG pathway analysis, the categorical and the continuous model revealed reduced expression of *UCP-1* in VAT from individuals with enlarged fat cells ($FDR_{\text{cat}} = 0.017$, $\log_2(\text{FC})_{\text{cat}} = -4.74$; $FDR_{\text{cont}} = 1.57e^{-05}$, Figure 3C). A detailed visualization of the KEGG thermogenesis pathway indicated concordant negative enrichment of genes involved in lipolysis (*ATGL*, *HSL*, *PLIN*), respiration and energy dissipation (*UCP-1*) in VAT from individuals with hypertrophic adipocytes (Figure 3D). Together, adipocyte hypertrophy in both SAT and VAT was associated with decreased marker gene expression of genes involved in processes crucial for WAT function and homeostasis, i.e. FA metabolism and mitochondrial activity.

bioRxiv preprint doi: <https://doi.org/10.1101/2021.11.20.468818>; this version posted November 20, 2021. The copyright holder for this preprint (which was not certified by peer review) is the author/funder, who has granted bioRxiv a license to display the preprint in perpetuity. It is made available under aCC-BY-NC-ND 4.0 International license.

Adipocyte size is inversely associated with the thermogenic adipocyte content of SAT and VAT

To further elucidate the link between adipocyte area and mitochondrial activity, the brown adipose tissue atlas (BATLAS) deconvolution tool was used to estimate brown and beige adipocyte content in GTEx WAT biopsies as a proxy of thermogenesis and browning capacity (27). BATLAS analysis revealed substantial differences in estimated thermogenic adipocyte content dependent on WAT depot and adipocyte area (Table 3). A 6.13 % higher brown/beige adipocyte content was predicted in paired VAT compared to SAT derived from 99 individuals ($p_{\text{paired t-test}} = 2.07e^{-06}$ Figure 4A, Table 3). In both VAT and SAT, BATLAS predicted a decrease in brown/beige adipocyte content with hypertrophic ($\text{bin}_{\text{X-Large}}$) compared to small adipocytes ($\text{bin}_{\text{small}}$). A 8.79 % and 13.57 % reduction in brown/beige adipocyte content was observed for SAT and VAT, respectively (SC: $n_{\text{binSmall}} = 20$, $n_{\text{binX-Large}} = 28$, $p_{\text{Wilcoxon}} = 0.0013$; VC: $n_{\text{binSmall}} = 41$, $n_{\text{binX-Large}} = 11$, $p_{\text{t-test}} = 0.0038$; Figure 4B, 4C, Table 3). Findings from the binned analysis were confirmed by correlating the estimated brown adipose tissue (BAT) content with adipocyte area across all samples from both adipose depots. In SAT, a negative relationship between brown/beige adipocyte content and adipocyte area was found ($n = 153$, $\rho_{\text{spearman}} = -0.16$, $p = 0.026$, Figure 4B). Similar results were observed in VAT where adipocyte area was inversely associated with BAT content estimated by BATLAS ($n = 141$, $r_{\text{Pearson}} = -0.3$, $p = 1.57e^{-04}$, Figure 4C). A slightly higher overall BAT content and a stronger negative relationship with adipocyte area were seen for VAT. In both depots, multiple of the 98 BAT marker genes published by *Perdikari et al.* (27) were also found to be significant with an FDR < 0.05 between the $\text{bin}_{\text{small}}$ and $\text{bin}_{\text{X-Large}}$ groups (Figure 4D, 4E). Among the significant genes, greater fold changes of BAT marker genes were observed in VAT compared to SAT (Figure 4D, 4E). From all BATLAS BAT marker genes *KCNK3* showed the strongest downregulation in SAT from individuals with large adipocytes (Figure 4D; $\log_2(\text{FC}) = -1.41$, $p = 2.54e^{-04}$). In VAT, *UCP-1* showed the strongest downregulation in individuals with large adipocytes (Figure 4E; $\log_2(\text{FC}) = -$

bioRxiv preprint doi: <https://doi.org/10.1101/2021.11.20.468818>; this version posted November 20, 2021. The copyright holder for this preprint (which was not certified by peer review) is the author/funder, who has granted bioRxiv a license to display the preprint in perpetuity. It is made available under aCC-BY-NC-ND 4.0 International license.

4.74, $p = 0.017$). Similarly, the continuous model indicated a significant negative relationship between *UCP-1* expression and VAT adipocyte area ($FDR = 1.57e^{-05}$).

RNA-Seq reveals differences in the transcriptomic signature between small and large adipocytes from the same individual involving FA metabolism and inflammation.

Results concerning the investigations on bulk adipose tissue from individuals with diverse genetic backgrounds (GTEx cohort) suggest substantial differences in transcriptomic signatures between individuals with large and small fat cells. To clarify, whether the observed differences in tissue can be explained by the transcriptomic signatures of large adipocytes themselves an investigation was carried out on the intra-individual gene expression patterns of size-separated mature adipocytes. Size separation based on buoyancy resulted in an average size difference of 2.98 fold between the small and large fraction (Figure 5A). RNA-Seq revealed 583 genes to be differentially expressed ($FDR < 0.05$) between small and large adipocytes (Table S4_A). 480 genes were upregulated in the large fraction, while 103 genes were higher expressed in the small fraction (Figure 5B; Table S4_A). KEGG pathway analysis revealed pathways analogous to the cross-sectional GTEx cohort to be enriched in the large (*hsa04151*:PI3K-Akt signaling, $FDR = 0.014$; *hsa03010*:Ribosome, $FDR = 0.0049$) and small fraction (*hsa04512*:Carbon metabolism, $FDR = 0.0013$; *hsa00020*:Citrate cycle, $FDR = 0.011$; *hsa00620*:Pyruvate metabolism, $FDR = 0.015$), respectively (Figure 5C; Table S4_B). In contrast to the GTEx tissue-based analysis, OXPHOS and thermogenesis were not significantly enriched in the KEGG gene set enrichment analysis. Further, no major differences in BATLAS predicted thermogenic adipocyte content was observed (data not shown). In conclusion, intra-individual variance of adipocyte size did not alter the expression of genes related to OXPHOS and thermogenesis. The evidence for a decreased expression of genes related to respiratory chain function and thermogenesis was therefore limited to the GTEx RNA-Seq analysis assessing inter-individual differences in gene expression with regard to adipocyte area.

Adipose tissue FA composition is related to adipocyte size

To further understand the link between adipocyte area and FA metabolism that the data revealed in the gene set enrichment analysis, i.e. size-, and depot-dependent expression of de novo lipogenesis (DNL) and FA elongation related marker genes, the relationship between WAT FA composition and adipocyte diameter was investigated. Comparisons of the FA composition between SAT and VAT revealed an increased relative abundance of the saturated FA species lauric acid (12:0, $p = 0.05$), myristic acid (14:0, $p = 0.026$) and arachidic acid (20:0, $p = 0.0091$) in VAT (Figure 6A). In contrast, ω -3 and ω -6 PUFAs with chain lengths of 20 or 22 carbon atoms were significantly higher in SAT (Figure 6A). Out of all FA species the ω -6 FA, arachidonic acid (ARA) showed the highest significance (FA20:4 (n-6), $p = 0.00082$, Figure 6A). Similar to depot-specific FA patterns the results indicate that FA composition is dependent on adipocyte diameter in both depots. In SAT a positive relationship between C20 & C22 PUFAs and adipocyte diameter was observed, while an inverse association was revealed predominantly for medium-chain saturated FAs in VAT (Figure 6B, 6C). Associations between SAT adipocyte diameter and capric acid (FA 10:0, $r_{\text{Pearson}} = -0.71$, $p = 2.28e^{-04}$), eicosapentaenoic acid (FA20:5 (n-3); $r_{\text{Pearson}} = 0.70$, $p = 2.66e^{-04}$) and ARA (FA20:4 (n-6); $r_{\text{Pearson}} = 0.70$, $p = 1.29e^{-03}$) were observed (Figure 6B, 6C). Inverse relationships of VAT adipocyte diameter with myristic acid (FA14:0, $r_{\text{pearson}} = -0.88$, $p = 1.51e^{-04}$), pentadecylic acid (FA15:0, $r_{\text{pearson}} = -0.84$, $p = 5.58e^{-04}$) and arachidic acid (FA20:0, $r_{\text{pearson}} = -0.71$, $p = 0.01$) were detected (Figure 6B, 6C).

MRS is suitable for the non-invasive and in-parallel characterization WAT fat cell size and FA composition

To facilitate the translation of adipocyte size associated changes in FA and transcriptomic signatures into clinical practice an MRS-based technique for the simultaneous characterization of FA composition and adipocyte cell size-based relaxation properties was developed. As previously shown by our group, water-fat emulsions are a valuable model system to generate lipid droplets

bioRxiv preprint doi: <https://doi.org/10.1101/2021.11.20.468818>; this version posted November 20, 2021. The copyright holder for this preprint (which was not certified by peer review) is the author/funder, who has granted bioRxiv a license to display the preprint in perpetuity. It is made available under aCC-BY-NC-ND 4.0 International license.

with highly defined size ranges for the MR-based morphological characterization of lipid-rich samples (water/fat content & droplet size) (18, 30).

Independent of the ratio of sunflower to linseed oil, increasing lipid droplet diameters were observed with decreasing revolutions per minute of the colloid mill (Figure S2 A – F, Table S8). At similar rpms a trend towards smaller lipid diameter with increasing linseed oil content was observed (Table S8). As published, linoleic acid (18:2 n-6) was the most abundant FA in sunflower oil (Figure S2 G), while linolenic acid (18:3 n-3) was the most frequent FA in linseed oil (Figure S2 H). ω -6 FAs (59 %) were predominant in sunflower oil, while linseed oil showed a high ω -3 FA (56 %) content (Table S9) (45).

The lipid droplet phantom experiment served as a control experiment and indicated that FA characteristics *ndb* ($r = 0.762$, $p < 0.001$) and *nmdb* ($r = 0.980$, $p < 0.001$) can be adequately quantified independent from the median lipid droplet size (Figure 7B). The carbon chain length (CL) parameter showed a negative correlation between MRS and GC-MS ($r = -0.900$, $p < 0.001$). Furthermore, the lipid droplet phantom experiment revealed that the T2 relaxation of the triglyceride's methylene frequency was highly correlated with the median lipid droplet size ($r = 0.988$, $p < 0.001$) independently from the presence of double bounds (Figure 7C). Also, the statistics for T1 relaxation of the triglyceride's methylene frequency vs. median lipid droplet size showed a negative correlation ($r = -0.845$, $p < 0.001$). In contrast, the water component exhibited a positive correlation for the T1 relaxation ($r = 0.711$, $p < 0.001$) and a negative more likely exponential correlation for the T2 relaxation ($r = -0.849$, $p < 0.001$) vs. the median lipid droplet size, respectively.

The *in vitro* WAT MRS experiment was conducted with samples from abdominoplasty, general surgery and laparoscopy. Matched MRS, histology and GC-MS data was available for 32 samples originating from 21 donors. Similar to the lipid droplet phantom experiment, a positive but weaker correlation between MRS and GC-MS for the FA characteristics *ndb* ($r = 0.446$, $p = 0.011$) and

bioRxiv preprint doi: <https://doi.org/10.1101/2021.11.20.468818>; this version posted November 20, 2021. The copyright holder for this preprint (which was not certified by peer review) is the author/funder, who has granted bioRxiv a license to display the preprint in perpetuity. It is made available under a [CC-BY-NC-ND 4.0 International license](#).

nmidb ($r = 0.773$, $p < 0.001$) was found. No correlation between MRS and GC-MS was observed for FA chain length (Figure 8B).

The linear regression analysis between the median fat cell size diameter and FA characteristics (Figure 8C) revealed significant moderate correlation for the GC-MS-based ndb ($r = 0.374$, $p = 0.035$), nmidb ($r = 0.512$, $p = 0.003$) and CL ($r = 0.419$, $p = 0.017$), but only showed a trend not reaching significance with the MRS-based ndb ($r = 0.192$, $p = 0.292$), nmidb ($r = 0.203$, $p = 0.265$) and CL ($r = 0.192$, $p = 0.292$). In contrast, the median fat cell diameter significantly correlated with both T1 ($r = 0.484$, $p = 0.005$) and T2 relaxation ($r = 0.472$, $p = 0.006$) of the methylene frequency (Figure 8D).

The histology matched MRS example (Figure 8A) of SAT in comparison from two female donors with comparable age (59 and 63 years) and BMI (36 and 34 kg/m²) revealed between the subjects a larger median fat cell size diameter (49.8 vs. 74.4 μm) together with a longer T1 (225 vs. 244 ms) and T2 relaxation time (51 vs. 57 ms) of the methylene frequency.

bioRxiv preprint doi: <https://doi.org/10.1101/2021.11.20.468818>; this version posted November 20, 2021. The copyright holder for this preprint (which was not certified by peer review) is the author/funder, who has granted bioRxiv a license to display the preprint in perpetuity. It is made available under aCC-BY-NC-ND 4.0 International license.

DISCUSSION

The depot-specific hypertrophic expansion of adipocytes has been identified as detrimental for the manifestation of metabolic disorders. Understanding the transcriptomic changes occurring with adipocyte hypertrophy and between different WAT depots is therefore of great relevance to identify the causal mechanisms underlying this relationship. Further, the translation of experimental findings into clinical practice remains a challenging task since morphology and composition analysis of WAT are laborious and heavily dependent on biopsy-based techniques. To overcome this limitation, the potential of MRS as a biopsy-free method for the in-parallel assessment of adipocyte size and FA composition was explored.

SAT and VAT display distinct transcriptomic signatures

Based on the differential expression of multiple developmental genes and transcription factors (*HOX* family, *IRX* family, *BARX1*) our study expands the currently existing body of evidence derived from lineage tracing studies and smaller transcriptional profiling studies indicating that SAT and VAT white adipocytes arise from different progenitors (46-51). Both KEGG gene set enrichment analysis and differential expression of individual genes (e.g. *ALOX15*) highlight that extensive hypertrophic VAT accumulation could lay the transcriptional foundation for the manifestation of metabolic disorders (4, 52-55). As a related finding we observed a significant reduction in the amounts of ARA in VAT. Decreased ARA levels in VAT compared to SAT could stem from an elevated expression of *ALOX15* and other transcripts of enzymes utilizing ARA for the production of pro-inflammatory mediators resulting in an exhaustion of the substrate (40, 56, 57)

Adipocyte hypertrophy leads to transcriptomic alterations in both SAT and VAT

Amongst other genes, we observed the strongest associations between gene expression and adipocyte size for *EGFL6* and *SLC27A2* in SAT. *EGFL6* has been previously associated with obesity and stimulates the proliferation of adipose tissue-derived stromal vascular cells (43). Further, *EGFL6* was found to be differentially expressed with adipocyte size in a recent spatial

bioRxiv preprint doi: <https://doi.org/10.1101/2021.11.20.468818>; this version posted November 20, 2021. The copyright holder for this preprint (which was not certified by peer review) is the author/funder, who has granted bioRxiv a license to display the preprint in perpetuity. It is made available under aCC-BY-NC-ND 4.0 International license.

transcriptomics-based characterization of SAT (13). *SLC27A2* is a FA transporter and an acyl-CoA synthase that shows substrate specificity towards long chain and very long chain ω -3 FAs (58). Expression of *SLC27A2* has previously been shown to be reduced after high fat overfeeding and correlated negatively with obesity and diabetes-related traits (59-61). In VAT a strong negative relationship between genes involved in DNL and elongation of its end products was observed (*FASN*, *ELOVL6*). In good agreement, a strong negative association between saturated FAs with ≤ 20 carbon atoms, typically representing products of DNL with adipocyte size was seen. Decreased rates of DNL could display a physiological response to limit adipocyte expansion and compensate for the increased availability of FAs derived from dietary sources.

Besides alterations in FA metabolism and DNL related genes, negative enrichment for KEGG ribosomal and mitochondrial pathways was observed in relation to adipocyte area in both depots. In contrast, immune and inflammatory pathways i.e. NF- κ B signaling were positively enriched and the expression of pro-inflammatory marker genes (*TNF- α* & *IL-6*) was increased in individuals with large adipocytes. Mitochondrial dysfunction due to a reduced expression of respiratory chain genes could i.e. lead to elevated levels of ROS production impacting the endocrine and metabolic functions of the tissue (62). While an elevated production of pro-inflammatory mediators was detected, gene set enrichment analysis suggested negative enrichment for genes involved in ribosomal processes and amino acid synthesis at least partially resembling a senescence associated phenotype (63). Together the identified adipocyte-size associated gene expression patterns provide a transcriptomic foundation for the manifestation of obesity and its related metabolic disorders.

To rule out possible confounding effects of the stromal vascular fraction and different genetic backgrounds mature adipocytes were separated based on size and their transcriptome was characterized using RNA-Seq. Similar pathways and genes were affected in size-separated adipocytes with the large adipocyte fraction displaying a metabolically more harmful expression profile. It is therefore concluded that the detrimental transcriptomic profile of WAT from individuals

bioRxiv preprint doi: <https://doi.org/10.1101/2021.11.20.468818>; this version posted November 20, 2021. The copyright holder for this preprint (which was not certified by peer review) is the author/funder, who has granted bioRxiv a license to display the preprint in perpetuity. It is made available under aCC-BY-NC-ND 4.0 International license.

with large fat cells is at least partially caused by enlarged mature adipocytes themselves. While inflammatory, ribosomal and metabolic pathways were affected in size-separated adipocytes in a similar manner to the cross-sectional analysis on WAT, OXPHOS and thermogenesis did not show significant enrichment. It is therefore hypothesized that OXPHOS gene expression is altered across the entire adipose tissue cell population in individuals with enlarged fat cells. These findings are in excellent agreement with respirometry studies from our group suggesting that mitochondrial respiratory chain capacity is inversely related to BMI and adipocyte size, while no differences in respiratory chain function were observed between size-separated adipocytes (19, 64-66). On the individual gene level, findings on size separated adipocytes are in good agreement with spatial transcriptomics results suggesting that mature adipocytes from different size quartiles display distinct transcriptomic signatures (13).

Significantly less genes were differentially expressed in size-separated adipocytes compared to WAT. While different size fractions from four individuals were compared, the bulk WAT analysis was conducted in more than 140 individuals. Further, in WAT next to mature adipocytes other cell types can contribute to gene expression (67). Another layer of complexity is added as gene expression of adipocytes is dependent on progenitor lineage, spatial localization within the tissue and proximity to other cell types (13).

Individuals with large adipocytes show a decrease in thermogenic adipocyte content

BAT can dissipate stored chemical energy (triglycerides) in the form of heat mediated by the inner mitochondrial membrane protein *UCP-1*. SAT and VAT browning could display a possible protective mechanism against excessive lipid storage, adipocyte hypertrophy, and at long last metabolic complications. Pathway analysis revealed negative enrichment for lipolysis and FA degradation-related genes in both depots, indicating that hypertrophic adipocytes favor lipid storage over lipid catabolism and thus provide a plausible mechanism for an increase in volume. In parallel, this phenomenon was accompanied by decreased expression of oxidative phosphorylation-related genes, indicating substantial mitochondrial aberrations with adipocyte

bioRxiv preprint doi: <https://doi.org/10.1101/2021.11.20.468818>; this version posted November 20, 2021. The copyright holder for this preprint (which was not certified by peer review) is the author/funder, who has granted bioRxiv a license to display the preprint in perpetuity. It is made available under aCC-BY-NC-ND 4.0 International license.

hypertrophy. As a novel finding, evidence for an inverse relationship between brown/beige adipocyte content and adipocyte size, especially in VAT is provided. A higher thermogenic adipocyte content in individuals with small adipocytes could be protective against excessive lipid accumulation, adipocyte hypertrophy and its associated metabolic complications. Vice versa, brown and beige adipocyte content seems to be blunted in individuals with large adipocytes giving a possible explanation for disproportionate lipid storage, an increased risk for adipocyte hypertrophy and an adverse transcriptomic and metabolic profile. As our study is associative, whether genetic predisposition, environmental stimuli or a bidirectional effect lead to the observed inverse relationship remains elusive and should be the object of future longitudinal studies. Together, with reduced expression of lipolytic and FA degrading genes our data indicate that a transcriptional shift from an energy-burning towards a lipid storing, pro-inflammatory phenotype is a central hallmark of hypertrophic WAT.

MRS-based methods for the simultaneous characterization of WAT morphology and FA composition

Being able to determine WAT FA composition and adipocyte size in parallel as prognostic biomarkers for metabolic disease using non-invasive diagnostic tools would be highly desirable. Therefore, an MR-based technique for the simultaneous characterization of fat cell size and FA composition was developed to pave the way towards a non-invasive assessment of WAT morphology and composition that could be applicable in a clinical context.

The lipid droplet phantom experiment demonstrated the feasibility of the characterization of the FA characteristics as described by ndb and nmidb , as previously reported (38). Beyond what was already known, the experiment empirically demonstrated for the first time the correlation of the methylene T2 relaxation with median lipid droplet size independent from the presence of double bounds in the considered range. Thus, the methylene T2 relaxation can be used as an indirect measure of lipid droplet size. As mature white adipocytes are unilocular with the lipid droplet taking up most of the intracellular space lipid droplet size characterization by T2 relaxation times can be

bioRxiv preprint doi: <https://doi.org/10.1101/2021.11.20.468818>; this version posted November 20, 2021. The copyright holder for this preprint (which was not certified by peer review) is the author/funder, who has granted bioRxiv a license to display the preprint in perpetuity. It is made available under aCC-BY-NC-ND 4.0 International license.

considered representative for the estimation WAT fat cell size. With MR relaxation properties being temperature-dependent it should be acknowledged that *in vivo* relaxation times at body temperature will differ from the reported relaxation times of excised room temperature WAT samples. Interestingly, SHORTIE MRS-based *ndb* and *nmdb* measures correlated well with those from GC-MS, but not with the median adipocyte diameter whereas SHORTIE MRS-based *ndb* and *nmdb* correlated with the GC-MS-based derivatives of *ndb* and *nmdb*. While we found a similar trend of increasing methylene T2 relaxation times with increasing lipid diameter in WAT, the significance of the correlation flipped for methylene T1 relaxation showing an increase in T1 with increasing diameter. The differences between the phantom and the WAT sample experiment maybe partly explained in consideration of a) the performed GC-MS and MRS are not characterizing the exact same pool of fatty acids and b) structural difference between emulsified lipid droplets and WAT microstructure. The relaxation-based characterization of the median fat cell size in WAT has several advantages compared to approaches based on the probing of restricted diffusion effects including reduced data acquisition times, reduced sensitivity to vibrational artefacts and reduced motion sensitivity (17, 18, 68). Furthermore, the reported MR parameter relationship pinpoints the possibility of a methodological translation of the proposed measurement framework into a quantitative imaging-based method allowing the spatially-resolved probing of multiple AT depots.

Therefore, an application towards an unperturbed *in-vivo* phenotyping of adipocyte size and FA composition is feasible and the object of future investigations. Being able to simultaneously probe morphological and compositional parameters of WAT in a non-invasive manner would offer the opportunity to longitudinally monitor adipocyte size and FA composition in various depots of the body. Further, parallel MR-based measurements of FA patterns and adipocyte hypertrophy could serve as a potential biomarker to detect early changes in WAT morphology and composition that might occur prior to the systemic manifestation of metabolic diseases.

bioRxiv preprint doi: <https://doi.org/10.1101/2021.11.20.468818>; this version posted November 20, 2021. The copyright holder for this preprint (which was not certified by peer review) is the author/funder, who has granted bioRxiv a license to display the preprint in perpetuity. It is made available under aCC-BY-NC-ND 4.0 International license.

Despite validating our findings from bulk tissue in size-separated adipocytes we cannot fully rule out a substantial contribution of other cell types from the stromal vascular fraction to the observed changes in gene expression in bulk tissue characterized by adipocyte hypertrophy. The reported MRS relaxation times could be also affected by other tissue properties beyond adipocyte size (e.g. tissue oxygenation) (69). The employed MRS sequence was not derived from a formal optimal design of experiment and could therefore be further optimized. J-modulations were considered neglectable and not accounted for in the signal modeling process which, however, may further improve FA characterization irrespective of its computational demand and modelling uncertainties.

The observed switch to an energy storing, pro-inflammatory transcriptome in individuals with large adipocytes, especially in metabolically more harmful VAT provides important novel mechanistic insights on the transcriptional background of hypertrophic obesity. The identified reduction in thermogenic adipocyte content in individuals with large fat cells could display a novel mechanism facilitating hypertrophic WAT expansion and manifestation of metabolic disorders. Our MR-based proof-of-concept approach could become a promising tool for the non-invasive estimation of FA composition and adipocyte size in-vivo. An earlier and better diagnosis of metabolic derangements based on adipose tissue morphology and FA composition before systemic manifestations occur could substantially improve the treatment and prevention of cardiometabolic disorders. The present work is a first step towards this goal, but needs confirmation in prospective human studies.

ACKNOWLEDGEMENTS

We are grateful to Prof. Dr. T. Huettl, Dr. U.Schulze-Eifling, Dr. C. Kleeberger, Dres. Hoffmann, Dr. O. Prokopchuk and their respective teams for obtaining adipose tissue samples. We thank S. Winkler for assisting with WAT sample collection, D. Weidlich for helpful discussions, M. Zamskiy, C. Held and L. Patzelt for helping with the logistics and execution of the MRS measurements.

bioRxiv preprint doi: <https://doi.org/10.1101/2021.11.20.468818>; this version posted November 20, 2021. The copyright holder for this preprint (which was not certified by peer review) is the author/funder, who has granted bioRxiv a license to display the preprint in perpetuity. It is made available under aCC-BY-NC-ND 4.0 International license.

TABLES

Table 1: Phenotype data, obtained sample types, and measured outcome variables of subjects that were included in the study.

Cohort	n [male/female]	Age [years]	BMI [kg/m ²]	Sample types	Outcome variables
GTEx SAT	153 100/53	20 – 29: 9 (5.9 %) 30 – 39: 11 (7.2. %) 40 – 49: 16 (10.5 %) 50 – 59: 46 (30.1 %) 60 – 69: 69 (45.1 %) 70 – 79: 2 (1.3 %)	N/A	WAT biopsies	RNA-Seq Adipocyte size
GTEx VAT	141 92/49	20 – 29: 10 (7.1 %) 30 – 39: 10 (7.1 %) 40 – 49: 16 (11.3 %) 50 – 59: 52 (36.9 %) 60 – 69: 49 (34.8 %) 70 – 79: 4 (2.8 %)	N/A	WAT biopsies	RNA-Seq Adipocyte size
GTEx Paired	99 64/35	20 – 29: 8 (8.1 %) 30 – 39: 8 (8.1 %) 40 – 49: 11 (11.1 %) 50 – 59: 35 (35.4 %) 60 – 69: 35 (35.4 %) 70 – 79: 2(2.0 %)	N/A	WAT biopsies	RNA-Seq Adipocyte size
Liposuction	4 0/4	39 ± 10	27.4 ± 5.8 1 N/A	Mature adipocytes separated by size	RNA-Seq Adipocyte size
Fatty acids SAT	22 1/21	45 ± 12	32.6 ± 6.7 1 N/A	WAT biopsies	FAME GC-MS Adipocyte size
Fatty acids VAT	12 5/7	53 ± 15	36.0 ± 11.4 1 N/A	WAT biopsies	FAME GC-MS Adipocyte size
Fatty acids Paired	7 2/5	46 ± 12	40.7 ± 7.6 1 N/A	WAT biopsies	FAME GC-MS Adipocyte size
MRS SAT	16 16/0	44 ± 12	30.6 ± 4.6	WAT biopsies	MRS-derived FA profile Methylene relaxation
MRS VAT	5 3/2	51 ± 14	34.7 ± 11.4	WAT biopsies	MRS- derived FA profile Methylene relaxation

Data is given as means ± SD. Age from GTEx individuals is specified as count (%) in 10 year brackets.

Table 2: Bin and depot specific GTEx phenotypes and adipocyte sizes

Bin	SAT				VAT			
	<i>Small</i>	<i>Medium</i>	<i>Large</i>	<i>X-Large</i>	<i>Small</i>	<i>Medium</i>	<i>Large</i>	<i>X-Large</i>
n	20	49	56	28	41	49	40	11
Mean Area ± SD [μm^2]	1,383 ± 241	2,261 ± 230	3,055 ± 270	3,797 ± 235	1,089 ± 240	2,043 ± 326	2,947 ± 255	3,860 ± 335
Area range min – max [μm^2]	907 – 1,759	1,790 – 2,598	2,618 – 3,468	3,487 – 4,325	482 – 1,503	1,556 – 2,540	2,570 – 3,403	3,580 – 4,612
Sex (Male/Female)	14/6	28/21	39/17	19/9	22/19	30/19	29/11	11/0
Age 20-29 [n/%]	3 (15%)	4 (8.2%)	2 (3.6%)	0 (0%)	8 (20%)	2 (4.1%)	0 (0%)	0 (0%)
Age 30-39 [n/%]	2 (10%)	1 (2.0%)	7 (12%)	1 (3.6%)	4 (9.8%)	1 (2.0%)	3 (7.5%)	2 (18%)
Age 40-49 [n/%]	2 (10%)	6 (12%)	7 (12%)	1 (3.6%)	5 (12%)	7 (14%)	4 (10%)	0 (0%)
Age 50-59 [n/%]	7 (35%)	14 (29%)	17 (30%)	8 (29%)	13 (32%)	16 (33%)	17 (42%)	6 (55%)
Age 60-69 [n/%]	6 (30%)	24 (49%)	21 (38%)	18 (64%)	11 (27%)	21 (43%)	14 (35%)	3 (27%)
Age 70-79 [n/%]	0 (0%)	0 (0%)	2 (3.6%)	0 (0%)	0 (0%)	2 (4.1%)	2 (5.0%)	0 (0%)

Data is given as means \pm SD. Age from GTEx individuals is specified as count (%) in 10 year brackets. Individuals were assigned to one of four bins with equally spaced adipocyte area intervals (small, medium, large, X-large).

bioRxiv preprint doi: <https://doi.org/10.1101/2021.11.20.468818>; this version posted November 20, 2021. The copyright holder for this preprint (which was not certified by peer review) is the author/funder, who has granted bioRxiv a license to display the preprint in perpetuity. It is made available under aCC-BY-NC-ND 4.0 International license.

Table 3: Tabular overview from the BATLAS analysis for the depot and size bin-specific changes in estimated brown adipocyte content as well as brown and white marker genes.

	% Change in brown adipocyte content predicted by BATLAS	BATLAS BAT marker genes with a FDR < 0.05	BATLAS WAT marker genes with a FDR < 0.05
SAT vs VAT	+ 6.13 %	5 ↓ / 61 ↑	9 ↓ / 5 ↑
SAT Bin_{small} vs- bin_{X-Large}	- 8.79 %	60 ↓ / 0 ↑	6 ↓ / 2 ↑
VAT Bin_{small} vs- bin_{X-Large}	- 13.57 %	42 ↓ / 0 ↑	1 ↓ / 1 ↑

bioRxiv preprint doi: <https://doi.org/10.1101/2021.11.20.468818>; this version posted November 20, 2021. The copyright holder for this preprint (which was not certified by peer review) is the author/funder, who has granted bioRxiv a license to display the preprint in perpetuity. It is made available under aCC-BY-NC-ND 4.0 International license.

FIGURES

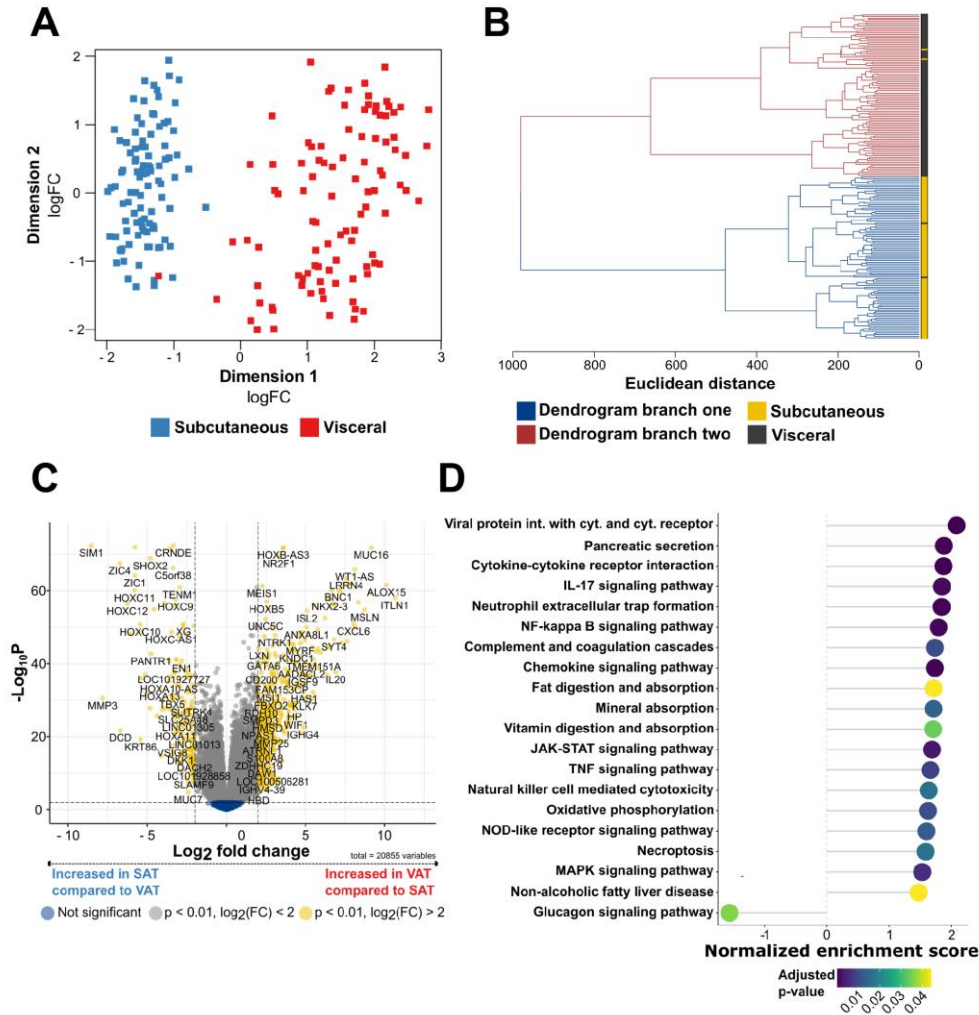
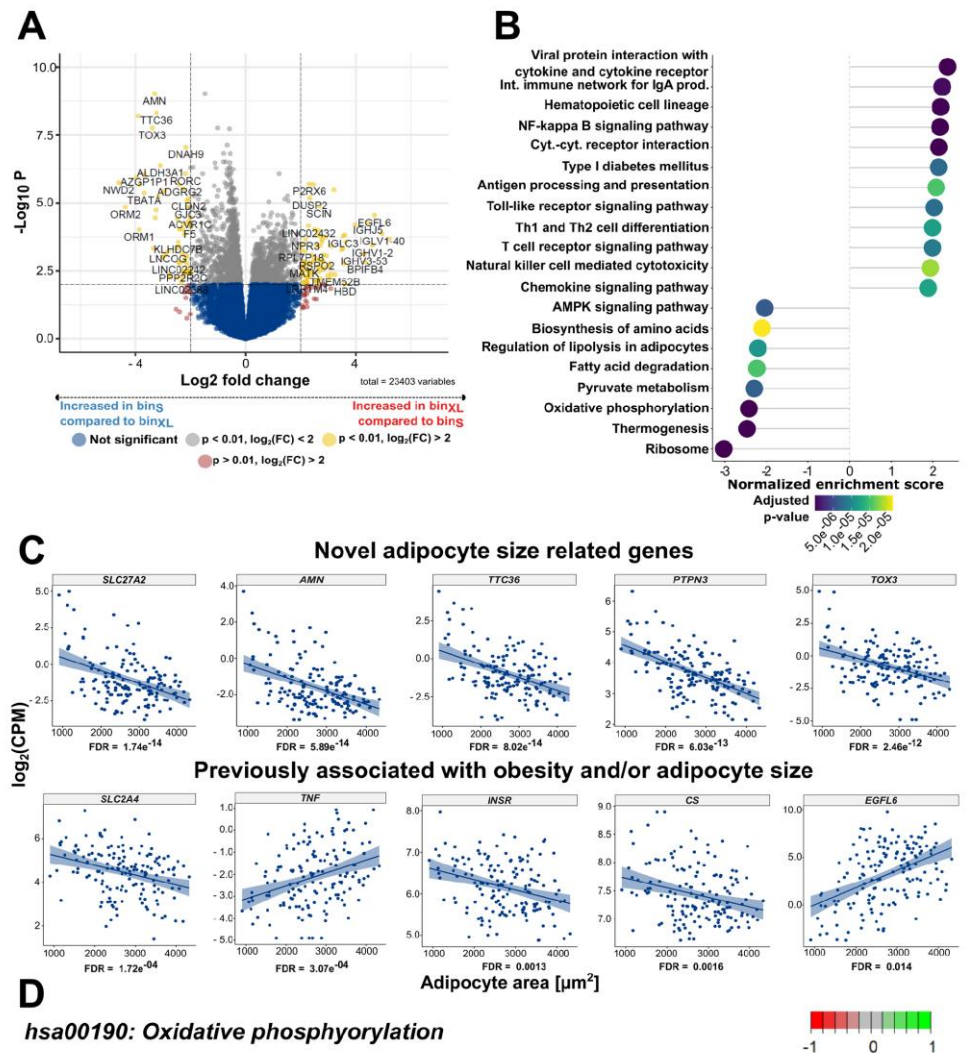


Figure 1: SAT and VAT are characterized by different transcriptomic signatures

(A) MDS plot displaying the first two dimensions of the data. (B) Hierarchical clustering of SAT and VAT samples based on euclidean sample distances. (C) Volcano plot showing differentially expressed genes between SAT and VAT (D) Lollipop plot displaying the top 20 enriched KEGG pathways with an adjusted p-value < 0.05 from gene set enrichment analysis, thereby comparing the expression of KEGG pathway associated genes from SAT and VAT depots.

bioRxiv preprint doi: <https://doi.org/10.1101/2021.11.20.468818>; this version posted November 20, 2021. The copyright holder for this preprint (which was not certified by peer review) is the author/funder, who has granted bioRxiv a license to display the preprint in perpetuity. It is made available under aCC-BY-NC-ND 4.0 International license.

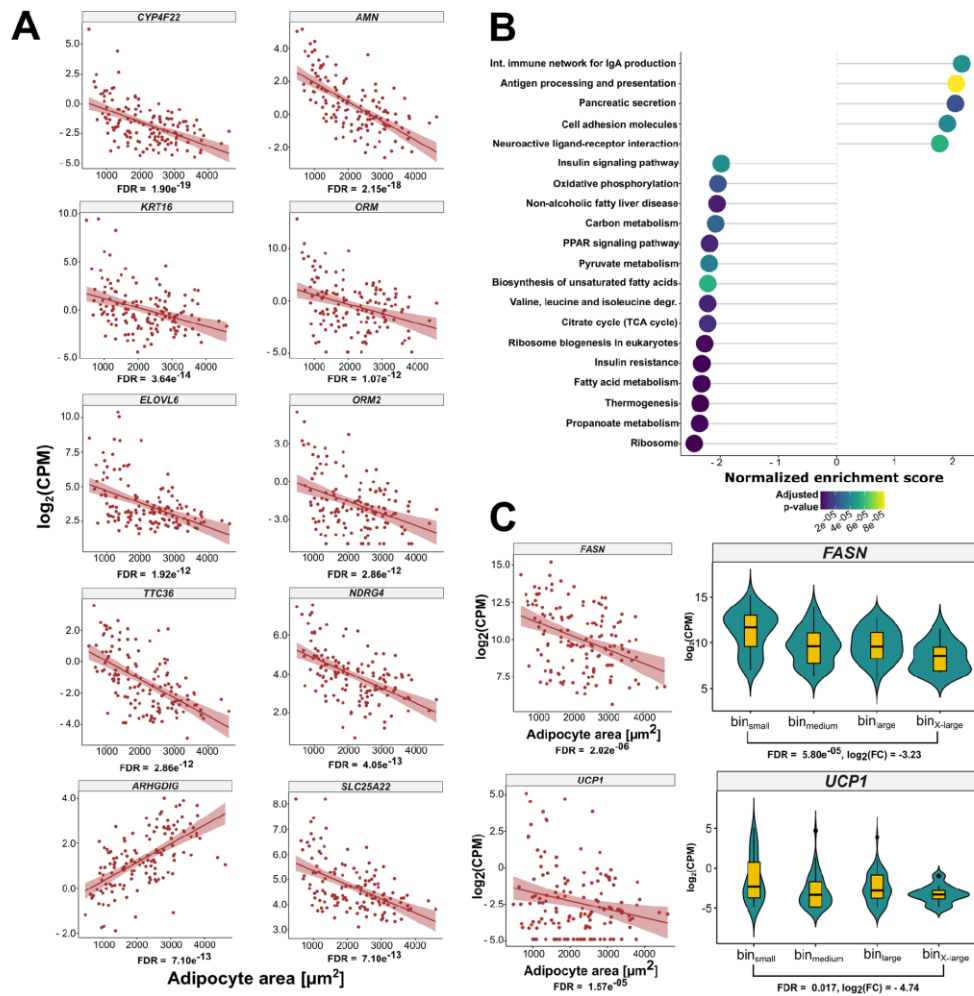


bioRxiv preprint doi: <https://doi.org/10.1101/2021.11.20.468818>; this version posted November 20, 2021. The copyright holder for this preprint (which was not certified by peer review) is the author/funder, who has granted bioRxiv a license to display the preprint in perpetuity. It is made available under aCC-BY-NC-ND 4.0 International license.

Figure 2: Adipocyte area is related to gene expression in SAT

(A) Volcano plot showing DE of genes between the $\text{bin}_{\text{small}}$ ($n = 20$) and $\text{bin}_{\text{X-Large}}$ ($n = 28$) in SAT. (B) Lollipop plot displaying the top 20 enriched KEGG pathways with an adjusted p-value < 0.05 from gene set enrichment analysis in SAT. The "Human Diseases" category of the KEGG pathway database was not displayed on the graph. (C) Scatterplots displaying the results of the continuous model-based analysis that was applied to GTEx RNA-Seq data from tSAT. Log_2 counts per million (CPM) are plotted against adipocyte area for 153 individuals. FDR is given for each gene below the plot. The upper half of the figure shows 5 of the top-ranked genes from the continuous model-based RNA-Seq analysis (*SLC27A2*, *AMN*, *TTC36*, *PTPN3*, *TOX3*). In the lower half 5 exemplary genes that are already known to be related to WAT biology and fat cell size that were also significant ($\text{FDR} < 0.05$) in our continuous model are depicted (*SLC2A4*, *TNF*, *INSR*, *CS*, *EGFL6*). A regression line including the standard error in a lighter shade of blue was added to the plots to visualize the relationship between gene expression and adipocyte area. (D) KEGG Pathview graph depicting the different complexes (I-V) of the respiratory chain (*hsa00190*: Oxidative phosphorylation). Red (-1) indicates mitochondrial complexes that are underrepresented in SAT from the $\text{bin}_{\text{X-Large}}$ group compared to the $\text{bin}_{\text{small}}$ group. In contrast, green (+1) displays complexes from the electron transport chain that are overrepresented in SAT from the $\text{bin}_{\text{X-Large}}$ group in relation to the $\text{bin}_{\text{small}}$ samples.

bioRxiv preprint doi: <https://doi.org/10.1101/2021.11.20.468818>; this version posted November 20, 2021. The copyright holder for this preprint (which was not certified by peer review) is the author/funder, who has granted bioRxiv a license to display the preprint in perpetuity. It is made available under aCC-BY-NC-ND 4.0 International license.



bioRxiv preprint doi: <https://doi.org/10.1101/2021.11.20.468818>; this version posted November 20, 2021. The copyright holder for this preprint (which was not certified by peer review) is the author/funder, who has granted bioRxiv a license to display the preprint in perpetuity. It is made available under aCC-BY-NC-ND 4.0 International license.

Figure 3: Adipocyte area is related to gene expression in VAT

(A) Scatterplots displaying the results of the continuous model-based analysis that was applied to GTEx RNA-Seq data from VAT. Log₂ counts per million (CPM) are plotted against adipocyte area for 141 individuals. FDR is given for each gene below the plot. Displayed is the relationship between adipocyte area and gene expression for 10 exemplary genes that were ranked highest in the analysis according to their FDR. A regression line including the standard error in a lighter shade of red was added to the plots to visualize the relationship between gene expression and adipocyte area. (B) Lollipop plot displaying the top 20 enriched KEGG pathways with an adjusted p-value < 0.05 from gene set enrichment analysis in VAT. The "Human Diseases" category of the KEGG PATHWAY database is not displayed on the graph. (C) Scatterplot and violin plot assessing the relationship between the expression of *FASN*, *UCP1* and adipocyte area. (D) KEGG Pathview graph depicting the different complexes and genes involved in the canonical thermogenesis pathway (hsa04714:Thermogenesis). Red (-1) indicates thermogenesis related genes that are underrepresented in VAT from the bin_{X-Large} group compared to the bin_{small} group. In contrast, green (+1) displays thermogenesis genes that are overrepresented in VAT from the bin_{X-Large} group in relation to the bin_{small} samples. Genes depicted in grey (0) did not show differences between the two groups.

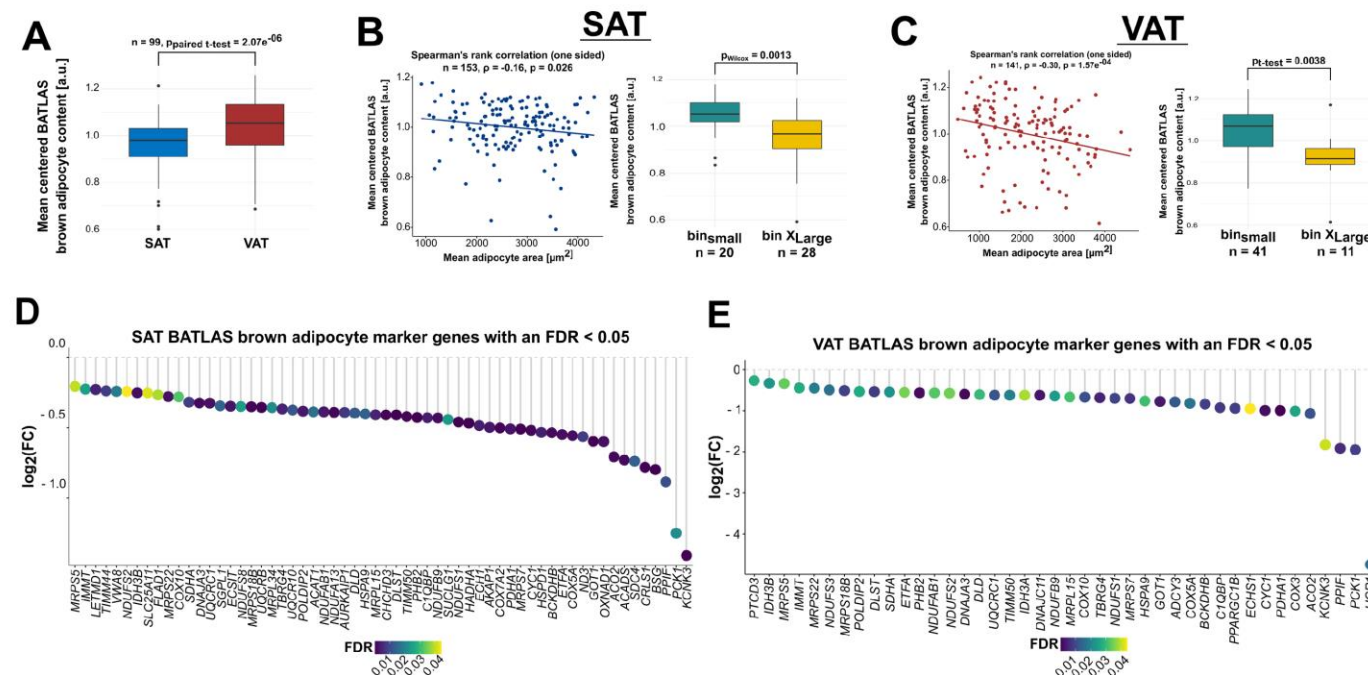


Figure 4: BATLAS analysis indicates differences in brown adipocyte content with adipocyte hypertrophy
(A) Tabular overview from BATLAS analysis for the depot and size bin-specific changes in estimated brown adipocyte content. Additionally, the number of the brown (n_{brown} marker genes = 98) and white (n_{white} marker genes = 21) marker genes from BATLAS that were differentially expressed with an FDR < 0.05 for the relevant group-wise comparisons are listed. **(B)** Boxplot comparing the mean-centered BATLAS estimated brown adipocyte content of paired SAT and VAT biopsies. **(C)** Scatterplot depicting the correlation between estimated brown adipocyte content and adipocyte area in SAT (left). Boxplot comparing the estimated brown adipocyte content between individuals with small ($\text{bin}_{\text{small}}$) and large subcutaneous adipocytes ($\text{bin}_{\text{XLarge}}$). **(D)** Scatterplot depicting the correlation between estimated brown adipocyte content and adipocyte area in VAT (left). Boxplot comparing the estimated brown adipocyte content between individuals with small ($\text{bin}_{\text{small}}$) and large visceral adipocytes ($\text{bin}_{\text{XLarge}}$) (right). **(E)** Lollipop plot depicting all BATLAS brown adipocyte marker genes that were found to be differentially expressed with a FDR < 0.05 in SAT group-wise comparisons between the $\text{bin}_{\text{small}}$ and $\text{bin}_{\text{XLarge}}$ group. **(F)** Lollipop plot depicting all BATLAS brown adipocyte marker genes that were found to be differentially expressed with a FDR < 0.05 in VAT group-wise comparisons between the $\text{bin}_{\text{small}}$ and $\text{bin}_{\text{XLarge}}$ group.

bioRxiv preprint doi: <https://doi.org/10.1101/2021.11.20.468818>; this version posted November 20, 2021. The copyright holder for this preprint (which was not certified by peer review) is the author/funder, who has granted bioRxiv a license to display the preprint in perpetuity. It is made available under aCC-BY-NC-ND 4.0 International license.

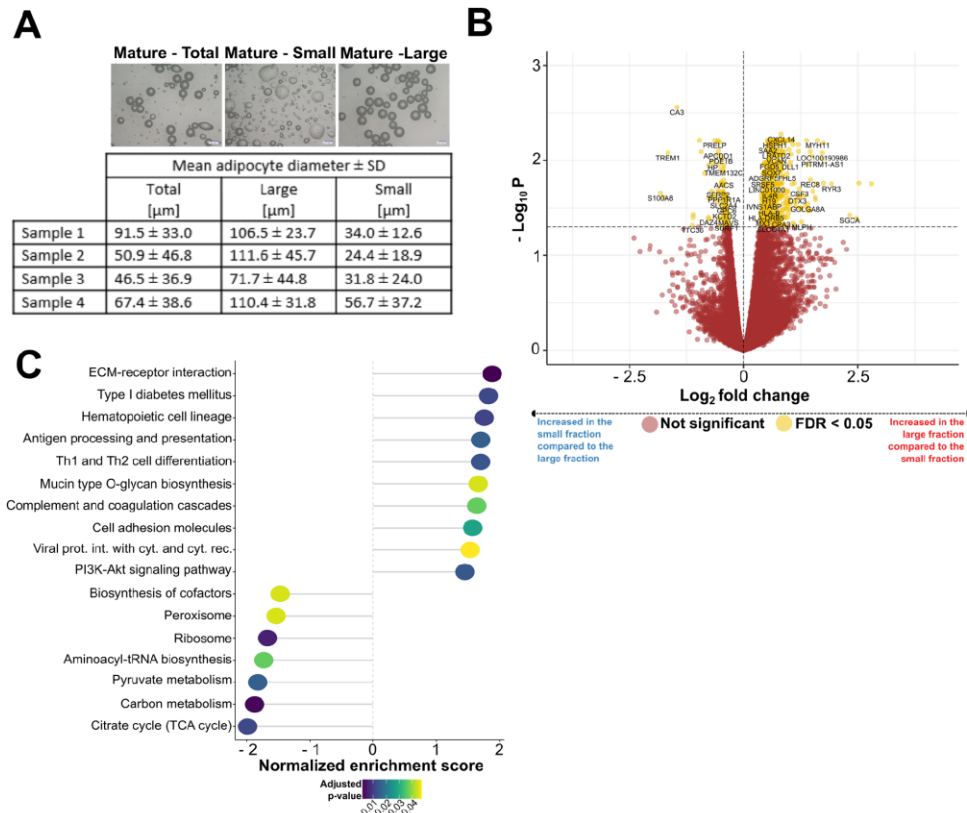


Figure 5: The transcriptomic signatures of size-separated mature adipocytes.

(A) Results from mature adipocyte size-separation experiments. Representative images of the total, small and large adipocyte fraction from one donor are shown in the top half of the graph. A tabular overview listing the mean adipocyte diameter \pm SD per fraction across all four different donors is given in the bottom half. (B) Volcano plot depicting the DE of genes between the small and large adipocyte fraction. (C) Lollipop plot displaying the top 20 enriched KEGG pathways with an adjusted p-value < 0.05 from gene set enrichment analysis comparing large and small fat cells that were size-separated based on buoyancy. The "Human Diseases" category of the KEGG PATHWAY database is not displayed on the graph.

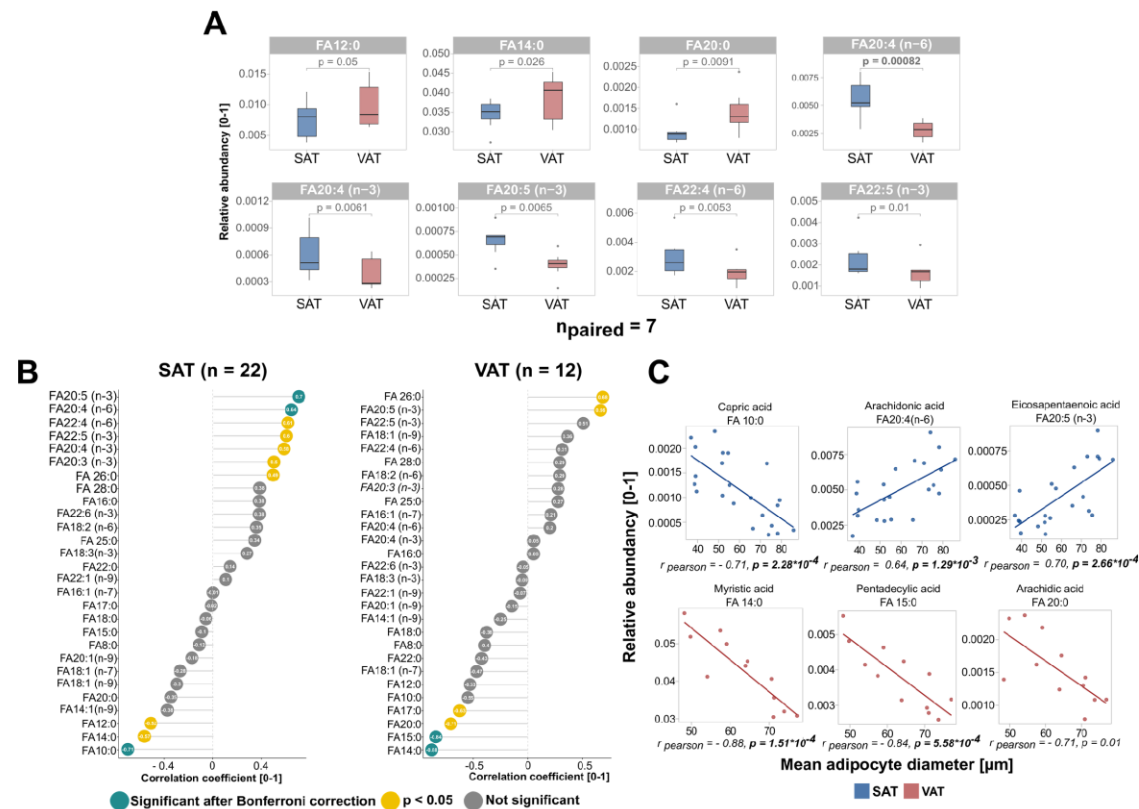


Figure 6: Differences in fatty acid composition with regard to adipose depot and fat cell size.

(A) Boxplots showing FA species that were found to show different abundancies in paired, SAT, and VAT. SAT samples are colored in red, while VAT samples are shown in blue. Out of the 28 FA species that were measured all FAs with a p-value < 0.05 are displayed. P-values written in bold are the ones that remained significant after Bonferroni adjustment for multiple testing ($p_{\text{bonf}} = 0.05/28 = 0.0018$). (B) Lollipop plot showing the correlation between adipocyte diameter and all 28 FA species assessed. SAT samples are displayed on the left, while VAT samples are shown on the right. (C) Scatterplots displaying the three FA species showing the strongest association with mean adipocyte diameter in SAT (blue) and VAT (red).

bioRxiv preprint doi: <https://doi.org/10.1101/2021.11.20.468818>; this version posted November 20, 2021. The copyright holder for this preprint (which was not certified by peer review) is the author/funder, who has granted bioRxiv a license to display the preprint in perpetuity. It is made available under aCC-BY-NC-ND 4.0 International license.

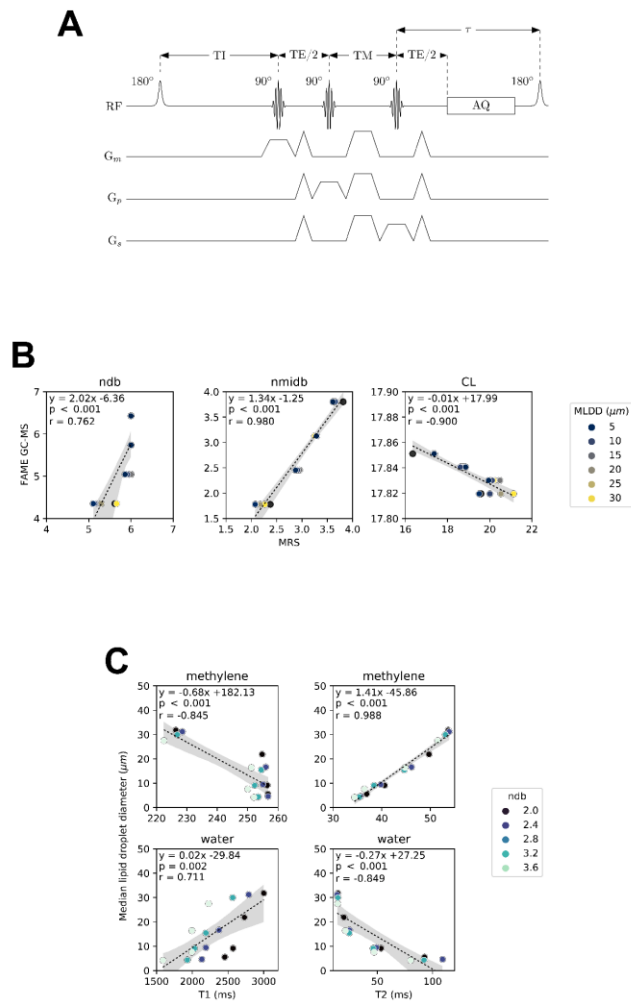


Figure 7: MRS-based characterization of fatty acid composition and lipid droplet size in phantoms

(A) MRS pulse sequence diagram of the single-voxel short-TR multi-TI multi-TE (SHORTIE) STEAM sequence. The sequence consists of a regular single-voxel STEAM sequence pattern with a minimal TR (constant recovery delay τ) combined with a non-selective 180-degree inversion RF-pulse. **(B)** Linear regression plots from the phantom experiment: GC-MS-based vs. MRS-based quantification of the FA characteristics ndb, nmldb, CL. The negative correlation for CL ($r=-0.900$, $p<0.001$) is considered an artifact arising from the difficulty of its accurate modelling and quantification in MRS. MLDD, median lipid droplet diameter. **(C)** Linear regression plots from the phantom experiment of the median lipid droplet diameter vs. the T1 and T2 relaxation of methylene and water, respectively. Very strong correlation between the median lipid droplet diameter and methylene T2 relaxation ($r=0.988$, $p<0.001$) independent from the fatty acid unsaturation suggests that methylene T2 is a promising indirect measure of lipid droplet size.

bioRxiv preprint doi: <https://doi.org/10.1101/2021.11.20.468818>; this version posted November 20, 2021. The copyright holder for this preprint (which was not certified by peer review) is the author/funder, who has granted bioRxiv a license to display the preprint in perpetuity. It is made available under aCC-BY-NC-ND 4.0 International license.

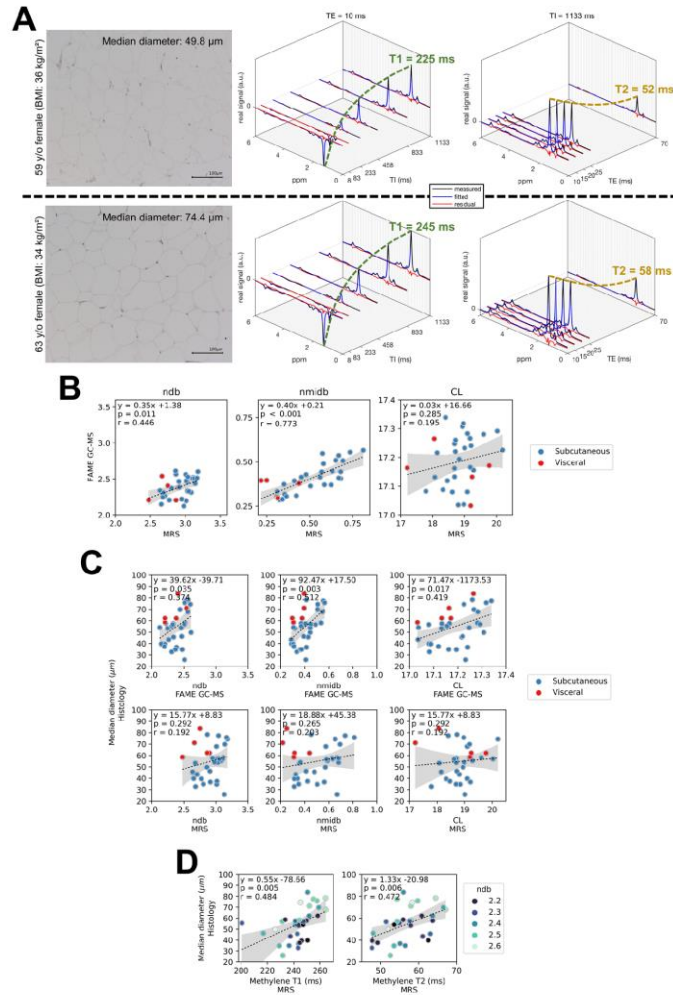


Figure 8: MRS-based characterization of fatty acid composition and fat cell size *in vitro* in adipose tissue samples.

(A) Exemplary MRS spectra with matched histology for two female subjects with similar age (59 and 63 year) and BMI (36 and 34 kg/m²) but difference median fat cell size (49.8 vs. 74.4 μ m) in abdominal subcutaneous AT. MRS spectra display signal variations with T1 (at TE = 10 ms) and TE (T1 = 1133 ms), respectively. Fitted methylene T1 and T2 relaxation times are given in green and orange, respectively. (B) Linear regression plots from the adipose tissue sample experiment: GC-MS-based vs. MRS-based quantification of the FA characteristics ndb, nmdb, CL. Sample origin is indicated by color. (C) Linear regression plots from the adipose tissue sample experiment: GC-MS-based and MRS-based FA characteristics ndb, nmdb, CL vs. median fat cell size. Sample origin is indicated by color. (D) Linear regression plot for the methylene T1 and T2 relaxation vs. median fat cell size. Sample ndb (binned) as measured by GC-MS is indicated by color encoding.

bioRxiv preprint doi: <https://doi.org/10.1101/2021.11.20.468818>; this version posted November 20, 2021. The copyright holder for this preprint (which was not certified by peer review) is the author/funder, who has granted bioRxiv a license to display the preprint in perpetuity. It is made available under aCC-BY-NC-ND 4.0 International license.

1. Morigny P, Boucher J, Arner P, and Langin D. Lipid and glucose metabolism in white adipocytes: pathways, dysfunction and therapeutics. *Nature Reviews Endocrinology*. 2021;17(5):276-95.
2. Laforest S, Labrecque J, Michaud A, Cianflone K, and Tchernof A. Adipocyte size as a determinant of metabolic disease and adipose tissue dysfunction. *Critical Reviews in Clinical Laboratory Sciences*. 2015;52(6):301-13.
3. Tandon P, Wafer R, and Minchin JEN. Adipose morphology and metabolic disease. *J Exp Biol*. 2018;221(Pt Suppl 1).
4. Verboven K, Wouters K, Gaens K, Hansen D, Bijnen M, Wetzels S, et al. Abdominal subcutaneous and visceral adipocyte size, lipolysis and inflammation relate to insulin resistance in male obese humans. *Scientific reports*. 2018;8(1):4677.
5. Veilleux A, Caron-Jobin M, Noël S, Laberge PY, and Tchernof A. Visceral adipocyte hypertrophy is associated with dyslipidemia independent of body composition and fat distribution in women. *Diabetes*. 2011;60(5):1504-11.
6. Hoffstedt J, Arner E, Wahrenberg H, Andersson DP, Qvisth V, Löfgren P, et al. Regional impact of adipose tissue morphology on the metabolic profile in morbid obesity. *Diabetologia*. 2010;53(12):2496-503.
7. Weyer C, Foley JE, Bogardus C, Tataranni PA, and Pratley RE. Enlarged subcutaneous abdominal adipocyte size, but not obesity itself, predicts type II diabetes independent of insulin resistance. *Diabetologia*. 2000;43(12):1498-506.
8. Laforest S, Michaud A, Paris G, Pelletier M, Vidal H, Geloën A, et al. Comparative analysis of three human adipocyte size measurement methods and their relevance for cardiometabolic risk. *Obesity (Silver Spring, Md)*. 2017;25(1):122-31.
9. Rydén M, Andersson DP, Bernard S, Spalding K, and Arner P. Adipocyte triglyceride turnover and lipolysis in lean and overweight subjects. *Journal of lipid research*. 2013;54(10):2909-13.
10. Arner P, Bernard S, Salehpour M, Possnert G, Liebl J, Steier P, et al. Dynamics of human adipose lipid turnover in health and metabolic disease. *Nature*. 2011;478(7367):110-3.
11. Skurk T, Alberti-Huber C, Herder C, and Hauner H. Relationship between adipocyte size and adipokine expression and secretion. *The Journal of Clinical Endocrinology and Metabolism*. 2007;92(3):1023-33.
12. Ye RZ, Richard G, Gévry N, Tchernof A, and Carpentier AC. Fat Cell Size: Measurement Methods, Pathophysiological Origins, and Relationships With Metabolic Dysregulations. *Endocrine Reviews*. 2021.
13. Bäckdahl J, Franzén L, Massier L, Li Q, Jalkanen J, Gao H, et al. Spatial mapping reveals human adipocyte subpopulations with distinct sensitivities to insulin. *Cell Metab*. 2021.
14. Lonsdale J, Thomas J, Salvatore M, Phillips R, Lo E, Shad S, et al. The Genotype-Tissue Expression (GTEx) project. *Nature genetics*. 2013;45(6):580-5.
15. The GTEx Consortium atlas of genetic regulatory effects across human tissues. *Science (New York, NY)*. 2020;369(6509):1318-30.
16. Glastonbury CA, Pullit SL, Honecker J, Censin JC, Laber S, Yaghootkar H, et al. Machine Learning based histology phenotyping to investigate the epidemiologic and genetic basis of adipocyte morphology and cardiometabolic traits. *PLoS computational biology*. 2020;16(8):e1008044.
17. Lehnert A, Machann J, Helms G, Claussen CD, and Schick F. Diffusion characteristics of large molecules assessed by proton MRS on a whole-body MR system. *Magn Reson Imaging*. 2004;22(1):39-46.
18. Weidlich D, Honecker J, Boehm C, Ruschke S, Junker D, Van AT, et al. Lipid droplet-size mapping in human adipose tissue using a clinical 3T system. *Magnetic resonance in medicine*. 2021;86(3):1256-70.

bioRxiv preprint doi: <https://doi.org/10.1101/2021.11.20.468818>; this version posted November 20, 2021. The copyright holder for this preprint (which was not certified by peer review) is the author/funder, who has granted bioRxiv a license to display the preprint in perpetuity. It is made available under aCC-BY-NC-ND 4.0 International license.

19. Fischer B, Schottl T, Schempp C, Fromme T, Hauner H, Klingenspor M, et al. Inverse relationship between body mass index and mitochondrial oxidative phosphorylation capacity in human subcutaneous adipocytes. *American journal of physiology Endocrinology and metabolism*. 2015;309(4):E380-7.
20. Dobin A, Davis CA, Schlesinger F, Drenkow J, Zaleski C, Jha S, et al. STAR: ultrafast universal RNA-seq aligner. *Bioinformatics (Oxford, England)*. 2013;29(1):15-21.
21. Liao Y, Smyth GK, and Shi W. The R package Rsubread is easier, faster, cheaper and better for alignment and quantification of RNA sequencing reads. *Nucleic acids research*. 2019;47(8):e47.
22. Robinson MD, McCarthy DJ, and Smyth GK. edgeR: a Bioconductor package for differential expression analysis of digital gene expression data. *Bioinformatics (Oxford, England)*. 2010;26(1):139-40.
23. Robinson MD, and Oshlack A. A scaling normalization method for differential expression analysis of RNA-seq data. *Genome biology*. 2010;11(3):R25.
24. Chen Y, Lun AT, and Smyth GK. From reads to genes to pathways: differential expression analysis of RNA-Seq experiments using Rsubread and the edgeR quasi-likelihood pipeline. *F1000Research*. 2016;5:1438.
25. Yu G, Wang LG, Han Y, and He QY. clusterProfiler: an R package for comparing biological themes among gene clusters. *Omics : a journal of integrative biology*. 2012;16(5):284-7.
26. Luo W, and Brouwer C. Pathview: an R/Bioconductor package for pathway-based data integration and visualization. *Bioinformatics (Oxford, England)*. 2013;29(14):1830-1.
27. Perdikari A, Leparc GG, Balaz M, Pires ND, Lidell ME, Sun W, et al. BATLAS: Deconvoluting Brown Adipose Tissue. *Cell Reports*. 2018;25(3):784-97.e4.
28. Ecker J, Scherer M, Schmitz G, and Liebisch G. A rapid GC-MS method for quantification of positional and geometric isomers of fatty acid methyl esters. *Journal of chromatography B, Analytical technologies in the biomedical and life sciences*. 2012;897:98-104.
29. Lepage G, and Roy CC. Direct transesterification of all classes of lipids in a one-step reaction. *Journal of lipid research*. 1986;27(1):114-20.
30. Weidlich D, Honecker J, Gmach O, Wu M, Burgkart R, Ruschke S, et al. Measuring large lipid droplet sizes by probing restricted lipid diffusion effects with diffusion-weighted MRS at 3T. *Magnetic resonance in medicine*. 2019;81(6):3427-39.
31. International Commission on Radiological Protection. *ICRP Publication 23, Reference Man: Anatomical, Physiological, and Metabolic Characteristics*. New York: Pergamon Press; 1975.
32. Thomas LW. The chemical composition of adipose tissue of man and mice. *Q J Exp Physiol Cogn Med Sci*. 1962;47:179-88.
33. Gmach O, Bertsch A, Bilke-Krause C, and Kulozik U. Impact of oil type and pH value on oil-in-water emulsions stabilized by egg yolk granules. *Colloids and Surfaces A: Physicochemical and Engineering Aspects*. 2019;581:123788.
34. Guilmineau F, and Kulozik U. Influence of a thermal treatment on the functionality of hen's egg yolk in mayonnaise. *Journal of Food Engineering*. 2007;78:648-54.
35. Ruschke S, Weidlich D, Wu M, Hoch A, and Karampinos DC. *Proceedings International Society for Magnetic Resonance in Medicine*. Montréal, QC, Canada 2019:27(4230).
36. Bydder M, Hamilton G, Yokoo T, and Sirlin CB. Optimal phased-array combination for spectroscopy. *Magn Reson Imaging*. 2008;26(6):847-50.
37. Dennis JE, Gay DM, and Welsch RE. Algorithm 573: NL2SOL—An Adaptive Nonlinear Least-Squares Algorithm [E4]. *ACM Trans Math Softw*. 1981;7(3):369–83.
38. Hamilton G, Yokoo T, Bydder M, Cruite I, Schroeder ME, Sirlin CB, et al. In vivo characterization of the liver fat ¹H MR spectrum. *NMR in biomedicine*. 2011;24(7):784-90.
39. R Core Team. Vienna, Austria: R Foundation for Statistical Computing; 2021.

bioRxiv preprint doi: <https://doi.org/10.1101/2021.11.20.468818>; this version posted November 20, 2021. The copyright holder for this preprint (which was not certified by peer review) is the author/funder, who has granted bioRxiv a license to display the preprint in perpetuity. It is made available under aCC-BY-NC-ND 4.0 International license.

40. Singh NK, and Rao GN. Emerging role of 12/15-Lipoxygenase (ALOX15) in human pathologies. *Progress in lipid research*. 2019;73:28-45.
41. Anderson CM, and Stahl A. SLC27 fatty acid transport proteins. *Molecular aspects of medicine*. 2013;34(2-3):516-28.
42. Wu Q, Ortegon AM, Tsang B, Doege H, Feingold KR, and Stahl A. FATP1 is an insulin-sensitive fatty acid transporter involved in diet-induced obesity. *Molecular and cellular biology*. 2006;26(9):3455-67.
43. Oberauer R, Rist W, Lenter MC, Hamilton BS, and Neubauer H. EGFL6 is increasingly expressed in human obesity and promotes proliferation of adipose tissue-derived stromal vascular cells. *Molecular and cellular biochemistry*. 2010;343(1-2):257-69.
44. Hammarstedt A, Graham TE, and Kahn BB. Adipose tissue dysregulation and reduced insulin sensitivity in non-obese individuals with enlarged abdominal adipose cells. *Diabetology & Metabolic Syndrome*. 2012;4(1):42.
45. Joint FAO/WHO Codex Alimentarius Commission. *Codex alimentarius : Standard for named vegetable oils*. Food and Agriculture Organization of the United Nations : World Health Organization; 1999.
46. Schleinitz D, Krause K, Wohland T, Gebhardt C, Linder N, Stumvoll M, et al. Identification of distinct transcriptome signatures of human adipose tissue from fifteen depots. *European Journal of Human Genetics*. 2020;28(12):1714-25.
47. Chau YY, Bandiera R, Serrels A, Martínez-Estrada OM, Qing W, Lee M, et al. Visceral and subcutaneous fat have different origins and evidence supports a mesothelial source. *Nature cell biology*. 2014;16(4):367-75.
48. Tang W, Zeve D, Suh JM, Bosnakovski D, Kyba M, Hammer RE, et al. White fat progenitor cells reside in the adipose vasculature. *Science (New York, NY)*. 2008;322(5901):583-6.
49. Tchkonja T, Lenburg M, Thomou T, Giorgadze N, Frampton G, Pirtskhalava T, et al. Identification of depot-specific human fat cell progenitors through distinct expression profiles and developmental gene patterns. *American journal of physiology Endocrinology and metabolism*. 2007;292(1):E298-307.
50. White UA, and Tchoukalova YD. Sex dimorphism and depot differences in adipose tissue function. *Biochimica et biophysica acta*. 2014;1842(3):377-92.
51. Karastergiou K, Fried SK, Xie H, Lee MJ, Divoux A, Rosencrantz MA, et al. Distinct developmental signatures of human abdominal and gluteal subcutaneous adipose tissue depots. *The Journal of Clinical Endocrinology and Metabolism*. 2013;98(1):362-71.
52. Hardy OT, Perugini RA, Nicoloso SM, Gallagher-Dorval K, Puri V, Straubhaar J, et al. Body mass index-independent inflammation in omental adipose tissue associated with insulin resistance in morbid obesity. *Surgery for obesity and related diseases : official journal of the American Society for Bariatric Surgery*. 2011;7(1):60-7.
53. Mraz M, and Haluzik M. The role of adipose tissue immune cells in obesity and low-grade inflammation. *The Journal of endocrinology*. 2014;222(3):R113-27.
54. Klötting N, Fasshauer M, Dietrich A, Kovacs P, Schön MR, Kern M, et al. Insulin-sensitive obesity. *American journal of physiology Endocrinology and metabolism*. 2010;299(3):E506-15.
55. Vohl M-C, Sladek R, Robitaille J, Gurd S, Marceau P, Richard D, et al. A Survey of Genes Differentially Expressed in Subcutaneous and Visceral Adipose Tissue in Men*. *Obesity research*. 2004;12(8):1217-22.
56. Cole BK, Morris MA, Grzesik WJ, Leone KA, and Nadler JL. Adipose Tissue-Specific Deletion of 12/15-Lipoxygenase Protects Mice from the Consequences of a High-Fat Diet. *Mediators of Inflammation*. 2012;2012:851798.
57. Simopoulos AP. The importance of the ratio of omega-6/omega-3 essential fatty acids. *Biomedicine & Pharmacotherapy*. 2002;56(8):365-79.

bioRxiv preprint doi: <https://doi.org/10.1101/2021.11.20.468818>; this version posted November 20, 2021. The copyright holder for this preprint (which was not certified by peer review) is the author/funder, who has granted bioRxiv a license to display the preprint in perpetuity. It is made available under a [CC-BY-NC-ND 4.0 International license](#).

58. Melton EM, Cerny RL, Watkins PA, DiRusso CC, and Black PN. Human fatty acid transport protein 2a/very long chain acyl-CoA synthetase 1 (FATP2a/Acsvl1) has a preference in mediating the channeling of exogenous n-3 fatty acids into phosphatidylinositol. *The Journal of biological chemistry*. 2011;286(35):30670-9.
59. Gillberg L, Perfilyev A, Brøns C, Thomasen M, Grunnet LG, Volkov P, et al. Adipose tissue transcriptomics and epigenomics in low birthweight men and controls: role of high-fat overfeeding. *Diabetologia*. 2016;59(4):799-812.
60. Alligier M, Meugnier E, Debard C, Lambert-Porcheron S, Chanseaux E, Sothier M, et al. Subcutaneous adipose tissue remodeling during the initial phase of weight gain induced by overfeeding in humans. *The Journal of Clinical Endocrinology and Metabolism*. 2012;97(2):E183-92.
61. Lappas M. Effect of pre-existing maternal obesity, gestational diabetes and adipokines on the expression of genes involved in lipid metabolism in adipose tissue. *Metabolism: clinical and experimental*. 2014;63(2):250-62.
62. Castro JP, Grune T, and Speckmann B. The two faces of reactive oxygen species (ROS) in adipocyte function and dysfunction. *Biological chemistry*. 2016;397(8):709-24.
63. Smith U, Li Q, Rydén M, and Spalding KL. Cellular senescence and its role in white adipose tissue. *International Journal of Obesity*. 2021;45(5):934-43.
64. Honecker J, Weidlich D, Heisz S, Lindgren CM, Karampinos DC, Claussnitzer M, et al. A distribution-centered approach for analyzing human adipocyte size estimates and their association with obesity-related traits and mitochondrial function. *International Journal of Obesity*. 2021.
65. Wessels B, Honecker J, Schöttl T, Stecher L, Klingenspor M, Hauner H, et al. Adipose Mitochondrial Respiratory Capacity in Obesity is Impaired Independently of Glycemic Status of Tissue Donors. *Obesity*. 2019;27(5):756-66.
66. Yin X, Lanza IR, Swain JM, Sarr MG, Nair KS, and Jensen MD. Adipocyte Mitochondrial Function Is Reduced in Human Obesity Independent of Fat Cell Size. *The Journal of Clinical Endocrinology and Metabolism*. 2014;99(2):E209-16.
67. Rosen Evan D, and Spiegelman Bruce M. What We Talk About When We Talk About Fat. *Cell*. 2014;156(1):20-44.
68. Weidlich D, Zamskiy M, Maeder M, Ruschke S, Marburg S, and Karampinos DC. Reduction of vibration-induced signal loss by matching mechanical vibrational states: Application in high b-value diffusion-weighted MRS. *Magnetic resonance in medicine*. 2020;84(1):39-51.
69. Morozov D, Quirk JD, and Beeman SC. Toward noninvasive quantification of adipose tissue oxygenation with MRI. *International journal of obesity (2005)*. 2020;44(8):1776-83.

7.2 | Letters of approval

Letter of approval - PLOS Computational biology, August 2021




Di 31.08.2021 09:07

PLOS Computational Biology <ploscompbiol@plos.org>

RE: Request to reproduce own work for the inclusion in a PhD dissertation

An Julius.honecker@outlook.de

 Klicken Sie hier, um Bilder herunterzuladen. Um den Datenschutz zu erhöhen, hat Outlook den automatischen Download von Bildern in dieser Nachricht verhindert.

Dear Dr. Honecker,

Thank you for your email. You are welcome to re-use the content from any PLOS articles.

All PLOS articles are published under a Creative Commons Attribution license (CC BY), further information about the terms of the license can be found at: <https://www.plos.org/license>.

All of our articles are available (through our websites) for anyone to download, re-use, reprint, modify, distribute, and/or copy so long as the original authors and source are cited.

Please let me know if you require any further assistance.


Kind regards,

Rachel Saunders-Singer
Journal Assistant, Editorial Office Ltd.
On behalf of PLOS Computational Biology

PLOS | [plos.org](https://www.plos.org)
Empowering researchers to transform science
1160 Battery Street, Suite 225, San Francisco, CA 94111

Case Number: 07285449
ref_00DU0Ifis_5004P1dRytc:ref

Letter of approval – International Journal of Obesity³

CCC | RightsLink[®] ? Help ▾  Live Chat

A distribution-centered approach for analyzing human adipocyte size estimates and their association with obesity-related traits and mitochondrial function

Author: Julius Honecker et al
Publication: International Journal of Obesity
Publisher: Springer Nature
Date: Jun 25, 2021
Copyright © 2021, The Author(s)

Creative Commons

This is an open access article distributed under the terms of the [Creative Commons CC BY](#) license, which permits unrestricted use, distribution, and reproduction in any medium, provided the original work is properly cited.

You are not required to obtain permission to reuse this article.
To request permission for a type of use not listed, please contact [Springer Nature](#)

© 2021 Copyright - All Rights Reserved | [Copyright Clearance Center, Inc.](#) | [Privacy statement](#) | [Terms and Conditions](#)
Comments? We would like to hear from you. E-mail us at customer-care@copyright.com

³ <https://s100.copyright.com/AppDispatchServlet?title=A%20distribution-centered%20approach%20for%20analyzing%20human%20adipocyte%20size%20estimates%20and%20their%20association%20with%20obesityrelated%20traits%20and%20mitochondrial%20function&author=Julius%20Honecker%20et%20al&contentID=10.1038%2Fs41366-021-00883-6©right=The%20Author%28s%29&publication=0307-0565&publicationDate=2021-06-25&publisherName=SpringerNature&orderBeanReset=true&oa=CC%20BY>; Retrieved on 08.09.2021; 13:45

Letter of approval – Bioarchives (bioRxiv)

This is an open access article distributed under the terms of the Creative Commons CC-BY-NC-ND 4.0 international license⁴ which permits unrestricted use, distribution and reproduction in any medium, provided the original work is properly cited⁵.

⁴ <https://creativecommons.org/licenses/by-nc-nd/4.0/>

⁵ <https://www.biorxiv.org/content/10.1101/2021.11.20.468818v1.article-info>

7.3 | Key resources table

Biomaterials	Cohort	Source
Subcutaneous adipose tissue	Abdominal surgery cohort	This study
	Plastic surgery cohort	This study
Visceral adipose tissue	Abdominal surgery cohort	This study
Buffy coat	Abdominal surgery cohort	This study
Human adipose mesenchymal stem cells	Plastic surgery cohort	This study
Mature adipocytes	Plastic surgery cohort	This study
Reagents	Source	Identifier
2-Mercaptoethanol	Sigma-Aldrich	#M6250
3,3'-5-Triiodo-L-Thyronin Sodium Salt (T3)	Sigma-Aldrich	#T-6397
3-Isobutyl-1-methylxanthine (IBMX)	Serva	#26445
4 % phosphate buffered formaldehyde pH 7	Carl-Roth	#P087
apo-Transferrin human	Sigma-Aldrich	#T2252
Bovine serum Albumin heat shock fraction (BSA)	Sigma-Aldrich	#A7906
Collagenase NB4	Nordmark	#S1745401
D-Biotin	Carl-Roth	#3822.1
Dexamethasone	Sigma-Aldrich	#D4902
D-Pantothenic acid hemicalcium salt	Sigma-Aldrich	#P5155
Dulbecco's Modified Eagle Medium/Nutrient Mixture F-12 (DMEM/F12)	Gibco	#31330-038
Epidermal growth factor (EGF)	R&D Systems	#236-EG
Ethanol absolute AnalR NORMAPUR	VWR	#20823.362
Ethylenediaminetetraacetic acid (EDTA), anhydrous	Sigma-Aldrich	#E9884
Fetal calf serum (FCS) F	Sigma-Aldrich	#F7524 (Lot:045M3270)
Fibroblast growth factor (FGF)	R&D Systems	#233-FB
Hydrocortisone	Sigma-Aldrich	#H4001
Insulin	Sigma-Aldrich	#19278c
Linseed Oil	Generic brand	N/A
Mounting medium, ROTI Histokitt	Carl-Roth	#6638.2
Oil-Red-O	Sigma-Aldrich	#O0625
Organic Solvents for FAME GC-MS	All from Merck, LiChrosolv	Diverse
Penicilin-Streptomycin	Sigma-Aldrich	#P0781
Phosphate buffered saline (PBS)	Sigma-Aldrich	#L182-50
Rosiglitazone	Sigma-Aldrich	#R2408
Salts	All from Sigma-Aldrich in ACS grade or higher	Diverse
Sodium benzoate	Sigma-Aldrich	#71300

7 | Appendix

Sunflower seed oil	Generic brand	N/A
Tris (hydroxymethyl)-aminomethan	AppliChem	#A1086
Trypsin/EDTA	Sigma-Aldrich	#T3924
Tween 80	Sigma-Aldrich	#P1754
Commercial assays & kits	Source	Identifier
Buffer RLT	Qiagen	#79216
DNeasy Blood & Tissue	Qiagen	#69504
Infinium Global Screening Array	Illumina	#20030770
mirVana miRNA isolation kit with phenol	Invitrogen	#AM1560
Quant-iT PicoGreen dsDNA Assay Kit	Invitrogen	#P7589
RNA 6000 Nano Chip	Agilent	#5067-1511
RNase A	Qiagen	#19101
Consumables	Source	Identifier
2000 µm nylon mesh	VWR	#510-9482
250 µm nylon gauze	VWR	#510-9526
25cm ² rectangular canted neck cell culture flask with vented cap	Falcon	#353109
384 Well Skirted PCR Plate, Roche Style	4titude	#4ti-1381
6-well clear flat bottom TC-treated multiwell cell culture plate	Falcon	#353046
75cm ² rectangular canted neck cell culture flask with vented cap	Falcon	#353136
Biosphere filter tips	Sarstedt	N/A
Borosilicate glass round bottom tube with screw cap	Pyrex	#10004654
Cell strainer 70µm	BD Falcon	#352360
Cellstar conical tubes (15 ml, 50 ml)	Greiner	N/A
Cellstar serological pipettes (50 ml, 25 ml, 10 ml, 5 ml, 2 ml)	Greiner	N/A
Circonia glas beads	Carl-Roth	#11079105
Coverslips	Carl-Roth	#H878.2
Thickness no. 1, 24x60 mm		
FrameStar 96 Well Plate, clear	4titude	#4ti-0960
Lysing matrix D	MP biomedicals	#116913050-CF
Safe-Lock Tubes (5 ml, 2ml, 1.5 ml)	Eppendorf	N/A
S-Monovette K3 EDTA, 9 ml	Sarstedt	#02.1066.001
Microscope slides	Carl-Roth	#1880.1
Superfrost corners grounded		

Equipment	Name	Manufacturer
Balances	Pinnacle, analytical balance	Sartorius
	Pinnacle, top loading balance	Sartorius
Bead beating grinder and lysis system	Fast Prep-24	MP biomedicals
Biological Safety Cabinet	HeraSafe Class II safety cabinet	Thermo Fisher Scientific
	Centrifuge 5415 R	Eppendorf
Centrifuges	Centrifuge 5415 D	Eppendorf
	Centrifuge 5810	Eppendorf
	Labor-Pilot 2000/4	IKA
Colloid mill		
High resolution automated electrophoresis	2100 bioanalyzer instrument	Agilent
Incubator	Heracell 240i CO2 incubator	Thermo Fisher Scientific
Magnetic stirrer	MR3001	Heidolph
Microplate reader	Infinite M200	Tecan
	VHX-6000 microscope	Keyence
	DMI4000 B inverted microscope	Leica Microsystems
Microscopes	Aperio AT2 whole slide scanning microscope	Leica Biosystems
	ST5020	Leica Biosystems
Multistainer		
Paraffin Embedding System	AP280 1-3	Microm
Particle Sizer	Mastersizer 2000 with Hydro 2000S dispersing unit	Malvern Panalytical
	Research plus pipette set	Eppendorf
	Multipette stream/Xstream	Eppendorf
Pipettes	Easypet 3	Eppendorf
	E1-ClipTip	Thermo Fisher Scientific
	MICROMAN positive displacement pipette	Gilson
Rotary microtome	HM 355 S	Thermo Fisher Scientific
	Mastercycler gradient	Eppendorf
Thermocycler	LightCycler 480, 384 well block	Roche
Tissue processor	TP1020 tissue processor	Leica Biosystems
Ultrapure water system	PURELAB flex 2	Elga Veolia
Water baths	CORIO CD Thermostat	Julabo
	GFL 1083 shaking water bath	Gesellschaft für Labortechnik

Software & Algorithms	Publication	URL
Adipocyte U-net	https://doi.org/10.1371/journal.pcbi.1008044	https://github.com/GlastonburyC/Adipocyte-U-net
BATLAS	https://doi.org/10.1016/j.celrep.2018.09.044	https://shiny.hest.ethz.ch/BATLAS/
CellProfiler	https://doi.org/10.1186/gb-2006-7-10-r100	https://cellprofiler.org/
CellProfiler, adipocyte sizing pipeline	https://doi.org/10.1016/b978-0-12-411619-1.00004-5	N/A
R	N/A; R Foundation for statistical computing	https://www.R-project.org/
Rsubread	https://doi.org/10.1093/nar/gkz114	https://bioconductor.org/packages/release/bioc/html/Rsubread.html
edgeR	https://doi.org/10.1093/bioinformatics/btp616	https://bioconductor.org/packages/release/bioc/html/edgeR.html
clusterProfiler	https://doi.org/10.1089/omi.2011.0118	https://bioconductor.org/packages/release/bioc/html/clusterProfiler.html
Pathview	https://doi.org/10.1093/bioinformatics/btt285	https://bioconductor.org/packages/release/bioc/html/pathview.html
QuPath	https://doi.org/10.1038/s41598-017-17204-5	https://qupath.github.io/
Collaborative experiments	Group name	URL
FAME GC-MS	ZIEL Research Group Lipid Metabolism Head: Dr. Josef Ecker	https://www.ziel.tum.de/ecker/
Genotyping, abdominal surgery cohort	Oxford Genomics Centre Body magnetic resonance research group (BMRR)	https://www.well.ox.ac.uk/ogc/
MR experiments	Head: Prof. Dimitrios Karampinos	https://www.bmrrgroup.de/
Mature adipocyte respiration	Wessels B., Honecker J. et al. (2019)	https://doi.org/10.1002/oby.22435
RNA-Seq of hAMSCs and mature adipocytes	Broad Institute Genomics platform	https://www.broadinstitute.org/genomics
Water-fat phantoms	Chair of Food and Bioprocess Engineering Head: Prof. Ulrich Kulozik	https://www.lmvt.wzw.tum.de/en/home/
Public data	Publication	URL
GTEX adipocyte size estimates	https://doi.org/10.1371/journal.pcbi.1008044	https://github.com/GlastonburyC/Adipocyte-U-net
GTEX phenotypes	https://doi.org/10.1038/ng.2653	https://gtexportal.org/home/datasets/dbGap accession phs000424.v8.p2
GTEX RNA-Seq data	https://doi.org/10.1038/ng.2653	https://gtexportal.org/home/datasets/dbGap accession phs000424.v8.p2

7.4 | Approval for a publication-based dissertation



Einverständniserklärung zur publikationsbasierten Promotion¹

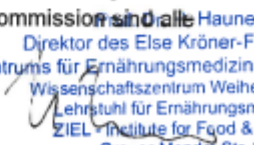
Anlage 6 (für § 6 Abs. 2)

Hiermit erkläre ich mein Einverständnis, dass die Dissertation von

Frau/Herrn Julius Honecker

als publikationsbasierte Dissertation eingereicht wird. Sie erfüllt die nachfolgenden Kriterien:

1. Einleitungs- und Methodenteil (20 Seiten). Ein themenübergreifender Diskussionsteil mit Reflexion zur bestehenden Literatur.
2. Kumulative Einbindung von mindestens zwei akzeptierten Erstautorenveröffentlichungen (full paper in einem englischsprachigen, international verbreiteten Publikationsorgan, peer reviewed)
3. Die eingebundenen Veröffentlichungen müssen federführend vom Doktoranden abgefasst sein.
4. Eingebunden muss sein: je eine einseitige Zusammenfassung der jeweiligen Veröffentlichungen unter Hervorhebung der individuellen Leistungsbeiträge des Kandidaten.
5. Einbindung von ausgewählten Originalveröffentlichungen nur mit einem separaten schriftlichen „Erlaubnisschreiben des jeweiligen Verlags“. Alle anderen Originalveröffentlichungen werden unter Nennung der bibliografischen Angaben aufgelistet. In den Exemplaren für die Mitglieder der Prüfungskommission sind alle Originalveröffentlichungen separat dazu abzugeben.


Ursula Hauner
Direktor des Else Kröner-Fresenius-
Zentrums für Ernährungsmedizin d. TU München
Wissenschaftszentrum Weißenstephan
Lehrstuhl für Ernährungsmedizin
ZIEL - Institute for Food & Health
Gregor-Mendel-Str. 2
85354 Freising, Germany

27.01.2022

Datum

Unterschrift Betreuerin

¹ Zur Vorlage bei der Einreichung der Dissertation.

7.5 | Declaration of Authorship

Eidesstattliche Erklärung

Ich, Julius Honecker, erkläre an Eides statt, dass ich die bei der promotionsführenden Einrichtung der TUM School of Life Sciences Weihenstephan der TUM zur Promotionsprüfung vorgelegte Arbeit mit dem Titel:

Development of novel adipocyte sizing strategies to decipher the genetic, transcriptomic and metabolic mechanisms of adipocyte hypertrophy.

am Lehrstuhl für klinische Ernährungsmedizin unter der Anleitung und Betreuung durch: Prof. Dr. Johann J. Hauner ohne sonstige Hilfe erstellt und bei der Abfassung nur die gemäß § 7 Abs. 6 und 7 angegebenen Hilfsmittel benutzt habe.

Ich habe keine Organisation eingeschaltet, die gegen Entgelt Betreuer*innen für die Anfertigung von Dissertationen sucht, oder die mir obliegenden Pflichten hinsichtlich der Prüfungsleistungen für mich ganz oder teilweise erledigt.

Ich habe die Dissertation in dieser oder ähnlicher Form in keinem anderen Prüfungsverfahren als Prüfungsleistung vorgelegt.

Die vollständige Dissertation wurde noch nicht veröffentlicht.

Ich habe den angestrebten Doktorgrad noch nicht erworben und bin nicht in einem früheren Promotionsverfahren für den angestrebten Doktorgrad endgültig gescheitert.

Ich habe keine Kenntnis über ein strafrechtliches Ermittlungsverfahren in Bezug auf wissenschaftsbezogene Straftaten gegen mich oder eine rechtskräftige strafrechtliche Verurteilung mit Wissenschaftsbezug.

Die öffentlich zugängliche Promotionsordnung sowie die Richtlinien zur Sicherung guter wissenschaftlicher Praxis und für den Umgang mit wissenschaftlichem Fehlverhalten der TUM sind mir bekannt, insbesondere habe ich die Bedeutung von § 27 PromO (Nichtigkeit der Promotion) und § 28 PromO (Entzug des Doktorgrades) zur Kenntnis genommen. Ich bin mir der Konsequenzen einer falschen Eidesstattlichen Erklärung bewusst.

Mit der Aufnahme meiner personenbezogenen Daten in die Alumni-Datei bei der TUM bin ich einverstanden,



Freising, 17.01.2022

8 | Publications and congress contributions

Included first-authored, peer-reviewed journal Publications

- [JF1] Glastonbury, C. A., Pulit, S. L., **Honecker, J.**, Censin, J. C., Laber, S., Yaghootkar, H., Rahmioglu, N., Pastel, E., Kos, K., Pitt, A., Hudson, M., Nellåker, C., Beer, N. L., Hauner, H., Becker, C. M., Zondervan, K. T., Frayling, T. M., Claussnitzer, M. & Lindgren, C. M. Machine Learning based histology phenotyping to investigate the epidemiologic and genetic basis of adipocyte morphology and cardiometabolic traits. *PLoS computational biology* **16**, e1008044, doi:10.1371/journal.pcbi.1008044 (2020).
- [JF2] **Honecker, J.**, Weidlich, D., Heisz, S., Lindgren, C. M., Karampinos, D. C., Claussnitzer, M. & Hauner, H.. A distribution-centered approach for analyzing human adipocyte size estimates and their association with obesity-related traits and mitochondrial function. *International Journal of Obesity*, doi:10.1038/s41366-021-00883-6 (2021).

JF = Journal, first authorship

Included first-authored, preprints

- [PF1] **Honecker, J.**, Ruschke, S., Seeliger, C., Laber, S., Strobel, S., Pröll, P., Nellaker, C., Lindgren, C. M., Kulozik, U., Ecker, J., Karampinos, D. C., Claussnitzer, M. and Hauner, H.. Transcriptome and fatty-acid signatures of adipocyte hypertrophy and its non-invasive MR-based characterization in human adipose tissue. *bioRxiv*; doi: 10.1101/2021.11.20.468818 Under review: *EBioMedicine*

PF = Preprint, first authorship

Related, first authored journal publications

- [JS1] Wessels, B., **Honecker, J.**, Schöttl, T., Stecher, L., Klingenspor, M., Hauner, H. & Skurk, T. Adipose Mitochondrial Respiratory Capacity in Obesity is Impaired Independently of Glycemic Status of Tissue Donors. *Obesity (Silver Spring)* **27**, 756-766, doi:10.1002/oby.22435 (2019).

JS = Journal, first authorship

Related, co-authored journal publications

- [JC1] Weidlich, D., **Honecker, J.**, Gmach, O., Wu, M., Burgkart, R., Ruschke, S., Franz, D., Menze, B. H., Skurk, T., Hauner, H., Kulozik, U. & Karampinos, D. C. Measuring large lipid droplet sizes by probing restricted lipid diffusion effects with diffusion-weighted MRS at 3T. *Magnetic resonance in medicine* **81**, 3427-3439, doi:10.1002/mrm.27651 (2019).
- [JC2] Weidlich, D., **Honecker, J.**, Boehm, C., Ruschke, S., Junker, D., Van, A. T., Makowski, M. R., Holzapfel, C., Claussnitzer, M., Hauner, H. & Karampinos, D. C. Lipid droplet-size mapping in human adipose tissue using a clinical 3T system. *Magnetic resonance in medicine* **86**, 1256-1270, doi:10.1002/mrm.28755 (2021).
- [JC3] Laber, S., Forcisi, S., Bentley, L., Petzold, J., Moritz, F., Smirnov, K. S., Al Sadat, L., Williamson, I., Strobel, S., Agnew, T., Sengupta, S., Nicol, T., Grallert, H., Heier, M., **Honecker, J.**, Mianne, J., Teboul, L., Dumbell, R., Long, H., Simon, M., Lindgren, C., Bickmore, W. A., Hauner, H., Schmitt-Kopplin, P., Claussnitzer, M. & Cox, R. D. Linking the FTO obesity rs1421085 variant circuitry to cellular, metabolic, and organismal phenotypes in vivo. *Sci Adv* **7**, doi:10.1126/sciadv.abg0108 (2021).

JC = Journal, co-authorship

Related, first authored conference abstracts

[CF1] **Honecker, J.**, Glastonbury, C., Weidlich, D., Gmach, O., Pulit, S., Nellåker, C., Laber, S., Kulozik, U., Karampinos, D., Hauner, H., Lindgren, CM., Claussnitzer, M., Novel strategies for the morphological profiling of adipose tissue, Keystone Symposia - Diabetes: Innovations, Outcomes and Personalized Therapies (X3), Poster presentation, Whistler, Canada

CF = Conference, first authorship

Related, co-authored conference abstracts

[CC1] Weidlich, D., **Honecker, J.**, Ruschke, S., Patzelt, L., Held, C., Wu, M.M., Franz, D., Winkler, S., Hauner, H., Karampinos, D.C., Comparison of adipocyte size measurements with histology and high b-value diffusion-weighted spectroscopy in human white adipose tissue at 3 T, 28th Annual Meeting of ISMRM (p. 4680), Virtual Meeting (digital poster)

[CC2] Ruschke, S., Weidlich, D., **Honecker, J.**, Seeliger, C., Ecker, J., Prokopchuk, O., Hauner, H., Karampinos, D.C., Estimation of the triglyceride fatty acid composition in human adipose tissue using multi-TE and SHORTIE STEAM: in vitro validation using GC-MS, 28th Annual Meeting of ISMRM (p. 4882), Virtual Meeting (digital poster)

[CC3] Weidlich, D., Zamskiy, M., Ruschke, S., **Honecker, J.**, Skurk, T., Wu, M., Hauner, H., Karampinos, D.C., Spatially resolved lipid droplet size mapping with a high b-value diffusion weighted 2D TSE sequence in phantoms, human adipose tissue samples and in vivo, in: ISMRM Workshop on MRI of Obesity and Metabolic Disorders. Singapore. (oral)

[CC4] Weidlich, D., **Honecker, J.**, Gmach, O., Wu, M.M., Burgkart, R., Ruschke, S., Franz, D., Menze, B., Skurk, T., Hauner, H., Kulozik, U., Karampinos, D.C., Measuring large lipid droplet sizes by probing restricted lipid diffusion effects with Diffusion-Weighted Magnetic Resonance Spectroscopy at 3 T, 27th Annual Meeting of ISMRM (p. 373), Montreal, Canada (oral) ISMRM Magna Cum Laude Award

[CC5] Weidlich, D., Wu, M.M., Ruschke, S., Franz, D., **Honecker, J.**, Gmach, O., Skurk, T., Hauner, H., Kulozik, U., Karampinos, D.C., Spatially resolved measurement of lipid droplet size in white adipose tissue with high b-value stimulated echo-prepared diffusion-weighted 2D single shot TSE, 27th Annual Meeting of ISMRM (p. 1927), Montreal, Canada (digital poster)

CF = Conference, co-authorship

9 | Acknowledgement

I would like to thank everybody, who supported me personally and scientifically during my Ph. D. project.

First and foremost, I would like to thank my doctoral supervisor, Prof. Hans Hauner, for the great opportunity to realize my Ph. D. thesis, here at the chair of nutritional medicine. Thank you for all the constructive feedback, experimental suggestions and impulses that have substantially contributed to the success at every stage of this research project.

I would like to thank Prof. Melina Claussnitzer for her mentorship and co-supervision. Your constant feedback, combined with countless experimental and analytical input markedly shaped this thesis and is highly acknowledged. Thank you for your continuous support and engagement.

Moreover, I would like to thank Prof. Dimitrios Karampinos, Dr. Stefan Ruschke and Dominik Weidlich (TUM, Body Magnetic Resonance Research Group) for the great interdisciplinary collaboration and pleasant teamwork at the interface of magnetic resonance and adipose tissue biology. I thank Prof. Cecilia Lindgren, Dr. Christoffer Nellaker and all individuals from the Big Data Institute at the University of Oxford for the fruitful collaboration over the last years. I have always felt as a part of the histology/image analysis team and thank you sincerely for the trust and involvement regarding the development of novel adipocyte sizing strategies. Moreover, I would like to thank all people of the Claussnitzer Lab at the Broad Institute for their countless support with RNA-Seq experiments and for their numerous feedback regarding experimental design and analysis.

I am beyond grateful for all my colleagues in the lab with whom I have worked over the years. The atmosphere and team spirit was unmatched. I have not only shared office space and lunch breaks with you, but also memorable times and I am grateful for your continuous support, scientific discussions and experimental help during the project.

I would like to express my sincere gratitude to my parents for their unconditional support, confidence and encouragement throughout my years of study and especially during this Ph.D. I am eternally grateful to Franzi for her unfailing support, uplifting nature and being always there for me.